The Horizontal Oculomotor System in Zebrafish: Binocular Coordination, Functional Architecture and Early Maturation

Dissertation

Zur Erlangung des Grades eines

Doktors der Naturwissenschaften

der Mathematisch-Naturwissenschaftlichen Fakultät

und

der Medizinischen Fakultät

der Eberhard-Karls-Universität Tübingen

vorgelegt

von

Christian Brysch

aus München, Deutschland

2023

Tag der mündlichen Prüfung: 11.05.2023

Dekan der Math.-Nat. Fakultät: Prof. Dr. Thilo Stehle

Dekan der Medizinischen Fakultät: Prof. Dr. Bernd Pichler

1. Berichterstatter: Prof. Dr. Aristides Arrenberg

2. Berichterstatter: Prof. Dr. Ziad Hafed

Prüfungskommission: Prof. Dr. Aristides Arrenberg

Prof. Dr. Ziad Hafed

Prof. Dr. Thomas Euler

Prof. Dr. Uwe Ilg

Erklärung / Declaration:

Ich erkläre, dass ich die zur Promotion eingereichte Arbeit mit dem Titel: „The Horizontal Oculomotor System in Zebrafish: Binocular Coordination, Functional Architecture and Early Maturation“ selbständig verfasst, nur die angegebenen Quellen und Hilfsmittel benutzt und wörtlich oder inhaltlich übernommene Stellen als solche gekennzeichnet habe. Ich versichere an Eides statt, dass diese Angaben wahr sind und dass ich nichts verschwiegen habe. Mir ist bekannt, dass die falsche Abgabe einer Versicherung an Eides statt mit Freiheitsstrafe bis zu drei Jahren oder mit Geldstrafe bestraft wird.

I hereby declare that I have produced the work entitled “The Horizontal Oculomotor System in Zebrafish: Binocular Coordination, Functional Architecture and Early Maturation”, submitted for the award of a doctorate, on my own (without external help), have used only the sources and aids indicated and have marked passages included from other works, whether verbatim or in content, as such. I swear upon oath that these statements are true and that I have not concealed anything. I am aware that making a false declaration under oath is punishable by a term of imprisonment of up to three years or by a fine.

Tübingen, den ....

Datum / Date Unterschrift /Signature

This page is intentionally left blank

Table of Contents

Abstract

The oculomotor integrator transforms an eye velocity input into an eye position signal that is essential for retinal image stabilization. This signal is stored for a prolonged amount of time in the brain and acts as a working memory for eye position. The oculomotor integrator is embedded into the vertebrate hindbrain circuit that drives horizontal eye movements. While the basic components of this circuit are known, we still have little knowledge about how those neurons achieve this integration and the exact coding properties of those neurons and of the connected oculomotor nuclei. Similarly, different theories exist that try to explain how the binocular coordination of the two individual eyes is achieved to drive precise binocular eye movements. No conclusive answer has been found to this question so far.

The larval zebrafish is becoming an increasingly popular choice for neuroscientists as a model organism due to its transparency and great accessibility for microscopy studies during early development. Therefore, I used calcium imaging in the developing brain of larval zebrafish to investigate those questions.

In the first set of experiments, I exploit a specific experimental paradigm to provoke monocular eye movements in one-week old larval zebrafish to investigate the eye specific tuning of oculomotor neurons and to coarsely map their eye position/velocity sensitivity. I imaged the hindbrain area encompassing the nucleus abducens, oculomotor integrator, inferior olive, and the velocity storage mechanism. The results of this experiment show that the neurons of those nuclei can be grouped into four response groups which differ in their activity during monocular eye movements. One group shows preferential activity during binocular eye movements. This points towards a certain degree of task separation at this developmental stage. Additionally, I show how the oculomotor integrator appears to extend into areas that were previously not identified as important for retinal image stabilization.

In the second part, I further investigate the precise tuning properties of those neurons by running a closed-loop experiment that was aimed at decoupling the eye position signal from eye velocity. I report how oculomotor neurons encode eye position and eye velocity to a varying degree and their different activation thresholds. I show how the neurons in the caudal hindbrain appear to integrate eye velocity into position along a gradient, but they are arranged in two separate eye position and eye velocity clusters.

In the last set of experiments, I examine the maturation of the previously investigated nuclei. I replicate the experiments on two-week old larvae, as the brains of zebrafish are still developing at that age. I show how several aspects of the oculomotor system are already established in young larvae, but some others are still undergoing refinement. Monocular neurons increase their eye specific sensitivity even further and the eye velocity system is becoming almost exclusively monocular with age. Neurons that show preferential binocular activity are more distributed in the brain and become less frequent with age, while neurons that are active regardless which eye is moving become more abundant.

This thesis characterizes the binocular coordination and coding sensitivities of the oculomotor hindbrain neurons at two different developmental stages. It expands our knowledge on how the nuclei controlling horizontal eye movements are tuned and provides the basis for further investigations on how persistent activity can be generated in the brain.

Zusammenfassung

Der okulomotorische Integrator wandelt ein neuronales Signal, welches Augengeschwindigkeit kodiert, in ein Augenpositionssignal um das für die Stabilität des Netzhautbildes wichtig ist. Dieses Signal wird über einen längeren Zeitraum im Gehirn gespeichert und dient als Arbeitsgedächtnis für die Augenposition. Der okulomotorische Integrator ist in den neuronalen Schaltkreis des Hinterhirns von Wirbeltieren eingebettet, der horizontale Augenbewegungen steuert. Während die grundlegenden Komponenten dieses Schaltkreises bekannt sind, wissen wir noch wenig darüber, wie die Integratorneurone diese Integration erwirken und welche genauen Kodierungseigenschaften diese Neurone und die angebundenen okulomotorischen Kerne haben. Es gibt verschiedene Theorien die zu erklären versuchen, wie die binokulare Koordination der beiden einzelnen Augen erreicht wird, um Augenbewegungen präzise zu steuern. Eine schlüssige Antwort auf diese Frage wurde bisher noch nicht gefunden.
Der larvale Zebrafisch wird als Versuchstier für Neurowissenschaftler immer beliebter, da er sich transparent entwickelt und dadurch für mikroskopische Untersuchungen empfänglich ist. Ich habe Kalzium-Bildgebungsverfahren im sich entwickelnden Gehirn des larvalen Zebrafisches verwendet, um diese Fragen zu beantworten.

In einem ersten Experiment benutze ich ein spezielles Stimulationsprotokoll, um monokulare Augenbewegungen in einwöchigen Zebrafischlarven auszulösen. Dies ermöglicht es mir die Augenspezifität der okulomotorischen Neurone zu untersuchen und ihre Sensitivität bezüglich Augenposition und -geschwindigkeit grob zu kartieren. Ich habe den Hinterhirnbereich untersucht der den Nucleus abducens, den okulomotorischen Integrator, den unteren Olivenkernkomplex und den Geschwindigkeitsspeichermechanismus beinhaltet. Die Ergebnisse dieses Experimentes zeigen, dass die Neurone dieser okulomotorischen Kerne in vier verschiedene Gruppen eingeteilt werden können, die sich in ihrer Aktivität während monokularer Augenbewegungen unterscheiden. Eine dieser Gruppen zeigt eine bevorzugte Aktivität bei binokularen Augenbewegungen, was auf ein gewisses Maß an Aufgabentrennung in diesem Entwicklungsstadium hinweist. Darüber hinaus zeige ich wie sich der okulomotorische Integrator in Bereiche ausdehnt, die bisher nicht als wichtig für die retinale Bildstabilität erachtet wurden.

Im zweiten Teil untersuche ich die genauen Abstimmungseigenschaften dieser Neurone, indem ich ein Closed-Loop Experiment durchführe, welches darauf abzielt, das Augenpositionssignal von dem Augengeschwindigkeitssignal zu entkoppeln. Ich beschreibe wie okulomotorische Neurone Augenposition und Augengeschwindigkeit in unterschiedlichem Maße kodieren und ich veranschauliche ihre unterschiedlichen Aktivierungsschwellen. Ich zeige, wie die Neurone im kaudalen Hinterhirn, die das Augengeschwindigkeitssignal in ein Positionssignal umwandeln, entlang eines Gradienten angeordnet erscheinen, aber in Wirklichkeit getrennt in zwei räumlich spezifischen Arealen liegen.

Im letzten Teil meiner Arbeit beschreibe ich die Entwicklung der zuvor untersuchten Gehirnbereiche. Ich wiederhole die Experimente an zwei Wochen alten Larven, da sich die Gehirne der Zebrafische in diesem Alter noch entwickeln. Ich zeige, dass einige Aspekte des okulomotorischen Systems in jungen Larven bereits etabliert sind, während sich andere noch in der Entwicklung befinden. Monokulare Neurone erhöhen ihre Spezifität noch weiter und das Augengeschwindigkeitssystem wird mit zunehmendem Alter fast ausschließlich monokular. Neurone, die bevorzugt binokulare Aktivität zeigen, sind gleichmäßiger im Gehirn verteilt und werden mit zunehmendem Alter seltener. Nervenzellen, die unabhängig davon welches Auge sich bewegt aktiv sind, kommen mit zunehmendem Alter häufiger vor.

In der vorliegenden Doktorarbeit untersuche ich die binokulare Koordination der Augen und die Kodierungsempfindlichkeit der okulomotorischen Hinterhirnneurone in zwei verschiedenen Entwicklungsstadien des larvalen Zebrafisches. Die Ergebnisse dieser Arbeit erweitern unser Wissen darüber, wie die Gehirnbereiche, welche horizontale Augenbewegungen steuern, kodieren und sie bildet eine Grundlage für weitere Untersuchungen wie persistente Aktivität im Gehirn erzeugt werden kann.

Chapter 1: Introduction

1.1 The "Neuron Doctrine" and "Functional Localization" in the context of studying neuronal circuits

In his pioneering work, Ramón y Cajal showed, using Golgi-staining in the cerebellum of birds, that the nervous system is composed of independent cells (Figure 1-1a; Ramón y Cajal (1888)). This discovery contradicted with the at the time popular idea of the "reticular theory", which states that the nervous system forms a continuous network which is physically connected, a theory which Golgi himself followed (Gerlach, 1872; Grant, 2007). However, the results of Cajal's work, together with the findings of other scientists, led to the postulation of the "neuron doctrine", which states that "the relationship between nerve cells was not one of continuity, but rather of contiguity" (López-Muñoz et al., 2006). The neuron doctrine developed over time into one of the most basic principles of modern neuroscience.

Another important neuroscientific tenet is the "functional specialization" (or sometimes called "functional localization"), which states that specific parts of the brain are specialized for different functions/behaviors (Finger, 2009; Glickstein, 2006). Originating from the school of Phrenology, of which most ideas are now refuted as pseudoscience (Zola-Morgan, 1995), the studies of Paul Broca on a patient who suffered from aphasia provided the first neurobiological evidence for functional localization in the brain (Broca, 1861; Finger, 2009). It has been shown that, especially in the visual domain, specific areas are selectively active not only for basic sensory and motor tasks but also for higher cognition (Kanwisher, 2010). However, as the most radical interpretation of the "functional specialization" might be too strict and not true for all high level perceptual functions, it has been proven that specific regions in the brain are associated to specific functions (Bartels & Zeki, 2004; Brett et al., 2002; Kanwisher, 2010; Schiller, 1996).

These two components, the fact that the brain is comprised of individual cells and that networks of these individual cells can be attributed to specific and well-defined behaviors, show that not only the properties of individual neurons, but also their interconnectivity and interactions matter when studying neuronal circuits. This is essential in understanding how sensory information is processed and how neuronal networks produce different behavioral responses.

1.2 The zebrafish as a model organism in neuroscience

1.2.1 Zebrafish: From genetics to neuroscience

To elucidate how circuits generate behavior and the complex interactions between the neurons involved, one needs to study the appropriate networks in a model organism that ideally can perform the underlying behavior in a well-defined and quantifiable way (i), is susceptible to the appropriate analytical tools and genetic manipulation (ii), imaging can be performed *in vivo* (iii), shares similarities to humans to allow for translational research (iv), and are easily bred and maintained in laboratories (v).

In recent time, zebrafish (*danio rerio*, Figure 1-1b) emerged as a prime model organism in neuroscience that fulfills all of the above mentioned requirements (Fetcho & Liu, 1998; Grunwald & Eisen, 2002; Rinkwitz et al., 2011; Rubinstein, 2003; Spence et al., 2008). Zebrafish are teleost tropical freshwater fish that belong to the family of Cyprinidae. They natively live in small streams and rice paddies in the north-eastern parts of India and neighboring countries. Zebrafish develop *ex utero* in transparent eggs, with a short generation time for vertebrates, and they produce a large number of offspring. They are very susceptible to genetic and molecular tools and their small size makes them ideal for laboratory use (Engeszer et al., 2007; Fetcho & Liu, 1998; Spence et al., 2008).

The remarkable success of zebrafish in today's scientific environment is attributed to the dedication of George Streisinger, who started to work on zebrafish in the 1960s. The first breakthrough for zebrafish came in the mid-1970s, though only published several years later, as Streisinger and colleagues produced clonal homozygous, diploid embryos from the maternal genome only (Grunwald & Eisen, 2002; Streisinger et al., 1981). Notably, at that

Figure 1-1: Neurons and zebrafish

a: Drawing of Purkinje and Granule cells in the pigeon cerebellum by Cajal. © Public Domain **b:** A picture of an adult, female zebrafish in an aquarium. © Wikimedia Commons **c:** 7-day old zebrafish larvae of the AB strain (wildtype, above) and from a mutated strain in a homozygous background that lacks melanophores (*nacre*, bottom). Left: dorsal view; right: sagittal view of the eye. Adapted under CC BY 4.0 from Antinucci & Hindges (2016).

time zebrafish were already used in neuroscientific research but more in the fields of genetics and developmental biology (Eisen et al., 1986; Kimmel, 1982). This is also highlighted by the 2nd phase of notable hallmark publications which came in the form of two forward genetic screens, the first large scale screens in vertebrae, which were published in a special issue of *Development* (volume 123, 1996) that encompassed a total of 37 individual zebrafish papers (Nüsslein-Volhard, 2012; Spence et al., 2008).

While wildtype larvae still develop their eponymous stripes, the resulting opacity limits their use after the first days of development for traditional microscopy studies. However, there are several established mutations and chemical treatment protocols available which allow to maintain the transparency of the fish and it is thus possible to study biological processes and their development *in vivo* until the adult stage (Figure 1-1c; Antinucci & Hindges (2016); Elsalini & Rohr (2003); Lister et al. (1999); White et al. (2008)). With the establishment of these lines and simultaneous advances in microscopy, zebrafish became more and more relevant for researchers interested not only in the development and genetics of neurons but also their circuitry (Denk et al., 1990; Fetcho et al., 1998; Fetcho & Liu, 1998). The small size of the zebrafish brain, and thus the small number of neurons (about 100.000), makes it easier to find causal links between neuronal activity and behaviors (Kimmel, 1982; Naumann et al., 2010). This provides the opportunity to study behavior and understand the underlying neurons and their circuitry in a vertebrae system, with easy access to genetic markers and sensors, and then test the resulting hypotheses in "higher" model organisms, like mammals (Fetcho & Liu, 1998).

1.2.2 The use of zebrafish in visual studies and ocular disease models

Though zebrafish are phylogenetically distant to humans, with a common ancestor ~440 million years ago, about 70 % of their genes are orthologous to humans and 82 % of disease related genes in humans have an orthologue in zebrafish (Figure 1-2; Amores et al. (2011); Howe et al. (2013)). Thus, it is not surprising that we share striking similarities, including the central nervous system morphology, a rather conserved genetic plan for brain development, neurotransmitters and receptors, structural and functional brain homology, and behavioral paradigms with zebrafish (Fadool & Dowling, 2008; Jurisch-Yaksi et al., 2020; Kalueff et al., 2014; Levin & Cerutti, 2009; Rinkwitz et al., 2011; Tropepe & Sive, 2003; Wilson & Houart, 2004).

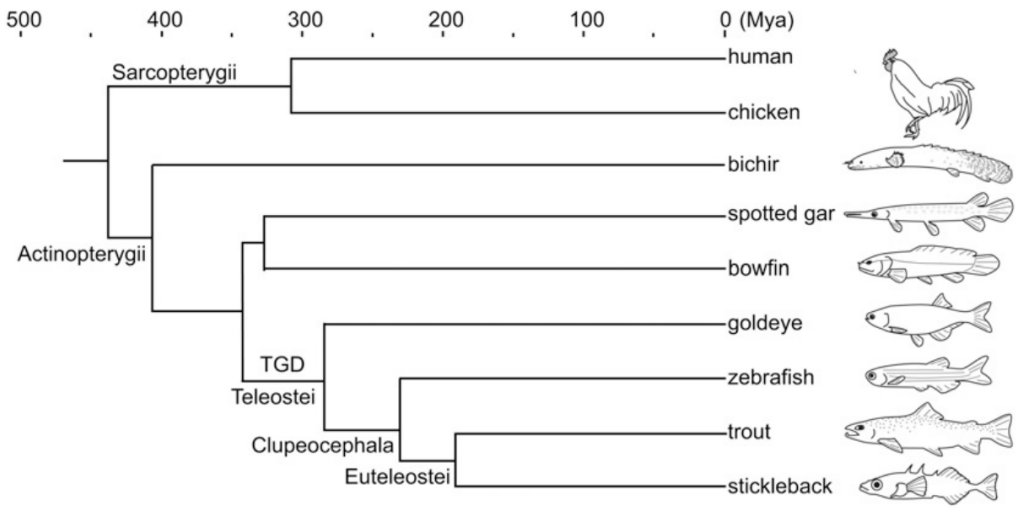

Figure 1-2: Phylogenetic relationship between humans and zebrafish

Phylogenetic relationship between several ray-fin (Actinopterygii) and lobe-fin fish (Sarcopterygii). Lineages between tetrapod and ray-fin fish diverged ~440 million years ago (MYA). TGD: teleost genome duplication; species: human (*Homo sapiens*), chicken (*Gallus gallus*), bichir (*Polypterus ornatipinnis*), spotted gar (*Lepisosteus oculatus*), bowfin (*Amia calva*), goldeye (*Hiodon alosoides*), zebrafish (*Danio rerio*), trout (*Oncorhynchus mykiss*), and stickleback (*Gasterosteus aculatus*). Adapted with permission from Amores et al. (2011).

Therefore, zebrafish are used to study a wide variety of brain and drug-related disorders from anxiety (Jesuthasan, 2012; Stewart et al., 2012b), cognitive behaviors (Yu et al., 2006), epilepsy (Stewart et al., 2012a; Yaksi et al., 2021), neuroactive drugs (Irons et al., 2010), social behaviors (Buske & Gerlai, 2012; Lemasson et al., 2018) to withdrawal syndrome (Cachat et al. (2010); reviewed in Basnet et al. (2019); Kalueff et al. (2013, 2014)).

One specific area where zebrafish have been used as a model organism with great success is in ophthalmological research and the study of visuomotor circuits. The visual development of zebrafish happens over a small timescale (see below). It is largely congenital and thus comparable between individual fish. Plus, zebrafish perform a variety of visually driven and quantifiable behaviors from a young age. This makes it convenient to use them in visual screens to check for developmental or degenerative diseases including glaucoma, photoreceptor degeneration, myopia, and even oculomotor diseases like human congenital nystagmus/infantile nystagmus syndrome (Chen, 2014; Chhetri et al., 2014; Gestri et al., 2012). Together with the other benefits of zebrafish for neuroscientific research mentioned above, they developed into a prominent model

organism for oculomotor studies (Orger, 2016; Portugues et al., 2014; Portugues & Engert, 2009).

1.2.3 The development of vision and visual behaviors in zebrafish

Oculomotor studies and visual circuit analysis in zebrafish are normally conducted at an age of 5-7 days post fertilization (dpf). At this age, zebrafish larvae already exhibit a number of different visual behaviors (Figure 1-3). The following part shows how the development of visual structures coincides with the emergence of several behavioral paradigms which have been used to investigate the underlying visual pathways (i) and that the development of the visual system is not complete at 7 dpf (ii).

The zebrafish eyes begin to form around 12 hours after fertilization and after 72 hours a sharp image is projected onto the retina, thus making the eye emmetropic (Easter & Nicola, 1996; Schmitt & Dowling, 1994). At that time, all extraocular muscles (EOMs) are already present and functional, though they are still maturing for another day. All opsins are also detectable and the synaptic ribbons become functional, though they are not yet fully mature (Chhetri et al., 2014; Easter & Nicola, 1996). The eye is now visually functional and it sends information towards 10 different retinorecipient brain areas (Baier & Wullimann, 2021; Burrill & Easter, 1994). Interestingly, at that age zebrafish already perform tracking eye movements (see chapter 1.4.1) and a visual startle response, which can be caused by a rapid luminance de-/increase. This shows that, simultaneously with the emergence of all

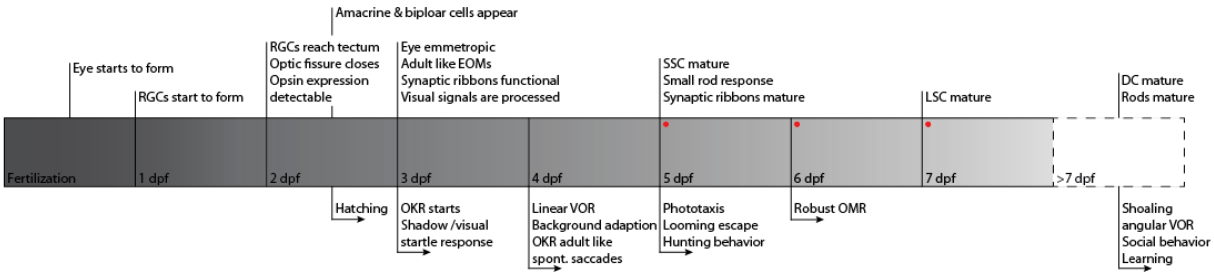

Figure 1-3: Development of vision and behavior in zebrafish

Schematic depicting several hallmarks in visual development (above) and the emergence of some behaviors (below). DC: double cone, dpf: days post fertilization, EOM: extraocular muscle, LSC: long single cone, OKR: optokinetic response, OMR: oculomotor response, RGC: retinal ganglion cell, SSC: short single cone, VOR: vestibulo-ocular reflex. Red dots show the developmental stages used for experiments in chapter 3. Data taken and slightly modified for artistic reasons from Bilotta & Saszik (2001), Chhetri et al. (2014), Neuhauss (2003, 2010), Walz (2011).

structural prerequisites (light sensor, processing structures, muscles), zebrafish start to react to visual stimulation, though the performance of those behaviors is still improving with age. While visually evoked eye movements are already present at 3 dpf, vestibular-induced eye movements and spontaneous rapid eye movements (saccades) become measurable one day later. At that age, zebrafish will only respond with compensatory eye movements to acceleration that is detected by their otoliths, namely to linear/translational head displacements. The corresponding behavior to angular acceleration is only measurable after ~35 dpf (Beck et al., 2004; Mo et al., 2010). This is due to the still immature semicircular canals. It has been shown that they must surpass a specific size before the endolymph movement inside them can reliably activate the vestibular hair cells and therefore zebrafish need additional time to grow before the angular acceleration gets detected (Beck et al., 2004; Branoner et al., 2016; Lambert et al., 2008). Zebrafish primarily rely on vision during foraging, which they start at 5 dpf, and it further highlights the rapid development of zebrafish vision that such a complex behavior is already established this fast (Bianco et al., 2011; Mearns et al., 2020).

Most studies investigating the visual processing in zebrafish use 5-7 dpf old larvae, as there are already a lot of different visually evoked behaviors present and the small size/minimal ossification does not interfere with imaging studies to a great extent. However, it should be noted that at 5-7 dpf the brain and other visual structures are still developing and are not yet mature. On the one hand, the anatomy and the physiology of the eye will change further during development (Gestri et al., 2012; Zhao et al., 2006). At 5 dpf, larval vision is mostly mediated by cone photoreceptors as rods, while already present and capable of driving behavior under specific circumstances, are not yet matured and only contribute little to larval vision (Bilotta et al., 2001; Venkatraman et al., 2020). Similarly, two of the four cone types, sensitive to blue light (LSC) and green/red sensitive double cones (DC), are also maturing at a later developmental stage (Bilotta & Saszik, 2001; Chhetri et al., 2014). On the other hand, further refinement will happen at other levels of visual processing as well. For instance, tectal receptive fields will shrink in size during the first three weeks of development to support a better acuity in visually guided behaviors (Bergmann et al., 2018; Zhang et al., 2011). Also, the already mentioned later detection of angular acceleration needs to be integrated into existing neuronal circuits (Branoner et al., 2016). The sustained development is also accompanied by behavioral changes as eye movements of older zebrafish become more conjugate and have a more than 2-fold

increase in the frequency of spontaneous saccades (Beck et al., 2004). Additionally, some behaviors such as learning, shoaling, and other social behaviors will only occur at stages later than 7 dpf (Buske & Gerlai, 2012; Valente et al., 2012; Walz, 2011). This shows that, while most imaging studies on zebrafish are conducted at an early stage, these results might not be comparable to adults.

1.3 Using calcium imaging to probe neuronal circuits in zebrafish

1.3.1 Using calcium indicators to image neuronal activity

Calcium (Ca^{2+}) is a ubiquitous secondary messenger that is involved in a large variety of cellular processes from fertilization, where calcium spikes initiate development, to apoptosis, where it is used in the expression of apoptotic signaling components (Berridge et al., 2000). In neurons, calcium triggers neurotransmitter release at the presynaptic terminal, where a large influx of calcium induces a release of vesicles with the stored neurotransmitters upon activation of voltage-gated calcium channels (VGCCs; Neher & Sakaba (2008)). The calcium signals triggered by VGCCs, due to depolarization of the membrane caused by neuronal activity, and by activation of receptor mediated calcium channels is also propagated into the nucleus where the nuclear calcium concentration changes show a strong interdependence to the spiking of a neuron (Bading, 2013; Bengtson et al., 2010; Bloodgood & Sabatini, 2007; Tian et al., 2012). The relative calcium concentration changes in the cytoplasm or nucleus can now be visualized with calcium indicators and the resulting signals can be used as a proxy for neuronal activity. Some of these indicators are derived from the bioluminescent protein Aequorin, which can easily be used in freely moving animals, do not require external excitation, and have already been used successfully in zebrafish (Naumann et al., 2010). However, the recharging of these indicators is slow and therefore chemical or genetically encoded calcium indicators (GECIs) have become more prominent over the years. GECIs in particular do not require any potentially harmful application procedure, like microinjections (Grienberger & Konnerth, 2012). The most widely used GECIs are GCaMPs. They are designed based on a circularly permuted enhanced green fluorescent protein (cpEGFP) fused to calmodulin, a calcium binding protein, and M13, a target sequence of calmodulin (Figure 1-4a & b). Upon binding of calcium to calmodulin, a conformational change is induced, which leads to an increase in fluorescence at a certain wavelength. When excitation is provided by an

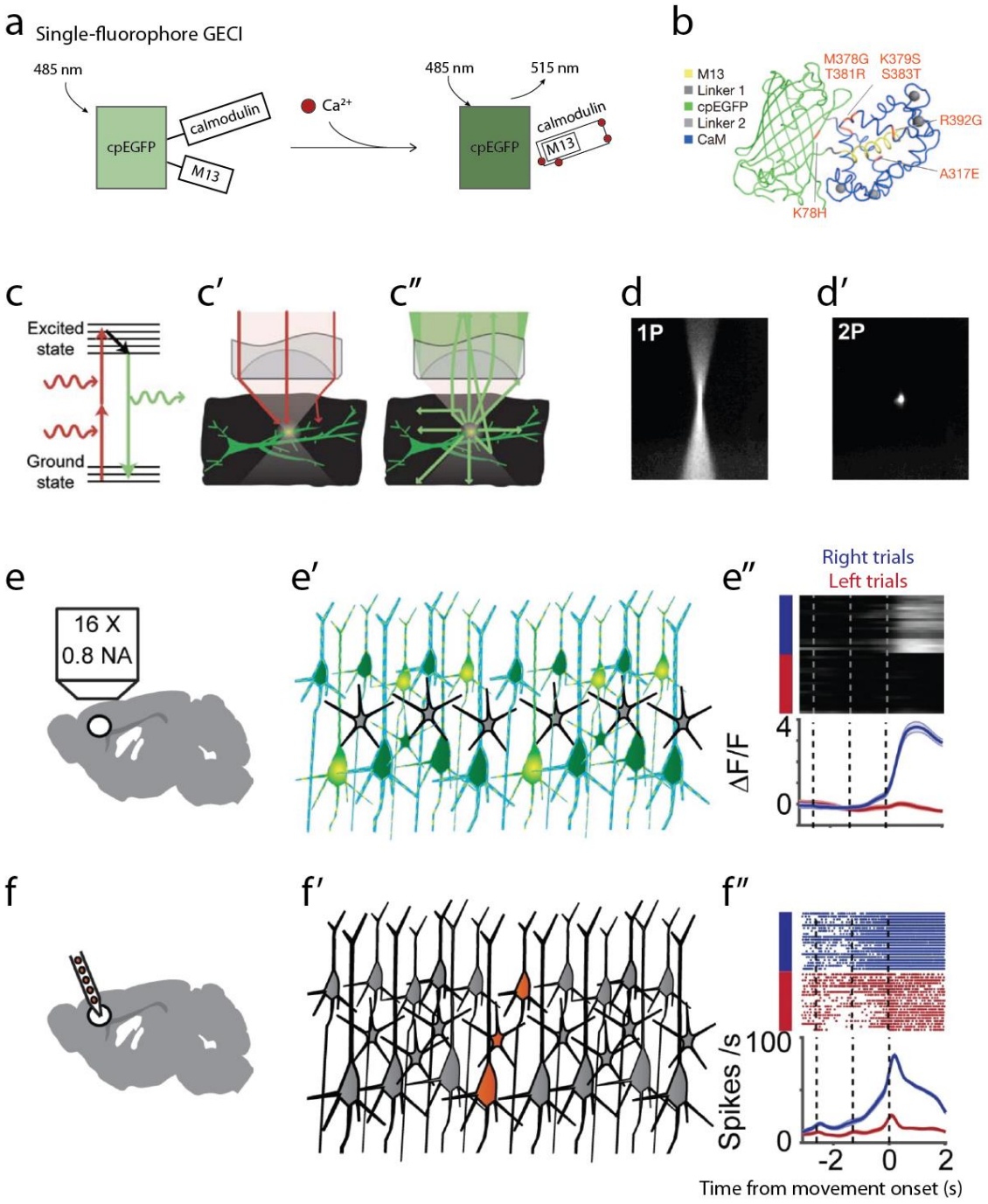

Figure 1-4: Calcium imaging and 2P-microscopy

a: Single-fluorophore GECI where conformational intramolecular changes lead to an increase in the emitted fluorescence of 515 nm, after binding of calcium to calmodulin. Adapted with permission from Grienberger & Konnerth (2012). **b:** GCaMP6 variant structure and its mutations relative to GCaMP5G. With permission from Chen et al. (2013). **c:** Simplified Jablonski diagram of the 2-photon excitation process; c': Localization of excitation in a scattering medium (black). 2 ballistic photons excite green fluorescence in a single diffraction-limited spot; scattered photons are too dilute to cause off-focus excitation. c'': Fluorescence collection in a scattering medium. Fluorescence photons are emitted isotropically from the excitation volume. Figure and legend taken with permission from Svoboda & Yasuda (2006). **d:** Fluorescence emission in a fluorescein solution. With traditional 1-photon excitation (1P) emission can be seen throughout the sample depth. d': Using 2-photon excitation it is localized to a single spot (2P). Adapted with permission from

Soeller & Cannell (1999). **e-f'':** Illustration showing sampling of population activity using calcium imaging (GCaMP, e & e') and electrophysiology (silicon probe that recorded multiple neurons at a time, f & f') of a delayed-response, two alternative forced-choice task experiment. Mice had to discriminate a pole position and report it by directional licking. Recordings were conducted in the left anterolateral motor cortex. e'': Individual trials (top) and mean activity (bottom) for calcium imaging. f'': Raster plot (top) and peri-stimulus time histogram (PSTH) for electrophysiological recordings. Note the differences for the decay time after neuronal activity. Adapted under CC BY 4.0 from Wei et al. (2020).

external source, the change in fluorescence intensity can then be used as a proxy for neuronal activity (Nakai et al., 2001).

1.3.2 2-photon microscopy with GCaMPs

Fluorescent indicators, like GCaMP, need an external light source to function. Lasers are an ideal way to provide the energy to the sensor, in particular 2-photon (2P) lasers. Here, the near simultaneous absorption of 2 lower energy photons is necessary for the electron to reach the excited state (Figure 1-4c; Denk et al. (1990)). In contrast to traditional 1-photon imaging, in a focused 2P laser this double absorption almost exclusively happens at the focal point, preventing excitation in areas above and below (Figure 1-4d & d'; Svoboda & Yasuda (2006)). Due to the longer wavelength of the excitation light in 2P microscopy, deeper tissue penetration and minimized light scattering is also achieved, which makes this technique quite powerful for functional *in-vivo* imaging in zebrafish.

In comparison to other recording techniques, like electrophysiology (ephys), 2P calcium imaging enables the researcher to record signals from populations of neurons with single cell resolution. However, some drawbacks should be addressed. Due to the kinetic of the indicator, the reported fluorescence changes are distorted in time and non-linear (Figure 1-4e-f''; Rose et al. (2014)). Furthermore, the temporal resolution for calcium imaging is lacking far behind ephys data (2 Hz in this study compared to kHz in ephys). On the other hand, calcium imaging provides a powerful tool for interrogating the population activity of neurons linked to specific behaviors, even if the true extent of the neuronal assemblies associated to that behavior are not yet known, and is therefore utilized in the present study (Wei et al., 2020).

1.4 The visual system of zebrafish for horizontal eye movements

Chapter 1.1 to 1.3 are intended to help readers become familiar with the importance of studying neuronal networks, the zebrafish with its advantages for imaging studies of visual systems, and some of the techniques utilized to do so. In the following chapter, the visual system of zebrafish is introduced, specifically the networks of neurons required for the execution of horizontal eye movements and the system required to maintain stable eye positions.

1.4.1 The optokinetic response

To maintain stable vision in response to movement of the surround or own body movements, vertebrates have developed two compensatory and reflexive eye movement behaviors to maintain a stable image on the retina. The vestibulo-ocular reflex (VOR) relies on information from the semicircular canals and otoliths and thus responds to head velocity. The optokinetic response (or optokinetic reflex, OKR) helps with retinal image stability in response to retinal slip signals by evoking compensatory eye movements. Both behaviors are complementary to each other, with the OKR capable of persistent responses to constant stimulation and acting as a low-pass filter while the other is more sensitive to rapid head rotations (Beck et al., 2004; Huang, 2008; Masseck & Hoffmann, 2009; Soodak & Simpson, 1988). As shown in chapter 1.2.3, the OKR is an innate behavior in zebrafish, develops rapidly, and is comparable among different larvae. It is thus an ideal candidate to provoke eye movements under laboratory conditions.

The OKR is usually evoked by rotating vertical gratings around the head of a tethered zebrafish (Figure 1-5a). The fish will then perform the OKR, which consists of two components. During the so-called slow-phase, the zebrafish eyes follow the movement of the gratings by rotating until they reach an eccentric position. In the resetting eye movement phase, the eyes move rapidly in the contraversive direction to a more neutral state. In general, the two phases alternate each other resulting in a sawtooth-like eye trace (Figure 1-5b). The resetting eye movement phase (quick-phase) is comparable in speed and amplitude to saccades and the same anatomical structures are involved in both of them (Garbutt et al., 2001; Schoonheim et al., 2010). The OKR is dependent on the angular velocity, spatial frequency, and contrast of the stimulus for both larval and adult zebrafish, with brightness not contributing above a certain threshold (Mueller & Neuhauss, 2010;

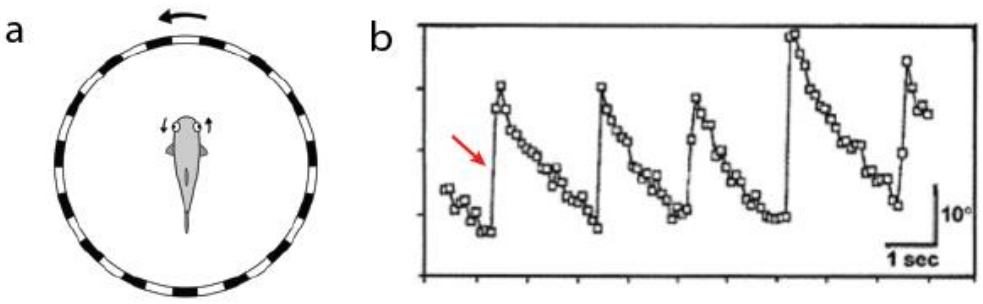

Figure 1-5: The optokinetic response

a: Setup schematic to evoke the OKR in zebrafish. The vertical stripes (large arrow) rotate horizontally around the fish which moves its eyes in the ipsiversive direction (small arrows). Reprinted under CC BY 4.0 from Bollaerts et al. (2018) **b:** Typical eye position trace for continuous OKR stimulation in one direction. Red arrow indicates one saccade. Reprinted with permission from Neuhauss et al. (1999).

Rinner et al., 2005). One form to quantify the OKR is its "gain", calculated by dividing the eye velocity with the stimulus velocity. The OKR gain is dependent on the location of the stimulus and is highest with the visual stimulation located around the equator laterally to the eyes. However, while the gain increases significantly with age, especially for higher temporal frequencies, it is always smaller than one, indicating that the eyes trail behind the stimulus and that zebrafish do not perfectly follow the stimulus (Beck et al., 2004; Dehmelt et al., 2021).

The OKR gain in zebrafish is asymmetrical and depends on the stimulus direction. Each eye shows a higher gain to stimulation moving in its temporal to nasal direction (e.g. counterclockwise movement for the right eye; Qian et al. (2005); Roeser & Baier (2003)). This is an OKR feature of many lateral-eyed animals, though several exceptions even within fish exist (Masseck & Hoffmann, 2009). In zebrafish, psychophysics studies showed that the spatial frequency of the stimulus has an influence on the degree of this asymmetry and is even capable of inverting the preferred direction if the frequency is high enough (Bögli et al., 2016; Qian et al., 2005).

Fish show a varying degree of correlation between the two eyes during optokinetic stimulation. When one eye is occluded, the butterflyfish (*Chaetodon rainfordi*) and pipefish (*Corythoichthyes intestinalis*) exhibit OKR in the non-stimulated eye as well. This is in contrast to the sandlance (*Limnichthyes fasciatus*) which only exhibit OKR in the stimulated eye (Fritsches & Marshall, 2002). Zebrafish also show yoked eye movements for monocular OKR stimulation, though with less gain in the unstimulated eye than in the

stimulated one. If the unstimulated eye is presented with a stationary pattern, the gain of this eye drops significantly to <0.1 and the zebrafish performs a monocular OKR. However, during this monocular OKR the gain of the stimulated eye is reduced and its quick-phase amplitudes are smaller compared to their values during binocular stimulation (Beck et al., 2004; Qian et al., 2005).

1.4.2 The accessory optic system mediating the OKR

The accessory optic system (AOS) mediates the OKR in the visual system of different species (Masseck & Hoffmann, 2009; Simpson, 1984). The AOS responds to the optic flow perceived by direction-selective (DS) retinal ganglion cells (RGCs) and is present in all vertebrates but differs between species (Figure 1-6a & a'). In mammals, the AOS is comprised of 3 individual nuclei (when the NOT-DTN is counted as one functional structure) of which each nucleus responds directional selectively to input from only one preferred direction (Giolli et al., 2006; Masseck & Hoffmann, 2009). In zebrafish, the area pretectalis (APT) is the homologous structure to these nuclei. Here, motion-sensitive, direction-selective neurons are sensitive to 4 directions, which are roughly tuned to the cardinal directions (up & down and left/right for each eye respectively; Wang et al., 2019)). When stimulated with moving gratings, two groups of neurons can be identified in the pretectum. Monocular neurons, which show response to movement in the temporal-nasal or nasal-temporal direction for each eye, or binocular neurons, which are responsive to translational and rotational movement along all 3 body axes but preferably respond to only translational stimulation (Kubo et al., 2014; Wang et al., 2019). A recent study also showed that zebrafish can decompose the rotation and translational optic flow components separately and behaviorally respond accordingly (Zhang et al., 2022).

In zebrafish, RGC projections terminate in 10 anatomically distinct areas in the brain, termed arborization fields (Afs; when counting the optic tectum as one entity (Robles et al., 2014)). The RGCs mediating the OKR are of the ON and ON-OFF type (Emran et al., 2007). Direction-selective RGCs innervate two of those AFs: the superficial layer of the optic tectum and AF5 in the pretectum (Kramer et al., 2019; Nikolaou et al., 2013), with one study identifying the pretectal AF6 rather than AF5 as a DS-recipient structure (Naumann et al., 2016). RGC axons completely cross the midline in zebrafish (Rick et al., 2000). Therefore, the input to the pretectum is monocular and thus some form of

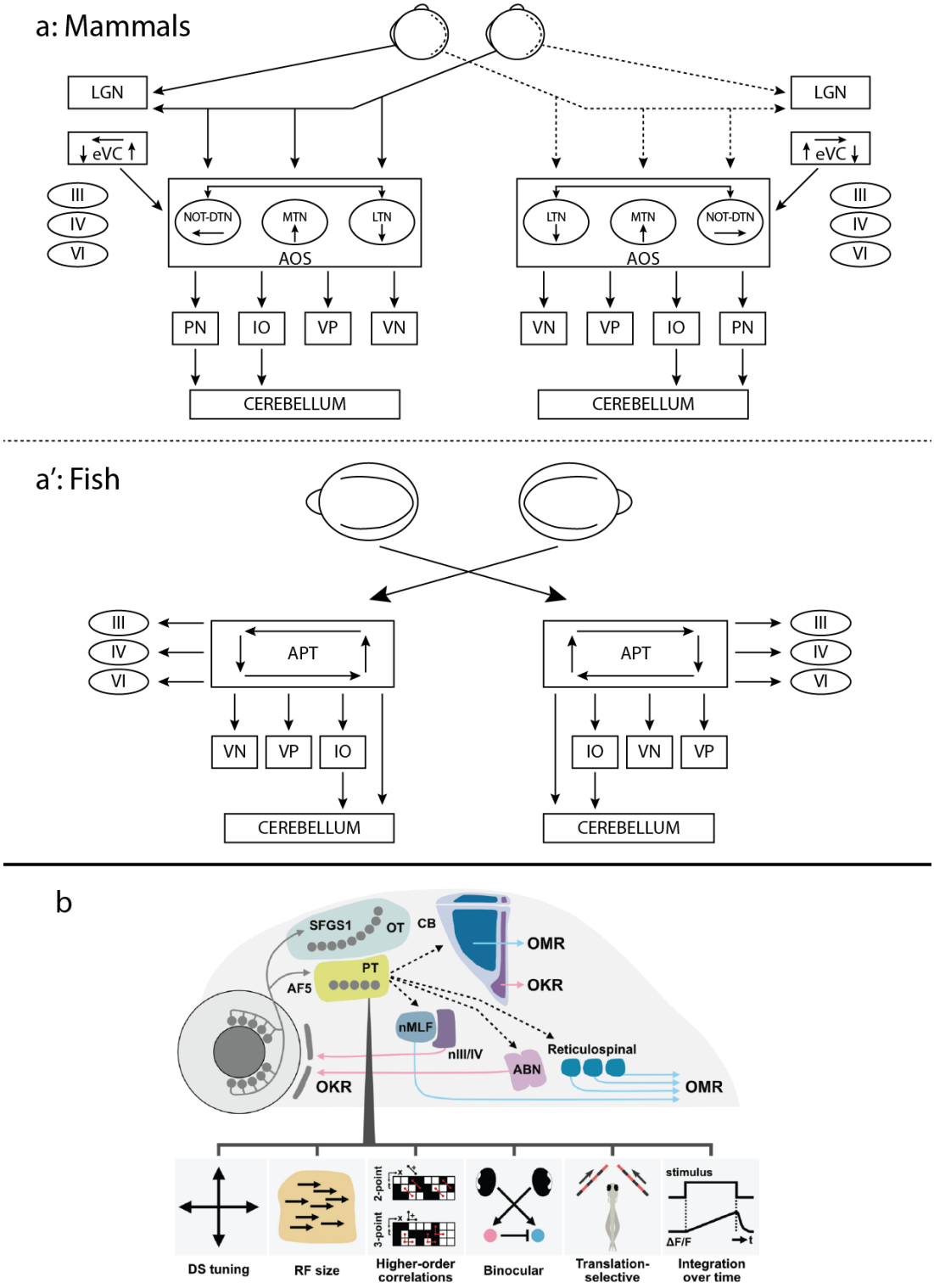

Figure 1-6: Neuronal circuitry of the OKR in mammals and fish

Neuronal circuitry of the OKR in frontal-eyed mammals (a) and fish (a'). Arrows between the boxes represent anatomically verified connections in each panel. **a:** Arrows in the box NOT-DTN, LTN and MTN indicate that only ipsiversive, down or up directions of stimulus movement are coded by neurons in these nuclei respectively. Arrows in the box eVC indicate that extrastriate visual neurons projecting to the AOS prefer ipsiversive, down or up, but not contraversive stimulus movements. **a'**: Arrows in the box APT

indicate that all directions of stimulus movement are coded by neurons in the left as well as in the right nucleus. APT: area pretectalis; eVC: extrastriate visual cortex; IO: inferior olive; LGN: lateral geniculate nucleus; LTN: lateral terminal nucleus; MTN: medial terminal nucleus; PN: pontine nuclei; VP: velocity-to-position integrator; VN: vestibular nuclei; III: nucleus oculomotorius; IV: nucleus trochlearis; VI: nucleus abducens. Figure adapted with permission from Masseck & Hoffmann (2009). **b:** Organization of the optic flow processing circuit in the larval zebrafish brain. The direction selective (DS) retinal ganglion cells (RGCs) project to the SFGS1 layer of the optic tectum (OT) neuropil and AF5 in the pretectal (PT) neuropil. For triggering the OKR, the pretectum sends a signal (either directly or indirectly) to the oculomotor system. In addition, rotation- and translation-selective information is represented in the rostromedial and caudolateral regions in the cerebellum (CB), respectively. Solid lines indicate projections that have been shown in zebrafish larvae, whereas dotted lines represent proposed connections. ABN: nucleus abducens, AF5: arborization field 5, CB: cerebellum, nIII/IV: oculomotor/trochlear nuclei, nMLF: nucleus of the medial longitudinal fasciculus, OKR: optokinetic response, OMR: oculomotor response, SFGS1: stratum fibrosum et griseum superficiale. Figure and legend adapted under CC BY 4.0 from Matsuda & Kubo (2021).

integration must happen at the level of the pretectum for the binocular responsive neurons. Ablation of the posterior commissure, a structure containing commissures from both hemispheric pretectal areas, disrupts binocular integration. This result is in line with a newer study showing that binocular integration happens in the neuropil area close to AF6, while one study hypothesizes that integration happens further downstream (Kramer et al., 2019; Naumann et al., 2016; Wang et al., 2019). Optogenetic perturbations and laser ablations of a small patch of neurons in the ventral-lateral pretectum result in an impaired OKR, further demonstrating that this area is responsible and necessary for driving the OKR (Kubo et al., 2014; Wu et al., 2020). Laser ablations of the optic tectum only interfere with the quick-phase of the OKR but not the slow-phase (Roeser & Baier, 2003). Neurons in the pretectum also have large receptive fields and are responsive to slower motion stimuli, in agreement with optic flow compensation behavior (Giolli et al., 2006; Wang et al., 2020). From the pretectum, the OKR command is then relayed to the oculomotor system (Figure 1-6b). In the caudo-lateral cerebellum, sensory OKR information is represented, likely encoding an error signal from the inferior olive (IO; Knogler et al. (2019); reviewed in Matsuda & Kubo (2021)).

1.4.3 The extraocular muscles and motoneurons that drive eye movements

Downstream of the AOS, several nuclei are involved in initiating and maintaining eye movements that are ultimately generated by the EOMs. There are three pairs of different EOMs: the medial rectus (responsible for eye adduction; MR) and lateral rectus (abduction; LR) are responsible for horizontal eye movements and work antagonistically.

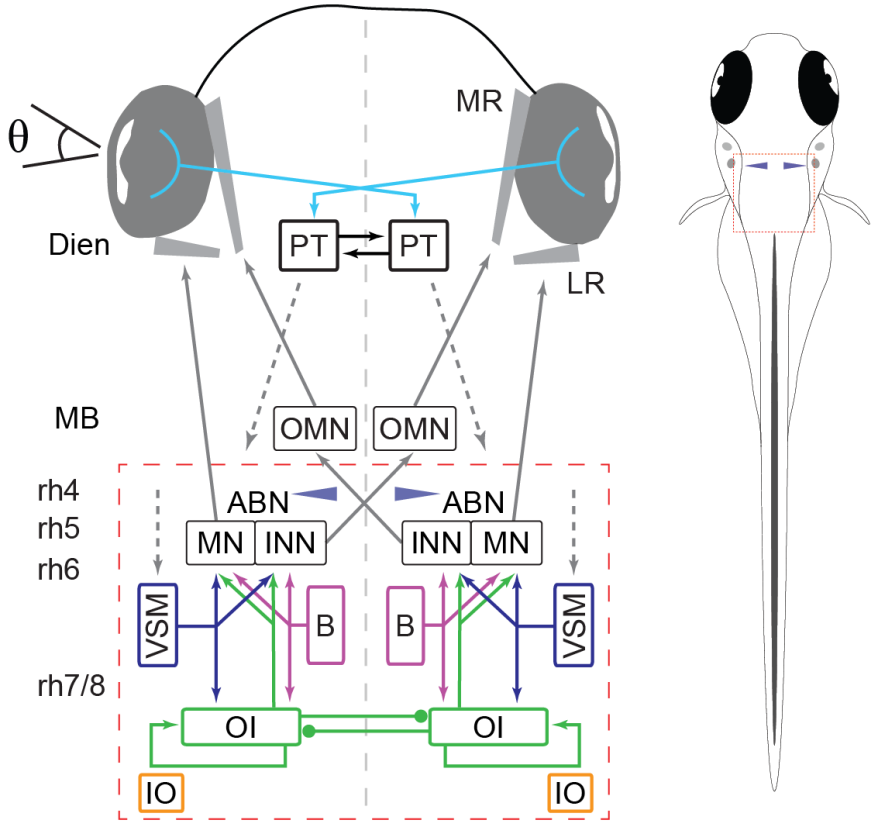

Figure 1-7: Oculomotor circuits in the hindbrain of larval zebrafish

Simplified circuit schematic for horizontal eye movements. Red dashed rectangle represents imaged brain area in this thesis; blue cones show location of Mauthner cells. ABN: nucleus abducens, B: burst neurons, Dien: diencephalon, INN: internuclear neurons, IO: inferior olive, LR: lateral rectus, MB: midbrain, MN: motoneurons, MR: medial rectus, OMN: nucleus oculomotorius, OI: oculomotor integrator, PT: pretectum, rh 4-8: rhombomere 4-8, VSM: velocity storage mechanism, Θ: eye position. The connection from the VSM to the ABN/OI in zebrafish is probably indirect via the cerebellum (Beck et al., 2006; Straka et al., 2006). Dashed lines indicate direct or indirect inputs from upstream visual areas (Figure 1-6; Cochran et al. (1984); Masseck & Hoffmann (2009)). Adapted under CC BY 4.0 from Brysch et al. (2019b).

The superior rectus (elevation, intorsion; SR) and inferior oblique (extorsion, elevation; IOb) work synergistically for eye elevation and the inferior rectus (depression, extortion; IR) and superior oblique (intorsion, depression; SOb) for eye depression respectively (Bruce & Friedman, 2002). The EOM arrangement is highly conserved across vertebrates (Büttner-Ennever, 2006), but there are several differences between zebrafish and humans: zebrafish don't have an EOM subdivision into a global and orbital layer, but they exhibit a subdivision into an inner and outer layer which both connect to the globe, though it is debated how severe this difference is (Dennhag et al., 2020; Horn & Straka, 2021; Kasprick et al., 2011). Furthermore, zebrafish have a different origin for the LR and oblique muscles and lack the trochlea for the SO, though the individual EOM function for

eye movements stay the same (Asakawa & Kawakami, 2018; Kasprick et al., 2011). The motoneurons (MNs) innervating the EOMs are located in three different nuclei: the oculomotor (OMN, cranial nerve nIII), the trochlear (cranial nerve nIV) and the abducens nucleus (ABN, cranial nerve nVI; Horn & Straka (2021); Schilling & Kimmel (1997)). The oculomotor nucleus is located in the mesencephalon, containing MNs innervating the ipsilateral IOb, IR, and MR and MNs innervating the contralateral SR. Within nIII, MNs are arranged in distinct pools with SR MNs located in the medio-ventral area, IOb MNs in the middle, and IR/MR MNs in the dorsal part. The nIV is directly adjacent to the IR/MR MN pool, slightly caudo-dorsally, and it contains SOb MNs that project to the contralateral eye (Greaney et al., 2016; Knüfer et al., 2020). LR MNs are found in the hindbrain within the ABN and are innervating the ipsilateral eye (Figure 1-7). In zebrafish, the ABN is subdivided into two separate nuclei, which reside in rhombomere 5 & 6 (rh) respectively (Chandrasekhar, 2004). Neither anatomical nor functional differences between the two rhombomeres were identified (Asakawa & Kawakami, 2018). MR MN in nIII are activated by internuclear neurons (INNs) in the contralateral ABN and thus reside in close proximity to the respective LR MNs that drive the conjugate eye movements (Cabrera et al., 1992; Ma et al., 2014; Straka & Dieringer, 1991).

MNs can be subdivided into two major classes. In the first group, MNs generally form multiple "*en grappe*" terminals and project to multiply innervated (non-twitch) muscle fibers (MIF). MIFs have slow, tonically muscle fiber properties and they are proposed to be primarily active for slow-phase eye movements. The other group forms a single "*en plaque*" terminal and are innervating singly innervated (twitch) muscle fibers (SIF) which respond with an "all-or-nothing" twitch. MIFs can be further subdivided: MIFs in the orbital layer can have one additional central *en plaque* endplate to their *en grappe* terminals (Horn & Straka, 2021). Recently a study also described a novel type of MIF that has multiple *en plaque* endings (Liu & Domellöf, 2018), which is also present in zebrafish (Dennhag et al., 2020). Additionally, SIF and MIF differ in their molecular/neuronal markers, ion channel composition, and afferent input (reviewed in Büttner-Ennever (2006); Horn & Straka (2021); Spencer & Porter (2006)). Both major types of MNs are found in each rhombomere for the LR in zebrafish (Asakawa & Kawakami, 2018). In monkeys, SIF and MIF MNs differ in their soma size and spatial location. SIF MNs have larger soma sizes and are located more centrally in the motor nuclei, while MIF MNs are located at the periphery and have smaller soma sizes (Büttner-Ennever et al., 2001). A soma size gradient

for LR MNs has also been reported in goldfish and zebrafish, but no connection to the targeted muscle fiber type could be established (Asakawa & Kawakami, 2018; Sterling, 1977).

1.4.4 The burst system for fast eye movements

As already mentioned in chapter 1.4.2, the saccades/quick-phases of the OKR are driven by a different system. Here, excitatory burst neurons (EBNs) in the brainstem drive saccade velocity with bursts of activity ~10 msec before the actual saccade onset (Strassman et al., 1986a). For ipsiversive horizontal saccades, this activity is relayed to the ipsilateral MN/INNs in the ABN (Igusa et al., 1980; Scudder et al., 2002; Van Gisbergen et al., 1981). Simultaneously, inhibitory burst neurons (IBNs) make connections to the MNs and INNs of the antagonistic muscle in the contralateral ABN to suppress activity in the OFF direction (Strassman et al., 1986b). Both types of burst neurons are inhibited by tonically active omnipause neurons (OPNs). 20 msec before a saccade occurs in either direction, OPNs stop firing thus causing disinhibition in the downstream EBNs/IBNs. OPNs stay inhibited by a "latch" command from EBNs until the saccade is executed and they resume their tonic activity (Curthoys et al., 1984; Scudder et al., 2002).

In zebrafish, the locations of these burst neurons have been reported (partly including by my own work but not presented in detail here) to be primarily throughout the dorsal parts of the hindbrain (Leyden et al., 2021). Another study reported a specific group of neurons that show ramping activity before saccades and are thus thought to be involved in their initiation (Ramirez & Aksay, 2021). Additionally, broad optogenetic silencing of neurons in rhombomere 5 suppressed ipsilateral saccade generation (Schoonheim et al., 2010). Neurons involved in saccadic control have also been reported in a dorsal cluster in rhombomere 7 (Ramirez & Aksay, 2021; Wolf et al., 2017) and in a specific dorsal region in the anterior hindbrain termed anterior rhombencephalic turning region (ARTR). Neurons in this region show alternating activity between each hemisphere and they are involved in gaze control and swimming (Ahrens et al., 2013; Dunn et al., 2016; Wolf et al., 2022). The input from the slow-phase OKR and burst system is also relayed to a structure termed the oculomotor integrator (OI).

1.4.5 The oculomotor integrator

1.4.5.1 The function of the oculomotor integrator

The oculomotor integrator (OI, or Velocity-to-Position-Neural-Integrator: VPNI) is an important structure that helps with maintaining retinal image stability. When someone performs a horizontal saccade and keeps the eyes stable at the new position, the EBNs only encode the saccade itself. However, the MNs in the ABN show not only a burst of activity for the saccade (pulse), but also persistent activity (step), which is linearly related to the eye position, after the saccade is finished (Figure 1-8a & b; Gestrin & Sterling (1977); Schiller (1970)). This "step"-command is important to keep the eyes stable at an eccentric position as the EOMs exhibit a passive pullback that would force the eyes back into a neutral position over time (Robinson, 1964; Seung, 1996). As this persistent activity is not generated by the EBNs, it must stem from a different source. The oculomotor integrator is serving that function by transforming the phasic eye velocity input into a persistent eye position encoding output signal via integration (in the mathematical sense) and thus forms a neuronal correlate for working memory of the current eye position. In mammals, this integrator consists of the medial vestibular nucleus (MVN) and the nucleus prepositus

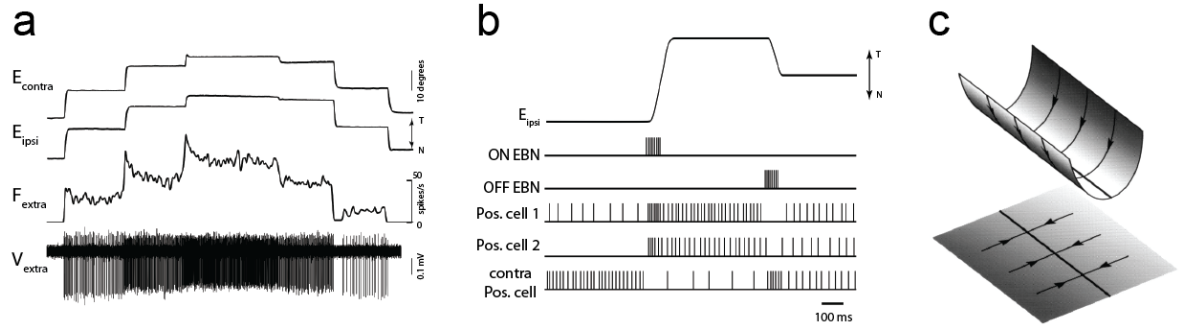

Figure 1-8: Oculomotor neurons encode eye position to hold the eyes still

a: Extracellular voltage recording (V_{extra}) and firing rate (F_{extra}) of a position neuron in goldfish area I (OI in zebrafish) during one back and forth cycle of saccades and fixation. E_{ipsi}: ipsilateral eye, E_{contra}: contralateral eye, T: temporal, N: nasal. **b:** Schematic showing eye position, EBNs discharge and discharge of three position neurons during transition in fixation position. ON burst cell activity briefly precedes saccades and produces burst discharges of ipsilateral position neurons. This transient command is transformed into persistent, elevated discharge of position neurons, supplying motoneurons with tonic drive necessary to maintain a new eye position. OFF burst cell activity initiates saccades in the opposite direction and induces pauses in discharge followed by lowered persistent firing. Changes in firing rate are opposite in sign for contralateral position neurons. Legend and figure adapted with permission from Aksay et al. (2001). **c:** Visual representation of a line attractor. Two of the dimensions of state space are depicted in the plane, with the height of the energy landscape as the third dimension. All trajectories in the state space of the memory network flow toward the line attractor (thick line). The corresponding trajectories on the energy landscape flow down the walls of a through, toward a line of minimum energy at the bottom. Figure and legend adapted from Seung (1996); written permission not required.

hypoglossi (NPH) for horizontal eye movements, while in goldfish the horizontal integrator is thought to be formed by a single structure in the medulla that was termed “area I” (Fukushima et al., 1992; Pastor et al., 1994; Robinson, 1989). The integration for vertical and torsional eye movements happens in the interstitial nucleus of Cajal (INC). While the overall integration process between the MVN/NPH and INC is thought to be similar, differences in their synaptic channel composition and modulation do exist (Fukushima et al., 1992; Saito & Sugimura, 2020, 2021).

How this integration is achieved and how neurons store a working memory of the current eye position is still actively researched. The integration and the memory storage capabilities of the OI are often described by a “line attractor” model. To characterize this model, we have to introduce the idea of a dynamic system in which several states can be encoded that represent a set of variables at a given time. In the OI, the activity of individual neurons for a given eye position are converging to a single point in this state space due to the eye position dependent firing relationship. When looking at the possible eye positions in the oculomotor range, these points will form a line in the state-space. This means that the activity of the OI will always converge to a stable point on this line and the location on this line is dependent on the current eye position of the zebrafish. Further, this activity lasts for a long time and thus can be seen as a form of working memory (Figure 1-8c; Khona & Fiete (2022); Seung (1996)). For each point on this line, the OI network has a significantly increased time constant compared to the short intrinsic, biophysical time constants of its individual neurons and synapses (Goldman, 2009; Seung, 1996). This line attractor dynamic is thought to be generated by a network of neurons that show strong recurrent, positive feedback connections. However, recent studies have found strong heterogeneity in the persistent response of neurons in the teleost and monkey OI that are inconsistent with a classical line attractor model (Aksay et al., 2003; Daie et al., 2015; Joshua et al., 2013; Miri et al., 2011a). In zebrafish, the time constant of OI neurons varies up to 10-fold and is arranged along a rostro-caudal and dorso-ventral gradient within the OI and neurons that are located close to each other show similar activity (Miri et al., 2011a). The authors proposed a recurrent model of the OI that is strongly biased in a feed-forward manner, where the fast-decaying neurons would perform the integration and the slower-decaying neurons would provide the output of the OI. A similar model can also explain the heterogeneity of neuronal responses in primates, while a purely feed-forward

model can theoretically also achieve the function of the OI (Goldman, 2009; Joshua & Lisberger, 2015).

To achieve that the eyes remain stable, the OI needs to be precisely tuned. Excessive feedback will cause an unstable integrator that provides an overly strong drive to the EOMs and therefore drives the eyes to an eccentric position, instead of keeping them stable. If there is not enough input, the integrator becomes leaky and the eyes will slowly drive back towards their neutral resting position. This is the case for the OI in zebrafish (Khona & Fiete, 2022; Miri et al., 2011a). The OI can be trained via artificially altered visual feedback to become more leaky or unstable. This shows that an external error signal is used to evaluate the integrator performance and to tune it accordingly (Debowy & Baker, 2011; Major et al., 2004a, 2004b; Mensh et al., 2004). This feedback is thought to be mediated via the cerebellum, in particular the flocculus (Optican et al. (1986), reviewed in Shadmehr (2017)). However, recent work suggested, theoretically and via experiments, that the integrator can also self-tune and no visual feedback is required for a stable integrator as dark-reared animals exhibit similar integrator performance (Gonçalves, 2012; Nygren et al., 2019).

1.4.5.2. Firing properties of OI neurons

Integrator neurons, together with INNs and MNs, exhibit a threshold-linear firing pattern. They are silent until they reach a neuron specific firing threshold and then their activity increases linearly with ipsilateral eye position (Figure 1-9a). This results in a push-pull mechanism, where neurons on the right side become more active for rightward eye positions and neurons on the left side become more silent respectively. Neurons that have their firing threshold more towards the OFF-side have a flatter increase in their firing rate relative with eye position, while neurons having more centered firing thresholds exhibit steeper slopes. This behavior was termed “recruitment order” (Figure 1-9a’). While OI position neurons almost exclusively have their firing thresholds on the OFF-side, MNs and INNs have more centered thresholds (Aksay et al., 2000, 2007; Fuchs et al., 1988; King et al., 1981; Pastor et al., 1991). The firing rate slopes increase exponentially when plotted against their relative firing thresholds (Figure 1-9a’, inset) and INNs have higher slopes for eye position and eye velocity than MNs. It is not clear if the recruitment order for MNs and INNs is independently established or inherited from their afferent connections (Aksay et al.

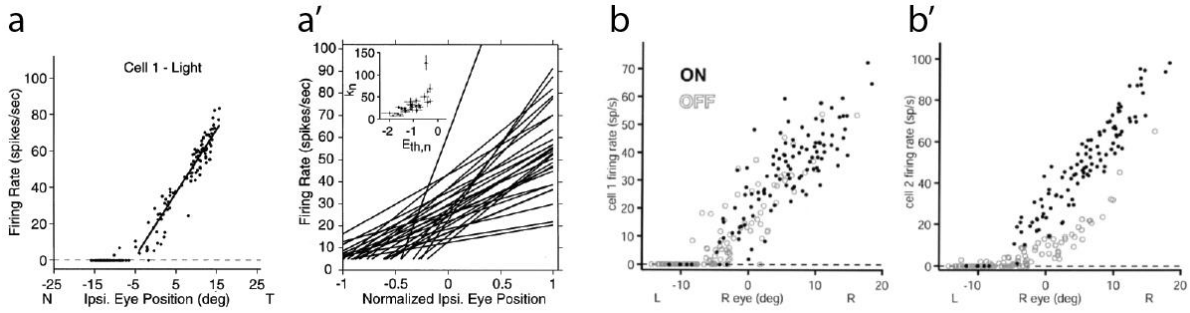

Figure 1-9: Firing properties, recruitment order and hysteresis of OI neurons

a: Threshold-linear firing rate of an eye position encoding neuron in area I in goldfish. **a':** Firing rate vs. eye position plot for 29 area I neurons (oculomotor range normalized). Inset shows the slope (see a; k_n) vs. eye position threshold ($E_{th,n}$) plot for those neurons. Error bars indicate 95 % confidence intervals. Reprinted with permission from Aksay et al. (2000). **b:** Firing rate vs. eye position relationship plot of goldfish area I position neurons for fixation periods after saccades in the ON direction (ipsilateral. black circles) or in the OFF direction (open circles). Some neurons show history dependence in their firing rate (**b'**). Reprinted with permission from Aksay et al. (2003).

2000; Broussard et al., 1995; Pastor & Gonzalez-Forero, 2003). Additionally, some integrator neurons and MNs show history dependence in their firing patterns that is termed "hysteresis". For those neurons, the firing rate of the step-period is higher when the eye position was reached by a saccade in the ON direction than it would be when the same eye position was reached via a saccade in the OFF direction (Figure 1-9b & b'). In goldfish, OI neurons with hysteresis have an average of 3.1 ± 3.7 spikes/s difference, with 8.2 ± 4 spikes/s for MNs (Aksay et al., 2003; Eckmiller, 1974; Goldstein & Robinson, 1986; Pastor et al., 1991). The amount of hysteresis is dependent on the eye position sensitivity of the neuron, with more hysteresis present for neurons with higher sensitivities (Aksay et al., 2000).

1.4.5.3. Anatomy & connectivity of the OI

In mammals, the NPH receives afferent connections from multiple brain areas that are aligned with oculomotor function, such as the vestibular nuclei (predominantly from the MVN), medullary and paramedian pontine reticular formation, INC, oculomotor nuclei, and the cerebellum. Most notably, it receives input from itself. In comparison, it sends efferent projections to the vestibular nuclei, inferior olive, cerebellum, reticular formation, thalamus, oculomotor nuclei, and various other areas (for a full list and review see: Fukushima et al. (1992); McCrea & Baker (1985); McCrea & Horn (2006)).

In gold- and zebrafish, the OI is located caudally to the ABN in the reticular formation in the medulla, dorsal of the IO in rhombomere 7 & 8 (Miri et al., 2011a; Pastor et al., 1994). Pharmacological/optogenetic inactivation or ablation of neurons in this area lead to gaze holding deficits that are in line with disrupted integrator function. Additionally, electrophysiological & calcium recordings show neurons with strong eye position sensitivity in two hemi-nuclei in this area, one in each brain hemisphere (Aksay et al., 2007; Gonçalves et al., 2014; Miri et al., 2011b; Pastor et al., 1994).

Electroporation with immunohistochemistry and electron microscopy (EM) studies have identified several groups of OI neurons within each hemi-integrator in zebrafish. Since zebrafish hindbrain neurons are arranged along rostro-caudal stripes, that share the same transcription factors and neurotransmitters, some predictions can be made based on their anatomical location (Kinkhabwala et al., 2011; Lee et al., 2015; Vishwanathan et al., 2017). OI neurons closest to the midline are glutamatergic and project to the ipsilateral OI and ABN, with some neurons sending projections to the cerebellum and spinal cord. This is in contrast to goldfish where no direct connection between the cerebellum and Area I was identified (Pastor et al., 1994; Straka et al., 2006). The second group of excitatory neurons is located more laterally, intermingled with predominantly GABAergic neurons. They project to the contralateral ABN, like the inhibitory neurons which also project to the contralateral OI. A third stripe along the lateral edge of the brain was just identified in EM recordings and appears to be excitatory, but no axons could be reconstructed and their projections are still unknown. The EM study from Vishwanathan and colleagues also identified chemical synapses between ipsilaterally projecting integrator neurons which can be the source for the recurrent excitation. Gap junctions have not been identified between goldfish integrator neurons, but their existence between zebrafish OI neurons cannot yet be ruled out (Aksay et al., 2000; Vishwanathan et al., 2017).

These projection patterns and inactivation studies are consistent with computational models where each hemi-integrator is functionally independent and maintains activity through recurrent, ipsilateral, excitatory connections. The inhibitory, contralateral projecting neurons are not thought to contribute to the generation of persistence through disinhibition of inhibition, but they would help to coordinate the activity between each hemi-integrator. This model is critically dependent on a threshold mechanism that could either be incorporated at the synaptic level, or it would be dependent on the neuron firing

threshold. In the neuronal recruitment threshold mechanism, a functional difference between high and low threshold neurons exists. The high threshold neurons would drive the integration process, while the low threshold neurons are thought to be used for the read-out of eye position (Aksay et al., 2007; Fisher et al., 2013).

Additionally, one study shows that the eye position is encoded in the amplitude of the persistent activity of OI neurons, but the spatial activity of the OI is dependent on the context of the preceding eye movement. After saccadic or OKR induced fixation periods, neurons in the OI show different persistence times (decay of persistent firing) based on their anatomical location, with caudal neurons having longer persistence times after saccadic eye movements and rostral neurons having longer persistence times after OKR induced saccades. The authors propose a multi-mode model of the OI, according to which the rostral OI neurons receive stronger saccadic input, but caudal neurons show a longer persistence time for saccadic input and vice versa for OKR induced fixations (Daie et al., 2015).

1.4.6 The velocity storage mechanism and the optokinetic afternystagmus

The slow-phase OKR, elicited by a unidirectional stimulus, can be subdivided into two components. The first part consists of a fast eye velocity onset that is mediated through a direct pathway and a second component that consists of a gradual eye velocity build-up until the OKR reaches a steady-state value. This build-up is mediated via an indirect pathway that includes a velocity storage mechanism (VSM). The VSM acts like an integrator which is charged over time and stores a working memory of the eye velocity (Figure 1-7). When the OKR stimulus is switched off and the animal is in the dark, the VSM will drive the eyes in the direction of the preceding stimulus until the eye velocity gradually decreases and the eyes stop moving (Cohen et al., 1977). This behavior is termed optokinetic after-nystagmus (OKAN) and is thought to help with stable OKR performance when the stimulus is briefly interrupted or during saccades. The VSM is also charged by vestibular input, primarily during low frequencies, which helps with perception and balance (Angelaki & Cullen, 2008; Raphan et al., 1979). The presence of the VSM and OKAN in teleost differs between species. While carp and goldfish show high amounts of OKAN with a time constant of >10 sec (Miki et al., 2020), the presence of the VSM in zebrafish is more elusive. One study did not find an OKAN in zebrafish (Beck et al.,

2004), while the previous study did find an OKAN but only with a much shorter time constant of 1.6 seconds. This is in agreement with the results of another study where the VSM time constant in larval zebrafish is estimated, using mathematical models, to be slightly less than 2 seconds. The authors of this study argue that in zebrafish the minimal manifestation of the OKAN behavior is caused by overshadowing activity from the leaky OI. Additionally, a negative OKAN that drives the eyes in the contraversive direction of the preceding stimulus was also shown to be present in larval zebrafish (Chen et al., 2014; Lin et al., 2019; Waespe & Henn, 1978).

In goldfish, a cluster of neurons rostral to area I, termed "area II", has been identified to encode eye/head velocity. Lidocaine inactivation of these neurons almost completely abolished the VSM time constant and thus these neurons were suggested to generate and store eye velocity. This was further supported by a study which shows that the neuronal firing rate of area II neurons closely match the decay time constant of the VSM (Beck et al., 2006; Pastor et al., 1994). Additional anatomical and electrophysiological studies in goldfish showed that brainstem loops between area II and the vestibular nuclei are necessary for the generation of the velocity storage (Hirata, 2021; Straka et al., 2006). In zebrafish, the locations of area II neurons were reported in the rostral parts of rh7/8 based on labelling studies, but not by functional imaging (Ma et al., 2009).

1.5 Aims of this thesis

While the basic components and the tuning properties from neurons of the horizontal oculomotor system and oculomotor integrator are already known, specific knowledge regarding the ocular tuning and precise eye position/velocity coding is still lacking. To understand how conjugate eye movements are controlled and how the persistent activity in the integrator is achieved, it is important to have a deeper understanding of these topics. In this thesis, a total of four different experiments were conducted at two different developmental stages to investigate these issues.

The first experiment was designed to identify neurons involved in horizontal oculomotor control and to investigate the coarse coding of those neurons, regarding their eye position or slow-phase eye velocity sensitivity and their ocular specificity in young larvae (5-7 dpf). Zebrafish show a high degree of conjugate eye movements, but they also exhibit a stereotypical eye convergence during hunting by which they change their binocular

vergence angle about 30 ° (Bianco et al., 2011). Additionally, our lab recently reported that zebrafish are capable of performing monocular saccades under specific conditions (Leyden et al., 2021). This raises the question how the motor commands for each eye are encoded in the underlying circuits. There are basically two different schools of thought how eye movement control is achieved. Ewald Hering postulated his hypothesis of "Equal Innervation" where each eye would receive the same input and monocular eye movements would be the results of a conjugate eye command superimposed with a special vergence command that cancels the movement for one eye and is added to the conjugate command for the other eye. This theory is contrasted by Hermann von Helmholtz's hypothesis, which states that each eye receives an independent, monocular specific input. So far no conclusive answer to this question has been found (Bridgeman & Stark, 1977; Coubard, 2013; Helmholtz, 2005; King, 2011).

In zebrafish, one study used a computational model to investigate post-saccadic eye drifts and concluded that, based on eye movements alone, the OI should be subdivided into four individual clusters that exhibit uniocular control for each eye and direction (Chen et al., 2016). Therefore, in my first experiment I used a specially designed stimulation protocol to decouple the normally yoked eye movements of zebrafish. I recorded the underlying neuronal activity in the hindbrain and provide a classification about the ocular specificity carried by each neuron and thus mapped the horizontal oculomotor system in zebrafish.

The second experiment was aimed to provide a better understanding about the specific eye position and/or slow-phase eye velocity encoding of each neuron and to provide 2D-tuning curves to investigate the firing thresholds of different clusters of neurons in young larvae (5-7 dpf). Since the initial eye movement command for saccades exists of a "pulse"-command to overcome the inertia of the eye plant, oculomotor neurons also receive velocity information via the cerebellum, vestibular nuclei and the VSM (see chapter 1.4.3; Pastor et al. (2022); Robinson (1964)). This will result in some additional eye velocity encoding on top of the already mentioned eye position encoding. Therefore, this experiment was geared towards eliciting different eye position/velocity combinations to better elucidate the differential coding for each neuron and to precisely highlight the anatomical distribution of eye position and eye velocity encoding neurons. With the already mentioned gradient for persistence time in the OI (see chapter 1.4.5.1), these results will potentially shed light onto the shift from eye velocity to eye position coding within the OI and thus visualize the integrator function (Delgado-García et al., 1989;

Joshua et al., 2013; Miri et al., 2011a). Based on 2D-tuning curves, I can calculate the firing thresholds for each neuron which will provide insights into the OI as neurons with different firing thresholds have been hypothesized to serve different purposes within the OI (Fisher et al., 2013).

The third and fourth experiments were the same as the ones described above but conducted at a later developmental stage (14-15 dpf). As already laid out in chapter 1.2.3, the visual development of zebrafish is not finished after the more traditional imaging time window of 5-7 dpf. In older larvae, new behaviors appear that contribute to retinal image stability (aVOR) and the OI shows an increased persistence time with more linear eye drifts in older animals (Beck et al., 2003). These experiments will investigate how the neuronal code is changing in the first two weeks, when newborn neurons are integrated into already existing and functioning circuits and potentially help to fine-tune the behavioral response. Additionally, the distribution of monocular and binocular neurons at a later stage should provide insights into the Hering vs. Helmholtz debate, as according to Helmholtz, the binocular coordination needs to be learned and would thus require visual feedback and time to be precisely calibrated which should be reflected by the underlying circuits. Therefore, the results of these experiments will supplement the findings from experiment 1 & 2 and investigate which tuning properties are already fully developed at 5-7 dpf and which are refined at a later developmental stage.

Chapter 2: Material & Methods

2.1 Animal welfare and transgenic lines

The following transgenic zebrafish lines were used in this study:

Table 1: Fish lines

Name	Source	Publication
Tg(ubb:nls-GCaMP6f)m1300Tg	Driever lab (Fenja Gawlas, Philipp Rustler), University of Freiburg, Germany	Present study and Brysch et al. (2019b)
Tg(elavl3:H2B-GCaMP6f)jf7Tg	Zebrafish International Resource Center (ZIRC), Oregon, USA	Dunn et al. (2016)
Tg(mnx1:TagRFP-T)vu504Tg	Driever lab, University of Freiburg, Germany	Jao et al. (2012)

Larvae used in the experiments were reared in an incubator at 29 °C in a 14/10 day/night cycle and kept in E3 medium with methylene blue (0.01 %). Fish used for the late-stage larvae experiments were screened for strong GCaMP6f expression under an epifluorescence microscope (Nikon SMZ25, Tokyo, Japan) and kept in the main fish facility from 5 dpf onwards. They were raised in system water and fed once per day with paramecia *ad libitum*. Between the late-stage larvae experiment days (14 to 15 dpf), they were fed with powdered artemia (NovoTom JBL, Neuhofen, Germany). The *Tg(ubb:nls-GCaMP6f)m1300Tg* and *Tg(mnx1:TagRFP-T)vu504Tg* fish were kept in a TL/N (nacre; Lister et al. (1999)) background. The *Tg(elavl3:H2B-GCaMP6f)jf7Tg* were delivered from the ZIRC in the casper background (*nacre* -/-, *roy* -/- ; White et al. (2008)), but were only screened for nacre expression. All imaged larvae were *nacre* -/-.

2.2 Animal Preparation for 2P-imaging

2.2.1 Young larvae (5-7 dpf):

Animal preparation was conducted as previously described in Brysch et al. (2019b). Larvae of both sexes (F2 or later) were screened for strong GCaMP6f expression in a *nacre* -/- background. They were immobilized, with the dorsal side up, within 1.6 % low-melting agarose (in E3 without methylene blue) in a 3.5 cm (in diameter) petri dish lid (627161,

Greiner Bio-One International GmbH, Kremsmünster, Austria). The agarose surrounding the eyes was cut off using a custom-made flattened platinum wire tool (see Supplemental Figure 1a; Arrenberg (2016)) to enable the larvae to move their eyes over the entire horizontal oculomotor range. After solidification of the agarose, the lid was filled with E3 devoid of methylene blue.

2.2.2 Late-stage larvae (14-15 dpf):

Late-stage larvae were taken from the main fish facility in the morning of the day of the experiments and the system water was gradually replaced with Ringer's solution to slowly accommodate them to the higher concentration saline solution. Late-stage larvae were embedded in 3 % low-melting agarose (in Ringer's solution) in a 6 cm (in diameter) petri dish lid (628161, Greiner Bio-One International GmbH, Kremsmünster, Austria). During the solidification of the agarose, 2 Luer connectors (IDEX H&S P-801, Techlab GmbH, Braunschweig, Germany) were mounted to the side of the petri dish lid, in line with the fish body, using hot glue. The connector closest to the head (input) was oriented in a way that oxygenated Ringer's solution would enter at the bottom part of the lid. The connector at the tail (output) was leveled with the top of the lid to ensure a water column large enough to cover the whole fish and to ensure the flow of oxygenated Ringer's solution over the gills of the fish (Supplemental Figure 1b). After complete solidification of the agarose, the whole lid was filled with Ringer's solution and the agarose surrounding the eyes and gills was removed (Supplemental Figure 1a). Immediately after that, the Luer connectors were attached to a 4-channel peristaltic pump (REGLO ICC Digital Peristaltic Pump, Ismatec, Barrington, USA) to provide constant flow of freshly oxygenated Ringer's solution to the petri dish (7 ml/min input, 10 ml/min output to prevent flooding). The Ringer's solution was oxygenated in a 500 ml glass flask with medical oxygen at 0.2 l/min (UN1072, provided by GTI medicare GmbH, Hattingen, Germany). From this flask, the oxygenated Ringer's solution was directly pumped into the petri dish containing the fish while deoxygenated solution was re-fed into the flask for oxygenation. With our setup, we were able to support 2 embedded late-stage larvae at the same time (Supplemental Figure 1c). As the rigidity of the tubing sometimes caused a slow drift of the petri dish, a small piece of modelling clay was put in front of the fish at the binocular zone, which was blocked with black aluminum foil during experiments 2 and 4, and behind the fish. This

ensured both, a stable mounting setup and unhindered view of the larvae to the areas of the visual field in which the highest OKR gains are evoked (Dehmelt et al., 2021).

2.3 Microscope and stimulation setup

2.3.1 Microscope:

Calcium imaging recordings were performed under a modified MOM-microscope (Movable Objective Microscope, Sutter Instruments, Novato, USA; Euler et al. (2009)) with C7319 preamplifiers (Hamamatsu Photonics K.K., Hamamatsu, Japan) and a 25x objective (Nikon CFI75, Tokyo, Japan) using the MScan software (Version 2.3.0.1). Hindbrain patches were imaged at 2 frames per second between ~280 x 280 µm and 420 x 420 µm, based on the size of the fish, to ensure that the appropriate hindbrain section was completely recorded. For excitation, a "Coherent Vision-S" Ti-Sa IR laser was used (Coherent Inc., Santa Clara, USA) at a wavelength of 920 nm.

For eye detection, an IR-LED ring (850 nm) was mounted onto the microscope and the light of 2 IR-LEDs was fed into the laser path using a T700lpxxr (Chroma Technology Corp, Vermont, USA) mirror. The reflected IR light from the mirror was strong enough to back illuminate the zebrafish eyes through the objective though the reflection of the mirror was just about 2 % (Figure 3-1a). To record eye movements, the stage holding the petri dish either had a hole in the center to allow the light to pass through (young larvae) or was made out of plexiglass (late-stage larvae) and a CMOS camera (DMK 23UV024, The Imaging Source Europe GmbH, Bremen, Germany) was mounted below the animal and stage. Eye detection and stimulation was accomplished using an adapted version of ZebEyeTrack (Dehmelt et al., 2018) running in the Labview environment (Version 2015, National Instruments, Austin, USA). Due to the increased body length of late-stage larvae, the illumination provided through the objective was often not large enough to completely highlight the eyes in the camera while running calcium imaging in rh 4-8. Therefore, an additional custom-made LED ring (24 IR LEDs, 850 nm) was mounted below the mounting stage at the level of the camera which provided broad range illumination from below. This enabled illumination of the eyes independent from the imaged brain region (Supplemental Figure 2).

2.3.2 Stimulation setup:

A custom-made, square, red LED arena consisting of four individual panels was used to stimulate the larvae with horizontally rotating vertical bars around the body of the fish. Each panel showed 3 bars at the same time (7 LEDs high, 12 LEDs wide, 660 nm). Two panels, linked together, provided stimulation either to the left or right eye. The stimulation setup was based on a previous publication (Kubo et al. (2014); Figure 3-1, Supplemental Figure 2). Stimulation was only provided during flyback of the scan mirrors to avoid stimulation artefacts in the recorded calcium imaging data. Stimuli were still perceived as continuous motion by the zebrafish (Kubo et al., 2014). For monocular stimulation experiments, the binocular zone between the eyes was blocked using either black aluminum foil (BKF12, Thorlabs, Newton, USA) or black tape directly glued to the arena (Conrad Components 541659, Conrad Electronic SE, Hirschau, Germany) to allow independent, eye-specific stimulation (Bianco et al., 2011).

2.4 Stimulation protocols

2.4.1 Binocular coordination (ocularity) tuning

The goal of this experiment was to evoke disconjugate, slow-phase eye movements and classify the neurons in the hindbrain based on their ocularity as well as a coarse specification of their eye position or eye velocity tuning. This was achieved with a 3-step stimulation protocol. In the first two steps, monocular eye movements were elicited for each eye respectively and conjugate eye movements during the last step (Figure 3-3a).

To provoke monocular eye movements and to circumvent the yoking of the eyes, a moving stimulus was shown to the stimulated eye (ON eye) while a stationary stimulus was shown to the non-stimulated eye (OFF eye). This technique almost completely abolishes the movement of the OFF eye (Beck et al., 2004). After a short adaption period of the fish (~5 min for young larvae, 30 min to 1 h for late-stage larvae), this stimulation approach decoupled slow-phase eye movements reliably. Each stimulation phase was 150 sec long (300 frames, young fish) and varied for late-stage larvae from 150 sec to 300 sec (300 to 600 frames, based on the occurrence of saccades). Stimulus direction changed between 7-10 sec with a pause of 1-4 sec between the direction changes. As both directions were mapped equally, no further actions were taken to account for hysteresis. Stimulation speed

was chosen for each larva individually to minimize the yoking of the eyes and the occurrence of saccades while simultaneously maximizing the explored motor range.
The stimulation speed during experiment 1 (young larvae) for the ON phases was 32.1 ± 11.4 °/sec and for experiment 3 (late-stage larvae) 32.0 ± 7.7 °/sec (mean ± STD). In experiment 1, the left eye was stimulated first in 233 recordings, while the right eye was stimulated first in 15 recordings. In experiment 3, the left eye was stimulated first for 76 out of 90 recordings. For data analysis and visualization purposes, in recordings where the right eye was stimulated first, the first and second stimulation phase were switched.

2.4.2 Eye Position/Velocity tuning

The goal of this experiment was to investigate the coding properties for each neuron regarding their exact eye position and/or eye velocity sensitivity. The first part of this stimulation protocol consisted of an alternating OKR stimulus which changed direction every 8 sec and ran for 6-12 repetitions (depending on the fish's performance) to ensure that the fish was exploring and to coarsely map a wide motor range. To decouple eye position from slow-phase eye velocity tuning, a closed-loop stimulation protocol in which eye position was monitored in real-time and desired eye movements were provoked by changing stimulus direction and speed respectively, was followed. In detail: Each eye position bin was defined as a fixed 2 ° wide space in the motor range and was mapped for different eye velocities. For experiment 2, 93 recordings were mapped between ± 10 ° and 3 recordings between ± 8 °. Due to the increased number of saccades in late-stage larvae, the oculomotor range was occasionally reduced to prevent z-drifts, which otherwise would happen in longer recordings. Therefore, the motor range in experiment 4 ranged from -8.9 ± 1.2 ° (mean ± STD, left hemisphere) to 8.7 ± 1.2 ° (right hemisphere). While z-drifts can be prevented in adult fish by fixating the fish with dental cement and tissue glue to a holding mechanism (Huang et al., 2020), the ossification in 14/15 dpf animals is just starting and does not yet support this fixation method (Cubbage & Mabee, 1996; Parichy et al., 2009). After the OKR stimulus, the eyes were steered towards the desired eye position bin via an OKR stimulus with the baseline stimulation speed, which was set for each fish individually. Once this bin was reached, the stimulus speed was set to zero to keep the eyes stable within that bin for 3-4 sec (Figure 3-10a - a''). Sometimes the eyes were drifting out of their respective bin, either because of overshoot caused by the inertia of the eye and/or the effect of the VSM, or because they drifted to a more nasal eye position due to the

passive pullback of the eye muscles and the leaky OI in zebrafish (Chen et al., 2016; Leigh & Zee, 2006; Miri et al., 2011a). If that happened, the whole "stable" part was restarted until the fish kept their eyes in the desired range for the entire time window. After successful completion of the "stable part", the eyes were steered in clockwise (CW) and counterclockwise (CCW) direction through the respective eye position bin at baseline, 1.2 times baseline and 1.4 times baseline speed to elicit different eye velocities. If a saccade occurred at any time during the stimulation protocol, the appropriate step was restarted. As each direction was mapped equally, no additional analysis steps were made to account for potential hysteresis effects.

The average stimulation speed for experiment 2 (young larvae) was 22.5 ± 6.4 °/sec and 24.3 ± 7.3 °/sec for experiment 4 (late-stage larvae, mean ± STD). Due to the decreased fish's performance in the latter experiment (see chapter 4.3), several changes to the original protocol were implemented. The "stable time" was reduced for some experiments (2-4 sec, rarely manually to 1 sec if the fish was stuck at a certain eye position bin and already had several seconds of that bin mapped) due to the more frequent occurrence of saccades in older animals (Beck et al., 2004). The motor range was sometimes lower as the late-stage larvae had more problems in exploring a similar motor range than the young ones.

2.5 2P-imaging analysis

2.5.1 Identification of ROIs

The raw calcium data timeseries recordings were converted into 8-bit and registered to their median or standard deviation in time using the ImageJ plugin "TurboReg" (Biomedical Imaging Group, Swiss Federal Institute of Technology Lausanne; Thevenaz et al. (1998)) to account for potential movement artefacts in x and y. If any drift in z was observed, the recording was excluded from further analysis.

The identification of regions of interest (ROIs) was based on a previously published method (Brysch et al., 2019b; Miri et al., 2011b). In short: For each recording, the raw fluorescence was correlated in 2x2 pixel bins to a modified behavioral trace (either from eye position or high/low speed eye velocity), termed regressor. The regressor was convolved with a calcium impulse-response function (CIRF) to account for the decay time of fluorescence caused by the kinetics of the calcium sensor GCaMP6f (Chen et al., 2013). For the *Tg(ubb:nls-GCaMP6f)m1300Tg* line the CIRF was measured at 1.1 sec, for the

Tg(elavl3:H2B-GCaMP6f)jf7Tg line at 1.6 sec (*in vivo*, based on the fluorescence decay of eye position encoding neurons after a saccade in the OFF direction). In the resulting heatmap, individual ROIs were semi-automatically selected (Figure 3-2a). The algorithm for the regression-based correlation analysis was based on a modified version of "MOM-Load" (Kubo et al., 2014).

As the original algorithm used only one regressor to generate the heat-map for cell selection (and therefore would only highlight neurons with one tuning specificity, e.g. only eye position encoding neurons), the resulting ROIs would have been suboptimal to detect neurons with different coding features. Therefore, this code was adapted in a way that each pixel that was surpassing the threshold z-score for any selected regressor was highlighted with its absolute, maximal z-score value in the final heat-map (Figure 3-2b).

The following 5 regressors were used in all experiments to highlight eye movement related neurons in each recording while still providing a high SNR ratio:

- Rectified, angular eye position
- Rectified, angular slow-phase eye velocity (capped at 20 °/s, for CW and CCW)
- Rectified, angular quick-phase eye velocity (above 20 °/s, for CW and CCW)

All regressors were averaged for both eyes. This method was used to initially select ROIs in the dataset and was sufficient to select neurons which were almost always active during the whole recording, or only during specific parts (Figure 3-2c, ROIs 9 and 19). Furthermore, it was sensitive enough to highlight pixels which only rarely showed any activity, even if this activity was probably not related to any eye movements (Figure 3-2c, ROI 47). Therefore, neurons were ultimately defined on more restrictive inclusion criteria, reported later, based on the respective experiments conducted.

As the GCaMP protein was either fused to "nls" (Kalderon et al., 1984) or "H2B" (Freeman et al., 2014; Kanda et al., 1998) to restrict expression to the nucleus, all of the recorded calcium signals correspond to somatic signals. Due to the strong interdependence between nuclear calcium concentration and the firing of a neuron, with only milliseconds delay, nuclear calcium can be used as a proxy for neuronal activity (Bengtson et al. (2010), reviewed in Bading (2013)). This helps to avoid ROIs encompassing multiple neurons and, together with the already low number of those in other studies using the same approach (Kubo et al., 2014; Wang et al., 2019), results in a reliable selection of single neurons only.

2.5.2 Registration of recordings to a reference frame

To account for drifting of the preparation and to combine multiple recordings of different brains to the same reference frame, each recording was manually aligned in x, y, and z to a z-stack of the respective larvae. This z-stack was recorded at 1x magnification at increased laser power/gain in 0.82 µm increments encompassing the whole area recorded during the normal experiments. To prevent bleaching due to the increased laser power, the z-stack was only recorded after all other experiments were finished. To correct for potential pitch, yaw and roll differences, made during the embedding of different larvae, the position of both Mauthner cells, the medial longitudinal fasciculus (MLF), and of the midline were extracted to be used as landmarks for each z-stack. Pitch and yaw were corrected based on the MLF position and the midline of the brain, with the intersect between the midline and Mauthner cells defined as the origin. Roll was corrected based on the difference between the Mauthner cell locations in z. This approach was based on a previous publication (Kubo et al., 2014) and the adapted method has previously been published (Brysch et al., 2019b).

For experiments 3 and 4 (late-stage larvae) the data was further modified to account for the differences between inter-individual hindbrain sizes. Here, the standard length (SL; Parichy et al. (2009)) for each fish was measured under the epifluorescence microscope after the recordings were finished. For experiment 3 the mean SL was 5130 ± 543 µm (STD, 12 larvae), for experiment 4 5209 ± 773 µm (11 larvae), which is well in the published range for 2 week old zebrafish (Parichy et al., 2009). Each ROI location was then normalized to the average brain size of all late-stage larvae (5167 ± 648 µm in RC, 275 ± 28 for LR). As the true DV extent of the brain could not be measured without potentially touching the agarose dorsal of the embedded fish with the objective, no further normalization in DV was made besides the registration to the z-stack (above).

2.6 Binocular coordination data analysis

2.6.1 General data analysis

This analysis approach was used for experiments 1 and 3. For experiment 1, data from 28 larvae was used (5-7 dpf) and for experiment 3 from 12 larvae (14-15 dpf). To ensure that stimulation phases which were tailored to elicit monocular eye movements were sufficient for the task, a Yoking Index (YI) was calculated. Recordings which did not pass this criterion were excluded from further analysis (YI < 0.5 for any monocular stimulation

phase, see chapter 2.6.2). For experiment 1, the hindbrain area extending from 90 µm (dorsal) to -60 µm (ventral) was imaged to ensure an 8-fold coverage in 5 µm intervals around the Mauthner cells (defined as 0 in z). For experiment 3, each z-level was imaged at least 3 times (in 10 µm intervals) between ± 100 µm around the Mauthner cells.
The x/y extent of the imaged patch was set in a way that a small area rostral to the Mauthner cells was still imaged (for landmark identification), partly containing the ARTR, and to ensure that rhombomeres 5-8 were imaged completely (aligned for z=0 and then kept stable for different z levels). This ensured that the areas reported to contain the OI, area II and moto-/internuclear neurons were imaged (Lee et al., 2015; Miri et al., 2011a; Portugues et al., 2014; Wolf et al., 2017).

After ROI selection, each trace was smoothed by a sliding window filter (over 5 frames):

$$DFF_k = \frac{DFF_{k-2}*0.25+DFF_{k-1}*0.5+DFF_k+DFF_{k+1}*0.5+DFF_{k+2}*0.25}{2.5} \qquad \text{(Eq. 1)}$$

With DFF_k being the $\Delta F/F$ at the time k.

To ensure that an individual eye position of zero was defined as the resting state of the eye (neutral view to the front), each eye trace was offset by its relative median eye position. This was necessary as the eyes at rest are rotated to the front (e.g. the right eye shows a slightly negative eye position when the fish is looking forward (Zimmermann et al., 2018)).

Neurons were grouped according to their response profiles by a similar regression-based analysis approach as reported by Kubo and colleagues (Kubo et al., 2014). The regressors used in this step of the analysis pipeline were designed in such a way that every stimulation phase (left eye: LE, right eye: RE, both eyes: BE) was either handled as “active” or “inactive”, which results in 8 general activity states (three phases with two activity states). The behavioral trace used for these regressors were either taken from the recorded eye position or eye velocity (as the derivative of eye position). If the regressor contained an “inactive” activity state, the appropriate section was filled with zeros. The “active” parts of the regressor were calculated in two different ways: In the 1st (non-averaged), the activity for the monocular phases were always taken from the stimulated (ON) eye. For the 2nd (averaged), the mean activity over both eyes (ON & OFF) was used. This was done because the explored motor range, and thus activity during the binocular phase, was often higher than for the monocular phases (own observations and Beck et al. (2004)). This

regressor captured the activity of “binocular always” neurons more reliably (see chapter 3.2). Given the threshold-linear firing properties of the recorded neurons (see chapter 1.4.5.2), the regressors were rectified in positive (right eye position/rightward eye velocity) and negative (left eye position/leftward eye velocity) direction to prevent that behavioral activity in the OFF state of the neuron would result in a smaller correlation value and thus prevent identification. In the end, this approach generated 52 different regressors (see Figure 3-4c & Supplemental Figure 3).

The regressors were convolved with the appropriate CIRF in a similar way as described in chapter 2.5.1. To prevent noise from saccades, regressors encoding eye velocity were capped at 8 °/sec. The DFF trace for each ROI was then correlated (Pearson correlation) with all 52 regressors and the ROI was only kept for further analysis if any of the regressors had a correlation value of at least 0.6. In total, 16413 ROIs were analyzed for experiment 1, with 4483 exhibiting a big enough correlation coefficient to be kept for further analysis and 1297 neurons for experiment 3, with a total of 4855 ROIs analyzed.

The explored motor range was usually larger during the binocular stimulation phase than during any of the monocular phases as zebrafish normally exhibit conjugate eye movements, with the exception of monocular saccades and eye convergence during hunting (Bianco et al., 2011; Leyden et al., 2021). In combination with eccentric firing thresholds, this could result in a misclassification of specific response types (binocular preferred or monocular exclusive; see chapter 3.2) due to potential under-sampling of the explored motor range during monocular phases. To prevent this from happening, the firing threshold (using the start of the fluorescence raise as a proxy) for each eye during the binocular stimulation was calculated. This was achieved by calculating the tuning curve from the deconvolved and smoothed DFF (using the same CIRF as for convolution of the regressors, Eq 1) and binning it in 2 ° increments for eye position and 1 °/sec increments for eye velocity for each eye separately. Starting from the OFF direction of the tuning curve, the first three bins were used as the starting baseline and a one-sided, iterative Wilcoxon rank-sum test was conducted against the neighboring bin in the ON direction. This bin was then pooled into the baseline and tested against the next bin in the ON direction. A Bonferroni correction was used to shield against multiple comparison errors. The firing threshold was defined as the first significant different bin where at least one of the following two bins in the ON direction was also significantly different. If the neuron did not reach this firing threshold for any of the relevant OFF stimulation phases it was

discarded from the analysis, e.g: if a neuron was classified as encoding for the right eye monocularly, it was assessed if its motor range during the left eye monocular stimulation was big enough to potentially have resulted in activity. This resulted in the elimination of 1181 neurons for experiment 1 (26.3 %, 3302 neurons approved, Figure 3-5) and 466 neurons for experiment 3 (35.9 %, 831 neurons approved). Please note that at this step the exclusion of the neurons was purely based on the behavior of the fish and, to some extent, on the intrinsic coding properties, as neurons with a more eccentric firing threshold would require a wider motor range on both eyes to be classified correctly. This means that the reported number of neurons is quite conservative and the total number of neurons involved in horizontal eye movement control is probably larger than what was identified in this study.

2.6.2 Yoking index (YI)

The yoking index was calculated using the following equation:

$$Yoking\ Index = \frac{\sum abs(Eye\ velocity_{ON}) - \sum abs(Eye\ velocity_{OFF})}{\sum abs(Eye\ velocity_{ON}) + \sum abs(Eye\ velocity_{OFF})} \qquad \text{(Eq. 2)}$$

For each stimulation phase, the absolute, smoothed eye velocity (Eq 1, capped at 8 °/sec) of the stimulated eye (ON) was summed up against the one of the non-stimulated eye. For the binocular coding phase, the left eye was defined as the ON eye. The resulting YI ranges from 1 (only stimulated eye moves) to -1 (only non-stimulated eye moves), with 0 meaning both eyes move the same amount (Figure 3-3b). Only recordings with a YI of 0.5 and higher during the monocular stimulation phases were used, except for four recordings during experiment 3 (see chapter 4.2).

2.6.3 Monocular coding difference

For each of the main position encoding groups (BA, BP, MLE, MRE), the biggest correlation for any of the monocular eye position encoding regressors (MLE: 7, 8, 19, 20; MRE: 3, 4, 21, 22) was taken and their correlation difference was standardized using the following equation:

$$Monocular\ coding\ difference = \frac{Corr_{\max\,(MRE)} - Corr_{\max\,(MLE)}}{Corr_{\max\,(MRE)} + Corr_{\max\,(MLE)}} \qquad \text{(Eq. 3)}$$

If the highest correlation for any of the monocular sets was negative, the respective value was set to zero. The index runs from -1 (exclusively coding for the left eye) to 1 (exclusively coding for the right eye).

2.6.4 $PV_{Influence}$

For all BA and BP position coding neurons, the highest scoring regressor was standardized against its respective velocity coding regressor with the same kinematic parameters (e.g. for regressor 1, it was regressor 9) using the following equation:

$$PV_{Influence} = \frac{Corr_P - Corr_V}{Corr_P + Corr_V} \qquad \text{(Eq. 4)}$$

If the appropriate velocity regressor was negative, it was set to zero. This index runs from 0 (equal position and velocity encoding) to 1 (exclusively position encoding).

2.6.5 Adjustment for unequally sampled z-levels in older animals

Due to the unequally sampled z-levels in late-stage larvae in experiment 3, the data had to be adjusted. To maintain the quality of the data, each z-level in 10 µm increments between ± 100 µm around the Mauthner cells was recorded at least three times (up to six) and then upscaled to eight brains in 5 µm increments to ensure comparability to the data from young larvae. To reach the minimum recording number, four recordings with a YI of smaller than 0.5 had to be included into the final data set. Great care was taken to only include recordings which missed the YI threshold of 0.5 by a marginal degree (0.49, 0.49, 0.44, 0.49; Figure 4-2e). In total, 90 recordings for late-stage larvae were analyzed of which 84 were in the range of ± 100 µm around the Mauthner cells. For plotting the cell maps with adjusted neuron numbers, each identified neuron was grouped into voxels of 10x10x10 µm and upscaled to 8 brains with 5 µm intervals in z to ensure comparability to the young larvae dataset (Supplemental Table 2).

2.7 Eye Position/Velocity data analysis

2.7.1 General data analysis

In experiment 2, a total of 16 larvae were recorded (5-7 dpf) from 90 (dorsal) to -60 µm (ventral) around the Mauthner cells (defined as z = 0). The same hindbrain area (in x and y) as for experiment 1 was imaged in 96 recordings which resulted in an equally sampled,

6-fold coverage of the hindbrain in 10 µm intervals. For experiment 4, 11 larvae (14-15 dpf) were recorded from 70 to -70 µm in 10 µm increments 5 times, which resulted in 75 recordings. After ROI selection and registration, a correlation analysis approach was applied, similar to the one described in chapter 2.6. Here, only neurons which were correlated to a rectified and convolved eye position or slow eye velocity (capped at 8 °/sec) regressor with at least 0.4 were analyzed. In contrast to experiment 1 and 3, a lower correlation coefficient was chosen here as the goal of this analysis step was only to ensure that neurons which showed some eye position and/or eye velocity coding were chosen for further analysis. The 2-dimensional tuning curves contain all data points from the whole recording (including OKR stimulation), only excluding frames that contain saccades (> 10 °/sec eye velocity) and the following three frames (1.5 sec).

2.7.2 PV_{Index}

To classify the eye position and/or eye velocity sensitivity of each neuron, a Position-Velocity Index (PV_{Index}) was calculated according to the following equation:

$$PV_{Index} = \frac{Corr(Eye\ position) - Corr(Eye\ velocity)}{Corr(Eye\ position) + Corr(Eye\ velocity)} \qquad \text{(Eq. 5)}$$

The highest scoring eye position and eye velocity regressor from the previous section was used for calculation. If a neuron had a negative correlation for both regressors of the same quality, it was discarded from this analysis step given that - due to the rectification - at least one should be positive. This was the case for 41 neurons in experiment 2 and for 25 neurons in experiment 4.

2.7.3 Firing threshold analysis

To extract the firing thresholds, the previously described iterative-baseline approach (see chapter 2.6.1) was used. To verify the firing threshold assessment and to provide confidence intervals, a bootstrap analysis was performed. Here, each data point from the baseline pool was randomly selected (with repetitions allowed, meaning the baseline could include one datapoint multiple times) and for each neuron this test was repeated 1000 times. The resulting firing thresholds were sorted and the 25^{th} and 975^{th} rank was used as the upper and lower confidence interval.

2.8 Quantification and statistical analysis

All statistical tests were conducted using Matlab 2015a. Significance level was set as $p < 0.05$. All statistical tests are reported in the appropriate sections. For multiple comparison analysis, if not stated otherwise, a Kruskal-Wallis test was performed (*kruskalwallis*) with a subsequent multiple comparison test (*multcompare*).

2.9 Chemicals and solutions

Table 2: Chemicals

NaCl	AppliChem, A3597
KCl	Carl Roth, 6781.1
$CaCl_2$	AppliChem, A1873
$MgSO_4$	Merck, 1.05886.050000
HEPES	AppliChem, A3724
Methylene blue	AppliChem, A4084
Low-melting agarose (Sieve GeneticPure)	Biozym, 850080

E3: NaCl (5 mM), KCl (0.17 mM), $CaCl_2$ (0.33 mM), $MgSO_4$ (0.33 mM) with 0.01 % methylene blue

Ringer's solution: NaCl (116 mM), KCl (2.9mM), $CaCl_2$ (1.8 mM), 5mM HEPES, pH 7.2

The above mentioned methods (except for chapter 2.6.5) and some of the data (for experiment 1 and 3) have previously been published by me (Brysch et al., 2019a, 2019b).

Chapter 3: Results for Young Larvae

3.1 Young larvae

In the first part of my thesis, I describe and present data of 2 experiments conducted using young zebrafish larvae (5-7 dpf). This is the timespan in which most calcium imaging and behavioral studies in zebrafish research are conducted (Ahrens et al., 2013; Bianco et al., 2011; Migault et al., 2018; Wang et al., 2020). At this developmental stage, the OKR can already reliably be evoked and the small brain size and transparency (in the nacre background) of the larvae, together with the still rudimental ossification, result in a good image quality (Easter & Nicola, 1996; Parichy et al., 2009). While some hallmarks of visual processing are still developing at this age (e.g.: OI linearity, OKR gain, aVOR), most of the underlying circuits are already functional and can be studied (Figure 1-3). Some of the data presented in chapter 3 has previously been published by me (Brysch et al., 2019a, 2019b).

3.1.1 Setup

The present and following chapter provide only a brief overview of the stimulation and recording setup together with a brief introduction how the data was analyzed. They are applicable for all conducted experiments. The full details are provided in chapter 2.

Young larvae (5-7 dpf), transgenic for the calcium indicator GCaMP6f, were embedded in 1.6 % low melting agarose with the eyes cut free and placed under a 2-P microscope inside a custom-made LED arena (Figure 3-1a). Brain activity was recorded in the hindbrain (rhombomeres 4-8) for different z-levels (Figure 3-1b), according to previous reports of the ABN, OI and VSM in this area (Ma et al., 2009; Miri et al., 2011a; Portugues et al., 2014; Vishwanathan et al., 2017; Wolf et al., 2017). Eye movements were elicited by horizontally rotating vertical bars around the zebrafish using a custom-made LED arena. This setup enabled me to provide monocular, binocular, and stationary stimuli for each eye individually (Figure 3-1c). During experiments with monocular stimulation, the binocular zone in front of the fish was blocked.

Due to the small size of the larvae's head, it was sufficient to provide back-illumination of the eyes only through the microscope's objective. This was enough to highlight the head with the eyes and to record eye movements on a separate PC (Figure 3-1d).

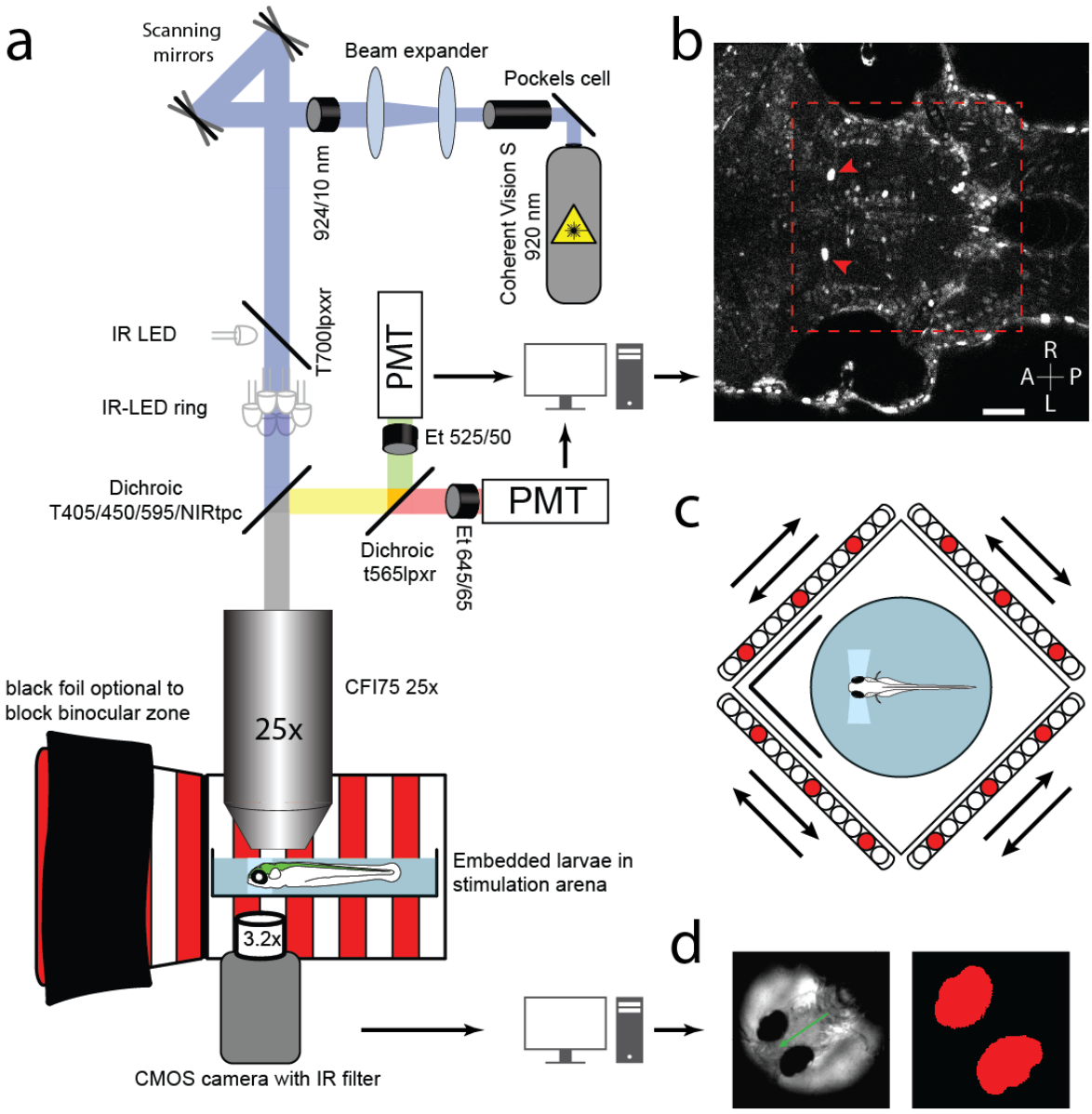

Figure 3-1: Experimental setup

Setup and stimulation arena schematic. **a:** Schematic of the microscope setup: GCaMP6f positive zebrafish larvae were embedded in agarose and placed under a 25x objective and imaged at 920 nm. IR-LEDs were used to illuminate the head to ensure tracking of horizontal eye movements. Not drawn to scale. **b:** Imaged hindbrain patch for one recording (red dashed line) at the level of the Mauthner cells (red arrows). Scale bar 50 µm. A: anterior, L: left, P: posterior, R: right. **c:** Schematic of stimulation arena: The petri dish lids with the embedded fish were placed inside a custom-made LED arena with the option to block the binocular zone at the front. **d:** Example picture showing the image recorded by the CMOS camera (below setup, green arrow indicates the fish's body axis) and the pixels identified as the eyes (right, magnified). Figure adapted under CC BY 4.0 after Brysch et al. (2019b).

3.1.2 Neuron selection

Regions of interest (ROIs) were selected using pixel-wise correlation of the calcium activity to behaviorally derived traces, called regressors (Kubo et al., 2014; Miri et al., 2011b). For initial neuron identification, regressors for eye position and quick/slow eye velocity were used. The correlation analysis was performed for each regressor separately and ROIs were chosen semi-automatically from one general heat-map which combined any active pixels from all regressors (Figure 3-2a & b). This approach was sensitive enough to highlight neurons which were only active under specific stimulation conditions (ROI 9 and 19 in Figure 3-2c) or seldom active (ROI 47), hardly with any activity related to eye movements. Therefore, more conservative inclusion criteria were applied in the downstream analysis to only analyze ROIs which show a clear eye movement related activity.

Using this method, I was able to reliably identify all neurons showing any degree of coding for eye position and/or fast/low eye velocity. Identified ROIs were aligned and registered to a reference coordinate system based on several anatomical landmarks in the larval brain, which negated any mounting differences in pitch, yaw, and roll between individual larvae. Therefore, the recordings of several larvae were combined into one picture.

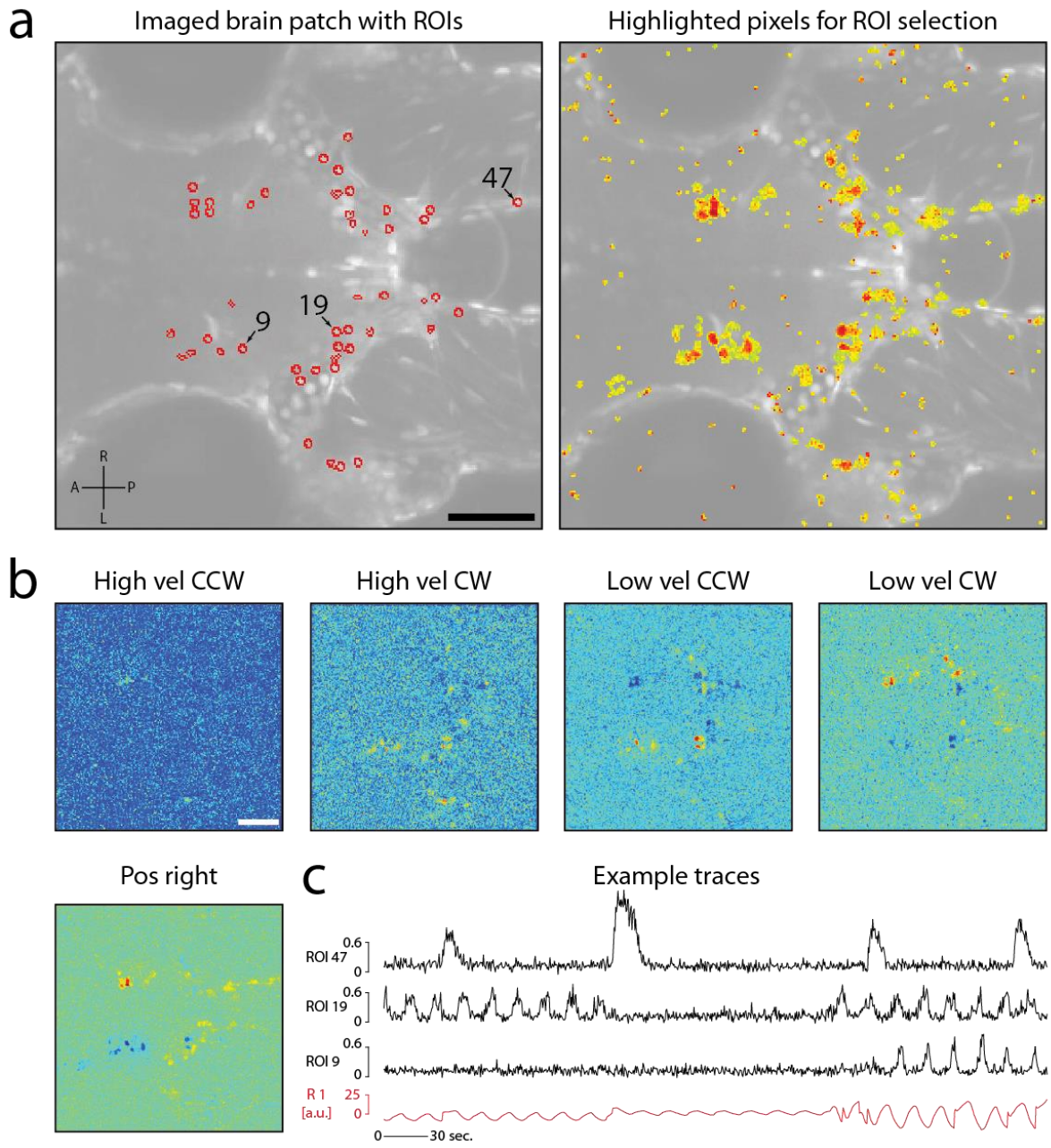

Figure 3-2: Example recording for ROI selection

Example showing the ROI selection and the generation of the heatmap from the five regressors used in the data analysis. **a:** Mean image of one timeseries recording with semi-automatically selected ROIs in red (left). Mean image with the heatmap generated from five different regressors superimposed used for ROI selection (right). Scale bar 50 µm. A: anterior, L: left, P: posterior, R: right. **b:** Original unscaled z-scores for each regressor used to generate heatmap in a (right, details on generation of these maps see Methods section and Kubo et al. (2014) & Miri et al. (2011b)). CCW: counterclockwise, CW: clockwise, Pos: eye position, right: positive colormap used for right eye positions, vel: velocity. **c:** Example traces (DFF, selection shown in a) for one ROI only active during one stimulation period (9), during 2 stimulation periods (19) and only seldom active (47). R1 (red) shows the Regressor used to generate the heatmap "Pos right" in b. Please note that in this recording the right eye was stimulated first.

3.2 Experiment 1 (eye coordination in young larvae)

3.2.1 Experimental framework:

The goal of this experiment was to investigate the coding properties and ocular specificity of horizontal eye movement related neurons in the hindbrain (see chapter 1.5). To decouple the conjugated eye movements, which zebrafish normally show to an alternating OKR stimulus, I applied a specific stimulation pattern which is capable of evoking monocular eye movements. The stimulation protocol was divided into three equally long parts. In the first part, only one eye (ON) was shown a moving bar stimulus which was rotating either in CW or CCW direction around the fish. To keep the other eye stable, a stationary stimulus was shown to the other eye (OFF), which is sufficient to decouple eye movements and to reduce the gain of the OFF eye below 0.1 (Beck et al., 2004). In the second part the ON and OFF eyes were switched and in the last step both eyes were shown the moving stimulus. This stimulation approach resulted in a very clear response pattern with monocular eye movements during the first two stimulation segments and binocular, conjugated eye movements during the last phase (Figure 3-3a). However, it should be noted that the fish were still capable of performing binocular eye movements during the monocular stimulation phases (e.g. saccades, see Figure 3-4b') and even the OFF eye can still show some residual stimulation related activity, though it was drastically reduced. This was not related to a suboptimal blocking of the binocular zone but due to intrinsic properties in zebrafish (Beck et al., 2004; Fritsches & Marshall, 2002; Qian et al., 2005). Therefore, I introduced a method to exclude recordings where the OFF eye showed too much movement, termed Yoking Index (Figure 3-3b, chapter 2.6.2).

The resulting decoupled monocular and conjugate binocular eye movements enabled me to group the recorded neurons based on their innervated eye(s), or at least to their correlation to the resulting eye movements, and their primary coding feature. To do this, a similar correlation approach was applied as in the ROI selection. Here, the regressors were derived from the recorded eye movement traces but adapted to the underlying stimulus protocol. Different regressors were generated based on combinations of the potential activity during each stimulation phase, eye position or slow-phase eye velocity coding, tuning direction, and two sets of regressors to address the reduced motor range during binocular stimulations. This resulted in a total set of 52 regressors (see chapter 2.4.1 & 2.6.1, Figure 3-4c and Supplemental Figure 3). These were comprised of two monocular groups for each

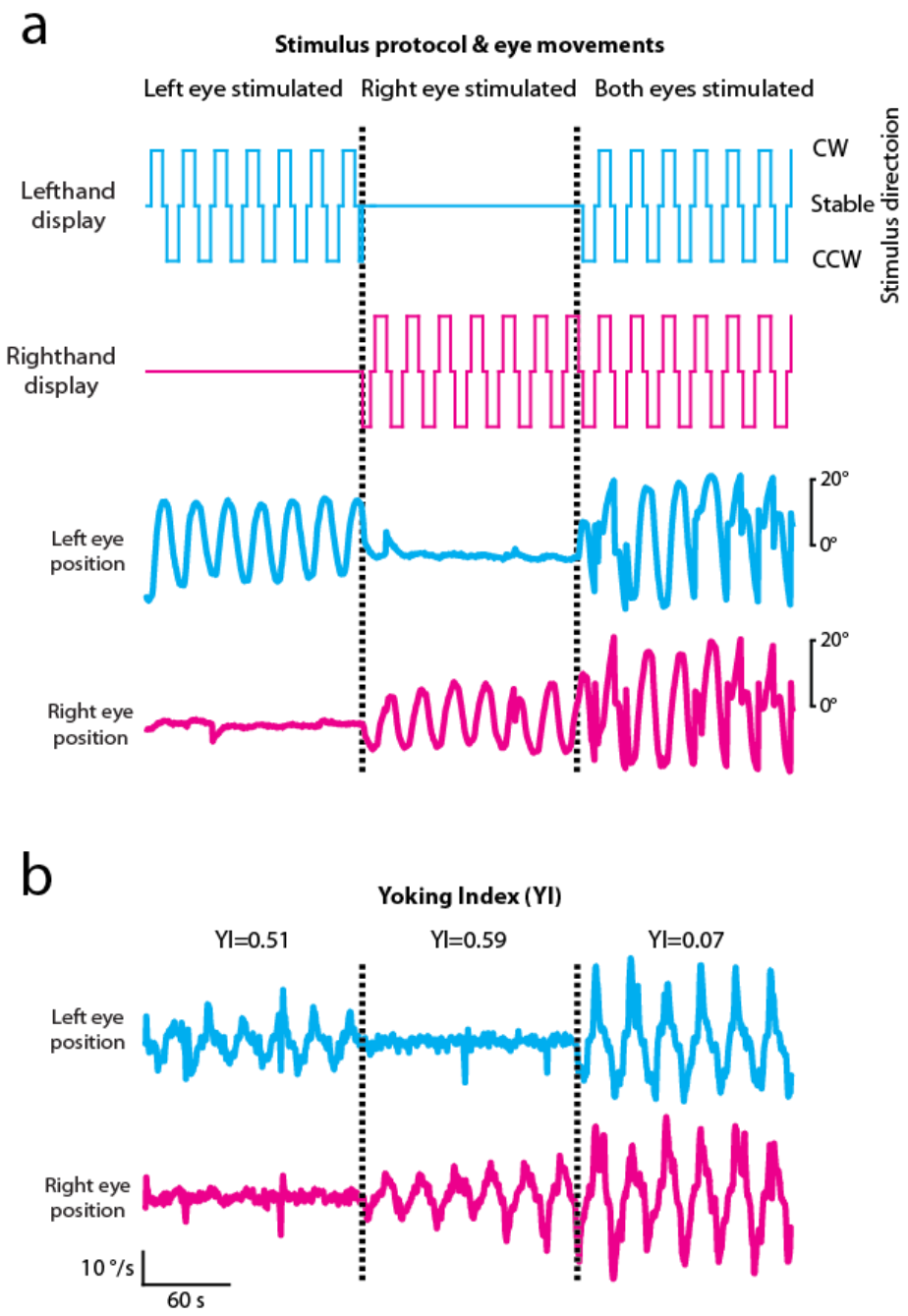

Figure 3-3: Stimulation protocol and example eye traces

Example picture showing the stimulus protocol and resulting eye movements with an example for the Yoking Index. **a:** Stimulus protocol schematic (top) showing the alternating OKR stimulation pattern. Bottom: Example eye traces resulting from the shown stimulation pattern. Dashed lines indicate transition between stimulus segments. **b:** Example eye traces from another recording showing one recording close to the YI threshold (0.5) for the left eye stimulation. This recording was still included into the final dataset. Figure modified under CC BY 4.0 from Brysch et al. (2019b).

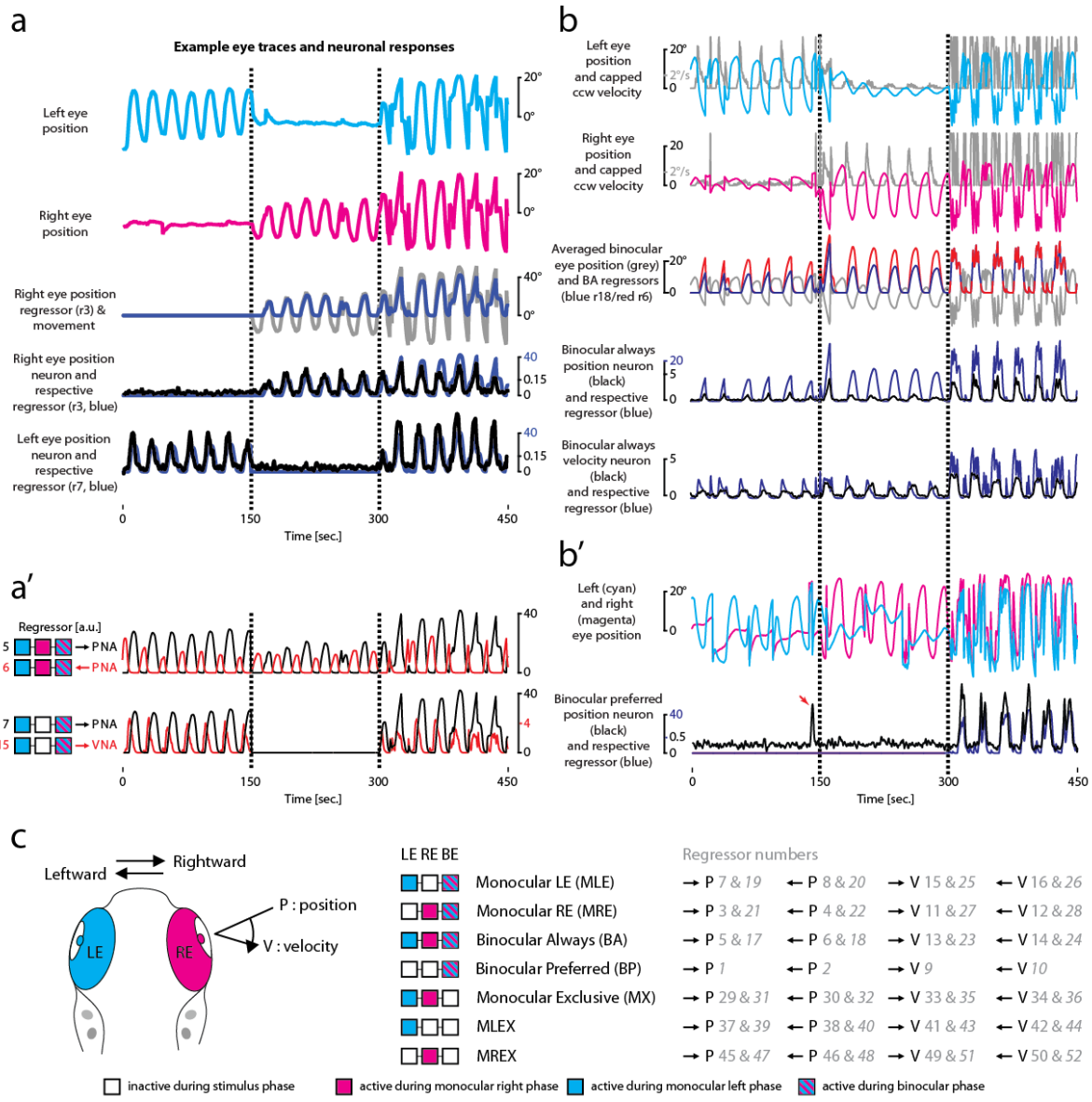

Figure 3-4: Regressor creation and example neuron traces

Analysis pipeline to classify neuronal response types. **a:** Eye traces (same as in Figure 3-3a) and two monocular example neurons from that recording (black, DFF). Blue traces show the respective highest scoring regressors (monocular right eye position encoding r3, monocular left eye position encoding r7) and, for r3, how it is derived from the right eye position. Dashed lines indicate transition between stimulus segments. **a':** Additional example regressors to highlight the rectification and the phase shift between the eye position and eye velocity regressors. Squares correspond to stimulation segment, filled squares indicate activity. Arrows show tuning direction. NA: non-averaged, P: position, V: velocity **b:** Example eye position and capped counterclockwise eye velocity traces (top 2 plots) and two "binocular always" (BA) regressors to show the difference between averaged and non-averaged regressors (red/blue) and the eye trace they were derived from (grey, middle plot). Example DFF traces for one BA position neuron (DFF, black) and its respective regressor (r18, blue) and one BA velocity neuron (r24, lower two traces). **b':** Example "binocular preferred" (BP) DFF trace and respective eye movements from that recording. Note the binocular event (red arrow). The blue trace shows the respective highest scoring regressor (r1). **c:** Overview showing all kinematic parameters (left) and all regressors used to group neurons into different response groups (right).

Italic numbers refer to averaged regressors, squares as in a'. BE: both eyes, LE: left eye, RE: right eye, MLEX: monocular left eye exclusive, MREX: monocular right eye exclusive. Figure modified under CC BY 4.0 from Brysch et al. (2019b).

eye (monocular right eye: MRE, monocular left eye: MLE) and two binocular groups (binocular always: BA, binocular preferred: BP). Additionally, there were regressors for exclusive monocular eye movements (MLEX: monocular left eye exclusive, MREX: monocular right eye exclusive, MX: monocular exclusive). The DFF for each neuron was correlated against all regressors and the neuron was grouped into one class according to its highest scoring regressor. Based on the different firing thresholds and differences in the explored motor ranges between the stimulation phases, potential misclassified neurons were excluded from the final dataset (Figure 3-5). In total, 4483 neurons from 28 young larvae (5-7 dpf) were identified using the regressor analysis and after application of the firing threshold assessment 3302 neurons remained (1181 excluded) and were analyzed further in detail.

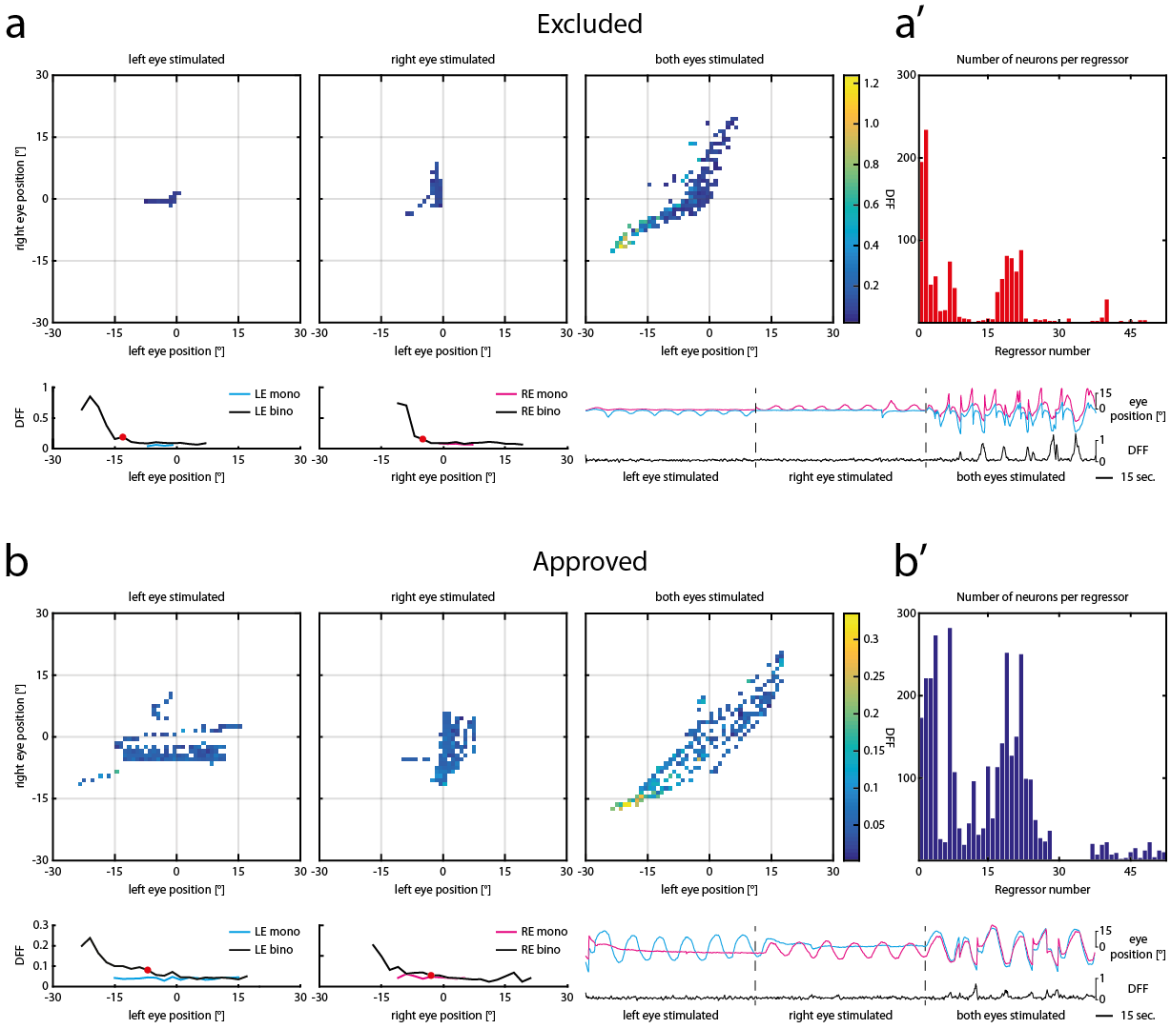

Figure 3-5: Exclusion of neurons with too little eye movement

This figure shows the process of eliminating neurons who might have been misclassified based on too little eye movements during individual stimulation phases. **a:** Example for one excluded BP neuron. Individual plots show the explored motor range (top) and the resulting monocular tuning curves (cyan/magenta, bottom) for the monocular left eye (left), monocular right eye (middle) and binocular stimulation phase (right). The black tuning curve shows the activity from the binocular stimulation phase with the respective firing threshold (red dot). If a neuron did not reach the firing threshold, it was excluded from the analysis. Monocular eye position traces and DFF are shown in the lower right corner. **a':** Bar plot showing the number of excluded neurons for each regressor. **b:** Example eye positions and tuning curves for one approved BP neuron. Note that the monocular tuning curves (cyan/magenta) exceed the binocular firing threshold (red dot). **b':** Bar plot showing the number of approved neurons for each regressor. Figure modified under CC BY 4.0 from Brysch et al. (2019b).

3.2.2 Oculomotor hindbrain neurons show distinct coding properties

Horizontal eye movement related neurons in the larval zebrafish hindbrain primarily fall into four groups, which account for 95 % of all neurons identified (BA, BP, MLE, MRE: 3125 of 3302 neurons; Figure 3-6a). These are the two monocular groups for the left and right eye and both binocular groups. Therefore, almost all identified neurons were active during the binocular stimulation phase and only differed in their activity during the monocular stimulation phases. Neurons exclusively active for movement of one eye only (MLEX, MREX) are quite infrequent and can possibly be attributed to noise rather than distinct coding preference. Neurons which were exclusively silent during the binocular phase and active irrespectively of the monocular phases (MX) are completely absent in the hindbrain.

Within the four major response groups, position encoding neurons are more frequent than slow-phase velocity encoding neurons (2359 P vs. 766 V; for 8 composite brains, 150 µm imaged brain volume in z, 5 µm increments). This is also reflected by the fact that the most frequent eye velocity group (MLE/MRE adduction) is less frequent than the least frequent eye position encoding group (BA; 303 vs. 295). Within the eye position encoding group, monocular neurons are the most frequent type with neurons carrying medial rectus information (adduction: 1057), followed by the respective monocular neurons coding for the lateral rectus (abduction: 605). For the binocular encoding neurons, BP neurons are more frequent than BA neurons (394 vs. 303). Monocular adducting neurons are also the most frequent eye velocity encoding neurons, but in contrast to eye position neurons, they are followed by eye velocity BA neurons before their respective antagonists (adduction: 295, BA: 267, abduction: 146). BP velocity neurons are surprisingly infrequent with only 58 neurons identified and are also outnumbered by monocular exclusive position neurons (adduction: 66). Other monocular exclusive groups are virtually non-existent.

While this analysis approach provides an easy first classification of the different coding properties of horizontal eye movement related neurons, it is ignorant to the fact that different response groups might exist alongside a continuum and neurons encode both eye position and eye velocity (Leigh & Zee, 2006), or are graded regarding their eye preference (King & Zhou, 2000). To highlight the differences in eye preference coding, I calculated the monocular coding difference for each eye position encoding neuron (see chapter 2.6.3, Figure 3-6b). It shows that binocular neurons group around 0 (Index running from -1 (left

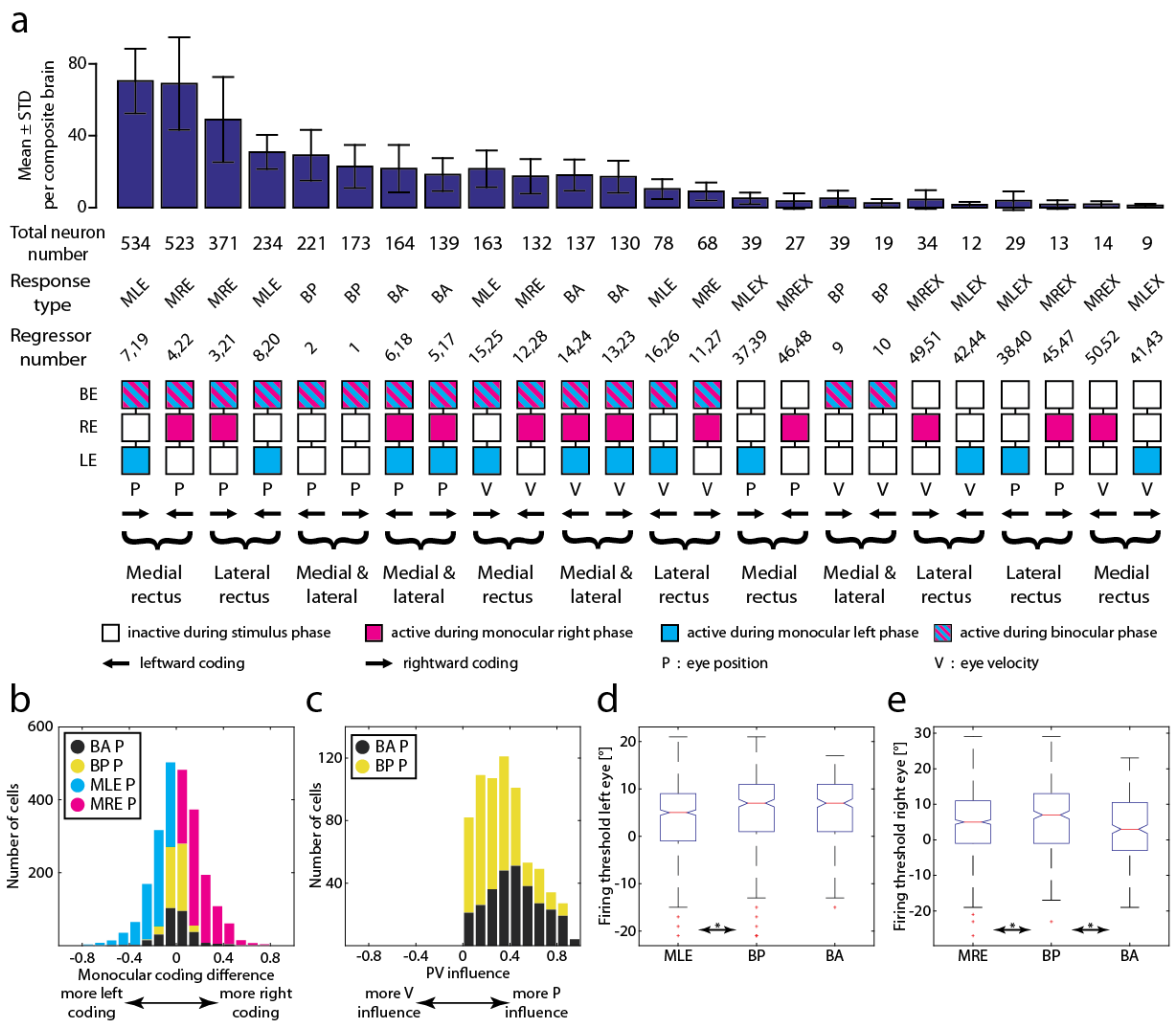

Figure 3-6: Response groups and their coding properties in young larvae

Figure showing the distribution of neurons for each response group and coding properties regarding their exclusivity and firing threshold. **a:** Number of identified neurons grouped pairwise according to their mono-/binocular coding and eye muscle(s). The bar plot shows the mean and STD for eight artificial, composite brains. **b:** Difference in monocular coding for position coding neurons for all four main response groups. Index runs from -1 (exclusively coding for the left eye) to 1 (exclusively coding for the right eye). **c:** Index showing the difference in position or velocity coding for BA P and BP P neurons. The index runs from zero (equal correlation of position and velocity coding) to 1 (exclusive position coding). **d:** Firing thresholds of position encoding neurons for the left eye derived from the firing threshold analysis pooled in ON (positive) direction (n: MLE=768, BP=394, BA=303). **e:** same as in d, but for the right eye (n: MRE=894). Figure modified under CC BY 4.0 from Brysch et al. (2019b).

eye) to 1 (right eye)), indicating a similar coding for the left and right eye. Monocular neurons are located more towards their respective sides. This indicates that these neurons indeed form gradients regarding their eye preference, but this effect could also be influenced by binocular events (saccades) and residual yoking of the eyes during the monocular stimulation phases (see chapter 5.2 for discussion). As mentioned above, the

explored motor range during the binocular stimulation was often greater than that during the monocular stimulation phases. This means that the exhibited eye velocity during the binocular phase is also higher than that during the monocular ones. This can lead to a potential misclassification of neurons, which have a certain degree of eye velocity encoding, as binocular neurons because they respond better during the binocular phase than during the first two monocular phases. Therefore, true BA neurons might end up in the BP group. To address this issue, I calculated the eye position/velocity influence ($PV_{Influence}$, Figure 3-6c, chapter 2.6.4) for BA and BP eye position encoding neurons. This index runs from 0 (equal eye position and velocity encoding) to 1 (exclusive eye position encoding). It should be noted that, due to the close cross-correlation of eye position and eye velocity (see Figure 3-4a', lower trace), values close to 1 should not be expected. This index shows that BA and BP neurons have a similar $PV_{Influence}$, but BP position neurons have indeed a slightly higher velocity contribution by 0.16 (Wilcoxon rank-sum test: $p < 0.05$).

Regarding the eye position firing thresholds for the left eye (Figure 3-6d, pooled in ON (positive) direction, extracted from the firing threshold analysis, see Figure 3-5), MLE neurons have significantly more centered firing thresholds than BP neurons (Kruskal-Wallis test: $p < 0.05$). However, there is no statistically significant difference between the firing thresholds of BP and BA neurons for the left eye. For the right eye, BP neurons have more eccentric firing thresholds than MRE and BA neurons (Kruskal-Wallis test: MRE-BP & BP-BA: $p < 0.05$; Figure 3-6e). It should be noted that in this analysis different anatomical functional groups have been combined, even though it is known that OI and ABN neurons have differently centered firing thresholds (see chapter 1.4.5.2). This analysis has been conducted to show the broad spread of firing thresholds for eye position and to highlight that the BP neuron classification might be slightly influenced by later firing thresholds, even though the absolute difference is rather small (BP-BA left eye: 0.83 °, right eye: 2.53 °; but see chapter 3.3.4 for a more detailed analysis of the firing thresholds). The difference regarding the firing thresholds and the slightly stronger eye velocity sensitivity in BP neurons might have a beneficial impact on the classification of BP neurons as I also observed some residual activity for some BP neurons during the monocular stimulation phases. However, that activity was not strong enough to classify those neurons as BA or monocular. Taken together, these findings suggest that BA and BP neurons might not be two distinct groups, but these neurons exist alongside a continuum

with the extreme cases being BA and BP on each side. This is also the reason I label BP neurons as “binocular preferred” rather than “binocular exclusive” as this might be a too extreme label for these neurons.

3.2.3 Spatial arrangement of monocular neurons

Regarding the spatial location of all identified oculomotor neurons, a strict hemispheric separation caudal to the Mauthner cells becomes visible. Neurons identified with either rightward eye velocity or right eye position regressors are primarily located in the right hemisphere (1426 of 1460 neurons, 98 %) as it is the case for the left hemisphere for left(ward) regressors (1358 of 1397 neurons, 97 %). Rostral to the Mauthner cells this clear separation is less pronounced (ipsiversive: 237 neurons, contraversive: 208 neurons).

Monocular neurons, which are only active during their respective monocular and for the binocular stimulation phases, are located throughout the whole hindbrain with some clear clusters visible (Figure 3-7). Notably, these hotspots are mirror symmetric for MLE and MRE neurons. MLE and MRE eye position encoding neurons range from 90 µm dorsal to -80 µm ventral, thus spanning the whole recorded dorsal-ventral extent. Along the AP axis, they range from 100 µm rostral to ~ -220 µm caudal. For the medial-lateral expanse, a clear dependency on their dorsal-ventral location is visible (Figure 3-7, left panels). While dorsally located neurons lie directly lateral from the midline to ~40 µm (with only some exceptions at the very top), the more ventrally the cells are, the more lateral they get (from ~75 µm up to 100 µm for some neurons). However, the most lateral cell cluster is located just about 20 µm below the MLF within rhombomeres 7-8.

The largest clusters of monocular eye position neurons are within the ABN. Here, two distinct columns are visible with one in each hemisphere (Figure 3-7a middle panel dashed line & grey areas in right panel). When looking at the transversal projections of these cells, a clear separation based on the underlying eye identity becomes visible. Monocular neurons encoding the ipsiversive eye position for the ipsilateral eye are located ventrally in this cluster ranging from about -40 to -80 µm with only some single cells located more dorsally. This area overlaps with the expression pattern of the *Tg(mnx1:TagRFP-T)vu504Tg* line (Jao et al., 2012), which labels motoneurons. The corresponding expression of three 5 dpf old vu504Tg larvae is highlighted in Figure 3-7a & b (mean vertices + STD, ignoring sparsely labeled cells in the dorsal region; Brysch

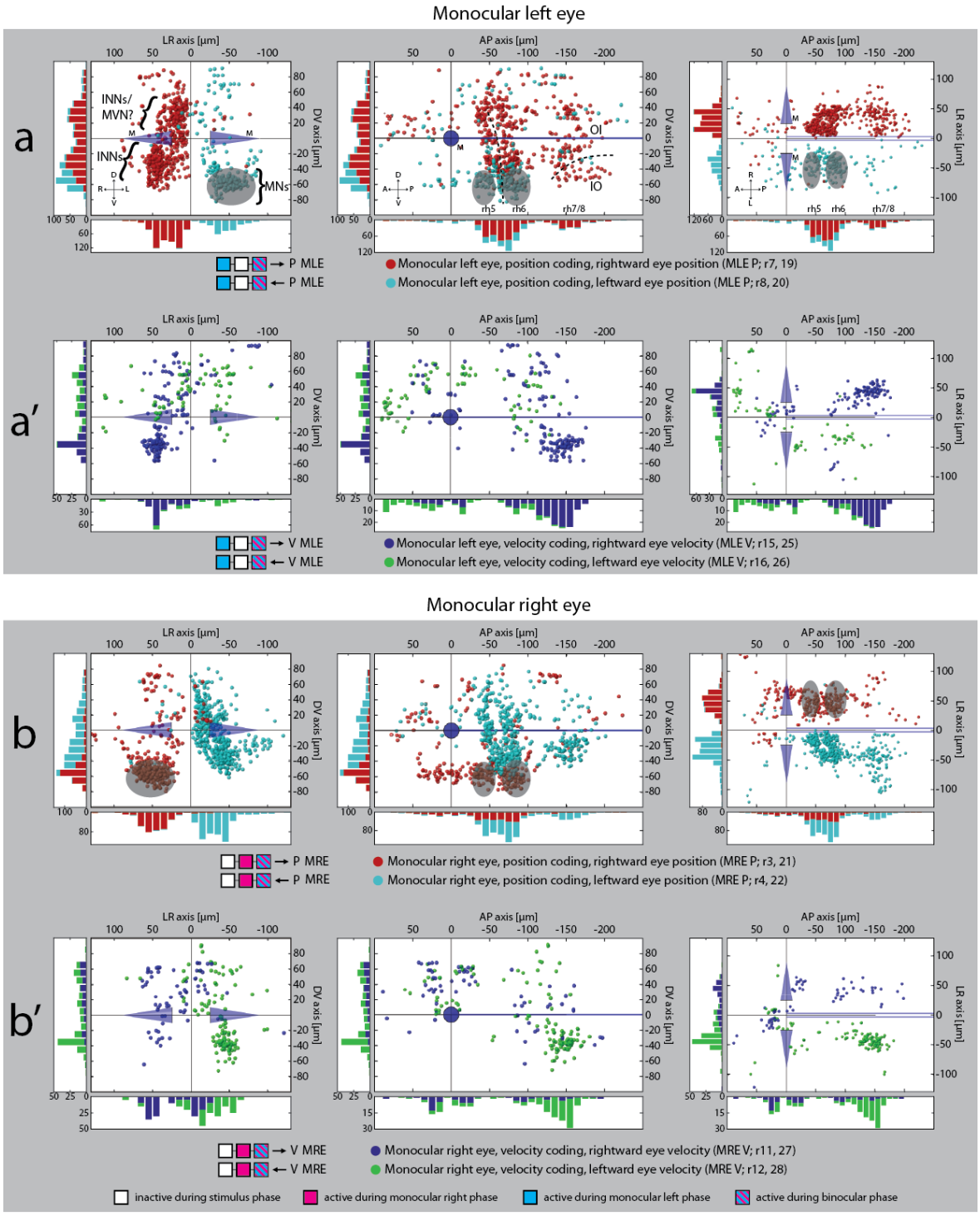

Figure 3-7: Monocular cell maps for young larvae

Spatial locations of identified monocular neurons. **a-b':** Transversal, sagittal and dorsal views for MLE position (a), MLE velocity (a'), MRE position (b), and MRE velocity (b') encoding neurons in the larval zebrafish hindbrain. Each dot represents one neuron identified in one recording with its highest correlation to the regressor in the respective legend. A: anterior, D: dorsal, INN: internuclear neuron, IO: inferior olive, L: left, M: Mauthner cells, MN: motoneuron, MVN: medial vestibular nucleus, OI: oculomotor integrator, P: posterior/position, R: right/regressor, rh: rhombomere, V: ventral/velocity. Shaded area in (a) and (b) show overlap with the *Tg(mnx1:TagRFP-T)vu504Tg* transgenic line highlighting motoneuron location. Dashed

lines show rough separation of anatomical clusters based on identified neuron locations. Figure modified under CC BY 4.0 from Brysch et al. (2019b).

et al. (2019b)). The coding pattern and spatial locations of these neurons coincide with the expected coding of motoneurons innervating the lateral rectus that are responsible for abducting eye movements. The INNs relaying the information for driving the antagonistic adducting eye movements should therefore encode for the same eye but for contraversive eye positions and should also be located within the ABN. These cells can be found in the contralateral ABN, in agreement with the above-mentioned hemispheric lateralization, and span a wide dorsal-ventral range from -60 to 90 µm. They spatially overlap to a little extent with contraversive MNs around -50 µm ventrally, but other than that are distinctly separated. Within the cluster of INNs, two smaller clusters can be distinguished with a small gap at around -20 µm at a ~30 ° angle (see Supplemental Figure 4a). Based on the eye command, monocular neurons in rh5 & 6 would separate to 39 % into MNs (n=411) and 61 % into INNs (n=654).

Outside of the ABN, some MN-like neurons extend from the group of identified MNs in rh5 & 6 rostrally into rh4 (best seen for MRE neurons, Figure 3-7b). However, this cluster is not labeled in the vu504Tg line and is not within the ABN where the MNs are located. Therefore, these neurons carry the same information as motoneurons, but probably do not innervate the lateral rectus. Their function might lie in providing a corollary discharge to upstream brain areas.

Another large group of monocular eye position encoding neurons can be found in rh7/8. Most of those neurons encode the contralateral eye position. These neurons span from -60 µm ventrally to ~60 µm dorsally. Some of these ventral neurons are located lateral and close to the ventral boarder of the brain. They are likely part of the IO, which is mostly monocular encoding. The neurons more medial and dorsal around the MLF, up to ~40 µm, and the ones more rostral and lateral in rh7/8 are likely part of the OI (Figure 3-7a, middle panel; Daie et al. (2015); Vishwanathan et al. (2017)). I only find very few monocular neurons in rh 7/8 coding for the ipsilateral eye. One cluster is around -150 µm caudal to the Mauthner cells and around 30 to 100 µm lateral to the MLF. The other group is around -150 µm to -230 µm caudal and only extends 40 µm from the MLF. Notably, the more medial group is also located more dorsally around and above the MLF. The latter cluster appears to be arranged in a rostro-caudal dependent fashion. Contralateral MLE and MRE

encoding neurons appear to be more rostral than ipsilateral neurons, with a switch around -180 µm, though only very few neurons were identified < -200 µm (Figure 3-7a & b, right panel).

MLE and MRE slow-phase velocity encoding neurons are less frequent and encompass different locations than their eye position encoding counterparts (Figure 3-7a' & b'). They are located primarily -120 to -180 µm caudal to the Mauthner cells and 25 to 60 µm lateral to the MLF in rh7/8. They range from -25 to -60 µm ventral to the MLF, which puts them a little more rostro-ventral to the above-mentioned lateral eye position encoding cluster with some overlap between them. Similarly, most of these cells encode the contralateral eye. Some sparsely scattered ipsi- & contralateral encoding monocular velocity neurons can be found rostral from this cluster, stretching up to the dorsal imaging border and up to the position encoding neurons in rh6, filling the area between the position encoding ABN and rh7/8 neurons. Rostral and above the Mauthner cells some velocity neurons, intermingled with eye position encoding neurons, are visible close to the midline. Their location corresponds to the ARTR (see chapter 1.4.4), which is supported by the fact that their coding preference regarding their velocity direction is flipped compared to the rest of the neurons. This is expected, as they are encoding anticipatory eye/tail movements (Ahrens et al., 2013; Dunn et al., 2016; Wolf et al., 2022).

Monocular exclusive neurons (MLEX, MREX, Figure 3-8) are only found very infrequently (177 of 3302 neurons) and do not appear to cluster in any specific locations. Additionally, their hemispheric separation regarding their coding direction is less pronounced compared to the other mono- and binocular groups (MLEX/MREX: 67 ipsiversive, 46 contraversive; MLE/MRE/BA/BP: 2717 ipsiversive, 27 contraversive; caudal to the Mauthner cells). This further supports the notion that these groups are probably not a functional entity in the zebrafish hindbrain. Neurons only active during any of the monocular stimulation phases were completely absent.

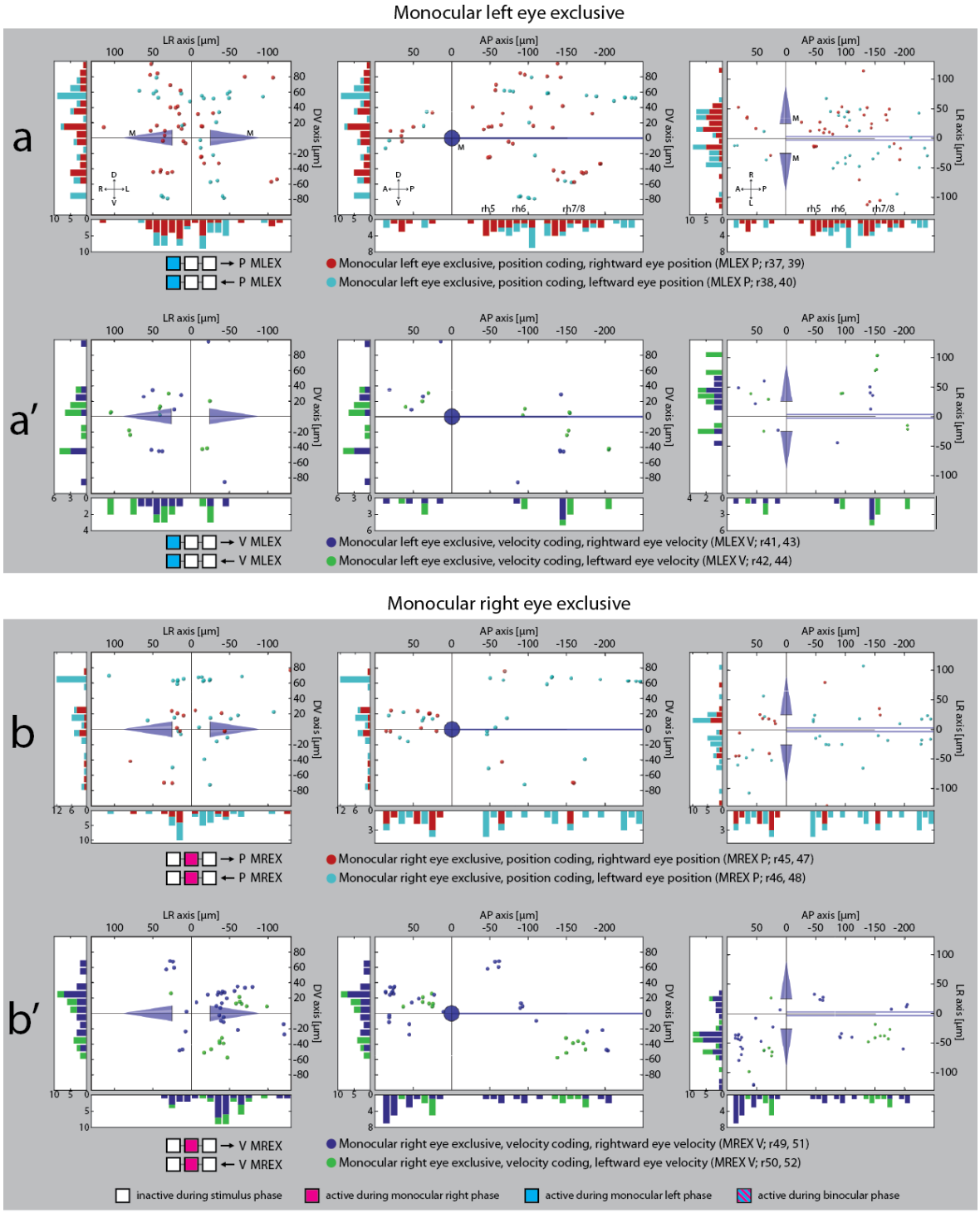

Figure 3-8: Monocular exclusive cell maps for young larvae

Spatial locations of identified monocular exclusive neurons. **a-b':** Transversal, sagittal and dorsal views for MLEX eye position (a), MLEX velocity (a'), MREX position (b) and MREX velocity (b') encoding neurons in the larval zebrafish hindbrain. Each dot represents one neuron identified in one recording with its highest correlation to the regressor in the respective legend. A: anterior, D: dorsal, L: left, M: Mauthner cells, P: posterior/position, R: right/regressor, rh: rhombomere, V: ventral/velocity. Figure modified under CC BY 4.0 from Brysch et al. (2019b).

3.2.4 Spatial arrangement of binocular neurons

For binocular neurons, the hemispheric lateralization is comparable to the monocular neurons mentioned above. BP neurons span the whole imaged patch in the rostro-caudal and dorso-ventral dimensions (Figure 3-9a). Notably, there is a huge difference in the number of identified BP eye position and BP slow-velocity neurons, with the latter being almost completely absent from the hindbrain (BP position: 394, BP velocity: 58). The few identified BP velocity neurons are found roughly in the same locations as their monocular counterparts, caudal to rh6 and around the ARTR.

BP position neurons are scattered throughout the hindbrain. Their biggest aggregation is in the ventral part of the ABN at the location of the MNs. A small protrusion ventrally into rh4 is also visible, even though it is less pronounced than the one from the monocular neurons. Other clusters are located above the Mauthner cells and around the ARTR. BP position neurons follow roughly the spatial arrangement of monocular position neurons, but only very few neurons were identified < -180 µm caudal to the Mauthner cells and in the dorsal part of the ABN.

BA neurons, active regardless of the stimulation phase, are found throughout the whole hindbrain and do not appear to form distinct clusters. Generally, they follow the distribution of the respective other eye position and eye velocity encoding neurons (Figure 3-9a'). In contrast to BP position neurons, they are also present in areas more caudally than 180 µm from the Mauthner cells and even appear to aggregate there, though the number is too low to draw a conclusion. However, the eye identity switch from ipsi- to contralateral monocular position neurons is around the same area as the faint separation of BA and BP position neurons.

BA velocity neurons are predominantly found in the area between rh6 and the position encoding clusters in rh7/8 through the whole dorso-ventral extent of the imaged brain area. Here, they form a narrow band, medially from the ABN to more lateral positions in the anterior regions of rh7/8, where they connect to the clusters of monocular velocity coding neurons (Figure 3-9a', right panel). With that, a slight gradient for slow-phase eye velocity encoding neurons is visible. Binocular velocity neurons caudal to the ABN are mostly found in the more dorsal regions, while monocular velocity encoding neurons are located more ventral and caudal (Supplemental Figure 4b & b'). The remaining BA velocity neurons are located around the Mauthner cells and in the ARTR.

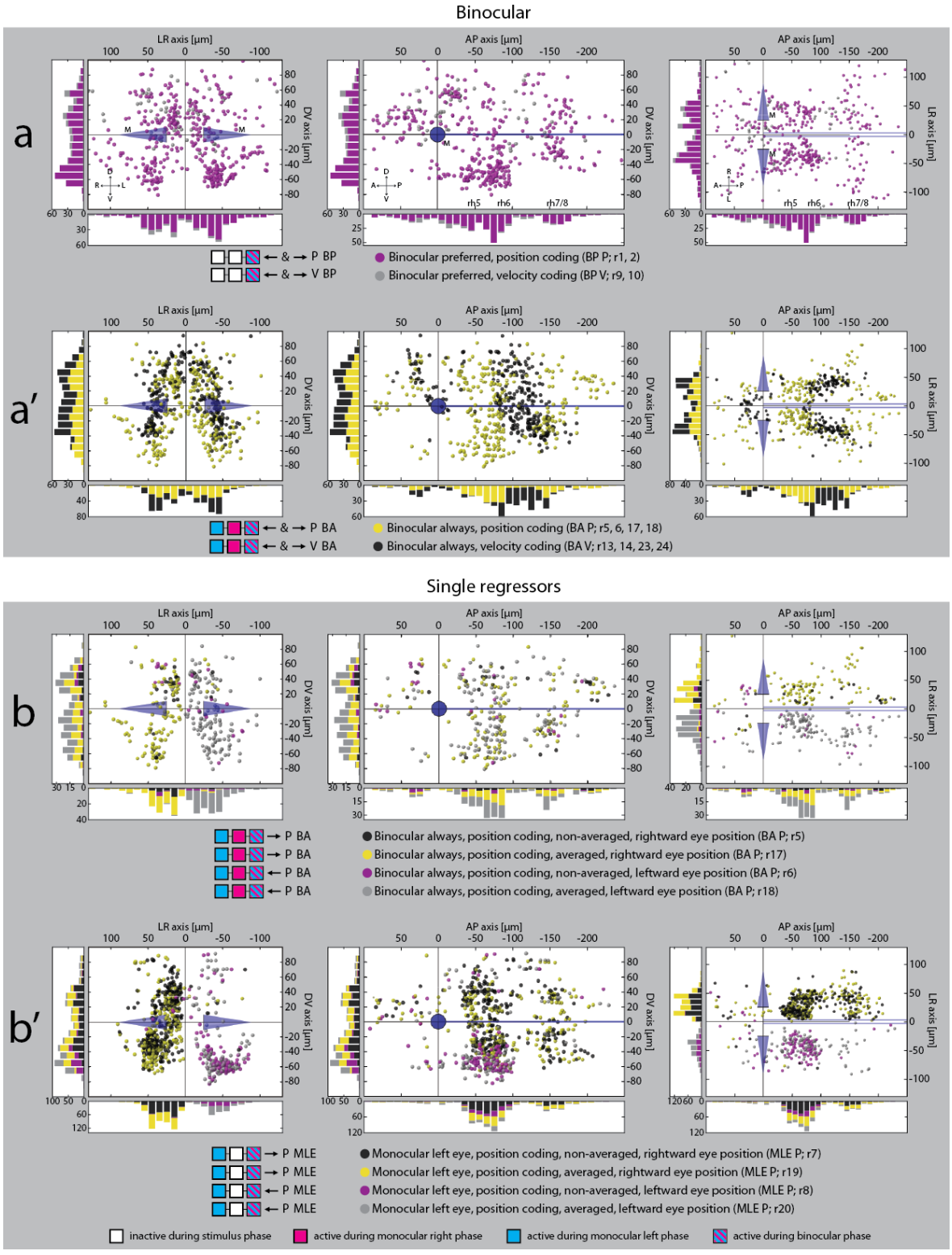

Figure 3-9: Binocular and single regressor cell maps for young larvae

Spatial locations of identified binocular neurons and maps highlighting the distribution of cells identified by averaged and non-averaged regressors. **a-b':** Transversal, sagittal and dorsal views for BP eye position and velocity (a), BA position and velocity (a'), BA position, separated for each regressor, (b) and MLE position (b') encoding neurons in the larval zebrafish hindbrain. Each dot represents one neuron identified in one recording with its highest correlation to the regressor in the respective legend. A: anterior, D: dorsal, L: left,

M: Mauthner cells, P: posterior, R: right/regressor, rh: rhombomere, V: ventral. Figure adapted under CC BY 4.0 from Brysch et al. (2019b).

As mentioned in chapter 2.6.1, with the difference in the explored motor range during the binocular stimulation, the introduction of “averaged”-regressors was necessary. As it is visible in Figure 3-9b, most of the BA P neurons were indeed identified with those regressors (averaged regressors: 255 neurons, non-averaged regressors: 48 neurons). There was no spatial aggregation of neurons identified by one specific regressor. For all other neuronal response types, the distribution of identified neurons for averaged and non-averaged regressors was roughly equal as it is exemplary shown for MLE P neurons in Figure 3-9b’ (averaged regressors: 379 neurons, non-averaged regressors: 389 neurons).

3.2.5 Summary

The experiment conducted here provides the basic layout of horizontal oculomotor neurons in the zebrafish hindbrain regarding their ocular specificity and basic coding features. It shows that oculomotor neurons in the zebrafish hindbrain can be categorized into four distinct response groups based on their ocular tuning. These groups only differ in their extent of monocular encoding and are always active during binocular eye movements.

The location of two clusters of putative INNs in the dorsal ABN was identified, with a faint gap separating them, and the location of MNs in the ventral ABN with MN-like neurons extending into rh4. In rh7/8, a rostro-ventral to dorso-caudal gradient from velocity to position encoding is visible, which coincides with the location thought to contain the OI. Also, a faint rostro-dorsal to caudo-ventral gradient for velocity encoding neurons is visible, switching from mono- & binocular to only monocular encoding neurons. In the caudal part of the medio-dorsal cluster of rh7/8 eye position encoding neurons, a response type flip for both monocular neurons (contra- to ipsilateral) and for binocular neurons (BP to BA) is visible.

3.3 Experiment 2 (neuronal tuning in young larvae)

3.3.1 Experimental framework:

While the previous experiment can provide a basic ground plan for the organization of eye position and slow-phase eye velocity encoding neurons in the zebrafish hindbrain, those neurons were grouped in a “winner takes it all” fashion and this analysis is thus ignorant to the fact that multidimensional response types might occur as well and it’s not capable to highlight the precise coding properties of each neuron (see chapter 1.5).

Therefore, this experimental stimulation protocol was tailored to map the eye position and eye velocity sensitivity of horizontal oculomotor neurons in the hindbrain. At the start, an alternating OKR stimulus was shown to coarsely map the explored motor range, which was followed by a closed-loop stimulation protocol to elicit different combinations of eye position and slow-phase eye velocity. This precisely mapped the influence of the slow-phase eye velocity towards the eye position encoding and vice versa (Figure 3-10a-a’’). Using this data, 2-dimensional tuning curves, which were covering almost all combinations of eye position and eye velocity in the well explored motor range between ± 15 ° and ± 7 °/sec, were constructed. The firing thresholds were calculated from the data with the least amount of influence from the opposite coding feature (e.g. the eye position tuning curve was calculated from the data between ± 1 °/sec eye velocity) with the previously described iterative baseline approach (see chapter 2.6.1).

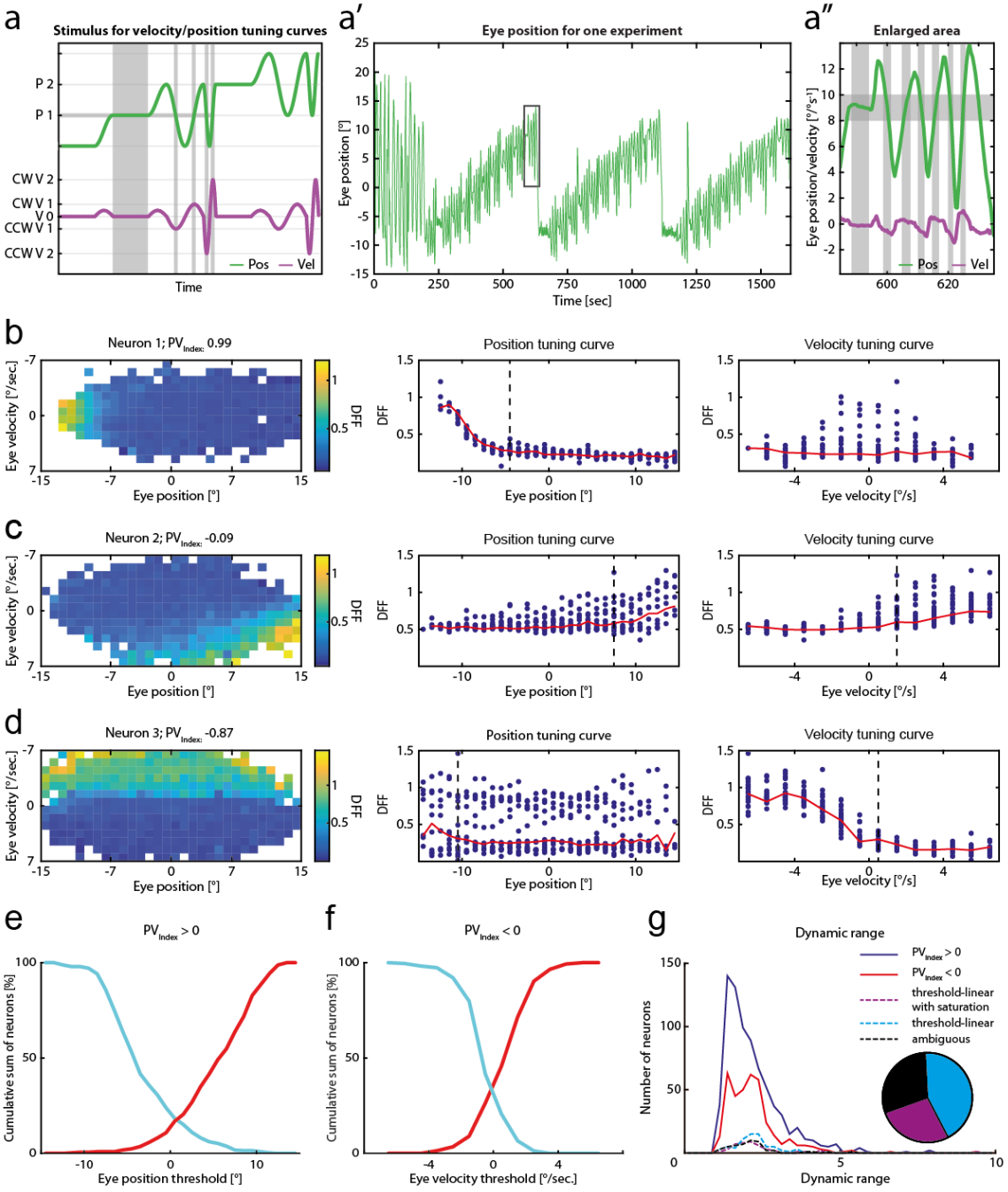

Figure 3-10: Stimulus and results for eye position/velocity assessment in young larvae

Example stimulus and results for the experiment assessing the different eye position & velocity coding. **a:** Schematic example for the different eye position (green) and velocity (magenta) combinations for one eye position bin (P1). For illustration purposes, only the stable and two of the three different velocity steps are shown (grey shaded areas). CCW: counterclockwise, CW: clockwise, P: position, V: velocity. **a':** Eye position trace for one example recording. In the beginning the alternating OKR stimulus is visible, followed by the three repetitions of the closed-loop stimulus. **a'':** Different stable and velocity steps for one eye position bin from highlighted area in a'. **b-d:** left column: two-dimensional tuning curves for one example eye position (b), one eye position/velocity (c) and one eye velocity encoding neuron (d), with the DFF color-coded for eye position (x-axis) and slow-phase eye velocity (y-axis). Middle column: eye position tuning curve. Red line shows the averaged eye position tuning between ± 1 °/sec. Blue dots show the remaining

datapoints for all different velocities. The black dashed line indicates the respective firing threshold (extracted from red trace), if identified. Right column: same as in middle column but for slow-phase eye-velocity, with the red line showing the eye velocity between ± 1 °. **e:** Cumulative sum of identified eye position thresholds for position encoding neurons ($PV_{Index}>0$) pooled in ON direction for left (cyan, n=343) and right (red, n=332) side. **f:** Cumulative sum of identified eye velocity thresholds for velocity encoding neurons ($PV_{Index}<0$) pooled in ON direction for left (cyan, n=228) and right (red, n=144) direction. **g:** Fluorescence dynamic range for different groups of neurons. Note that there is no significant difference in the dynamic ranges between the different groups of velocity encoding neurons ($PV_{Index}<0$, dashed lines, Kruskal-Wallis test: $p > 0.05$). Pie chart showing the distribution of the different strong velocity encoding groups (w/ saturation: 27 % (44/162), w/o saturation: 43 % (70/162), ambiguous: 30 % (48/162)). Figure adapted under CC BY 4.0 from Brysch et al. (2019b).

3.3.2 Eye position and slow-phase eye velocity tuning curves

I identified 1181 neurons with this protocol in the same imaging area of the hindbrain as in experiment 1. Using the richer dataset from this new experiment, I calculated a Position/Velocity-Index (PV_{Index}; see chapter 2.7.2). This index ranges from 1 (completely eye position encoding) to -1 (completely eye velocity encoding) with 0 indicating equal eye position/velocity coding. Neurons with a PV_{Index} larger than 0.5 were classified as "strong position encoding" while neurons with a $PV_{Index} < -0.5$ were identified as "strong velocity encoding".

To show the precise coding features of each neuron, I created 2-dimensional tuning curves for eye position and slow-phase eye velocity. Here, some neurons show only fluorescence increase along the x-axis (eye position coding) but not along the y-axis (eye velocity, Figure 3-10b left panel neuron 1, Supplemental Figure 5a & b). Note that the "exponential-like" tuning curve pattern for eye position tuned neurons is caused by non-linearities of the indicator and not by the actual firing properties of the neurons (Akerboom et al., 2012; Chen et al., 2013; Pologruto et al., 2004; Rose et al., 2014). Consistently, these neurons also show the highest PV_{Index}. The other "extreme" are neurons with a strongly negative PV_{Index} which only show activity changes along the y-axis (Figure 3-10d). Neurons which have their PV_{Index} around 0 have an intermingled response and show activity increases for both eye position and eye velocity changes. The vast majority of those intermingled neurons ($0.5 > PV_{Index} > -0.5$) have their eye position and velocity ON direction to the same side (93 %, 565/608; neurons which encode the eye position to the right, also encode rightward eye velocity). This is in line with the results from experiment 1, where neurons with the same tuning directions were also located in the same brain hemisphere (caudal to the Mauthner cells). When looking at the tuning of neurons with an intermingled response,

the influence of the eye velocity tuning towards the eye position tuning becomes visible (and vice versa, Figure 3-10c). The eye position and eye velocity tuning curve both show an increase in fluorescence, even before the respective firing threshold is reached, when the other movement quality is present (compare Figure 3-10c middle and left panel). This shows how the eye position/velocity responses are summed up and further highlights the intermingled coding for those neurons.

3.3.3 Eye position and slow-phase eye velocity firing thresholds

The firing thresholds for eye position encoding neurons (343 neurons for the left side, 332 for the right side with an identified firing threshold, $PV_{Index} > 0$) span a wide range between roughly ± 10 ° (Figure 3-10e). About 20 % of neurons for both tuning directions have their firing threshold already on the OFF-side, meaning that neurons encoding the right eye position already start firing for slightly leftward eye positions. This was slightly but significantly increased for neurons with a leftward eye position encoding (Wilcoxon rank-sum test: $p < 0.05$, mean for left coding neurons: 3.8 °, right: 5.7 °; pooled in ON).

For slow-phase eye velocity encoding neurons ($PV_{Index} < 0$), the identified firing thresholds span a smaller range of about ± 2 °/sec, with roughly 35 % of neurons exhibiting a firing threshold already on the OFF-side (Figure 3-10f). Therefore, their firing thresholds are more centered around 0 °/sec and have a larger portion of neurons already active on the contralateral side. There was no difference observed for the firing thresholds between leftward and rightward coding neurons, but I identified a larger fraction of neurons encoding for leftward eye velocity (Wilcoxon rank-sum test > 0.05, firing threshold mean for leftward coding neurons (n=228): 1.13 °/sec, rightward (n=144): 1.06 °/sec; pooled in ON). In line with the identified firing thresholds, the strongest fluorescence increases for the 2D tuning curves are visible around 0 °/sec.

During visual inspection of the strong eye velocity encoding neurons, it became obvious that a subset of those neurons show fluorescence saturation for their eye velocity tuning curves (e.g. Figure 3-10d, Supplemental Figure 5f & g, right panel) while other neurons still showed the expected threshold-linear firing response (Supplemental Figure 5d & e). This was only the case for some strong eye velocity encoding neurons and never for strong eye position encoding neurons. All strong velocity encoding neurons were manually classified as either “with saturation” (n=44), “without saturation” (n=70) or “ambiguous”

(n=48). To investigate if the observed saturation for slow-phase eye velocity was indeed caused by intrinsic coding and not by indicator saturation, I calculated the dynamic range of the indicator for eye position and eye velocity coding neurons and for each subset of eye velocity coding neuron (F_{Max}/F_{Min}, Figure 3-10g). With these results, I can rule out indicator saturation as there was no statistical difference between any group (Kruskal-Wallis test: $p > 0.05$) and the dynamic range was well below the published range of 51.7 (Chen et al., 2013).
Given that there is no observable spatial clustering between saturating and non-saturating neurons, and the probability that the non-saturating neurons might still saturate at higher velocities, they were merged into one group for further analysis (Figure 3-11a).

When looking at the firing thresholds of different groups of neurons, it becomes evident that the thresholds for eye position encoding neurons in rh7/8 are significantly shifted towards the ON direction compared to those of the MNs and INNs (and thus also to rh5 & 6, Figure 3-11b-b'', Supplemental Figure 6a, Kruskal-Wallis test: $p < 0.05$). In contrast, eye velocity encoding neurons in rh7/8 have their velocity firing threshold significantly shifted into the OFF direction compared to rh5 (Figure 3-11c-c'', Supplemental Figure 6b). However, the low number of velocity encoding neurons outside of rh7/8 limits the comparability.

To judge the robustness of the firing threshold assessment, a bootstrap analysis was performed (see chapter 2.7.3, Figure 3-11d & d'). This analysis shows that the measured firing thresholds are constantly very close to the upper confidence intervals. Further, as the onset of fluorescence change was used as a proxy for the firing threshold and the difficulties to detect single action potentials using GCaMP6f (Chen et al., 2013; Huang et al., 2021), the identified firing thresholds are probably shifted towards the ON direction. Therefore, the reported firing thresholds might be underestimated compared to their real-life counterparts.

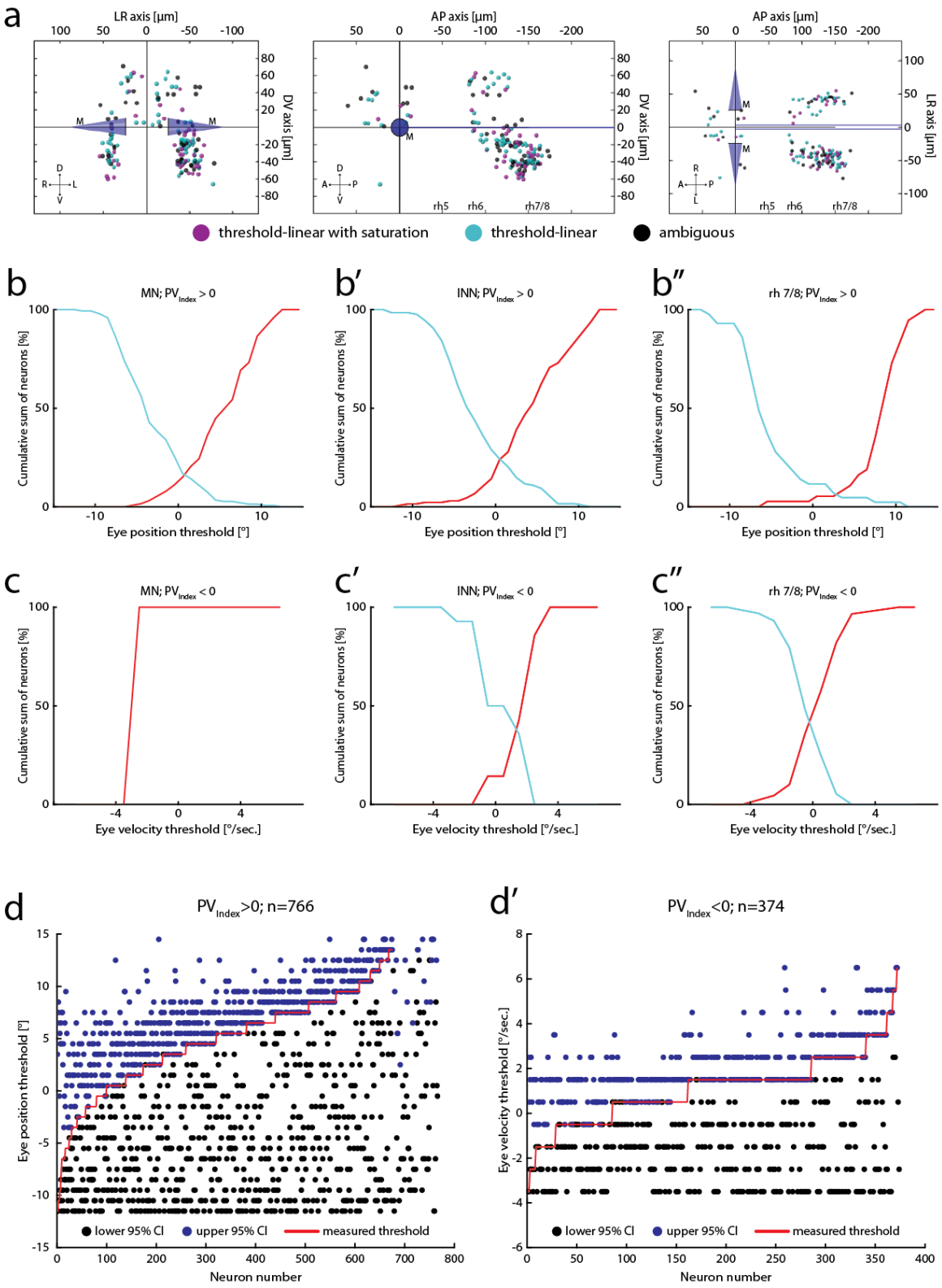

Figure 3-11: Firing threshold analysis in young larvae

a: Transversal, sagittal and dorsal view of all strong velocity encoding neurons grouped according to their eye velocity tuning curves (w/ saturation: 27 % (44/162), w/o saturation: 43 % (70/162), ambiguous: 30 % (48/162)). No specific clusters for each type are visible. **b:** Cumulative sum plots of the eye position firing

threshold for motoneurons (b, left: 147, right: 127), internuclear neurons (b', left: 128, right: 133) and rh 7/8 (b'', left: 43, right: 37) position encoding neurons pooled in the ON direction. The different neuronal groups were defined based on their anatomical location and the boundaries were set according to Figure 3-7a. **c:** Cumulative sum plots of the eye velocity firing threshold for motoneurons (c, left: 0, right: 1), internuclear neurons (c', left: 14, right: 7) and rh 7/8 (c'', left: 131, right: 89) velocity encoding neurons pooled in the ON direction. **d:** Bootstrap analysis for all eye position (d) and eye velocity encoding neurons (d') pooled in ON direction. Note how the identified thresholds (red) are always close to the upper 95 % confidence interval (blue dots). Confidence intervals were calculated for 1000 repetitions. Figure adapted under CC BY 4.0 from Brysch et al. (2019b).

3.3.4 Anatomical PV_{Index} and firing threshold maps

To investigate the distribution of firing thresholds, color-coded maps for eye position ($PV_{Index}>0$, n=675) and eye velocity ($PV_{Index}<0$, n=372) were created (Figure 3-12).

Along the dorsal-ventral axis, eye position firing thresholds (P_{Thres}) are more centered below the Mauthner cells and the MLF, with more shifted thresholds in the dorsal and ventral areas. However, the mean for each bin never falls below zero. While this slight shift towards more centered thresholds is present for the whole rostro-caudal extend, it is most notable in rh5 & 6. It is at the same location as the gap described earlier separating the 2 INN groups (Supplemental Figure 4a). In rh7/8, this shift is also present with more dorsal neurons showing similarly increased firing thresholds towards the ON direction. The aforementioned delayed firing thresholds for eye position encoding neurons in rh7/8 are also clearly visible in this figure (Figure 3-12, Supplemental Figure 6). Given a previously identified anatomical soma size gradient for MNs in zebrafish (Asakawa & Kawakami, 2018), the firing thresholds for MNs were separately analyzed, but no visible gradient was identified (based on their spatial location, Kruskal-Wallis test: $p > 0.05$). Eye velocity firing thresholds (V_{Thres}) show no gradients nor any anatomical clustering as it is expected given their small activation range (Figure 3-12b).

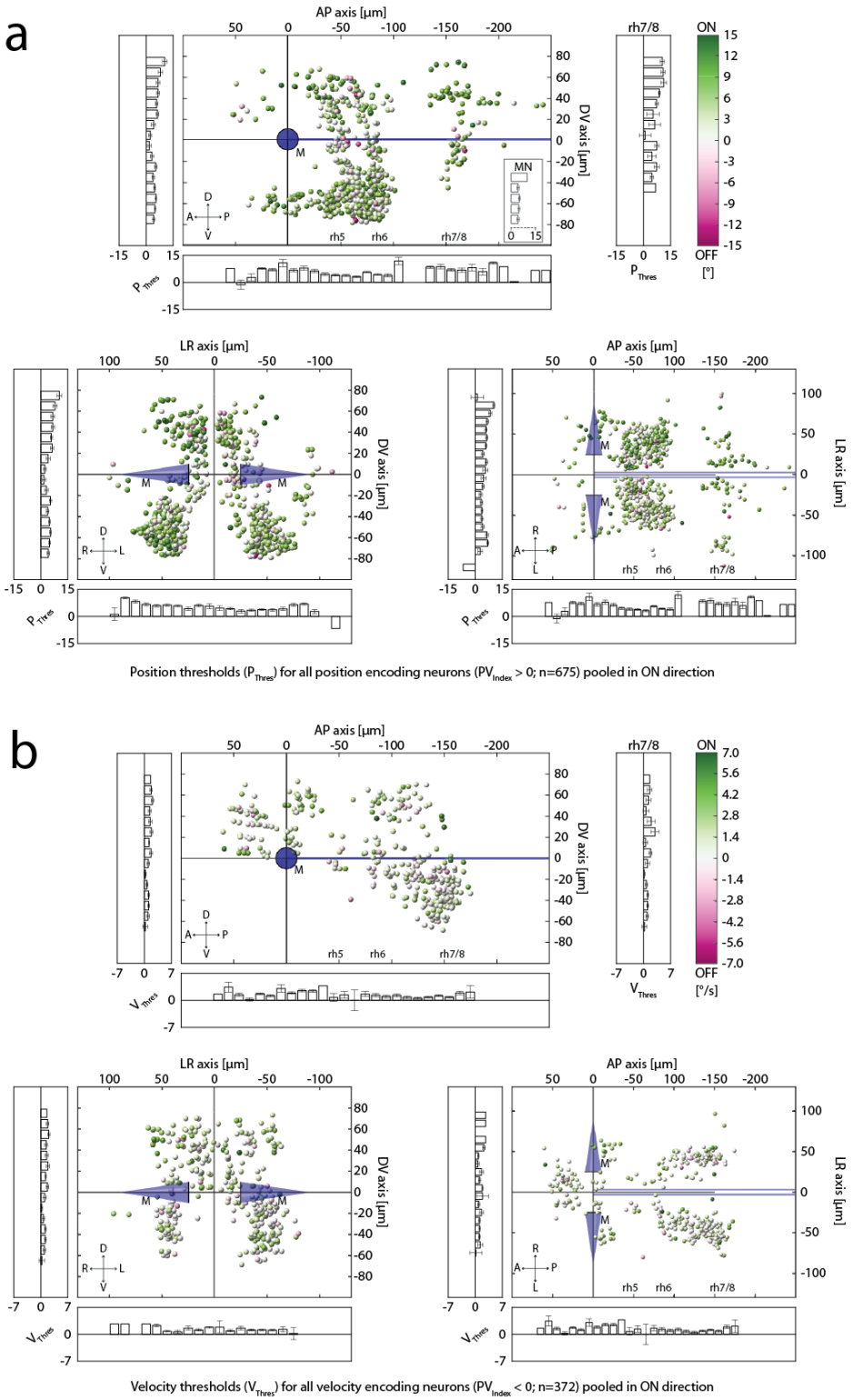

Figure 3-12: Firing threshold maps

Sagittal, transversal and dorsal views of eye position and velocity firing thresholds tuned in the respective ON direction. **a:** Eye position threshold color-coded for eye position encoding neurons (PV_{Index}>0, n=675) with an identified threshold. Inset shows threshold for motoneurons (based on anatomical location). **b:** Eye velocity threshold color-coded for eye velocity encoding neurons (PV_{Index}<0, n=372) with an identified threshold. Error bars are SEM. Figure modified under CC BY 4.0 after Brysch et al. (2019b).

To visualize the different coding for each neuron, color-coded maps of the PV_{Index} were created (Figure 3-13). Those maps show a close resemblance to the maps generated from experiment 1 (Figure 3-7 & Figure 3-9a & a') regarding the spatial location and tuning properties of oculomotor neurons.

In the dorso-rostral area to the Mauthner cells, most neurons show velocity tuning, following the expected coding for the ARTR. Neurons in rh5 & 6 have an average PV_{Index} of 0.42 ± 0.27 (STD, n=571), thus showing strong eye position sensitivity. Notably, the "gap" described above, -20 µm below the MLF between the two INN clusters, is visible again. Here, neurons thus show not only a shift in their firing threshold but also exhibit a more intermingled eye position/velocity encoding with more eye position sensitivity in the clusters above and below. This experiment also reveals eye position encoding neurons in the ventral parts of rh4 as it was expected from experiment 1. This further underlines that these neurons were not identified by chance and unveils a previously unreported cluster of eye position sensitive neurons.

Oculomotor neurons in rh7/8 have an average PV_{Index} of -0.26 ± 0.51 (STD, n=300), thus showing a strong amount of eye velocity encoding. However, when looking at the spatial distribution of the individual neurons, a clear coding shift from eye velocity (rostro-ventral) to eye position (dorso-caudal) can be seen. Here, the ventral cluster overlaps with the eye velocity encoding neurons from experiment 1 (MLE, MRE, BA), showing velocity encoding in the most ventral areas and a more intermingled encoding the further dorsal the neurons are located. The strongest position encoding neurons in rh7/8 can be seen in the dorsal part around the midline overlapping with the OI neurons described in experiment 1.

However, from a dorsal view (Figure 3-13b) it appears that most eye position encoding neurons are limited to the medial-most regions in the caudal part of rh7/8, while eye velocity encoding neurons are located along a rostro-medial to caudo-lateral stripe, with only few neurons with intermingled responses between them and the eye position encoding neuron cluster. This stricter anatomical separation between a strong eye position and a strong eye velocity encoding cluster somewhat disagrees with the visible rostro-caudal and dorso-ventral gradients from velocity to position encoding as seen in the PV_{Index}-panels in Figure 3-13a.

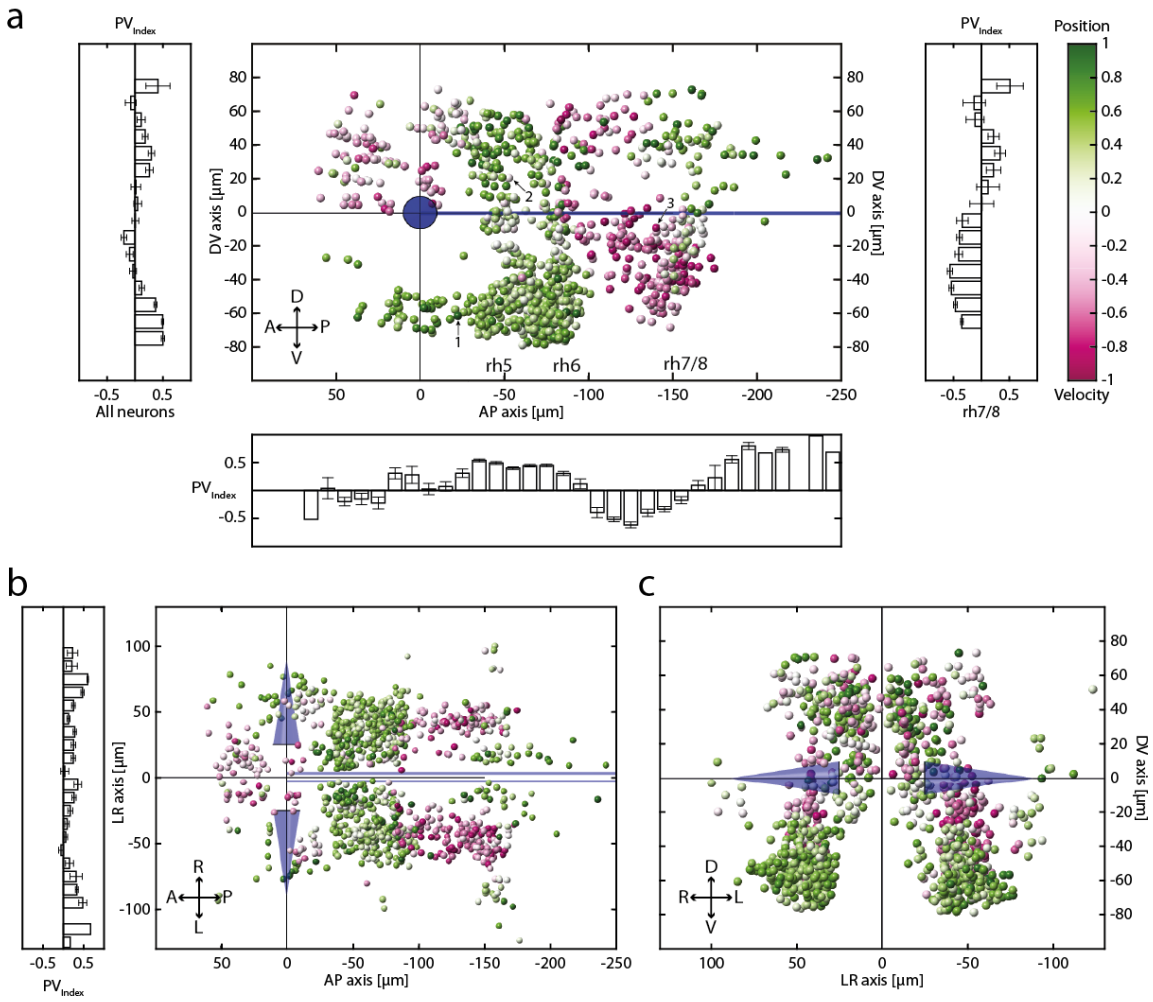

Figure 3-13: PV_{Index} maps for young larvae

Spatial location of all neurons color-coded for their PV_{Index}. **a-c**: Sagittal, dorsal and transversal views of all neurons with an identified PV_{Index} from experiment 2. Numbers show the locations of neurons highlighted in Figure 3-10b-d. A: anterior, D: dorsal, L: left, P: posterior, R: right, V: ventral; error bars are SEM. Adapted under CC BY 4.0 from Brysch et al. (2019b).

3.3.5 Summary

Oculomotor neurons in the hindbrain of zebrafish show a broad response profile of eye position and/or eye velocity encoding. Eye position firing thresholds are distributed along a wide range. In contrast, eye velocity firing thresholds are centered around the midline with only a minor fraction of neurons having their threshold in the OFF-side before crossing the midline. Strong eye velocity encoding neurons sometimes show saturation for their velocity tuning, but those neurons do not cluster anatomically.

The distribution of eye velocity and eye position encoding neurons reported for this experiment closely resembles the one reported in experiment 1. Furthermore, this experiment shows that the gap between the two INN clusters is not only of an anatomical nature, but also that the neurons close to this gap exhibit a shift for their eye position firing thresholds into the OFF direction and a stronger eye velocity encoding. Last, an eye velocity to position encoding gradient in the hindbrain along the rostro-caudal and dorso-ventral axis in the area which is thought to contain the OI was identified.

Thus, the findings reported here support the data from experiment 1 and precisely show the coding preferences for oculomotor neurons in the hindbrain.

This page is intentionally left blank

Chapter 4: Results for Late-Stage Larvae

4.1 Late-stage larvae

As already shown in the introduction, most of the imaging experiments in zebrafish are conducted in young and still developing brains (5-7 dpf), due to the easier accessibility of the brain for calcium imaging and the relatively few technical requirements to keep young larvae alive during microscopy at that age (Xu et al., 2015).

However, several visually guided behaviors undergo changes during the larval development or even only emerge after the conventional imaging timeframe of 5-7 dpf (see chapter 1.2.3). As behavior is the readout from neuronal activity, changes and the emergence of new behaviors are represented in altered neuronal activities and the neuronal code changes with development of the animal (Avitan & Goodhill, 2018). Therefore, I investigate the ontogeny of those circuits examined earlier by repeating experiments 1 & 2 in late-stage larvae (14-15 dpf) in the second part of my thesis.

4.1.1 Modifications to the recording setup:

Several modifications to the recording setup were implemented to adapt to the physiological changes of the older larvae.

With the increased body size and age, it becomes harder for the fish to breathe through their skin (Rombough & Drader, 2009). Therefore, it is necessary to provide a constant water flow over the gills to provide oxygen to the larvae and to ensure their survival at 14 dpf, but also to ensure proper ionoregulation from 7 dpf onwards (Rombough, 2002, 2007). This was achieved by pumping oxygenated Ringer's solution through the recording chamber and by removal of the agarose around the gills (Supplemental Figure 1).

Due to the increased length of the older animals, the passive illumination through the objective was not sufficient to fully illuminate the eyes while simultaneously record the whole hindbrain. Thus, an additional LED ring was mounted around the CMOS camera at the bottom of the stage to provide additional illumination from the bottom (Supplemental Figure 2). A more detailed description of the setup is provided in the Method section (see chapter 2.2.2).

4.1.2 Replacement of the transgenic reporter line

In a pilot experiment, it became obvious that the *Tg(ubb:nls-GCaMP6f)m1300Tg* line is not feasible for imaging older zebrafish larvae (Figure 4-1). In these preliminary experiments, the expression levels of two GCaMP6f lines were compared to assess which is more suitable for recordings in late-stage larvae. In a set of recordings using the same experimental paradigm from experiment 1, only 9 % of identified oculomotor neurons originated from the m1300Tg line, while 36 % of all recordings were conducted in that line. 91 % of identified neurons were found using the *Tg(elavl3:H2B-GCaMP6f)jf7Tg* line. This difference was not observed when imaging 5-7 dpf old larvae (Omejc, 2019). Thus, continuing the experiments with the m1300Tg line would have resulted in deprecated neuronal maps as this line loses much expression with age. This came as a surprise, as it was specifically chosen to combat the expected weaker expression of the *elavl3* line in older animals. It is the most commonly used promotor for pan-neuronal expression, but it is primarily active in young, differentiating neurons (Kim et al., 2014; Park et al., 2000). However, the newer GCaMP6f line *Tg(elavl3:H2B-GCaMP6f)jf7Tg* (Dunn et al., 2016) shows higher baseline fluorescence and the expression stays active >7 dpf in a homozygous background. Therefore, the m1300Tg line was replaced by the jf7Tg line, given that the sensor is still the same and pan-neuronal expression is guaranteed in both lines.

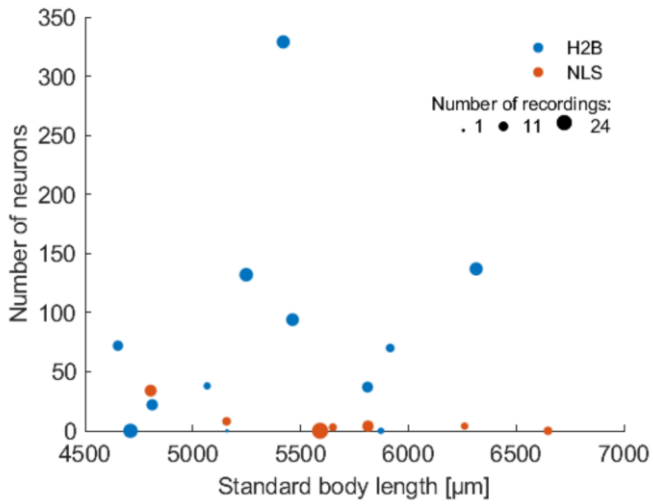

Figure 4-1: Comparison of two different GCaMP lines by identified neurons

Number of neurons obtained from individual zebrafish, based on their standard body length, the transgenic line they belong to, and the number of recordings they went through. Animals are represented by a circle and are color-coded based on their transgenic insert. The number of recordings is coded by the size of the circles. Figure, legend and data from Omejc (2019).

4.2 Experiment 3 (eye coordination in late-stage larvae)

4.2.1 Experimental framework:

The goal of this experiment was to reassess the organization of the circuits responsible for horizontal eye movements in the larval zebrafish hindbrain and to investigate how changes during development influence the neuronal tuning. The results from this experiment will show how mature the oculomotor circuits already are at the larval stage and how the mono-/binocular arrangement of neurons changes at a later developmental stage (see chapter 1.5). The stimulation and data analysis were the same as for experiment 1, with only minor changes due to the increased size of the larvae and due to some behavioral differences (see next chapter, 2.4.1 & 2.6.1 for details).

4.2.2 Late-stage larvae show decreased yoking and increased saccadic activity:

Late-stage larvae show several behavioral differences during the OKR stimulation compared to young larvae. First, the occurrence of saccades during each stimulation phase increased significantly from 0.024 ± 0.020 Hz to 0.068 ± 0.048 Hz in older animals (mean ± STD, Wilcoxon rank-sum test: $p < 0.05$, Figure 4-2a & b, Supplemental Figure 7a). While there were no differences in the saccade direction, most of the saccades happened during the binocular stimulation phase due to the increased gain present during binocular stimulation (Supplemental Figure 7a & b; Beck et al. (2004)). Notably, for some of the late-stage larvae the saccade frequency was comparable to the values of young larvae (Figure 4-2a top three traces), while other recordings exceeded that frequency range (bottom three traces). A lot of these saccades were spontaneous and not triggered by eccentric eye positions and thus not preventable.

The developmental progress of zebrafish larvae from the same clutch raised under identical conditions can vary greatly with increased age. Therefore, age is not an appropriate indicator for maturation and the standard length (SL) of the fish is often used to approximate the developmental stage (Parichy et al., 2009). Given the rather broad range of the SL for the late-stage larvae, it could be possible that the late-stage larvae group in this experiment consists of several subgroups and could be further subdivided. However, when plotting the saccade frequency against the SL, no increase is visible for the higher SL larvae and a linear regression fit shows a slight decrease in saccade frequency for the larger animals (Figure 4-2c). Therefore, all late-stage larvae were pooled into the same group.

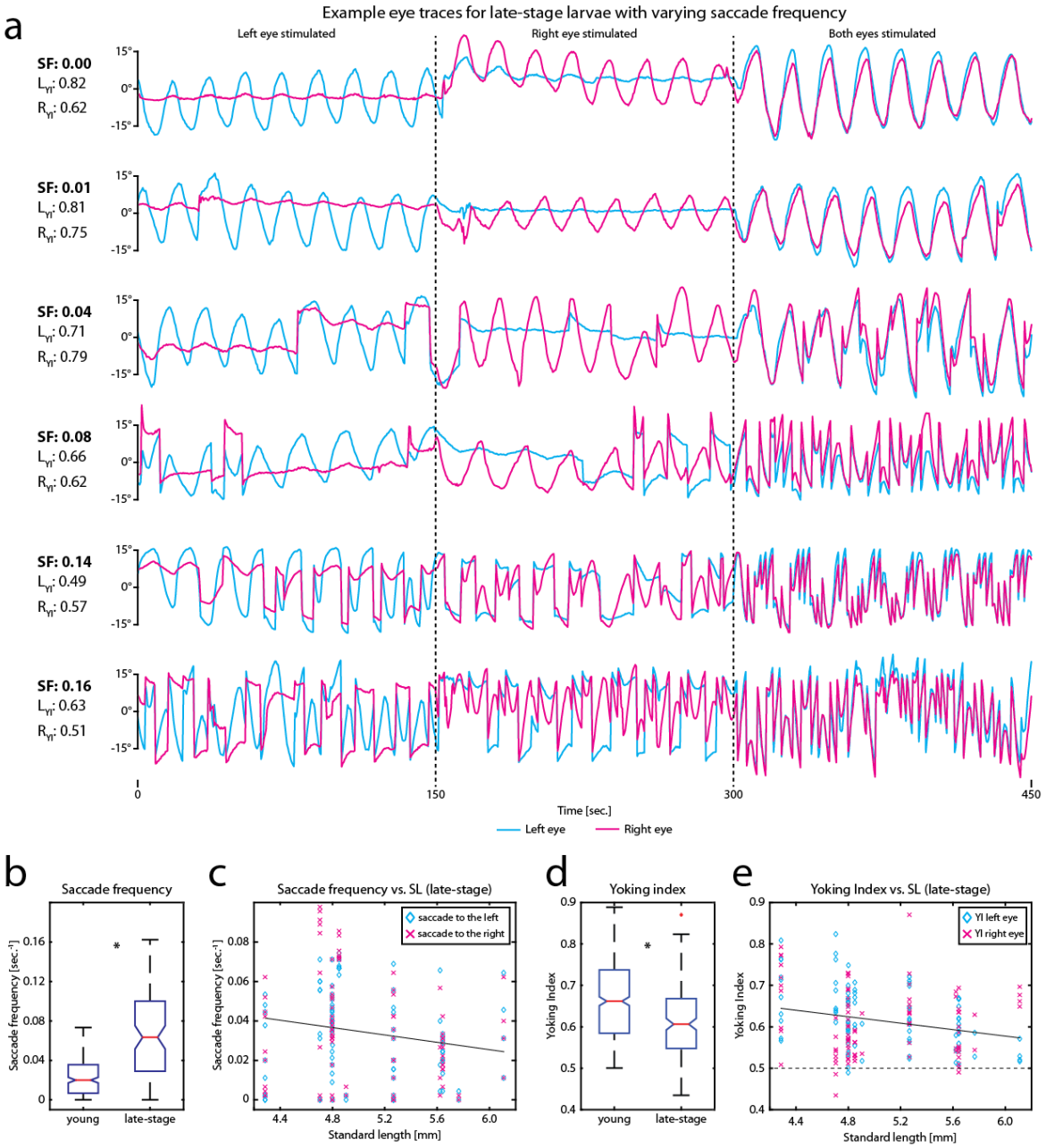

Figure 4-2: Saccade frequency and YI for different developmental stages

Zebrafish show increased saccadic activity and more yoked eye movements at later stages. **a:** Example eye traces from late-stage larvae showing the range of saccade frequency for this experiment. L_{YI}: left eye stimulation yoking index, R_{YI}: right eye stimulation yoking index, SF: saccade frequency. **b:** Saccade frequency for young and late-stage larvae during experiment 1 & 3 (Wilcoxon rank-sum: $p < 0.05$, young: n=248, late-stage: n=90). **c:** Saccade frequency for each late-stage recording in each direction (cyan diamond: left, magenta cross: right) plotted against their SL. Black line shows the linear fit for both saccade directions (R^2: 0.03). **d:** Yoking index from each monocular stimulation phase for young and late-stage larvae (Wilcoxon rank-sum: $p < 0.05$). **e:** Yoking index for each monocular stimulation phase (cyan diamond: left, magenta cross: right) for all late-stage recordings plotted against the SL. Black line shows the linear fit for both stimulation phases (R^2: 0.06). Black dashed line shows the Yoking index cutoff (see chapter 2.6.2).

Second, late-stage larvae have a decreased ability to perform monocular eye movements. While 5-7 dpf old fish had an average yoking index of 0.66 ± 0.09, late-stage larvae have 0.61 ± 0.09 (mean ± STD, Wilcoxon rank-sum test: $p < 0.05$, Figure 4-2d). In contrast to the saccade frequency, a small decrease for the YI in larger larvae is observable. Taken together, these two changes in behavior make it more difficult to perform this experiment with late-stage larvae. Thus, fewer successful recordings were achieved for late-stage larvae compared to young larvae (90 vs. 248). To ensure a minimum sampling size of three recordings for each 10 µm increment, four recordings with a $YI < 0.5$ for one eye were included (Figure 4-2e, chapter 2.6.2). Apart from the YI in those recordings, all recordings for late-stage larvae were analyzed in the same way as the ones from young larvae. This led to the identification of 1297 neurons in 12 individual larvae (14-15 dpf). After the firing threshold assessment, which excluded 466 neurons, a total number of 831 individual neurons were analyzed further.

4.2.3 Late-stage larvae exhibit an increased amount of eye position sensitivity

Similar to the case of young larvae, oculomotor neurons from late-stage larvae fall into the same four previously identified response groups (MLE, MRE, BA, BP), but their distribution shows some differences as the relative number of those neurons decreased from 95 % (young) to 87 % (late-stage, 723 of 831 neurons, Figure 4-3a). Respectively, the number of MLEX and MREX neurons increased. Similar to young larvae, no monocular exclusive neurons (not active during binocular stimulation, MX) were identified. Another notable difference between the two developmental stages is the relative increase of eye position encoding neurons over eye velocity encoding neurons (86 %, 718 position and 113 eye velocity encoding neurons) compared to young larvae (75 %).

The most frequent response groups for late-stage larvae are monocular neurons encoding nasal eye position, like in young larvae (Figure 4-3a). However, those neurons were unequally distributed for the left eye (157) and for the right eye (90), but no difference between the left and right eye was found in young larvae (534 left, 523 right eye). The second most common response group in late-stage larvae are BA P neurons, which were only on rank 4 in young larvae. This raises the question whether the missing MRE P left encoding neurons were erroneously classified as BA P neurons. As MRE left eye position encoding neurons would correspond to the INNs in the left hemisphere (see chapter 1.4.3),

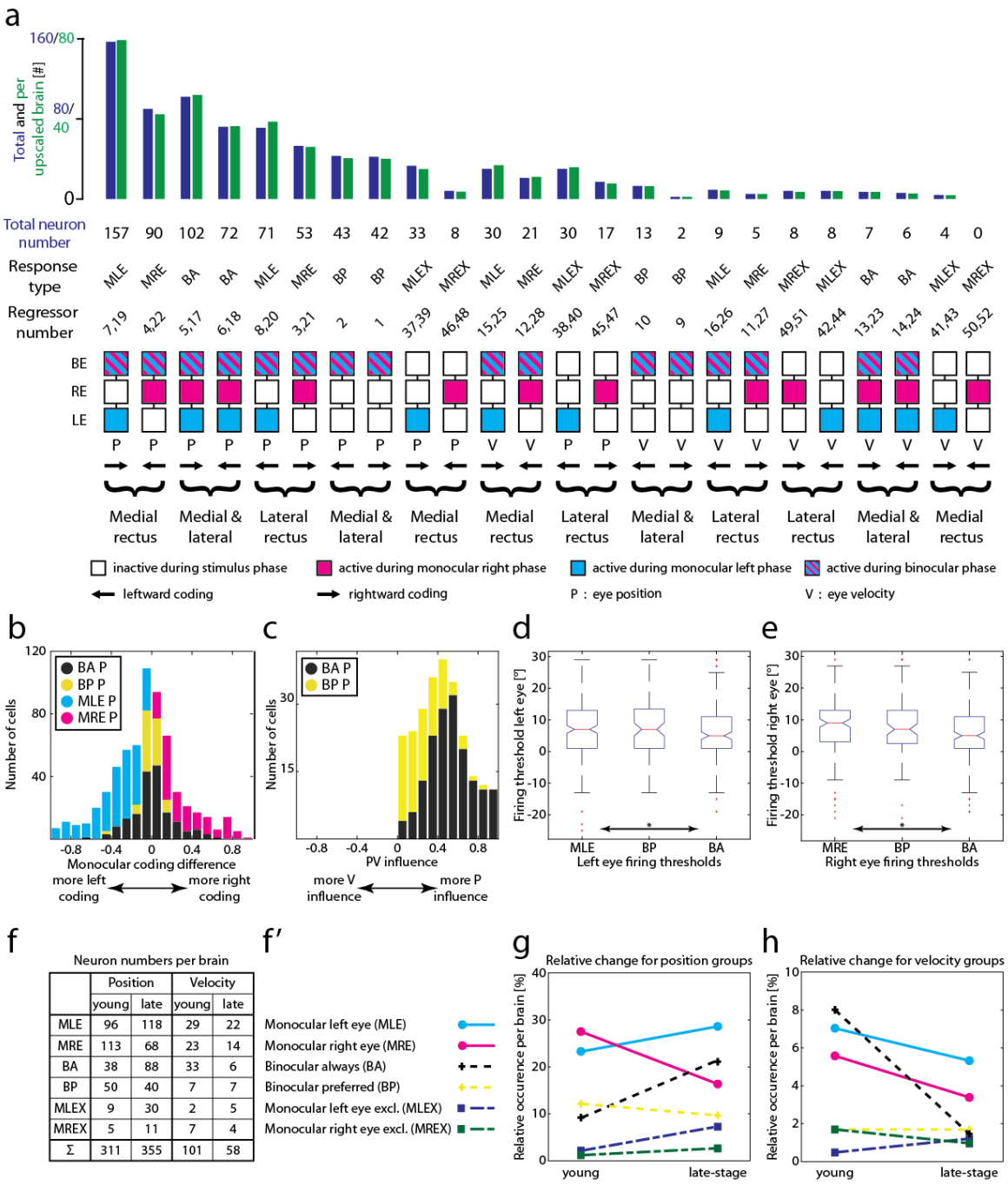

	Position		Velocity	
	young	late	young	late
MLE	96	118	29	22
MRE	113	68	23	14
BA	38	88	33	6
BP	50	40	7	7
MLEX	9	30	2	5
MREX	5	11	7	4
Σ	311	355	101	58

Figure 4-3: Response groups for late-stage larvae and their coding properties

Distribution of late-stage response groups and coding properties regarding their exclusivity and firing threshold. **a:** Number of identified neurons grouped pairwise according to their mono-/binocular coding and eye muscle(s) coding. The bar plot shows the total number of identified neurons (blue) and the adjusted & upscaled number per brain in 5 µm (green, comparable to Figure 3-6). **b:** Difference in monocular coding for position encoding neurons for all four main response groups. Index runs from -1 (exclusively coding for the left eye) to 1 (exclusively coding for the right eye). **c:** Index showing the difference in position or velocity coding for BA and BP P neurons. The index runs from zero (equal correlation from position and velocity coding) to 1 (exclusive position coding). **d:** Firing thresholds of position encoding neurons for the left eye, derived from the firing threshold analysis pooled in ON (positive) direction (n: MLE=228, BP=85, BA=174). **e:** same as in d, but for the right eye (n: MRE=143). **f:** Number of identified neurons for each group per brain

(mean, upscaled for late-stage). **f':** Color-code for subfigures g & h. **g:** Change of each eye position encoding response group for young and late-stage larvae (relative to the total, average number of neurons identified for the respective developmental stage). **h:** same as in g, but for velocity encoding groups.

one would expect an increase of BA P neurons there. However, neither the regressor identification (due to the hemispheric restriction) nor the anatomical location of BA P neurons show an increase to the left side (left: 72 neurons, right: 102 neurons, both for regressor and anatomical classification; Figure 4-3a & Figure 4-6a'). Similarly, the increased amount of MLE P right encoding neurons might be falsely classified and fall into the BA P left category. However, this can be excluded due to their hemispheric location on the right side. Sampling errors and a potential different explored motor range for different fish are likely the cause of these differences, rather than a functional asymmetry between the different eye muscles.

Interestingly, the most common velocity type for both developmental stages are also neurons encoding monocular adducting eye movements and they show an increased number of neurons encoding the left eye, though their total number is much smaller. Overall, the number of velocity encoding neurons decreased dramatically, mostly for the BA type which drop from the 6^{th} rank in young larvae to the 2^{nd} to the last in late-stage larvae.

MLEX and MREX neurons are found very infrequently, apart from MLEX P right and MLEX P left encoding neurons. Notably, their respective counterpart is always underrepresented (MLEX P right: 33 vs 8; MLEX P left: 30 vs 17). Even though MLEX P right neurons were found in 10 different recordings, 22 of the identified neurons stem from only two recordings from the same fish. Even though no apparent movement in z is visible in those recordings and neuronal activity is still observable during the last stimulation phase, the isolated occurrence in predominantly one fish suggests that these neurons do not comprise a specified response group. The specific eye movements during that recording and the fact that the SL for that fish was the smallest of all the recorded larvae (4.2 mm) probably contributed to the classification of those neurons. The same holds true for MLEX P left encoding neurons though these were found in larger animals (SL 5.2 & 6.1 mm).

Although the number of binocular events in the form of saccades is increased in the late-stage data, the monocular coding difference shows a significant larger fraction of

monocular neurons with a stronger monocular coding preference (young vs late MLE: -0.18 vs. -0.36, MRE: 0.20 vs. 0.35; Wilcoxon rank-sum: $p < 0.05$; Figure 3-6b, Figure 4-3b). On the other hand, both binocular groups show a different $PV_{Influence}$ (Figure 4-3c). While BP neurons exhibited a small but significantly increased velocity sensitivity for young larvae, this significant effect is further increased for late-stage larvae (mean difference: 0.29, Wilcoxon rank-sum test: $p < 0.05$). Whether this is a real coding shift or influenced by the increased saccade frequency remains to be elucidated. However, as the classification of BP neurons in young larvae might have been influenced beneficially by later firing thresholds compared to the monocular groups, this is not the case for late-stage larvae where BP neurons have their firing thresholds shifted more into the OFF direction (median monocular left: 7 °, right: 9 °, respective BP: 5 °; firing thresholds pooled in ON). The only significant difference is found for BA neurons with their firing threshold shifted towards the OFF direction compared to monocular neurons (Kruskal-Wallis test: $p < 0.05$, Figure 4-3d & e).

When comparing the response groups for young and late-stage larvae, several differences are observable (Figure 4-3f-h). While the mean number of identified neurons per brain is almost identical (412 young vs. 413 late-stage upscaled, Figure 4-3f), an increase for position encoding neurons in late-stage larvae is noticeable (with the aforementioned exception of MRE neurons). Velocity encoding neurons are found more seldom in late-stage larvae. Especially BA V encoding neurons, which are the most frequent velocity group in young larvae, are almost absent in late-stage larvae (see below for anatomical maps). Given the low number of BP, MLEX and MREX velocity neurons in young larvae to start with, only monocular velocity neurons appear to form a distinctive velocity group in late-stage larvae.

Due to the increased size of the brain in late-stage larvae, the area rostral of the Mauthner cells is under-sampled compared to young larvae. Therefore, large parts of the ARTR are missing, but this did not affect the amount of identified velocity/position neurons in a notable way (compare Figure 4-3f-h to Supplemental Figure 8).

4.2.4 Spatial arrangement of monocular neurons in late-stage larvae

The strict hemispheric separation for neurons caudal of the Mauthner cells is also observable for late-stage larvae, with 96 % (436 of 452) of neurons in the right and 95 %

(346 of 365) of neurons in the left hemisphere having their preferred direction to the ipsiversive side. Monocular eye position encoding neurons are generally found in the same areas as in experiment 1 and are also mirror-symmetric for MLE and MRE neurons. The unequal sampling in z did not affect the monocular cell maps in a noteworthy way (compare Figure 4-4 & Supplemental Figure 10). Monocular oculomotor neurons in the hindbrain are predominantly found in the ABN in rh5 & 6. Here they form two ventro-dorsal columns, though they are less obvious than in young larvae due to the decreased number of identified neurons (but see Supplemental Figure 9 for a better anatomical overview). The clear separation of INNs and MNs does not appear to be as prominent as in young larvae. However, the more ventral MN clusters and the larger dorsal extent of INNs is still visible. Again, neurons in the dorsal areas are located closer to the midline and only span to ~50 µm laterally, while ventral neurons are located more towards the sides (~40 µm to 100 µm, best seen for INN, Figure 4-4a & b). Neurons carrying the information for abducting, ipsiversive eye movements in late-stage larvae are also stretching from the ventral ABN rostral into rh4, though the number of identified neurons is probably underrepresented since this area is under-sampled and cutoff directly rostral to the Mauthner cells. Expression of the vu504Tg line would suggest that even more MNs are present in the ventral areas ~ -150 µm, but the total imaging depth of >250 µm, together with the problem of reliably identifying single neurons at this level in a pilot study, made more ventral recordings unfeasible (Omejc, 2019). While there is a small gap in the INN cluster for MLE neurons ~ -40 µm below the Mauthner cells, this gap is not visible for MRE neurons. Thus, it appears that the gap separating the INN neurons into two sub-clusters is only present for young larvae, but the extensive adjustment to address the different SLs might have influenced that alignment.

Outside of rh5 & 6, monocular eye position neurons are in rh7/8 which predominantly encode the contralateral eye. The majority of those neurons are clustered medially around the MLF and thus likely correspond to the OI, but some MLE P neurons are located more towards the rostral/ventral end of rh7/8. This cluster was not found for MRE P neurons, and it is thus questionable whether this cluster forms a distinctive group or whether it’s caused by experimental intricacies as the anatomical location of these neurons corresponds more to the IO than the OI. Few ipsilateral encoding neurons can be seen towards the caudal end of rh7/8. This is consistent with the monocular organization in the OI observed in young larvae, where contralateral MLE and MRE neurons were located more rostral

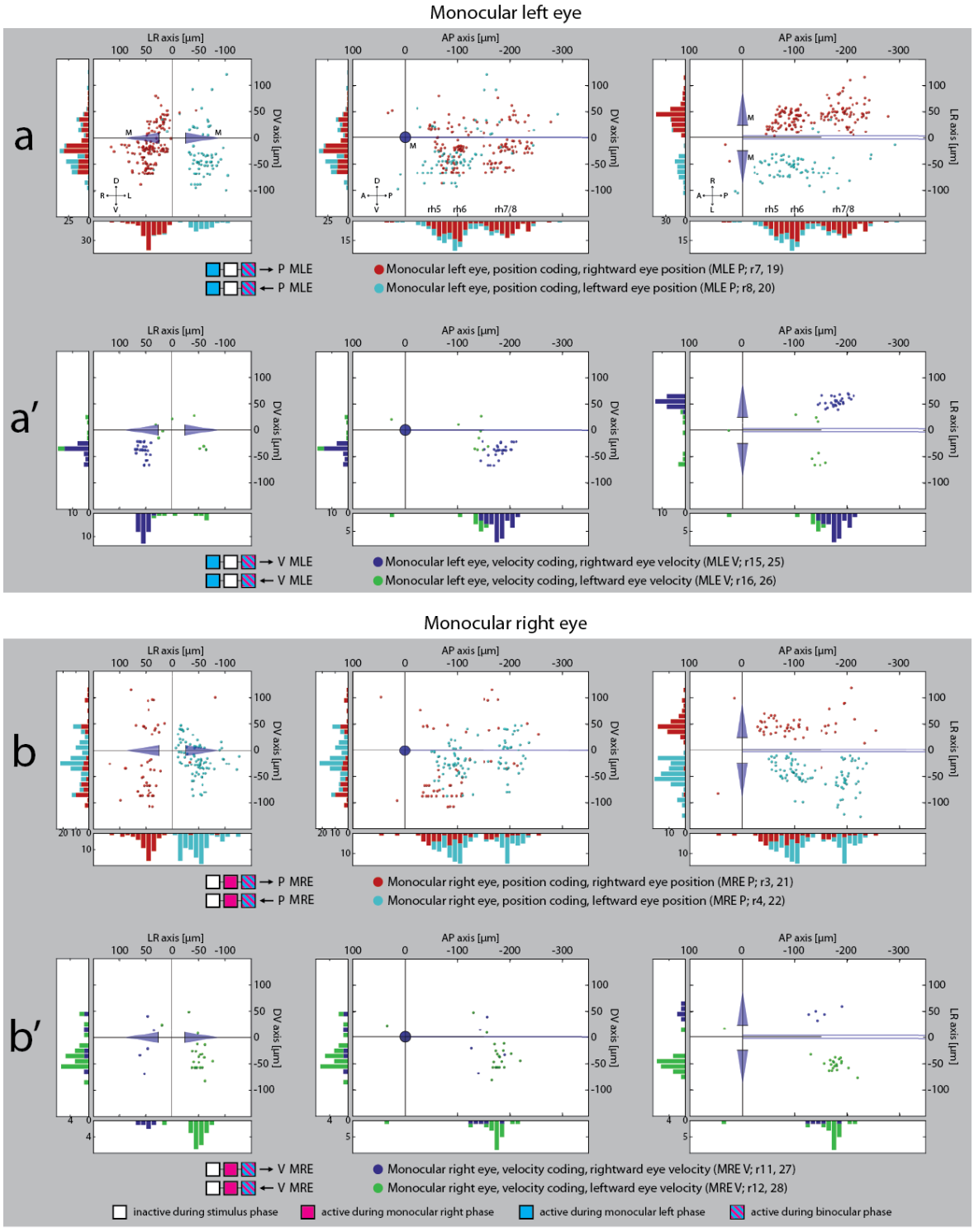

Figure 4-4: Monocular cell maps for late-stage larvae

Spatial locations of identified monocular neurons. **a-b':** Transversal, sagittal and dorsal views for MLE eye position (a), MLE velocity (a'), MRE position (b) and MRE velocity (b') encoding neurons. Each dot represents one neuron identified in one recording with its highest correlation to the regressor in the respective legend. A: anterior, D: dorsal, L: left, M: Mauthner cells, P: posterior/position, R: right/regressor, rh: rhombomere, V: ventral/velocity.

than ipsilateral neurons. However, hardly any ipsilateral encoding neurons in the OI were identified in the first place.

Monocular eye velocity neurons are found less frequently and they are restricted to the contralateral and ventral area of rh7/8. Except for the ventral MLEP cluster, they are located more ventro-rostrally than their respective eye position counterparts and, in contrast to young larvae, almost no monocular eye velocity neurons are found dorsal of the MLF. Ipsiversive monocular eye velocity neurons are almost absent and are only located in the more rostral regions of the eye velocity neuron clusters.

Monocular exclusive neurons in late-stage larvae are scattered throughout the hindbrain (MLEX, MREX, Figure 4-5, Supplemental Figure 11). Though their number increased relatively compared to young larvae, their hemispheric separation is less constrained than that of the other response groups, with MREX velocity neurons almost exclusively on the contraversive side (MLEX/MREX: 81 ipsiversive, 27 contraversive, MLE/MRE/BA/BP: 782 ipsiversive, 35 contraversive). They are still identified very infrequently and the already mentioned fact that most MLEX neurons were identified in only two recordings indicates that these neurons don't form a functional unit in the oculomotor system. Like in young larvae, neurons only active during both monocular stimulation phases and inactive for the binocular phase are completely absent.

4.2.5 Spatial arrangement of binocular neurons in late-stage larvae

Binocular neurons in late-stage larvae fall into the BA and BP group, but they exhibit some notable differences compared to young larvae. While the number of BP P neurons decreased, they are also more loosely distributed throughout the hindbrain. Therefore, no clear clusters of BP neurons are visible in late-stage larvae (Figure 4-6a), which contrasts with the strong aggregation of BP P neurons in the ventral ABN of young larvae (Figure 3-9a). Though some of the ventral areas are under-sampled, only a small increase in the amount of BP P neurons is visible in the upscaled dataset (Supplemental Figure 12a). While BP P neurons in the ABN still aggregate in the ventral area, no clear difference between the number of neurons in the ventral ABN and rh7/8 is visible. This suggests that BP P neurons in young larvae are only a transient group and might not be present in the adult brain. In contrast to young larvae, no protrusion into rh4 from the ventral ABN is visible. However, this was also less prominent for BP neurons than for monocular neurons

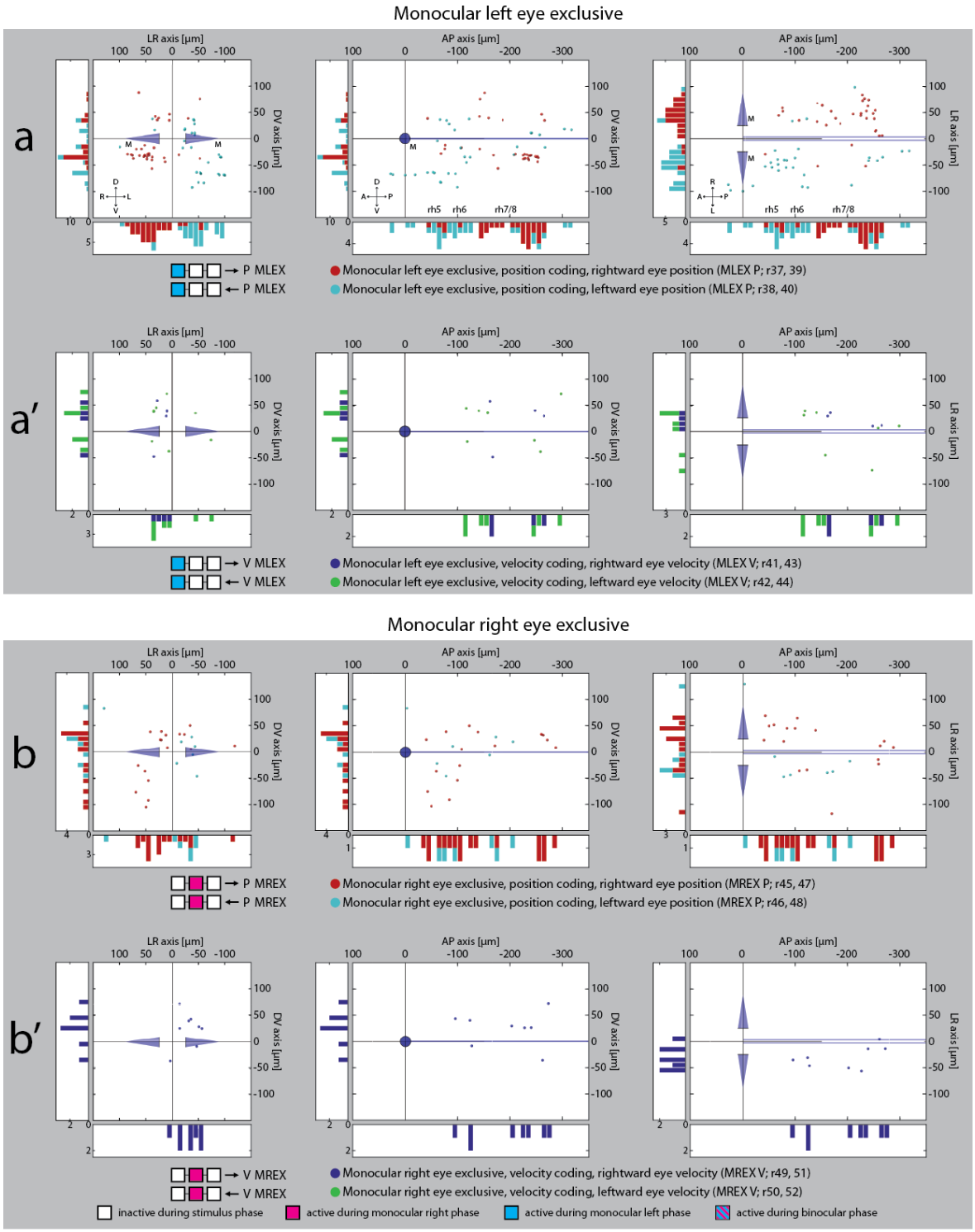

Figure 4-5: Monocular exclusive cell maps for late-stage larvae

Spatial locations of identified monocular exclusive neurons. **a-b':** Transversal, sagittal and dorsal views for MLEX eye position (a), MLEX velocity (a'), MREX position (b) and MREX velocity (b') encoding neurons in the larval zebrafish hindbrain. Each dot represents one neuron identified in one recording with its highest correlation to the regressor in the respective legend. A: anterior, D: dorsal, L: left, M: Mauthner cells, P: posterior/position, R: right/regressor, rh: rhombomere, V: ventral/velocity.

in young larvae. BP V neurons are almost absent from the hindbrain and the few present ones are in the area between the ABN and the OI in rh7/8 but restricted to more ventral areas than in young larvae.

BA P neurons are found in the whole hindbrain. They appear to be clustered denser throughout the ABN below the MLF (Figure 4-6a'), but they are also found in great number in rh7/8. Their distribution did not change in a notable way compared to that in young larvae, though their overall number increased dramatically (young: 38, late-stage: 88, per brain). This raises the question whether BA P neurons might be misclassified BP P neurons, which could explain the increase of the former and the decrease of the latter. However, like in young larvae, BP P neurons in the ABN are almost exclusively found in the most ventral parts (below -50 µm) in a much more clustered space than BA P neurons, which span a much broader area within rh5/6 (compare Figure 3-9 & Figure 4-6). Given that the increased number of saccades in the late-stage larvae experiments might have influenced the neuron classification of those groups and the fact that BP P neurons have a stronger velocity sensitivity than BA P neurons (Figure 4-3c), the increased number of binocular velocity events in the binocular stimulation phase (Supplemental Figure 7b) should actually increase the chance of identifying BP P neurons than for BA P neurons. Due to the anatomical location of BP P neurons and the already discussed differences between monocular and BA P neurons (see above), a systematical misclassification of BA P neurons to the disadvantage of one specific response group is unlikely.

BA V neurons in late-stage larvae are almost absent from the hindbrain. This is in sharp contrast to the case of young larvae in which BA V neurons were the most frequent velocity group (Supplemental Figure 13a & a'). The few BA V neurons in late-stage larvae are still found in the area between the ABN and the position clusters in rh7/8, with few BA P neurons intermingled between them. Given that the $PV_{Influence}$ for late-stage larvae's BA P neurons is larger (young: 0.46, old: 0.56; Figure 3-6c, Figure 4-3c), this renders a misclassification of neurons that could have led to the decrease in velocity encoding BP neurons unlikely. The spatial location of eye position encoding neurons outside of the eye velocity encoding cluster further supports this notion.

When comparing the clusters of eye position and eye velocity encoding neurons, a clear decrease of eye velocity encoding neurons in late-stage larvae becomes visible (Supplemental Figure 4b & b', Supplemental Figure 9, Supplemental Figure 13a & a').

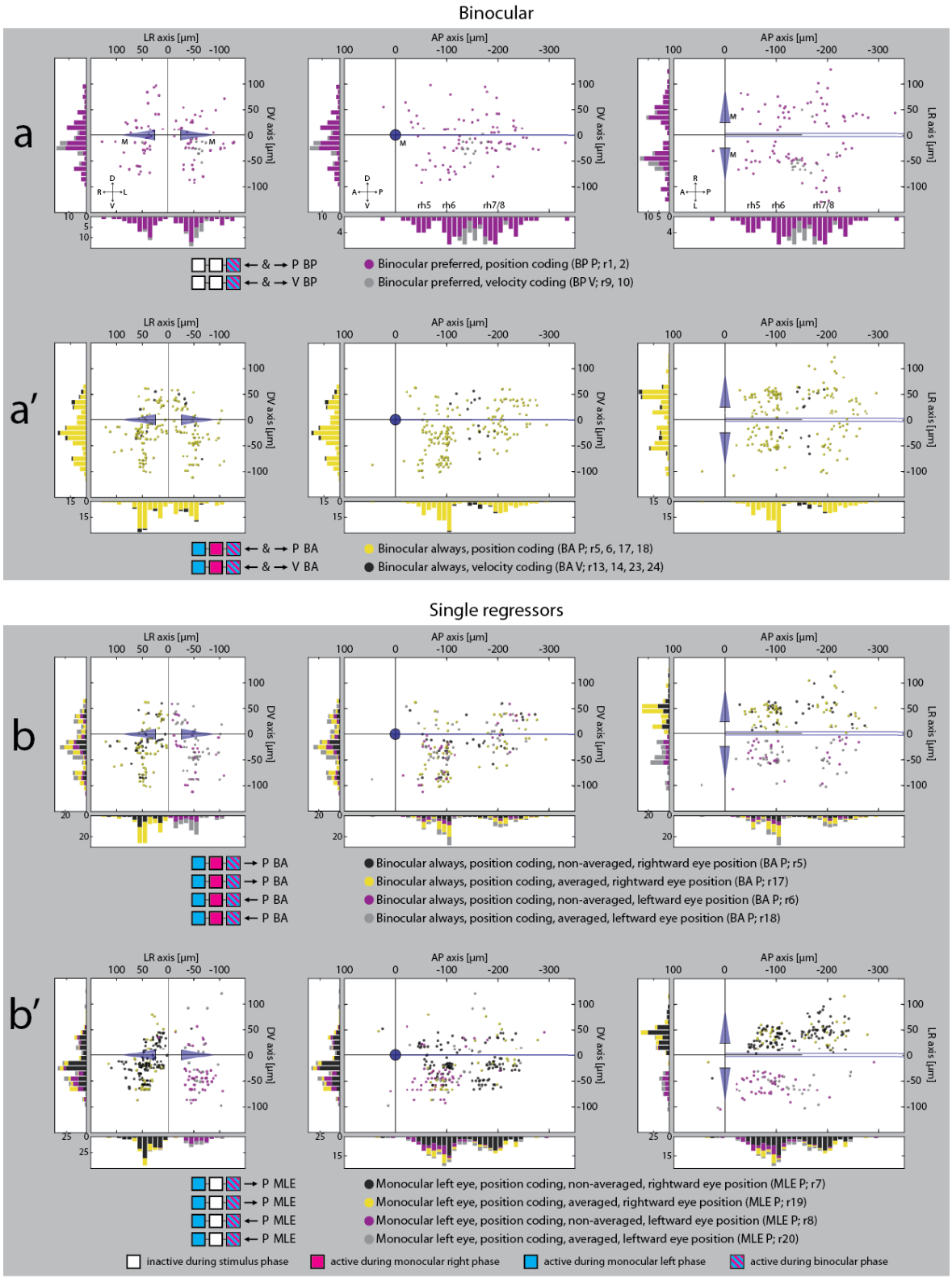

Figure 4-6: Binocular and single regressor cell maps for late-stage larvae

Spatial locations of identified binocular neurons and maps highlighting the distribution of cells identified by averaged and non-averaged regressors. **a-b':** Transversal, sagittal and dorsal views for BP eye position and velocity (a), BA position and velocity (a'), BA position, separated for each regressor, (b) and MLE position (b') encoding neurons in the larval zebrafish hindbrain. Each dot represents one neuron identified in one

recording with its highest correlation to the regressor in the respective legend. A: anterior, D: dorsal, L: left, M: Mauthner cells, P: posterior, R: right/regressor, rh: rhombomere, V: ventral.

While the general area occupied by velocity neurons is still between the ABN and caudal eye position encoding clusters in rh7/8, most velocity neurons are found below the MLF, in the area around the IO which is occupied by monocular eye velocity encoding neurons. Therefore, the earlier reported gradient from binocular eye velocity encoding neurons to monocular eye velocity encoding neurons in the rostral areas of rh7/8 in young larvae is not present for late-stage larvae anymore (Supplemental Figure 4b & b').

4.2.6 Summary

This experiment shows that late-stage larvae have a decreased ability to perform monocular eye movements and exhibit higher saccade frequencies than young larvae. The oculomotor neurons for horizontal eye movements of 14/15 dpf old zebrafish larvae can be classified into the same response groups as those of 5-7 dpf old larvae, but there are some notable differences. While monocular neurons in older larvae are generally comparable in number and location to young larvae, BP P neurons are less frequent and appear not to be clustered in the ventral ABN anymore. For BA P neurons, a strong increase in their cell number in the ABN is observed, which is accompanied by an almost complete lack of BA V neurons in the rostral parts of rh7/8, leaving the velocity system under almost exclusive monocular control. While the gap separating the putative INNs into two smaller clusters is not visible anymore, a rostro-ventral to dorso-caudal gradient from velocity to position encoding neurons is still present in rh7/8. In the caudal part of rh7/8, a flip from contralateral to ipsilateral monocular position encoding neurons can still be seen, but the switch from BP to BA neurons, as in young larvae, is not present anymore though the smaller number of identified neurons in this area renders this conclusion preliminary.

This shows that within just one week, key components in the oculomotor organization of zebrafish larvae undergo remarkable developmental changes and further highlights that the maturation of the oculomotor system is still ongoing after the conventional imaging time window of 5-7 dpf.

4.3 Experiment 4 (neuronal tuning in late-stage larvae)

4.3.1 Experimental framework:

Similar to experiment 3, the tests from experiment 2 were conducted with 14-15 dpf old zebrafish larvae. The results from this experiment will shed further light on the eye position/velocity tuning properties for each oculomotor neuron at a later developmental stage. The observed coding shift from eye velocity to eye position in the OI will be investigated to a greater degree than the more constrained analysis pipeline of the previous experiment was able to do (see chapter 1.5). The stimulation and data analysis were the same as for experiment 2, with only minor changes due to the increased size and behavioral differences (see next chapter, 2.4.2 & 2.7.1 for details).

4.3.2 Late-stage larvae show less velocity encoding and have shifted eye velocity thresholds

The aforementioned behavioral differences between young and late-stage larvae (Figure 4-2) were also affecting the larval performance during this experiment. To ensure the complete behavioral performance of larvae during the entire protocol in a timely manner and to prevent movement along the z-axis over time, some stimulation parameters were altered (e.g. repetition numbers, motor range, OKR duration; see chapter 2.4.2). This led to varying recording durations, since larvae which performed saccades frequently had problems finishing specific parts of the protocol especially in the “stable”-stimulation part (Figure 4-7a). In total 593 neurons were identified in 5 composite brains, between ± 70 µm around the Mauthner cells, of which 568 neurons could be attributed with a PV_{Index}. The 2-dimensional tuning curves show the presence of eye position, eye velocity, and intermingled encoding neurons, despite the decreased SNR compared to young larvae (Figure 4-7b-d). The decreased SNR was likely caused by the reduced recording time and the fact that saccades and 1.5 seconds after each saccade were excluded from data analysis which reduced the amount of data available.

The distribution of velocity encoding neurons between young and late-stage larvae changed in agreement with experiment 3. While the relative amount of strong eye position encoding neurons caudal to the Mauthner cells between young and late-stage larvae remained similar (young: 33 %, n=346; late-stage: 35 %, n=192), the relative number of strong eye velocity encoding neurons is strongly reduced in late-stage larvae in favor for

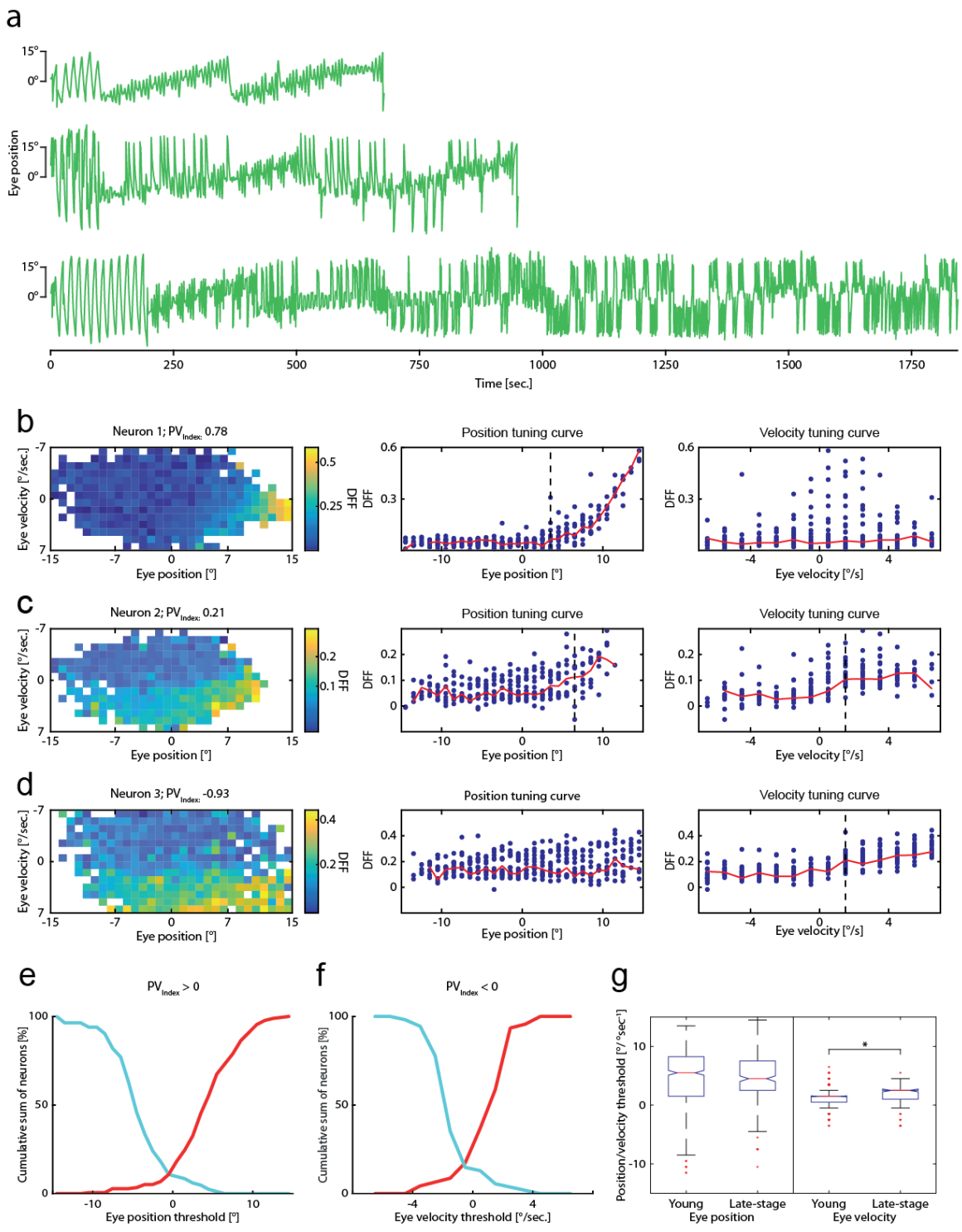

Figure 4-7: Eye position/velocity assessment for late-stage larvae

Example eye traces, 2D-tuning curves and threshold analysis for late-stage larvae. **a:** Eye position trace for 3 example recordings. Note the different number of saccades between the recordings. **b-d:** same as in Figure 3-10, but for late-stage larvae. **e:** Cumulative sum of identified eye position thresholds for position encoding neurons ($PV_{Index}>0$) pooled in ON direction for left (cyan, n=83) and right (red, n=175) side. **f:** Cumulative sum of identified eye velocity thresholds for velocity encoding neurons ($PV_{Index}<0$) pooled in ON direction for left (cyan, n=54) and right (red, n=46) direction. **g:** Comparison of eye position (left) and eye velocity

(right) thresholds pooled in ON direction for young and late-stage larvae. Data from e & f and Figure 3-10e & f.

intermingled encoding neurons (velocity: young: 14 %, n=149; late-stage: 3 %, n=16; intermingled: young: 53 %, n=550; late-stage: 62 %, n=341). Intermingled encoding neurons ($-0.5 < PV_{Index} < 0.5$) have their preferred direction for eye position and velocity to the same side (96 %, 79/82), similar to young larvae. Since no eye velocity threshold could be identified for most intermingled neurons (206 of 341 neurons), due to the above-mentioned reduced SNR, the number of neurons in this comparison is quite small.

The firing thresholds for eye position encoding neurons span the same range as in young larvae, roughly between ± 10 ° (Figure 4-7e). Despite a strong difference in the number of neurons identified for the left (n=83) and right side (n=175), no difference for the firing threshold in ON was identified (Wilcoxon rank-sum test: $p > 0.05$).
For the firing threshold of slow-phase eye velocity encoding neurons, late-stage larvae show a broader distribution than young larvae, starting around 4 °/sec (Figure 4-7f). However, the overall number of neurons exhibiting a firing threshold in the OFF-side decreased compared to young larvae and they are now more in line with eye position encoding neurons. While the number of velocity encoding neurons with an identified threshold was similar for the left and right side, neurons who encode leftward eye velocity have their thresholds shifted towards the ON-side by a small but still significant amount (mean firing eye velocity threshold in ON for leftward encoding neurons (n=54): 2.06 °/sec, rightward (n=46): 1.28 °/sec; Wilcoxon rank-sum test: $p < 0.05$).

No significant difference is observed for the eye position firing threshold between young and late-stage larvae (young: 4.73 °, late-stage: 4.61 °; Wilcoxon rank-sum test: $p > 0.05$). This shows that even with the integration of additional cell clusters into the group of eye position encoding neurons for late-stage larvae ($PV_{Index} > 0$, Figure 4-3f-h, Figure 4-10), the overall population coding does not change and is already optimized at a young age, assuming all measured signals are motor related.

In contrast, late-stage larvae have significantly increased eye velocity firing thresholds compared to their younger counterparts (young: 1.10 °/sec, n=372; late-stage: 1.70 °/sec, n=100; Wilcoxon rank-sum test: $p < 0.05$, Figure 4-7g). Similar to young larvae, some

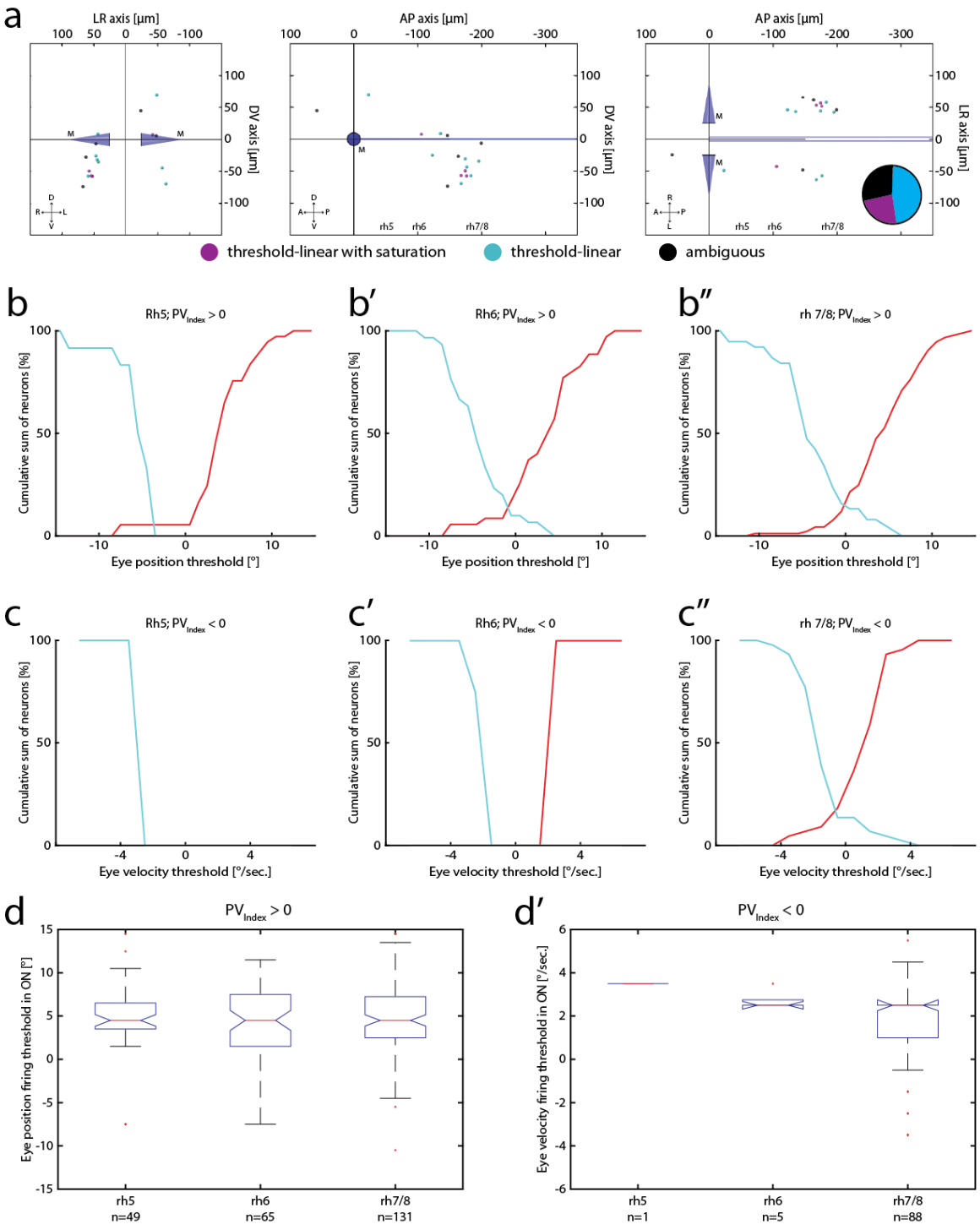

Figure 4-8: Firing threshold analysis for late-stage larvae

a: Transversal, sagittal and dorsal view of all strong velocity encoding neurons grouped regarding their velocity tuning curve (w/ saturation: 24 % (4/17), w/o saturation: 47 % (8/17), ambiguous: 29 % (5/17)). Pie chart showing the distribution of the different strong velocity encoding groups **b:** Cumulative sum plots of the eye position firing threshold for rh5 (b, left: 12, right: 37), rh6 (b', left: 30, right: 35) and rh 7/8 (b'', left: 38, right: 93) position encoding neurons pooled in the ON direction. **c:** Cumulative sum plots of the eye velocity firing threshold for rh5 (c, left: 1, right: 0), rh6 (c', left: 4, right: 1) and rh 7/8 (c'', left: 44, right: 44) velocity encoding neurons pooled in the ON direction. **d:** Eye position and velocity firing threshold pooled in

ON direction for different neuronal groups. (d: eye position. d': eye velocity, Kruskal-Wallis test, $p > 0.05$). Note the low number of velocity encoding neurons outside of rh7/8, which limits comparability.

late-stage high velocity encoding neurons show firing saturation as well. The relative distribution between saturating and non-saturating strong velocity encoding neurons stayed the same between both observed developmental stages (w/ saturation: 24 % (4/17), w/o saturation: 47 % (8/17), ambiguous: 29 % (5/17); compare Figure 4-8a with Figure 3-10g). Due to the change in velocity encoding neurons (as seen in experiment 3), all velocity encoding neurons were in the ventral parts of rh7/8 with no specific visible clusters between saturating and non-saturating neurons.

The clear separation between INNs and MNs in experiment 3 does not appear to be as prominent as in young larvae, though this could be an artifact resulting from the different fish sizes. Therefore, MNs and INNs in this experiment could not reliably be identified based on their anatomical location and only firing threshold comparisons between the different rhombomeres were conducted (Figure 4-8b-d'). While rh5 has a smaller range for the eye position threshold ($PV_{Index} > 0$), no significant difference between the individual rhombomeres could be identified (Figure 4-8d, Kruskal-Wallis test: $p > 0.05$). This changed from young larvae, in which rh7/8 had significantly later thresholds (Supplemental Figure 6a). Similarly, no difference for the eye velocity firing threshold is observed, though the low number of eye velocity encoding neurons outside rh7/8 strongly limits this comparison (Figure 4-8c-c'' & d').

A shift of eye position firing thresholds (P_{Thres}) for late-stage larvae into the OFF direction below the Mauthner cells and MLF is visible in rh 5 & 6 when looking at their anatomical arrangement (Figure 4-9a). This shift is comparable to the one found in young larvae and it is at the same location as the gap that separated the two INN groups in young larvae (Figure 3-12a, Supplemental Figure 4a).
Eye velocity firing thresholds (V_{Thres}) for late-stage larvae do not show any clustering or gradient, similar to their younger counterparts (Figure 4-9b).

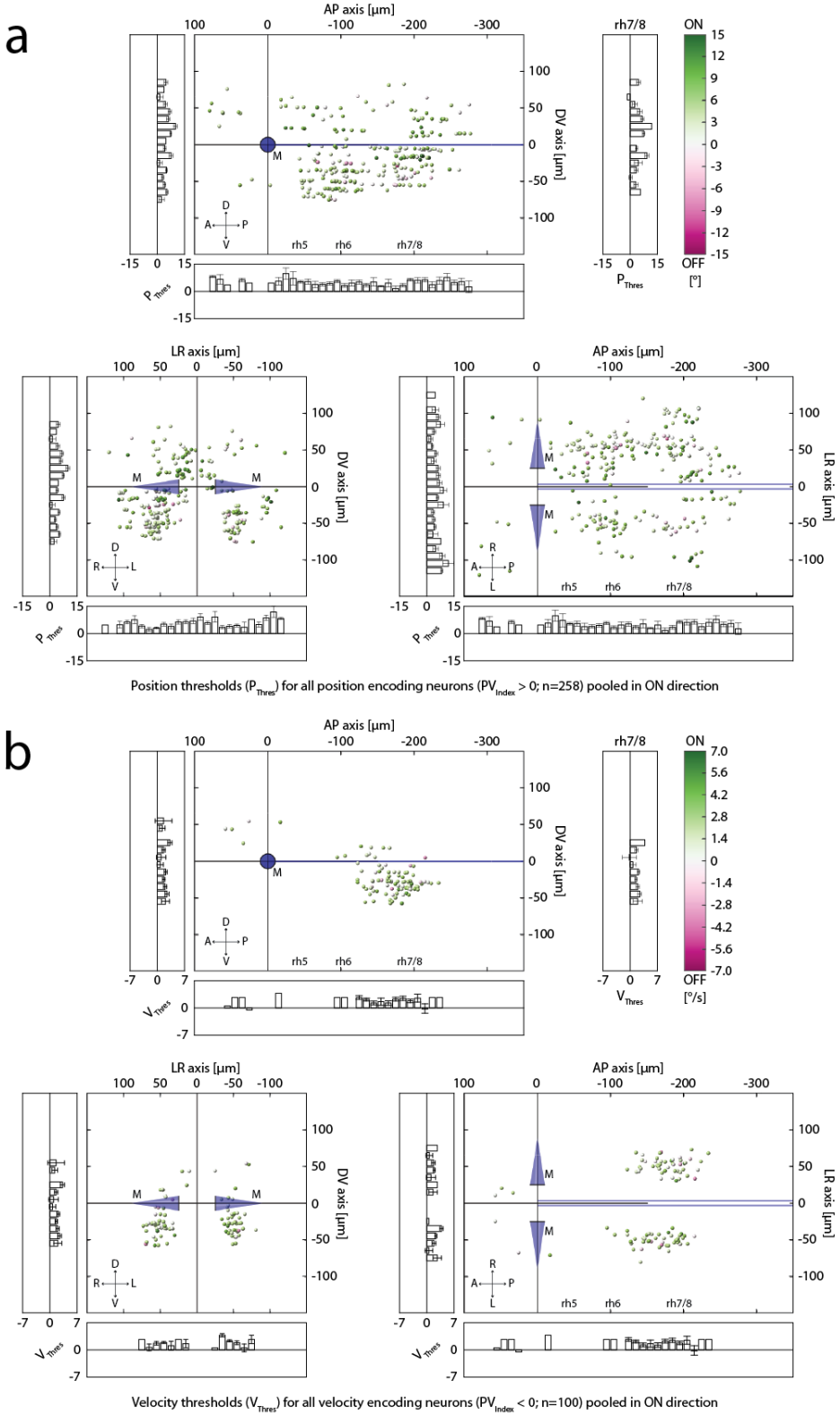

Figure 4-9: Firing threshold maps for late-stage larvae

Sagittal, transversal and dorsal views of eye position and velocity firing thresholds tuned in the respective ON direction. **a:** Eye position thresholds color-coded for all eye position encoding neurons (PV_{Index}>0, n=258) with an identified threshold. **b:** Eye velocity thresholds color-coded for all eye velocity encoding neurons (PV_{Index}<0, n=100) with an identified threshold. Error bars are SEM.

4.3.3 Oculomotor neurons in late-stage larvae are more eye position sensitive, but coding gradients still exist

The color-coded PV_{Index} maps (Figure 4-10) show a similar distribution of eye position and eye velocity encoding neurons as the maps obtained from the monocular/binocular experiments (Figure 4-4, Figure 4-6a & a'). To fully image the caudal hindbrain of late-stage larvae, the ARTR and the rostral parts of rh4 could only be imaged in animals with a small SL. Therefore, only few neurons in these areas were recorded and a comparison between young and late-stage larvae is not possible for those areas.

Oculomotor neurons in rh5 & 6 are predominantly eye position encoding with a PV_{Index} of 0.53 ± 0.34 (mean ± STD, n=176) and late-stage larvae thus exhibit a stronger eye position tuning than young larvae (0.42 ± 0.27, Figure 3-13). Within rh 5 & 6, around -30 µm below the MLF, a drop in the eye position sensitivity is present, like in young larvae. While these neurons do not form a clear "gap", as in 5-7 dpf old larvae due to the rigid body registration to a reference brain, the coding shift is still clearly visible when comparing the dorsal-ventral PV_{Index} plots in Figure 4-10a.

Neurons in rh7/8 have an average PV_{Index} of 0.18 ± 0.39 (mean ± STD, n=366) and are thus predominantly eye position encoding, but they still have a stronger eye velocity component than oculomotor neurons in rh5 & 6. The rostro-ventral and dorso-caudal eye velocity to eye position coding gradient is still present in late-stage larvae, but the overall velocity encoding is less than in young larvae (young larvae: -0.26 ± 0.51). Notably, the dorsal area between rh6 and the caudal part of rh 7/8, which contains the binocular eye velocity encoding neurons in experiment 1 (Figure 3-9a', Supplemental Figure 4b), is mostly devoid of oculomotor neurons, as it was the case for experiment 3 (Supplemental Figure 13b & b'). Along the left-right axis, neurons on the lateral extremes and closest to the midline show the strongest eye position encoding with eye velocity encoding neurons ~ ±50 µm lateral to the midline. Thus, the anatomical separation between medial eye position encoding neurons and more eye velocity encoding neurons in the rostro-lateral part of rh7/8 is still visible, as it is for young larvae (Figure 3-13).

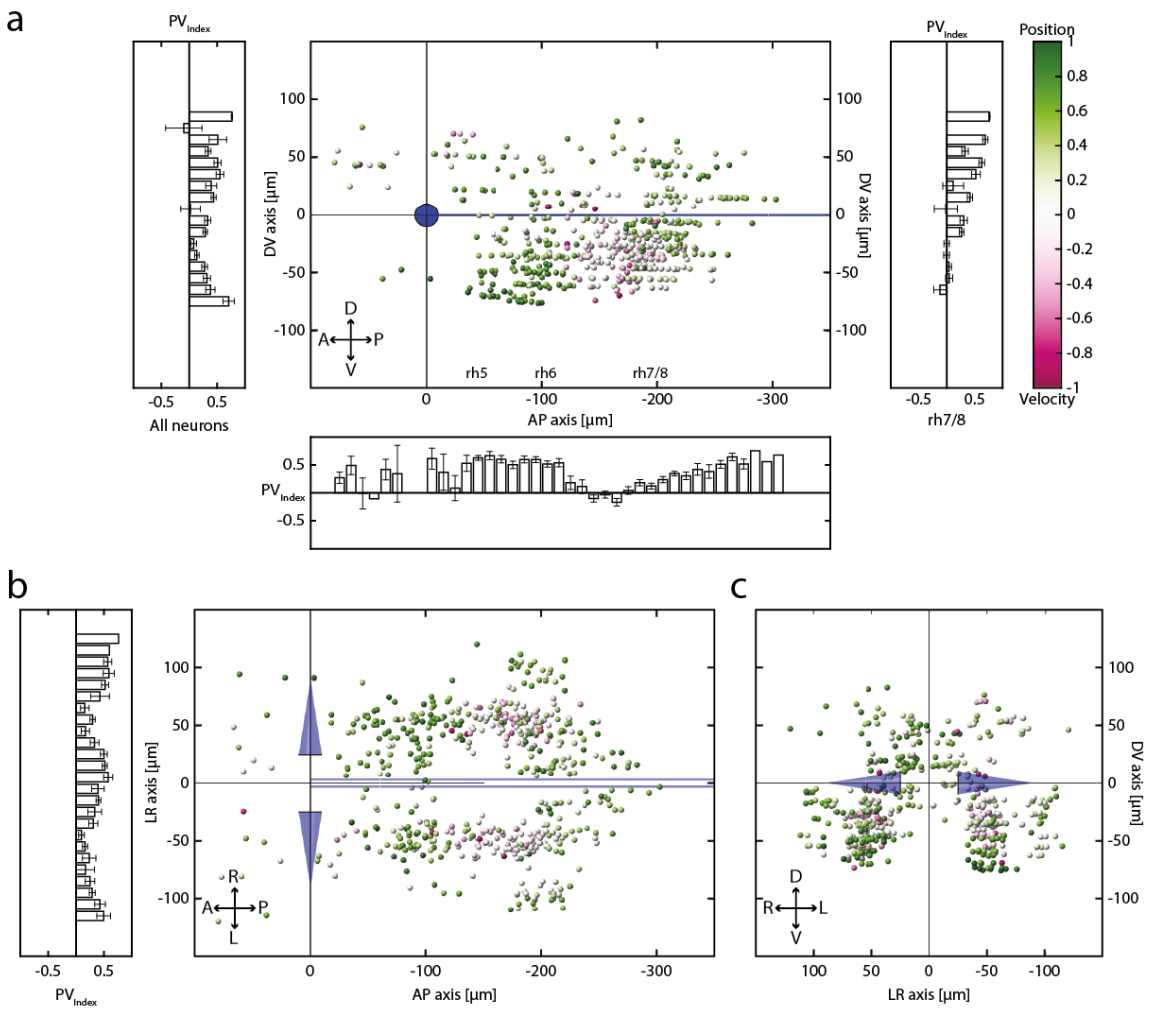

Figure 4-10: PV_{Index} maps for late-stage larvae

Anatomical location of all neurons color-coded for their PV_{Index}. **a-c**: Sagittal, dorsal and transversal views of all neurons with an identified PV_{Index} from experiment 4. A: anterior, D: dorsal, L: left, P: posterior, R: right, V: ventral; error bars are SEM.

4.3.4 Summary

The results presented here further support the findings from experiment 3 regarding the decrease of the number of eye velocity encoding neurons, especially the lack of identified neurons in the binocular cluster in the rostro-dorsal area of rh7/8. For the identified neurons, a strong shift from eye velocity encoding towards a more intermingled coding is observed. However, the identified gradient in rh7/8 is still present for late-stage larvae despite this coding shift.

The population coding for eye position neurons in the hindbrain is already quite mature in 5-7 dpf old larvae. Even with the integration of more neurons, the overall firing thresholds, and therefore the recruitment order, stay the same. The only observable difference is the shift in rh7/8, which is not significantly different from the other rhombomeres anymore.

However, eye velocity encoding neurons undergo some changes in the second week of development. While their relative numbers are strongly reduced, some neurons still exhibit the firing saturation in their velocity component. Even though eye velocity firing thresholds span a wider range, fewer neurons have their V_{thres} in the OFF direction, making them more similar to their eye position encoding counterparts. Late-stage larvae exhibit significantly later V_{Thres} than young larvae. Together with the overall drop in eye velocity encoding in the hindbrain, these results mark striking differences in the oculomotor tuning between the two developmental stages and shows that the oculomotor system is still maturing after one week of development.

Chapter 5: Discussion

5.1 Key results

The present study investigates the binocular coordination and eye position/velocity sensitivity of horizontal oculomotor neurons in the zebrafish hindbrain at two different developmental stages. This includes their anatomical distribution and a firing threshold assessment. These results provide insights into the organization of the OI and VSM. Additionally, it shows that the oculomotor system in young zebrafish is already well set to a large fraction after only one week of development. However, some notable differences are identified in late-stage larvae.

Oculomotor neurons are overwhelmingly encoding ipsiversive eye movements and can be classified into four distinct response groups, depending on their contribution to monocular eye movements. Monocular neurons, active during binocular and eye specific monocular stimulation, are the most frequent response type over all investigated structures (MNs, INNs, IO, OI, VSM). Based on those response profiles, the location of LR MNs are in the ventral part of the ABN and MR INNs are located dorsal to them. Putative INNs are separated into two subclusters by a faint gap, with reduced eye position sensitivity around that border. The OI consists mostly of monocular neurons that are encoding the contralateral eye, with only a few caudal neurons encoding eye movements for the ipsilateral eye.

Oculomotor neurons exhibit a wide range of eye position and/or eye velocity sensitivity with more centered firing thresholds for eye velocity neurons. Some of them exhibit firing rate saturation. In the region of the OI, a rostro-ventral to caudo-dorsal gradient from eye velocity to eye position encoding neurons is visible. Anatomically those neurons form two separate eye position and eye velocity clusters with only few neurons between them that show an intermingled response. No distinct gradients or spatial clusters for eye position nor eye velocity thresholds are visible within the OI.

With age, zebrafish show less decoupled eye movements and perform saccades more frequently. The amount of eye velocity encoding neurons drastically decreases in older animals, which is mostly caused by an almost complete absence of BA V neurons. This leaves the velocity system almost exclusively under monocular control. In the dorsal ABN, fewer eye position encoding neurons are found. BP P neurons are slightly less frequent in older animals, but they are not primarily clustered in the ventral ABN anymore and show a

more homogenous distribution throughout the hindbrain. On the other hand, there is a large increase in the amount of BA P neurons in the ventral ABN. Late-stage eye velocity encoding neurons exhibit later firing thresholds and a similar amount of saturation.

5.2 Oculomotor response groups

In the following chapters, the results regarding the different neuronal response groups are discussed. These chapters refer to the results from the 5-7 dpf old larvae of which some results have already been published and discussed by me earlier (Brysch et al., 2019b). Differences to late-stage larvae are discussed in chapter 5.4.

5.2.1 Rhombomeres 4-6

Neurons in the caudal hindbrain predominantly encode ipsiversive eye velocity or eye position. This agrees with other studies in zebrafish and goldfish (Aksay et al., 2000; Portugues et al., 2014). Based on the inferred coding properties of MR INNs and LR MNs as monocular, ipsiversive, eye position encoding, either as abducting (MN) or adducting (INN), MNs are located in the ventral part with a few sparsely scattered neurons in the dorsal areas of rhombomeres 5 & 6. Neurons that are following the INN code are located dorsal to the MNs and span a wide area closely up to the dorsal imaging border. They have only a small overlap with MNs. This clear separation in distinct MN/INN and rostral/caudal (rh5 & 6) pools resembles the arrangement in goldfish (Cabrera et al., 1992; Torres et al., 1992). In other species MNs and INNs also form distinct clusters e.g. in chick (Labandeira-Garcia et al., 1987) or intermingle to a variable degree e.g. in pigeon (Cabrera et al., 1989) or in mammals (Cabrera et al., 1988; Evinger et al., 1987; McCrea et al., 1986; Steiger & Büttner-Ennever, 1978). It should be noted that this functional identification is based on the tuning properties of individual neurons and not on their anatomical projections. I tried to validate the MN/INN classification using double transgenic larvae with photoactivatable GFP (*Tg(ubb:nls-GCaMP6f)m1300Tg* x *Tg(Cau.Tuba:c3paGFP)a7437*), but to no avail due to co-expression problems. Therefore, the MN location in the ventral parts of rh5 & 6 were only verified with genetic markers (Chandrasekhar, 2004; Jao et al., 2012). Monocular position neurons that share the neuronal code of MNs and some binocular neurons can also be found in the ventral areas of rh4, rostral to the ABN. As they are not labelled in MN specific lines, they are unlikely

to innervate the LR and probably provide an efference copy signal, since they carry a duplicate of the motor command and MNs do not provide the efference copy themself (Ghasia et al. (2008), Sparks et al. (1987); discussed in Shadmehr (2017)).

The INNs are subdivided into two clusters in each rhombomere by a faint gap with neurons with reduced eye position sensitivity around it (Supplemental Figure 4a, Figure 3-13a). As with MNs, this raises the question whether all putative INNs project to the OMN, or whether some neurons just share the same eye command with INNs and the two separate clusters are functionally different. While MNs generally outnumber INNs in the ABN by a significant amount (see the aforementioned publications), I find more INNs than MNs based on the monocular eye command code (experiment 1, see chapter 3.2.3) or a roughly equal amount based on the total number of neurons in each MN/INN containing region (experiment 2, Supplemental Figure 6). While there could be interspecies differences, a more plausible explanation is that not all neurons of the dorsal cluster innervate the OMN. A study reported the location of the MVN in zebrafish in the dorsal, medio-lateral part of rh5 & 6 (Schoppik et al., 2017). Here, the authors identify nose up/down tilt responsive neurons that project to nIII and nIV. While ablation of those neurons did not interfere with horizontal saccades, optogenetic activation of the general area in a pan-neuronal line did evoke some degenerated horizontal eye movements. Although the area identified by Schoppik and colleagues is more restricted than the dorsal INN cluster identified here, and includes only a smaller dorso-ventral extent, there is still some overlap. Therefore, these neurons might be part of the MVN and thus the OI, since the MVN is part of the OI in mammals (Leigh & Zee, 2006; McFarland & Fuchs, 1992; Mettens et al., 1994). This is in agreement with a recent pre-print study in which the authors used EM data to reconstruct neurons and their synaptic connections in the zebrafish hindbrain (Vishwanathan et al., 2022). Based on the obtained wiring diagram and network models, this study also proposes that some neurons in the dorso-medial areas of rh4-6 are part of the OI. Thus, it appears that the previously reported location of the OI exclusively in rh7/8 was too spatially constrained and the OI extends more rostrally (Daie et al., 2015; Miri et al., 2011a; Vishwanathan et al., 2017).

Binocular neurons in rh4-6 overlap with the monocular eye position encoding clusters (BA P), or cluster in the ventral ABN and intermingle primarily with MNs (BP P). It is not guaranteed that the BP P neurons innervate the LR and are therefore spatially concentrated with MNs. Given that MNs innervate only one eye, it is surprising that these neurons

would be active for both eyes and show preferential activity for conjugate eye movements. However, this is consistent with studies in monkeys in which ABN neurons have been shown to encode information for both eyes, though they just innervate one eye (King et al., 1994; Sylvestre & Cullen, 2002; Zhou & King, 1996). The binocular coordination and the preferential activity of some neurons for certain behaviors is further discussed in detail in chapter 5.2.3.

Several methodological constrains must be addressed regarding the classification of neurons as BP. Given the decreased OKR gain during monocular stimulation, especially in larger animals (Beck et al., 2004; Qian et al., 2005), neurons with stronger eye velocity sensitivity will show increased activity during the binocular stimulation phase. Figure 3-6c and Figure 4-3c show that BP P neurons have a small but significantly stronger eye velocity sensitivity than BA P neurons. This could have caused that some neurons appear to be preferentially binocular encoding due to the beneficial conditions for them in the binocular stimulation phase. Identified BP P neurons have surpassed the firing threshold analysis, meaning that they reached eye positions in the monocular stimulation phases that should result in increased fluorescence if they are not true BP encoding. Yet, the increased velocity sensitivity might have caused a higher fluorescence during the binocular phase and made them appear to be preferentially binocular encoding, as some BP P neurons also exhibit residual activity during monocular stimulation. However, this activity was not enough to classify them as either monocular or BA encoding (see chapter 3.2.2). Additionally, it should be noted that the BP P neurons are still primarily eye position encoding and were predominantly found in the ventral ABN in young larvae, an area that shows some of the strongest eye position sensitivity in the whole dataset (Figure 3-13a). Therefore, the increased sensitivity to eye velocity should be largely overshadowed by the actual encoding of eye position in BP P neurons.

5.2.2 Rhombomere 7/8

In rh7/8, three functional groups are the prime areas that contain oculomotor neurons: the IO, OI and the VSM (Area II). Each of these areas is discussed separately in detail in the following chapters.

5.2.2.1 Inferior olive

The IO is located medially at the ventral floor in the caudal part of the hindbrain (Figure 3-7; Takeuchi et al. (2015)). In this area, monocular eye velocity neurons and some eye position sensitive neurons were identified, with binocular neurons only at the very rostral part of the IO. However, all regressors that were used to identify those neurons are based on eye movements and are thus motor related. IO neurons project to Purkinje cells in the contralateral cerebellum via climbing fibers. While the zebrafish Purkinje cell output is modulated by eye and swim signals, the motor components in Purkinje cells likely stems from Granule cells rather than the IO (Knogler et al., 2017, 2019). Though some zebrafish IO neurons also show activity associated with eye and tail movements, this activity is rather limited for most cells ($R^2 < 0.3$), and those neurons are heavily outnumbered by sensory responsive IO neurons, though some show modulation during swimming events (Félix, 2020). Therefore, the IO neurons presented here could encode sensory information and just appear eye motor related due to the close resemblance of visual stimuli and eye movement signals during the OKR behavior (Portugues et al., 2014). One preprint study was investigating the responses of IO neurons to translational and rotational stimuli in zebrafish (Felix et al., 2021). The authors identified binocular rotation sensitive neurons in the rostro-lateral part of the IO. This cluster overlaps with the BA neurons in the rostral part of the IO (Figure 3-7 & Figure 3-9). Similarly, these neurons have their preferred direction to the ipsiversive side. However, given the already-mentioned lack of sensory regressors and the fact that most IO neurons were responsive to forward and backward motion in the preprint study, a stimulus not utilized in my experiments, the amount of IO neurons identified here is likely underestimated due to the underlying experimental conditions.

5.2.2.2 Oculomotor integrator

In zebrafish, OI neurons have been reported ~50 µm lateral from the midline in the ventro-caudal hindbrain, closely located to the IO. From there, they are stretching into more medial and dorsal regions up to ~30 µm dorsal of the MLF (Lee et al., 2015; Miri et al., 2011a, 2011b). The eye position encoding neurons identified in this study follow that pattern, but they also extend into the area of the IO. While the distribution of oculomotor neurons across individual zebrafish larvae is very conserved (Portugues et al., 2014), neuron location alone is generally a bad predictor of their function as oculomotor neurons

often intermingle with neurons that do not show any eye movement related activity (e.g. Fig. 5 in Lee et al. (2015), Fig. 4 in Miri et al. (2011b)). Therefore, functional groups of neurons in zebrafish do not necessarily cluster in distinctive nuclei and it is thus not surprising that no clear separation between the IO and OI is present (Arrenberg & Driever, 2013; Vishwanathan et al., 2022). The anatomy of eye position sensitive neurons in this area was investigated before and those results align well with the proposed integrator function for these neurons (see chapter 1.4.5.3). Additionally, I find some eye position sensitive neurons at the lateral edges of the hindbrain, roughly 100 µm away from the midline. Eye position sensitive neurons in this rough area have been reported previously in an EM study, but no axons for this cluster could be identified. Thus, anatomical evidence that these neurons belong to the integrator is still missing (Vishwanathan et al., 2017). While this EM study did only identify medial (<30 µm) integrator neurons at the border of rh6 & 7, a follow up EM and an additional imaging study found more medially located OI neurons in the caudal part of rh7/8 as well (Daie et al., 2015; Vishwanathan et al., 2022). In the data presented here (also see chapter 5.3.2 & Figure 3-13), a large proportion of the eye position sensitive neurons is located in the dorso-medial area of rh7/8. These neurons predominantly code for the contralateral eye, whereas ipsilateral eye sensitive neurons are hardly present and more restricted to the caudal end of rh7/8. While the eye specificity was assessed based on the fish's behavior, the rostro-caudal separation and ocular tuning of monocular neurons are conforming to the connectivity of reconstructed integrator neurons (Vishwanathan et al., 2022).

In monkeys, NPH/MVN neurons have been described as predominantly monocular encoding (Chen-Huang & McCrea, 1999). While some studies found an equal amount of ipsi- and contralateral monocular neurons (McConville et al., 1994; Sylvestre et al., 2003), other studies identified more monocular neurons for the ipsilateral eye (Zhou & King, 1996, 1998). In goldfish, 57 % of area I neurons (goldfish equivalent of the OI) are encoding for the ipsilateral eye and only 4 % for the contralateral eye during disconjugate eye movements (Debowy & Baker, 2011). Therefore, it is rather surprising that only few ipsilateral eye sensitive neurons were identified in this study. In zebrafish, eye specific time constants for post-saccadic eye drifts have been observed and they can be modified independently by altering visual feedback monocularly. This led to the hypothesis that the OI is subdivided into two clusters in each brain hemisphere that follow the Helmholtzian model for eye movement commands and each eye is independently controlled (Chen et al.,

2016; Debowy & Baker, 2011). While this hypothesis is supported by the strong eye specific wiring of oculomotor neurons in zebrafish (Vishwanathan et al. (2022), but see chapter 5.2.1), the lack of ipsilateral OI neurons here and of contralateral OI neurons in goldfish contradicts this assumption as the underrepresented eye would primarily be encoded only in the binocular context. However, unilateral lidocaine inactivation of the OI in goldfish showed that a single functional hemi-integrator can drive both eyes during ipsilateral eye positions, showing that each hemi-integrator encodes both eyes (Pastor et al., 1994).

Given the low number of ipsilateral encoding neurons in the caudal hindbrain, the question arises if they are a distinct functional group, or whether they were only identified due to noise. Based on my analysis protocol, the number of reported neurons is underrepresented. The conservative estimation of firing thresholds, while preventing a false-positive classification, will reduce the number of identified neurons. Integrator neurons have their firing threshold on the OFF-side (see chapter 1.4.5.2), but the iterative baseline approach, which was used to estimate the threshold, is skewed towards reporting thresholds as late. In combination with the challenge to detect single action potentials with GCaMP6f (Chen et al., 2013), the measured thresholds are shifted towards the ON-side (see chapter 3.3.3 & Figure 3-11). Therefore, the firing threshold analysis (Figure 3-5) will eliminate a large fraction of neurons solely because the fish could sometimes not offset the late firing thresholds with its explored motor range. This led to the exclusion of 26 & 36 % (experiment 1 & 3) of strong eye movement correlated neurons as no reliable classification of their ocular specificity could be made. Given the low fraction of contralateral monocular neurons in goldfish (4 %; Debowy & Baker (2011)), combined with the number of 25-40 neurons in each hemi-integrator (Daie et al., 2015; Pastor et al., 1994) and the caveats mentioned above, it can't be ruled out that the ipsilateral neurons form a functional relevant group. Similarly, ablation or optogenetic activation of only 6-12 neurons in the zebrafish pretectum is sufficient to abolish or provoke OKR behavior (Wu, 2019). Thus, partial sparse coding might be a common feature in the OKR circuit of zebrafish.

In the caudo-dorsal hindbrain, a coding shift for binocular neurons is also visible. While BP P neurons are more restricted to the rostral parts of rh7/8, BA P neurons are found more caudally, with a shift roughly at the same location as for the monocular neurons. While binocular neurons have been identified in the mammalian and teleost OI before (Debowy & Baker, 2011; Sylvestre et al., 2003; Zhou & King, 1996, 1998), no study reported the

preferential activity of neurons for only conjugate eye movements. Given the changes for BP neurons in late-stage larvae (see chapter 5.4), it is questionable whether the differences in coding between BA and BP neurons are a functionally relevant feature of the OI, or whether this phenomenon is only caused by immature neurons. However, it has been shown that the executed behavior has an influence on the eye preference of some neurons. 25 % of burst-tonic integrator neurons in the rhesus monkey changed their eye preference to a variable degree between disjunctive saccades and fixation (Sylvestre et al., 2003). Behavioral coding differences have also been reported for the zebrafish OI. Here, Daie and colleagues report that the spatial pattern of persistent firing for eye fixations changes depending on how this eye position was reached, either via saccades or via OKR (Daie et al., 2015). Based on their multi-mode model of the integrator, monocular ipsilateral & BA neurons in our data would primarily receive optokinetic input and the more rostrally located contralateral monocular & BP neurons would primarily receive saccadic input. Therefore, it would be interesting to see in a future study if the eye specification in zebrafish also changes with the executed behavior.

Several limitations regarding the ocular tuning should be addressed. Like the eye position and eye velocity classification, the ocular specificity was decided in a “winner takes it all” fashion that puts each neuron into a discrete group. Some of the above-mentioned studies also describe the eye sensitivity for integrator neurons to be more graded and not necessarily following a strict monocular or binocular classification (Debowy & Baker, 2011; Sylvestre et al., 2003), while one study did only find graded eye specificity in the abducens but not in the integrator (Zhou & King, 1996). The monocular coding index (Figure 3-6b) in my thesis also shows that MLE and MRE neurons are not clustered at the extremes but are more evenly distributed across the whole range with binocular neurons centered in the middle. Binocular events, such as saccades, might have influenced this analysis, but late-stage larvae, despite exhibiting saccades more frequently, show a stronger monocular sensitivity for MLE and MRE neurons (Figure 4-3b). This shows that zebrafish oculomotor neurons are also distributed along a gradient regarding their eye specificity. However, differences in the stimulation/analysis protocols limit the comparability to the other studies.

Apart from the differences in the OI activity based on the executed eye movements, one current preprint study investigated the activity of zebrafish neurons in tail-immobilized and

tail-free conditions (Sun et al., 2019). The authors identified a caudo-dorsal cluster of neurons in the hindbrain that overlaps with the location of the OI. Those neurons showed a strong correlation to eye position when the tail was immobilized, but their activity was reduced when the tail was free to move. The authors hypothesize that a tail movement efference copy is inhibiting the activity of the OI. Tail movement sensitive neurons have also been identified in the general vicinity of the integrator (Aksay et al., 2000; Lee et al., 2015; Sun et al., 2019; Vishwanathan et al., 2022) and the lack of specific locomotion regressors in my analysis could have masked some tail movement sensitive neurons as oculomotor neurons, comparable to the case of some early studies of the ARTR (see chapter 1.4.4). However, I can exclude that tail movements did influence OI activity in this study or that a large quantity of tail movement related neurons were identified in the first place for the following reasons: zebrafish that showed struggle behavior while being embedded were discarded from the analysis/not recorded in the first place (i), restrained zebrafish perform spontaneous swimming very infrequently (ii; Portugues et al. (2015)), and zebrafish become passive if movement commands do not produce the desired outcome (iii; Mu et al. (2019)) as it is the case in tail-immobilized larvae. Similarly, another current preprint study investigated neurons that form an integrator for self-location in the dorsal areas of rh7/8. This integrator biases future swimming events (Yang et al., 2021). While the authors hypothesize that these neurons are located in the NPH, their location is more lateral and dorsal than the eye position encoding neurons identified in my thesis.

5.2.2.3 Area II (VSM)

Area II neurons in zebrafish have been described in rh7/8, stretching from more medial locations at the border of rh6 & 7 to lateral positions in the caudal part of rh7/8 (Ma et al., 2009). The behaviorally identified eye velocity neurons follow the same pattern, best visible for the cluster of BA V neurons. The zebrafish's organization of area II and the OI thus resembles the same basic layout as found in goldfish, with area II being rostral and slightly ventral to the OI (Pastor et al., 1994), when following the traditional view of the OI being restricted to rh7/8. Given the above mentioned lack of nuclear organization in parts of the zebrafish oculomotor system, the close proximity of area II neurons to the IO (Ma et al., 2009; Straka et al., 2006) and the partial velocity encoding of the integrator (Delgado-García et al., 1989; Escudero et al., 1992; Miri et al., 2011a; Pastor et al., 1994), it is challenging to draw clear spatial boundaries between area II, the OI, and the IO.

However, the ocular specificity of proposed area II neurons also shows a lack of monocular encoding for the lateral rectus (ipsilateral eye), similar to the OI. Unilateral inactivation of area II causes deficits in both eyes (Pastor et al., 1994), showing that the BA V neurons compose an integral part of area II. In contrast to eye position encoding neurons, no distinct clusters of BP V neurons were identified. While BP P neurons are primarily found in the ABN and the OI, an area that makes direct connection to the ABN, area II neurons exhibit no direct connection to oculomotor nuclei (Straka et al., 2006). Therefore, the "binocular preferred" command might be motor exclusive and only needed in the position but not in the eye velocity domain. This separation of eye position and eye velocity commands likely represents an "ancestral condition" in teleosts compared to mammals (discussed in Pastor et al. (2019)).

5.2.3 Ocular control and task specificity in the larval zebrafish

Ever since their postulations more than a century ago, scientists tried to find an answer to which of the two competing theories from Ewald Hering and Hermann von Helmholtz regarding eye movement control is correct. While there is evidence in support of Hering's law of equal innervation (Mays, 1984; Mays et al., 1986; Zhang et al., 1991), recent findings tend to favor Helmholtz (King & Zhou, 1995; Sylvestre & Cullen, 2002; Zhou & King, 1998). However, so far no conclusive answer has been found as there is evidence that (dis)agrees with both theories (for review see Coubard (2013), Cullen & Van Horn (2011), King, (2011)).

Similarly, the results presented here do not conform to either theory completely. Most of the oculomotor neurons in the zebrafish hindbrain are monocular and thus correspond to the theory of Helmholtz, comparable to the large number of monocular premotor neurons in primates and goldfish (see chapter 5.2.1 & 5.2.2). On the other hand, the BA neurons are in line with the conjugate neurons in Hering's hypothesis, but the BP neurons are not as they are silent during monocular eye movements. The infrequent number of MLEX & MREX neurons and complete lack of MX neurons also support Helmholtz rather than Hering as these neurons encode a disconjugate eye movement signal. It would be interesting to see whether the zebrafish has dedicated vergence neurons for slow eye movements as well. The experiments presented here did not include a specific convergent/divergent stimulus and neurons specifically encoding vergence signals have

been identified in primates in the midbrain (Judge & Cumming, 1986; Mays, 1984; Mays et al., 1986; Quinet et al., 2020), an area not imaged here. Thus, our data cannot conclusively exclude the existence of slow-phase vergence neurons. A previous whole-brain imaging study using vergence stimuli did not find evidence for their existence either, though this study was not designed with that goal in mind (Portugues et al., 2014).

A recent study from our lab was investigating the ocular control during monocular, conjugate, and vergence saccades (Leyden et al., 2021). Similarly, burst neurons in zebrafish are also not following either theory completely. The largest group of burst neurons are of the conjugate type and thus conform to Hering's hypothesis. Vergence neurons, particularly for convergent saccades, were also identified. However, they show inconsistent activity during monocular saccades and thus do not strictly conform to Hering. Helmholtz specific burst neurons were also identified, but they showed inconsistent activity during conjugate and monocular saccades. Therefore, in zebrafish the control for the slow and fast eye movement system exhibit components from both hypotheses. Likewise to the preferential activity of BP neurons during conjugate eye movements, zebrafish burst neurons show saccadic-specific recruitment as some burst neurons show preferential activity for specific saccade-types (Figure 7 in Leyden et al. (2021)).

Such differential recruitment is reminiscent to the presence of SIF and MIF motoneurons. SIF/MIF are discussed to participate differently for specific eye movements, with SIF being responsible for fast eye movements and MIF for gaze holding and slow eye movements. However, newer studies suggest that they are not exclusively recruited, but rather act conjointly as both participate to a varying degree during all eye movements (Carrero-Rojas et al., 2021; Hernández et al., 2019). Similarly, a study in *Xenopus leavis* identified two distinct MN pools that encode different features during VOR but act in concert when generating eye motor commands (Dietrich et al., 2017). However, this study, and other work from the same lab, identified a specific class of motoneurons that were silent during slow eye movements and only active during saccades and for swimming efference-copy driven eye movements (Schuller, 2017). While these neurons were found infrequently, their reported activity would reflect true task-specificity between the slow- and quick-phase of the OKR. While BP neurons in the ABN are likely MNs (see chapter 5.2.1), their activity is better described as "preferential" rather than "exclusive". This response profile might result from the fact that they are primarily comprised of one specific

group of MNs. Their location in the ventral ABN suggest that they are SIF MNs, due to the increased soma size of ventral ABN MNs and their spatial overlap with the vu504Tg line, but in contrast to monkeys (Büttner-Ennever et al., 2001) no distinct connection between the soma size and the targeted muscle-fiber can be established in zebrafish (Asakawa & Kawakami, 2018). No relation between the firing threshold and the spatial location for the ventral MN group was found either (Figure 3-12). This indicates that MIF and SIF are intermingled in zebrafish, as MIF in cats exhibit lower firing rates and earlier recruitment (Carrero-Rojas et al., 2021; Hernández et al., 2019). However, this conclusion should be considered preliminary as the spatial information of BP neurons from experiments 1 & 3 can't be easily combined with the firing threshold data from experiments 2 & 4.

Regardless of their contribution as "exclusive" or "preferential", BP neurons provide an additional motor command that is only present during conjugate eye movements. This signal is not generated for monocular eye movements, as monocular exclusive neurons (MREX/MLEX/MX) are scarce or completely absent. MN activity for the LR & MR can be increased for the same eye position for convergent gaze in comparison to conjugate gaze. Further, this MN activity does not necessarily reflect the exhibited force of the innervated muscle (Miller et al., 2002, 2011). Thus, while the activity profile of BP neurons would argue for a stronger muscle activation during conjugate eye movements, further studies are needed to investigate if this activity also results in higher exhibited muscle force. A potential compartmentalization of the zebrafish EOMs, that hypothetically adds a secondary vertical and/or torsional action to the primary adduction/abduction movement (Clark & Demer, 2014; da Silva Costa et al., 2011; Peng et al., 2010), potential polyneuronal innervation of MIFs (Dimitrova et al., 2009; Jacoby et al., 1989; Liu & Domellöf, 2018), or muscle tension encoding (Davis-Lopez de Carrizosa et al., 2011) could account for differences in MN activity to the expected eye position.

The preferential innervation and activity of MNs for different types of eye movements has long been discussed (Horn & Straka, 2021; Pastor et al., 2022). The different activity of saccade associated burst neurons from Leyden et al. (2021) during quick eye movements and the response profile of BP neurons during slow-phase OKR provides further evidence for task separation in the oculomotor system that is present even within the same type of eye movement and not just between different types.

5.3. Coding properties of oculomotor hindbrain neurons

The following chapters discuss the coding properties of hindbrain neurons for 5-7 dpf old larvae. Some results have already been published and discussed by me earlier (Brysch et al., 2019b). Some differences to late-stage larvae are discussed but see chapter 5.4.

5.3.1 Firing thresholds

Eye position firing thresholds span a wide range, with some neurons having their threshold already on the OFF-side. MNs, INNs, and rh7/8 position neurons have their mean firing threshold on the ON-side, with rh7/8 position neurons exhibiting significant later thresholds (Supplemental Figure 6). This disagrees with previous reports where integrator neurons had their firing thresholds almost exclusively on the OFF-side (Aksay et al., 2000, 2007; McFarland & Fuchs, 1992) and more centered thresholds for ABN neurons, especially for MNs (Delgado-Garcia et al., 1986a, 1986b; Fuchs et al., 1988; Pastor et al., 1991; Pastor & Gonzalez-Forero, 2003). My conservative estimation of the firing threshold (see chapter 5.2.2.2) can account for a population shift towards the ON-side, but this should not affect the distribution between different neuronal populations. While these inconsistencies to the previous studies could have been unraveled by the clear separation of eye position from eye velocity in this study, inter-species differences could also exist. However, a more probable explanation is that the limited classification based on the anatomical position of MNs and INNs alone is insufficient and not every eye position encoding neuron in rh7/8 is necessarily an integrator neuron. Together with the possible extension of the OI into more rostral parts of the hindbrain, a clear separation between the OI and other oculomotor neurons without specific genetic markers is challenging and thus potential differences between the groups might be washed-out by a suboptimal neuronal classification. However, the significant differences between rh5 & 6 and rh7/8 vanish in late-stage larvae as the eye position firing thresholds in rh7/8 are shifting towards the OFF-side. This points towards a maturation/fine-tuning of integrator neurons with age, though this development is not yet complete at 14/15 dpf as they are still predominantly shifted towards the ON-side.

Eye velocity encoding neurons have more centered thresholds distributed across a narrower range. Some have their firing thresholds on the OFF-side, similar to reports in goldfish (Beck et al., 2006; Pastor et al., 1991). While my thesis was just investigating the

tuning for slow-phase eye velocity neurons, zebrafish saccadic burst neurons generally also show the same tuning towards one preferred direction, but they are also not exclusively direction selective and exhibit activity during small OFF direction saccades as well. This coding preference points towards a push-pull arrangement in which the activity of two opposing populations of excitatory and inhibitory neurons are summed up and potentially cancel out at the level of motoneurons (Leyden et al., 2021; Van Gisbergen et al., 1981). Thus, the weak activity in the non-preferred direction is a feature that is not restricted to the level of the MNs alone but also of higher up-stream areas, including the OI. This might help in fine-tuning the activity around the resting eye position. However, the vast majority of slow-phase eye velocity neurons in our recordings should correspond to area II neurons and are thus not innervating the MNs directly, but provide mossy fiber input to Granule cells in the cerebellum (Beck et al., 2006; Straka et al., 2006). They are a likely source of the eye movement signals that have been shown to be present in zebrafish Granule cells (Knogler et al., 2017, 2019) and supplement the limited motor signals stemming from the IO (Félix, 2020).

The saturation of some eye velocity neurons came as a surprise, as oculomotor neurons in the OI are described as threshold-linear and no saturation is observed for MNs and INNs within the oculomotor range (see chapter 1.4.5.2; Delgado-Garcia et al. (1986a, 1986b)). However, some OI neurons in goldfish have been reported to show a "nonmonotonic persistent firing" where their activity either stopped increasing or decreased at more eccentric eye positions (Aksay et al., 2003; Major et al., 2004b). Some models of the OI achieve the proposed line-attractor dynamics based on the progressive recruitment of neurons to compensate for hypothetical saturation (Gonçalves et al., 2014; Seung et al., 2000). However, in these models the saturation is constrained to the synapses and not to the neuronal firing itself. In a more recent approach to model the OI, it was shown that circuits based on synaptic saturation do not comply to other biological constraints of the integrator and linear/sigmoidal synaptic activation functions are more likely to be present (Fisher et al., 2013). We only find saturation in slow-phase eye velocity neurons outside of areas linked to the OI in zebrafish, predominantly in area II neurons. Based on the anatomical location and the newer models of the OI, I conclude that the observed saturation in the present study is not a necessary component for the integrator to function.
In goldfish, some area II neurons have been reported to show non-linearities with increased stimulation frequencies for both OKR & VOR and, especially for vestibular stimulation, a

decreased sensitivity for larger eye velocities. While decreased sensitivity can lead to the observed saturation, a contribution of stimulus/slip velocity in the area II activity can be neglected (Beck et al., 2006). The saturation and narrow range of eye velocity thresholds might help to fine-tune the oculomotor system around the resting state and the tuning to low frequencies acts as a low-pass filter to stabilize the OKR performance during brief stimulus interruptions (Beck et al., 2004, 2006; Chen et al., 2014).

Apart from the slight shift towards the non-preferred direction around the gap separating the two putative INN clusters in the ABN, no spatial arrangement for the firing thresholds could be identified within the ABN or the OI. This conforms to the limited data available in squirrel monkeys and goldfish (Aksay et al., 2000; McCrea et al., 1986). Similarly, no connection between a reported soma size gradient for MNs and the firing thresholds could be established (Asakawa & Kawakami, 2018). Based on the aforementioned modelling study, Fisher and colleagues reported that there can be a functional difference between high and low threshold neurons in the OI. In a neuronal recruitment threshold mechanism model, the low threshold neurons would be used for read-out while the high threshold neurons would be used to maintain the persistent firing (Fisher et al. (2013), but see Major et al. (2005)). While there is no real gradient visible for the eye position threshold distribution in rh7/8, more dorsal neurons appear to have higher eye position thresholds. This is predominantly true in the medial areas that overlap with the location of the OI. Neurons in this area are excitatory and they are the only OI neurons that project to the ipsilateral OI (Lee et al., 2015). Neurons with this projection pattern are expected to form the recurrent network that is thought to generate the persistent activity (see chapter 1.4.5.1). However, OI neurons are generally described as having their firing threshold shifted towards the non-preferred side while in our dataset they exhibit significantly later thresholds than any of the other neuronal groups (see above).

5.3.2 Eye position/velocity encoding & OI circuit organization

In rh7/8, there is an anatomical rostro-ventral to caudo-dorsal gradient of eye velocity to eye position encoding neurons (as shown by the PV_{Index}), spanning from supposedly area II neurons to areas previously reported to contain the OI. This gradient resembles a feedforward model of the OI in which the integration from eye velocity to eye position happens gradually with neurons encoding intermediate steps between dedicated input

(velocity) and output clusters (position encoding). A similar rostro-caudal gradient has been identified for the persistence time in the zebrafish OI before, with caudal neurons exhibiting longer persistence times than rostral neurons in rh7/8. This heterogeneous activity would similarly favor a network model of the OI that is biased in a feedforward manner and the neurons with a longer persistence time would be used as a readout of the OI (Miri et al., 2011a). The potential readout neurons from Miri and colleagues overlap anatomically with the previously discussed eye position neurons with somewhat late firing thresholds (see chapter 5.3.1) and the PV_{Index} maps show the highest eye position encoding in these parts as well. Together, the spatial aggregation of neurons with long persistent firing, strong eye position encoding, and late firing thresholds would support the notion that these neurons are the final step of the velocity to position transformation in the OI. However, this heterogeneity of neuronal responses does not conform to the classical line attractor model of the OI. Additionally, Miri and colleagues recently showed in a follow-up study that this heterogeneity is needed to counteract the viscoelastic components of the oculomotor plant. The OI achieves this by integrating the eye velocity command not in an uniformly manner but via multiple distributed timescales (Miri et al., 2022). Similarly, studies in primates (Joshua et al., 2013; McFarland & Fuchs, 1992) and cats (Delgado-García et al., 1989; Escudero et al., 1992; Lopez-Barneo et al., 1982) also showed strong heterogeneity in the MVN/NPH regarding the eye velocity/position encoding. They are in line with a more hierarchical model of the OI (Joshua & Lisberger, 2015) “in which a progressive decrease of eye velocity sensitivity [is] accompanied by a proportional increase in eye position sensitivity” (Delgado-García et al., 1989). While these results argue against a strict implementation of the classical line attractor theory, a recent study investigated the short-term memory formation in the anterolateral motor cortex in mice that predicts the direction of upcoming motor actions (Daie et al., 2021). The authors found that smaller, interconnected, recurrent modules in the circuit produce and maintain the persistent activity independently from each other. They propose a modular attractor model with a tunable heterogeneous connectivity between each module. A similar modular model was already proposed for the oculomotor integrator in the past (Crawford & Vilis, 1993). To fully understand the role of single neurons in this network, knowledge about their precise connections was needed to explain some of their heterogeneous behaviors (Daie et al., 2021). Thus, information about the neurotransmitters/transcription factors (Lee et al., 2015), anatomical connections (Vishwanathan et al., 2022), and coding preferences (Daie

et al., 2015; Miri et al., 2011a) of zebrafish OI neurons would be needed, ideally from a single experiment, to investigate whether the OI is also comprised of a similar modular structure. Additionally, optogenetic studies could also be used.

While the PV_{Index} and several other publications describe the neuronal code in the OI as heterogeneous, the exact anatomical locations of eye position and eye velocity neurons in rh7/8 are more separated than the distribution of the PV_{Index} along the RC and DV axis might suggest (Figure 3-13). This stricter spatial separation follows the arrangement in goldfish (Pastor et al., 1994) in which no position/velocity gradient was identified (Aksay et al., 2000). Additionally, the above-mentioned rostro-caudal gradient for the persistence time, that aligns with the PV_{Index} gradient, is present after saccadic input but it is flipped for OKR driven eye movements (Daie et al., 2015). However, saccadic events were cropped from the data presented here and they are absent in the 2D-tuning curves and the PV_{Index} which were only generated from the slow-phase part of the OKR or during stable stimulation. It is thus questionable, if the PV_{Index} gradient resembles the persistence time gradient described earlier as Miri and colleagues used spontaneous (saccadic) eye movements to generate their data. Furthermore, they only imaged neurons 20-70 µm lateral of the midline (Miri et al., 2011a), which excludes most of the caudo-dorsal eye position encoding neurons identified in this thesis. Therefore, the eye position/velocity gradient shown by the PV_{Index} might just stem from the partial overlap of eye position/velocity encoding neurons along the RC/DV axis in the caudal hindbrain (Figure 3-13b) but does not necessarily reflect the continuum of eye position/velocity encoding within the OI as seen in mammals. Additionally, midline lesions and unilateral inactivation of the OI in mammals causes severe bilateral gaze holding deficits (Anastasio & Robinson, 1991; Arnold & Robinson, 1997; Arnold et al., 1999; Cheron & Godaux, 1987; Straube et al., 1991), which is not the case in gold- and zebrafish (Aksay et al., 2007; Debowy & Baker, 2011; Pastor et al., 1994), highlighting additional inter-species differences. Selective inactivation and anatomical tracings are needed to determine whether the velocity and intermediate encoding neurons in zebrafish are actually involved in the generation of the OI command, are just immature neurons who are not yet fully integrated into the circuit (see chapter 5.4), or whether they belong to area II.

5.4 Ontogeny of the oculomotor system

5.4.1 Experimental constrains

In experiments 3 & 4, the already discussed experiments were repeated in 14-15 dpf old larvae. While it would be interesting to compare this data to even older animals, as the maturation of the zebrafish brain is not complete at two weeks of age, several limitations that come with older larvae had to be considered to achieve reliable recordings. First, for older animals the passive water flow over the gills is not sufficient for survival and therefore intubation, pumping oxygenated water through the mouth, is required (Olt et al., 2016; Xu et al., 2015). This potentially interferes with eye movements/behavior and requires anesthetization of the fish via MS-222, a sodium channel blocker, which needs to be washed out for up to 90 min until neuronal activity is restored to native levels (Johnston et al., 2013; Palmer & Mensinger, 2004). Secondly, the increased thickness of the skull in older/adult animals requires removal of the skin and thinning of the skull to reliably image deeper tissues (Barbosa et al., 2016). Thirdly, with increased age/SL it became harder for the software to reliably identify the eyes. The 2nd LED ring would cause reflections and the start of the ossification, primarily the development of the anguloarticular and interopercle (Cubbage & Mabee, 1996; Parichy et al., 2009), would start to overshadow the eyes as the CMOS camera, which was used for eye detection, was mounted at the bottom part of the stage. Taken together, this resulted in a sharp drop of successful recordings after 15 dpf in a pilot study (Omejc, 2019) and, together with the decreased behavioral performance discussed below, limited the age at which these types of experiments could be performed reliably with the available setup/experimental paradigm. However, while some behaviors are only developing after 14 dpf (e.g. aVOR), some notable changes are already happening within the zebrafish OI at that age. The time constant significantly increases (starting at 4.2 mm SL) and in larger animals (>5.3 mm SL) the leaky decay of eye position after spontaneous saccades changes from an exponential decay to a more linear decay as seen in adults (Beck et al., 2003). However, the additional week of development is enough for newborn neurons to fully integrate into existing neuronal circuits (Boulanger-Weill et al., 2017). Therefore, the use of 14/15 dpf old zebrafish is justified to investigate the ontogeny of the OI, though it should be noted that the maturation of the OI is not yet finished at this stage. At the developmental stages investigated in this study, the input to the OI is primarily driven by the OKR, tVOR and spontaneous eye movements (Lambert et al., 2008; Mo et al., 2010). With the integration of the aVOR signal at a later developmental

stage, the OI has to adapt to an additional input stream (Beck et al., 2003). Therefore, the results presented here show how a system matures and optimizes its performance under somewhat constant biological conditions, while any future changes to the OI circuit have to acknowledge the changed task profile by the future integration of the aVOR-signal.

5.4.2 Increased yoking and saccadic frequency in older larvae

Older larvae perform more saccades and show a decreased capability to execute monocular eye movements. Similarly to the data presented here, an earlier study in zebrafish, medaka, and goldfish reported an increased frequency for the quick-phase of the OKR and for spontaneous saccades in larger animals (Beck et al., 2004). This study also reported the decreased capability of older zebrafish to perform monocular eye movements. On the other hand, *Xenopus laevis* larvae, at a comparable developmental stage, exhibit a slight decrease in conjugacy (stages 47-59), until it drastically drops for larvae at metamorphic climax and for froglets. However, this decrease is likely caused by the transformation from a lateral eyed, swimming larvae into a frontal eyed tetrapod which limits the comparability to zebrafish (Schuller, 2017).

In zebrafish, the gain during binocular OKR stimulation increases with development. However, during monocular stimulation the gain of the unstimulated eye largely stays the same while the gain of the stimulated eye decreases (Beck et al., 2004). This shows that the increase in conjugacy in older animals is mainly caused by an inability to move the stimulated eye, rather than increased yoking of the OFF eye as a naïve interpretation of my YI might suggest. At the beginning of each experiment, every zebrafish was tested for its ability to perform monocular eye movements. In young larvae, only ~5 min of an adaption period was needed to achieve a reliable decoupling of the eyes, while up to 1 h was necessary for some late-stage larvae (see chapter 2.4.1). Unfortunately, this period was not recorded and no quantifications can be made. Nevertheless, this shows that the binocular response to monocular stimulation can be actively altered in older larvae. In the context of oculomotor control, Helmholtz proposed that oculomotor control is monocular and binocular coordination must be learned. A decreased capability to perform monocular eye movements and an increase in conjugacy in zebrafish with age can thus be seen as a small win for Helmholtz. Similarly, the longer adaption time needed for experiment 3 might

indicate that zebrafish “unlearn” the previously learned conjugacy to exhibit a higher degree of monocular eye movements.

5.4.3 Changes in eye specific encoding

As already described in chapter 5.2.2.2, oculomotor neurons form a continuum regarding their eye specificity (Debowy & Baker, 2011; Sylvestre et al., 2003; Zhou & King, 1996). The results from this thesis show that the monocular preferences for MLE & MRE position neurons become significantly stronger with age (Figure 4-3b). In combination with the additional changes discussed below, this shows that the oculomotor system in zebrafish is still maturing after 7 dpf, which is reflected in the tuning of the underlying neurons. Furthermore, it has been proposed that the visual system in zebrafish is under adaptive control in which neurons can change their relative connection strengths between the eyes to counteract changes caused by disease and aging (Chen et al., 2016). Somewhat similarly, some neurons in the mouse dorsal lateral geniculate nucleus have binocular connections but are functionally monocular. Synaptic refinement and input selection has been identified to drive the monocular specification, with inputs from the preferred eye resembling values in adult mice and inputs from the non-preferred eye remaining in a juvenile state (Bauer et al., 2021). A similar synaptic maturation can be the underlying cause for the increased monocular encoding of MRE/MLE neurons.

It is unclear from this data if these changes are hard-wired or whether they are shaped by visual experience. Early oculomotor development in zebrafish, including that of the OI, has been described as primarily genetically driven, with neuronal activity used for optimization but not required for development (Ulrich et al., 2016). Other studies in zebrafish showed that visual input shapes the visual sensitivity and tectal activity during a critical period between 5-7 dpf (Avitan et al., 2017; Xie et al., 2019), while other studies (partially) argue for a predetermined development as well (Nevin et al., 2008; Pietri et al., 2017). Regardless the cause, neuronal changes happening during/after the time window of the young larvae’s experiments lead to an optimized behavioral output (Avitan et al., 2020), or completely change the outcome of the underlying behavior (Harpaz et al., 2021). Thus, the increased monocular specificity identified in this thesis could underlie a similar optimization process.

With the increase of the monocular coding strength of MLE/MRE neurons, their relative number in late-stage larvae also changed. MLE P neurons are slightly more common in older larvae, but at the same time the amount of MRE P neurons drastically decreases (Figure 4-3f-g). Given the relative equal number of MRE P neurons in young larvae, it is rather surprising that their distribution changed with age, given that most horizontal eye movements in zebrafish are conjugate under natural conditions. Asymmetric projections of vestibular interneurons have been identified in zebrafish, where motoneurons that move the eyes downwards receive stronger innervation (Schoppik et al., 2017). However, these asymmetries, which are already present at 7 dpf, are not eye specific but direction specific, for which environmental requirements do exist. On the other hand, behaviorally different eye specific usage has been described in zebrafish. The left eye is preferentially used to investigate a novel stimulus, while the right eye is used to approach a target and for biting (Miklósi & Andrew, 1999, 2006; Miklósi et al., 2001). Teleost fish also have a preferential eye when viewing conspecifics (Sovrano, 1999). This preference is flipped in situs-inversus zebrafish (*fsi*), in which the neuroanatomical and visceral organization is mirror symmetric, indicating that these behavioral asymmetries are reflected in the neuronal code (Barth et al., 2005). While the difference of monocular eye specific neurons might reflect a different eye usage, it is still unclear why the right eye would be controlled by fewer neurons with age. Potential experimental intricacies might be the underlying cause for these differences, such as lighting differences between the two half arenas or unequal blocking of the binocular zone as no systemic OKR asymmetries between the eyes were identified in a previous study (Dehmelt et al., 2021). The authors contributed external factors and individual fish biases as the cause for some small asymmetries in the OKR gain between the left and right eye, rather than a general asymmetry of the OKR system.

Together with the increased monocular MLE/MRE encoding, BP P neurons also exhibit developmental changes. Their relative amount decreases only slightly, but they do not cluster in the ventral ABN anymore. While it is possible that the missing BP P neurons went into apoptosis before the 2nd week, they also might have changed their eye specificity to either monocular or BA P. The latter are much more common in older larvae, implying a possible transformation of BP P into BA P neurons. However, BA P neurons are more spread out in the ABN below the Mauthner cells and occupy areas dorsal to the location of BP P neurons in younger larvae. The increased amount of BA P neurons is therefore not the sole cause for the decrease of BP P neurons. The increased number of saccades likely

contributed beneficially to the increase of identified BA P neurons, but a systematic misclassification to the disadvantage of one particular oculomotor group seems unlikely (see chapter 4.2.5). Similar to the increased monocular specificity of MLE/MRE P neurons described above, a strengthening of eye specific connections for BP P neurons can lead to the observed results. However, this would mean that at 5-7 dpf a large part – and at later developmental stages potentially the whole group – of BP P neurons are just immature and their specific binocular response profile might vanish during development. But why would that class of neurons be needed in the first place? Given their ventral location, these neurons are relatively old and already had enough time to get fully integrated into the oculomotor system (Kinkhabwala et al., 2011). If they truly form a specific subgroup of MNs, why would their unique response profile be needed at 5-7 dpf, when EOMs are already adult-like at 3 dpf (Easter & Nicola, 1996)? A major reorganization of a neuronal circuit with increased age is not unheard of in zebrafish. Spinal locomotor neurons have been reported to alter their connectivity and even change the function of the underlying circuit in adults compared to larval fish (Pallucchi et al., 2022). However, the neuronal reorganization reported in my thesis is happening on a much shorter timescale and is thus unlikely to be necessary due to the increased size of the fish as it was concluded for the locomotor neurons. Future studies at later developmental stages are needed to investigate the fate of the remaining BP P neurons, the origin of the additional BA P neurons, and to identify if the BP class is a functional relevant group or whether it's just comprised of immature neurons. Similarly, the decreased amount of eye position encoding neurons in the dorsal ABN/putative MVN remains to be elucidated. A possible coding shift with the emergence of the aVOR might be a plausible cause.

5.4.4 Decreased eye velocity encoding and the maturation of the OI

One striking feature in late-stage larvae is the decreased eye velocity encoding in all four major response groups, primarily in the BA type (Supplemental Figure 13a & a'). This leaves the velocity system under almost exclusive monocular control. Based on the stereotypical spatial organisation of the velocity encoding neurons, a large dorsal cluster of velocity encoding neurons in the rostral area of rh7/8 is now missing. Given their location, it is likely that the remaining rostro-dorsal neurons are putative OI neurons and the question arises if this coding shift reflects the more mature integrator in older larvae (Beck

et al., 2003). In young zebrafish, the OI has been hypothesized to be topographically organized with strong persistence time heterogeneity, exhibiting a more distributed connectivity with less heterogeneity in adult fish (Fisher et al., 2013; Miri et al., 2011a). The decrease in velocity encoding in the rostral area of rh7/8 does reflect such a decrease in heterogeneity for the encoded eye movement quality, but not in the persistence time domain.

Several studies investigated the maturation of working memory during a delayed oculomotor response task in the prefrontal cortex of non-human primates (Li et al., 2021; Zhou et al., 2013, 2014, 2016). Here, specific neurons show persistent firing after the animal is presented with a spatial cue and this activity predicts an ocular behavioural response. While this brain region serves a different function than the OI, and is comprised of a different set of neurons, the underlying neurons act as a continuous attractor, which achieve their persistent activity due to their recurrent connectivity, similar to the OI (Khona & Fiete, 2022; Li et al., 2020; Liu et al., 2021; Riley & Constantinidis, 2016). On the neuronal level, the maturation of this system is characterized by an increased activity during the delay period (Zhou et al., 2013, 2016) and by a decrease in the functional connectivity of inhibitory neurons while the excitatory connections stay the same (Zhou et al., 2014). Similarly, the dorso-medial cluster in late-stage larvae, which forms excitatory recurrent connections (Lee et al., 2015), show no noteworthy changes compared to their younger counterparts. However, it's not possible to draw a conclusion regarding a potential increase in their monotonic firing pattern as different larvae were used for each experiment. Based on their location, a large part of the missing eye velocity encoding neurons could be inhibitory (Lee et al., 2015; Vishwanathan et al., 2017), which can reflect a similar maturation mechanism. Given their unique relevance in the OI (see chapter 1.4.5.3), it would be interesting to see what this maturation means for models of the integrator (Fisher et al., 2013). However, the question still remains why these changes are happening in eye velocity encoding neurons. It is possible that these neurons only appear eye velocity encoding and sharpen their tuning over time and are thus not part of the OI. Neurons rostral to the OI/VSM in goldfish exhibit postural signals, somewhat linked to head velocity/position, but their inactivation does not lead to oculomotor deficits (Pastor et al., 1994). Similarly, the stimulation velocity might have an influence on the underlying tuning. In adult goldfish, neurons become more velocity encoding during increased VOR stimulation (Major et al., 2005). Though the stimulation speed was very similar between

young and late-stage experiments (see chapter 2.4.1 & 2.4.2), the gain of the oculomotor system might change during development. However, the decrease in eye velocity encoding neurons is not reflected by a similar increase in eye position encoding neurons at the same spatial location as it would be expected if a similar process exists in the larval zebrafish.

5.5 Conclusion and future directions:

In this study, I investigated the binocular coordination and coding sensitivities of oculomotor neurons in the hindbrain of larval zebrafish. This analysis is supplemented by an investigation of the maturation of those neurons.

The results regarding the ocular tuning of hindbrain neurons show that the binocular coordination is not achieved in a way that fully conforms to either the theory of Helmholtz or Hering. While most of the underlying neurons are monocular, a large fraction of binocular neurons was also discovered, with one specific binocular type that is preferentially active during conjugate eye movements. These results show that a certain degree of task separation is not only implemented in the premotor areas but also potentially at the level of the motoneurons. The possibility of preferential recruitment of (pre)motor areas should be considered in future studies of oculomotor control. The tuning of oculomotor neurons regarding eye position/velocity is best described as graded, with true position/velocity encoding neurons being the extremes of a continuum. The firing thresholds of eye position and eye velocity encoding neurons both show activity during a limited range in the non-preferred direction that helps in encoding the resting eye position and act as a low-pass filter of the oculomotor system.

The spatial location of the OI in larval zebrafish likely spans into more rostral areas, previously not considered important for gaze holding stability. This requires reanalysis of earlier experiments of the zebrafish OI, as certain findings might change due to the more distributed location of the OI. The organization of the OI appears to form a gradient from eye velocity to eye position encoding along a rostro-caudal axis. However, the exact locations of eye position/velocity neurons are more separated and do not appear to form a gradient as my PV_{Index} might suggest. This points towards a more recurrent organization of the OI, which is mostly comprised of eye position encoding neurons. This highlights differences in the organization of the OI between teleost and mammals, in which a gradient of eye velocity to eye position encoding is reported. While this limits the capability of

zebrafish to explain the oculomotor integrator organization in mammals, it provides the opportunity to investigate how neuronal circuits solve the same biological problem in different ways.

On the other hand, my study shows how one must be careful when interpreting data from larval zebrafish. My investigation into the maturation of the oculomotor system in the hindbrain already shows striking differences after only one week of additional development. Eye velocity encoding neurons become less frequent in older animals and neurons that show preferential activity are more spread out. These changes are only expected to become more significant after the maturation of the aVOR in older zebrafish. My results show that, while providing useful insights, findings in larval zebrafish should always be considered to come from an immature organism until validated in adult fish. Similarly, future studies are needed to investigate how the oculomotor tuning of adult neurons differs to the findings we usually see in larval fish. However, the basic components of the OI can still be investigated in young larvae to probe circuit organization. Future OI studies are required to incorporate more rostral hindbrain neurons to fully investigate their involvement into the OI. Optogenetic activation/silencing of specific subsets of oculomotor neurons would provide a useful foundation to further elucidate how the different threshold neurons contribute to the OI.

Overall, this study expands our knowledge on how neurons that control and maintain horizontal eye positions are tuned and shows that the zebrafish is a competitive model organism for studying neuronal circuits and mechanisms of persistent activity generation.

References

Ahrens, M. B., Orger, M. B., Robson, D. N., Li, J. M., & Keller, P. J. (2013). Whole-brain functional imaging at cellular resolution using light-sheet microscopy. *Nature Methods*, *10*(5), 413–420. https://doi.org/10.1038/nmeth.2434

Akerboom, J., Chen, T.-W., Wardill, T. J., Tian, L., Marvin, J. S., Mutlu, S., Calderón, N. C., Esposti, F., Borghuis, B. G., Sun, X. R., Gordus, A., Orger, M. B., Portugues, R., Engert, F., Macklin, J. J., Filosa, A., Aggarwal, A., Kerr, R. a, Takagi, R., … Looger, L. L. (2012). Optimization of a GCaMP calcium indicator for neural activity imaging. *The Journal of Neuroscience : The Official Journal of the Society for Neuroscience*, *32*(40), 13819–13840. https://doi.org/10.1523/JNEUROSCI.2601-12.2012

Aksay, E., Baker, R., Seung, H. S., & Tank, D. W. (2000). Anatomy and discharge properties of pre-motor neurons in the goldfish medulla that have eye-position signals during fixations. *Journal of Neurophysiology*, *84*(2), 1035–1049. https://doi.org/10.1152/jn.2000.84.2.1035

Aksay, E, Gamkrelidze, G., Seung, H. S., Baker, R., & Tank, D. W. (2001). In vivo intracellular recording and perturbation of persistent activity in a neural integrator. *Nature Neuroscience*, *4*(2), 184–193. https://doi.org/10.1038/84023

Aksay, Emre, Major, G., Goldman, M. S., Baker, R., Seung, H. S., & Tank, D. W. (2003). History dependence of rate covariation between neurons during persistent activity in an oculomotor integrator. *Cerebral Cortex (New York, N.Y. : 1991)*, *13*(11), 1173–1184. https://doi.org/10.1093/cercor/bhg099

Aksay, Emre, Olasagasti, I., Mensh, B. D., Baker, R., Goldman, M. S., & Tank, D. W. (2007). Functional dissection of circuitry in a neural integrator. *Nature Neuroscience*, *10*(4), 494–504. https://doi.org/10.1038/nn1877

Amores, A., Catchen, J., Ferrara, A., Fontenot, Q., & Postlethwait, J. H. (2011). Genome Evolution and Meiotic Maps by Massively Parallel DNA Sequencing: Spotted Gar, an Outgroup for the Teleost Genome Duplication. *Genetics*, *188*(4), 799–808. https://doi.org/10.1534/genetics.111.127324

Anastasio, T. J., & Robinson, D. A. (1991). Failure of the oculomotor neural integrator from a discrete midline lesion between the abducens nuclei in the monkey. *Neuroscience Letters*, *127*(1), 82–86. https://doi.org/10.1016/0304-3940(91)90900-E

Angelaki, D. E., & Cullen, K. E. (2008). Vestibular System: The Many Facets of a Multimodal Sense. *Annual Review of Neuroscience*, *31*(1), 125–150. https://doi.org/10.1146/annurev.neuro.31.060407.125555

Antinucci, P., & Hindges, R. (2016). A crystal-clear zebrafish for in vivo imaging. *Scientific Reports*, *6*(March), 1–10. https://doi.org/10.1038/srep29490

Arnold, D. B., & Robinson, D. A. (1997). The oculomotor integrator: testing of a neural network model. *Experimental Brain Research*, *113*(1), 57–74. https://doi.org/10.1007/BF02454142

Arnold, Donald B., Robinson, D. A., & Leigh, R. J. (1999). Nystagmus induced by pharmacological inactivation of the brainstem ocular motor integrator in monkey. *Vision Research*, *39*(25), 4286–4295. https://doi.org/10.1016/S0042-6989(99)00142-X

Arrenberg, A. B. (2016). Fiber Optic-Based Photostimulation of Larval Zebrafish. In K. Kawakami, E. E. Patton, & M. Orger (Eds.), *Zebrafish: Methods and Protocols* (Vol. 1451, pp. 343–354). Springer New York. https://doi.org/10.1007/978-1-4939-3771-4_24

Arrenberg, A. B., & Driever, W. (2013). Integrating anatomy and function for zebrafish circuit analysis. *Frontiers in Neural Circuits*, *7*(April), 74. https://doi.org/10.3389/fncir.2013.00074

Asakawa, K., & Kawakami, K. (2018). Protocadherin-Mediated Cell Repulsion Controls the Central Topography and Efferent Projections of the Abducens Nucleus. *Cell Reports*, *24*(6), 1562–1572. https://doi.org/10.1016/j.celrep.2018.07.024

Avitan, L., & Goodhill, G. J. (2018). Code Under Construction: Neural Coding Over Development. *Trends in Neurosciences*, *41*(9), 599–609. https://doi.org/10.1016/j.tins.2018.05.011

Avitan, L., Pujic, Z., Mölter, J., McCullough, M., Zhu, S., Sun, B., Myhre, A.-E., & Goodhill, G. J. (2020). Behavioral Signatures of a Developing Neural Code. *Current Biology*, *30*(17), 3352-3363.e5. https://doi.org/10.1016/j.cub.2020.06.040

Avitan, L., Pujic, Z., Mölter, J., Van De Poll, M., Sun, B., Teng, H., Amor, R., Scott, E. K., & Goodhill, G. J. (2017). Spontaneous Activity in the Zebrafish Tectum Reorganizes over Development and Is Influenced by Visual Experience. *Current Biology*, *27*(16), 2407-2419.e4. https://doi.org/10.1016/j.cub.2017.06.056

Bading, H. (2013). Nuclear calcium signalling in the regulation of brain function. *Nature Reviews. Neuroscience*, *14*(9), 593–608. https://doi.org/10.1038/nrn3531

Baier, H., & Wullimann, M. F. (2021). Anatomy and function of retinorecipient arborization fields in zebrafish. *Journal of Comparative Neurology*, *529*(15), 3454–3476. https://doi.org/10.1002/cne.25204

Barbosa, J. S., Di Giaimo, R., Götz, M., & Ninkovic, J. (2016). Single-cell in vivo imaging of adult neural stem cells in the zebrafish telencephalon. *Nature Protocols*, *11*(8), 1360–1370. https://doi.org/10.1038/nprot.2016.077

Bartels, A., & Zeki, S. (2004). Functional brain mapping during free viewing of natural scenes. *Human Brain Mapping*, *21*(2), 75–85. https://doi.org/10.1002/hbm.10153

Barth, K. A., Miklosi, A., Watkins, J., Bianco, I. H., Wilson, S. W., & Andrew, R. J. (2005). Fsi Zebrafish Show Concordant Reversal of Laterality of Viscera, Neuroanatomy, and a Subset of Behavioral Responses. *Current Biology*, *15*(9), 844–850. https://doi.org/10.1016/j.cub.2005.03.047

Basnet, R. M., Zizioli, D., Taweedet, S., Finazzi, D., & Memo, M. (2019). Zebrafish larvae as a behavioral model in neuropharmacology. *Biomedicines*, *7*(1). https://doi.org/10.3390/BIOMEDICINES7010023

Bauer, J., Weiler, S., Fernholz, M. H. P., Laubender, D., Scheuss, V., Hübener, M., Bonhoeffer, T., & Rose, T. (2021). Limited functional convergence of eye-specific inputs in the retinogeniculate pathway of the mouse. *Neuron*, *109*(15), 2457-2468.e12. https://doi.org/10.1016/j.neuron.2021.05.036

Beck, Gilland, Tank, & Baker. (2004). Quantifying the Ontogeny of Optokinetic and Vestibuloocular Behaviors in Zebrafish, Medaka, and Goldfish. *Journal of Neurophysiology*, *92*(6), 3546–3561. https://doi.org/10.1152/jn.00311.2004

Beck, J. C., Rothnie, P., Straka, H., Wearne, S. L., & Baker, R. (2006). Precerebellar Hindbrain Neurons Encoding Eye Velocity During Vestibular and Optokinetic Behavior in the Goldfish. *Journal of Neurophysiology*, *96*(3), 1370–1382. https://doi.org/10.1152/jn.00335.2006

Beck, J., Tank, D., & Baker, R. (2003). Ontogeny of persistent neural activity: maturation of gaze holding in zebrafish. 391.1; 2003 Neuroscience Meeting Planner. New Orleans, LA: Society for Neuroscience, 2003. Online. https://www.sfn.org/meetings/past-and-future-annual-meetings/abstract-archive/abstract-archive-details?absID=7088&absyear=2003

Bengtson, C. P., Freitag, H. E., Weislogel, J. M., & Bading, H. (2010). Nuclear calcium sensors reveal that repetition of trains of synaptic stimuli boosts nuclear calcium signaling in CA1 pyramidal neurons. *Biophysical Journal*, *99*(12), 4066–4077. https://doi.org/10.1016/j.bpj.2010.10.044

Bergmann, K., Santoscoy, P. M., Lygdas, K., Nikolaeva, Y., MacDonald, R. B., Cunliffe, V. T., & Nikolaev, A. (2018). Imaging neuronal activity in the optic tectum of late stage larval zebrafish. *Journal of Developmental Biology*, *6*(1). https://doi.org/10.3390/jdb6010006

Berridge, M. J., Lipp, P., & Bootman, M. D. (2000). The versatility and universality of calcium signalling. *Nature Reviews Molecular Cell Biology*, *1*(1), 11–21. https://doi.org/10.1038/35036035

Bianco, I. H., Kampff, A. R., & Engert, F. (2011). Prey Capture Behavior Evoked by Simple Visual Stimuli in Larval Zebrafish. *Frontiers in Systems Neuroscience*, *5*(December), 1–13. https://doi.org/10.3389/fnsys.2011.00101

Bilotta, J., & Saszik, S. (2001). The zebrafish as a model visual system. *International Journal of Developmental Neuroscience*, *19*(7), 621–629. https://doi.org/10.1016/S0736-5748(01)00050-8

Bilotta, J., Saszik, S., & Sutherland, S. E. (2001). Rod contributions to the electroretinogram of the dark-adapted developing zebrafish. *Developmental Dynamics*, *222*(4), 564–570. https://doi.org/10.1002/dvdy.1188

Bloodgood, B. L., & Sabatini, B. L. (2007). Nonlinear Regulation of Unitary Synaptic Signals by CaV2.3 Voltage-Sensitive Calcium Channels Located in Dendritic Spines. *Neuron*, *53*(2), 249–260. https://doi.org/10.1016/j.neuron.2006.12.017

Bögli, S. Y., Afthinos, M., Bertolini, G., Straumann, D., & Huang, M. Y.-Y. (2016). Unravelling stimulus direction dependency of visual acuity in larval zebrafish by consistent eye displacements upon optokinetic stimulation. *Investigative Ophthalmology and Visual Science*, *57*(4). https://doi.org/10.1167/iovs.15-18072

Bollaerts, I., Veys, L., Geeraerts, E., Andries, L., De Groef, L., Buyens, T., Salinas-Navarro, M., Moons, L., & Van Hove, I. (2018). Complementary research models and methods to study axonal regeneration in the vertebrate retinofugal system. *Brain Structure and Function*, *223*(2), 545–567. https://doi.org/10.1007/s00429-017-1571-3

Boulanger-Weill, J., Candat, V., Jouary, A., Romano, S. A., Pérez-Schuster, V., & Sumbre, G. (2017). Functional Interactions between Newborn and Mature Neurons Leading to Integration into Established Neuronal Circuits. *Current Biology*, *27*(12), 1707-1720.e5. https://doi.org/10.1016/j.cub.2017.05.029

Branoner, F., Chagnaud, B. P., & Straka, H. (2016). Ontogenetic Development of Vestibulo-Ocular Reflexes in Amphibians. *Frontiers in Neural Circuits*, *10*(NOV), 1–17. https://doi.org/10.3389/fncir.2016.00091

Brett, M., Johnsrude, I. S., & Owen, A. M. (2002). The problem of functional localization in the human brain. *Nature Reviews Neuroscience*, *3*(3), 243–249. https://doi.org/10.1038/nrn756

Bridgeman, B., & Stark, L. (1977). The Theory of Binocular Vision. In B. Bridgeman & L. Stark (Eds.), *The Theory of Binocular Vision*. Springer US. https://doi.org/10.1007/978-1-4613-4148-2

Broca, P. P. (1861). Perte de la parole: ramollissement chronique et destruction partielle du lobe antérieur gauche du cerveau. *Bulletins de La Societe d'anthropologie*, *2*, 235–238.

Broussard, D. M., DeCharms, R. C., & Lisberger, S. G. (1995). Inputs from the ipsilateral and contralateral vestibular apparatus to behaviorally characterized abducens neurons in rhesus monkeys. *Journal of Neurophysiology*, *74*(6), 2445–2459. https://doi.org/10.1152/jn.1995.74.6.2445

Bruce, C. J., & Friedman, H. R. (2002). Eye Movements. In *Encyclopedia of the Human Brain* (Vol. 2, pp. 269–297). Elsevier. https://doi.org/10.1016/B0-12-227210-2/00142-4

Brysch, C., Leyden, C., & Arrenberg, A. B. (2019a). *Data and code for the manuscript "Functional architecture underlying binocular coordination of eye position and velocity in the larval zebrafish*

hindbrain." G-Node. https://doi.org/10.12751/g-node.6521de

Brysch, C., Leyden, C., & Arrenberg, A. B. (2019b). Functional architecture underlying binocular coordination of eye position and velocity in the larval zebrafish hindbrain. *BMC Biology*, *17*(1), 110. https://doi.org/10.1186/s12915-019-0720-y

Burrill, J. D., & Easter, S. S. (1994). Development of the retinofugal projections in the embryonic and larval zebrafish (Brachydanio rerio). *The Journal of Comparative Neurology*, *346*(4), 583–600. https://doi.org/10.1002/cne.903460410

Buske, C., & Gerlai, R. (2012). Maturation of shoaling behavior is accompanied by changes in the dopaminergic and serotoninergic systems in zebrafish. *Developmental Psychobiology*, *54*(1), 28–35. https://doi.org/10.1002/dev.20571

Büttner-Ennever, Horn, A. K. E., Scherberger, H., & D'Ascanio, P. (2001). Motoneurons of twitch and nontwitch extraocular muscle fibers in the abducens, trochlear, and oculomotor nuclei of monkeys. *The Journal of Comparative Neurology*, *438*(3), 318–335. https://doi.org/10.1002/cne.1318

Büttner-Ennever, J. A. (2006). The extraocular motor nuclei: organization and functional neuroanatomy. In *Progress in Brain Research* (Vol. 151, pp. 95–125). https://doi.org/10.1016/S0079-6123(05)51004-5

Cabrera, B., Pásaro, R., & Delgado-García, J. M. (1989). Cytoarchitectonic organisation of the abducens nucleus in the pigeon (Columbia livia). *Journal of Anatomy*, *166*, 203–211. https://www.ncbi.nlm.nih.gov/pmc/articles/PMC1256753/

Cabrera, B., Portillo, F., Pásaro, R., & Delgado-García, J. M. (1988). Location of motoneurons and internuclear neurons within the rat abducens nucleus by means of horseradish peroxidase and fluorescent double labeling. *Neuroscience Letters*, *87*(1–2), 1–6. https://doi.org/10.1016/0304-3940(88)90135-8

Cabrera, B., Torres, B., Pásaro, R., Pastor, A. M., & Delgado-García, J. M. (1992). A morphological study of abducens nucleus motoneurons and internuclear neurons in the goldfish (Carassius auratus). *Brain Research Bulletin*, *28*(1), 137–144. https://doi.org/10.1016/0361-9230(92)90241-O

Cachat, J., Canavello, P., Elegante, M., Bartels, B., Hart, P., Bergner, C., Egan, R., Duncan, A., Tien, D., Chung, A., Wong, K., Goodspeed, J., Tan, J., Grimes, C., Elkhayat, S., Suciu, C., Rosenberg, M., Chung, K. M., Kadri, F., … Kalueff, A. V. (2010). Modeling withdrawal syndrome in zebrafish. *Behavioural Brain Research*, *208*(2), 371–376. https://doi.org/10.1016/j.bbr.2009.12.004

Carrero-Rojas, G., Hernández, R. G., Blumer, R., de la Cruz, R. R., & Pastor, A. M. (2021). MIF versus SIF motoneurons, what are their respective contribution in the oculomotor medial rectus pool? *Journal of Neuroscience*, *41*(47), 9782–9793. https://doi.org/10.1523/JNEUROSCI.1480-21.2021

Chandrasekhar, A. (2004). Turning Heads: Development of Vertebrate Branchiomotor Neurons. *Developmental Dynamics*, *229*(1), 143–161. https://doi.org/10.1002/dvdy.10444

Chen-Huang, C., & McCrea, R. A. (1999). Effects of Viewing Distance on the Responses of Horizontal Canal–Related Secondary Vestibular Neurons During Angular Head Rotation. *Journal of Neurophysiology*, *81*(5), 2517–2537. https://doi.org/10.1152/jn.1999.81.5.2517

Chen, C.-C., Bockisch, C. J., Straumann, D., & Huang, M. Y.-Y. (2016). Saccadic and Postsaccadic Disconjugacy in Zebrafish Larvae Suggests Independent Eye Movement Control. *Frontiers in Systems Neuroscience*, *10*(October), 80. https://doi.org/10.3389/fnsys.2016.00080

Chen, C.-C. C., Bockisch, C. J., Bertolini, G., Olasagasti, I., Neuhauss, S. C. F. F., Weber, K. P., Straumann, D., & Ying-Yu Huang, M. (2014). Velocity storage mechanism in zebrafish larvae. *The Journal of Physiology*, *592*(1), 203–214. https://doi.org/10.1113/jphysiol.2013.258640

Chen, C. C. (2014). Optokinetic nystagmus in fish and man. *Ph.D. Thesis*. University of Zurich. http://doi.org/10.5167/uzh-98405

Chen, T.-W., Wardill, T. J., Sun, Y., Pulver, S. R., Renninger, S. L., Baohan, A., Schreiter, E. R., Kerr, R. a, Orger, M. B., Jayaraman, V., Looger, L. L., Svoboda, K., & Kim, D. S. (2013). Ultrasensitive fluorescent proteins for imaging neuronal activity. *Nature*, *499*(7458), 295–300. https://doi.org/10.1038/nature12354

Cheron, G., & Godaux, E. (1987). Disabling of the oculomotor neural integrator by kainic acid injections in the prepositus-vestibular complex of the cat. *The Journal of Physiology*, *394*(1), 267–290. https://doi.org/10.1113/jphysiol.1987.sp016870

Chhetri, J., Jacobson, G., & Gueven, N. (2014). Zebrafish—on the move towards ophthalmological research. *Eye*, *28*(4), 367–380. https://doi.org/10.1038/eye.2014.19

Clark, R. A., & Demer, J. L. (2014). Lateral Rectus Superior Compartment Palsy. *American Journal of Ophthalmology*, *157*(2), 479-487.e2. https://doi.org/10.1016/j.ajo.2013.09.027

Cochran, S., Dieringer, N., & Precht, W. (1984). Basic optokinetic-ocular reflex pathways in the frog. *The Journal of Neuroscience*, *4*(1), 43–57. https://doi.org/10.1523/JNEUROSCI.04-01-00043.1984

Cohen, B., Matsuo, V., & Raphan, T. (1977). Quantitative analysis of the velocity characteristics of optokinetic nystagmus and optokinetic after-nystagmus. *The Journal of Physiology*, *270*(2), 321–344. https://doi.org/10.1113/jphysiol.1977.sp011955

Coubard, O. A. (2013). Saccade and vergence eye movements: a review of motor and premotor commands. *The European Journal of Neuroscience*, *38*(10), 3384–3397. https://doi.org/10.1111/ejn.12356

Crawford, J. D., & Vilis, T. (1993). Modularity and parallel processing in the oculomotor integrator. *Experimental Brain Research*, *96*(3), 537. https://doi.org/10.1007/BF00234112

Cubbage, C. C., & Mabee, P. M. (1996). Development of the cranium and paired fins in the zebrafishDanio rerio (Ostariophysi, Cyprinidae). *Journal of Morphology*, *229*(2), 121–160. https://doi.org/10.1002/(SICI)1097-4687(199608)229:2<121::AID-JMOR1>3.0.CO;2-4

Cullen, K. E., & Van Horn, M. R. (2011). The neural control of fast vs. slow vergence eye movements. *European Journal of Neuroscience*, *33*(11), 2147–2154. https://doi.org/10.1111/j.1460-9568.2011.07692.x

Curthoys, I. S., Markham, C. H., & Furuya, N. (1984). Direct projection of pause neurons to nystagmus-related excitatory burst neurons in the cat pontine reticular formation. *Experimental Neurology*, *83*(2), 414–422. https://doi.org/10.1016/S0014-4886(84)90109-2

da Silva Costa, R. M., Kung, J., Poukens, V., Yoo, L., Tychsen, L., & Demer, J. L. (2011). Intramuscular Innervation of Primate Extraocular Muscles: Unique Compartmentalization in Horizontal Recti. *Investigative Opthalmology & Visual Science*, *52*(5), 2830. https://doi.org/10.1167/iovs.10-6651

Daie, K., Goldman, M. S., & Aksay, E. R. F. (2015). Spatial Patterns of Persistent Neural Activity Vary with the Behavioral Context of Short-Term Memory. *Neuron*, *85*(4), 847–860. https://doi.org/10.1016/j.neuron.2015.01.006

Daie, K., Svoboda, K., & Druckmann, S. (2021). Targeted photostimulation uncovers circuit motifs supporting short-term memory. *Nature Neuroscience*, *24*(2), 259–265. https://doi.org/10.1038/s41593-020-00776-3

Davis-Lopez de Carrizosa, M. A., Morado-Diaz, C. J., Miller, J. M., de la Cruz, R. R., & Pastor, A. M. (2011). Dual Encoding of Muscle Tension and Eye Position by Abducens Motoneurons. *Journal of*

Neuroscience, *31*(6), 2271–2279. https://doi.org/10.1523/JNEUROSCI.5416-10.2011

Debowy, O., & Baker, R. (2011). Encoding of eye position in the goldfish horizontal oculomotor neural integrator. *Journal of Neurophysiology*, *105*(2), 896–909. https://doi.org/10.1152/jn.00313.2010

Dehmelt, F. A., Meier, R., Hinz, J., Yoshimatsu, T., Simacek, C. A., Huang, R., Wang, K., Baden, T., & Arrenberg, A. B. (2021). Spherical arena reveals optokinetic response tuning to stimulus location, size, and frequency across entire visual field of larval zebrafish. *ELife*, *10*, 1–26. https://doi.org/10.7554/eLife.63355

Dehmelt, F. A., von Daranyi, A., Leyden, C., & Arrenberg, A. B. (2018). Evoking and tracking zebrafish eye movement in multiple larvae with ZebEyeTrack. *Nature Protocols*, *13*(7), 1539–1568. https://doi.org/10.1038/s41596-018-0002-0

Delgado-Garcia, J. M., Del Pozo, F., & Baker, R. (1986a). Behavior of neurons in the abducens nucleus of the alert cat—I. Motoneurons. *Neuroscience*, *17*(4), 929–952. https://doi.org/10.1016/0306-4522(86)90072-2

Delgado-Garcia, J. M., Del Pozo, F., & Baker, R. (1986b). Behavior of neurons in the abducens nucleus of the alert cat—II. Internuclear neurons. *Neuroscience*, *17*(4), 953–973. https://doi.org/10.1016/0306-4522(86)90073-4

Delgado-García, J. M., Vidal, P. P., Gómez, C., & Berthoz, A. (1989). A neurophysiological study of prepositus hypoglossi neurons projecting to oculomotor and preoculomotor nuclei in the alert cat. *Neuroscience*, *29*(2), 291–307. https://doi.org/10.1016/0306-4522(89)90058-4

Denk, W., Strickler, J. H., & Webb, W. W. (1990). Two-Photon Laser Scanning Fluorescence Microscopy. *Science*, *248*(4951), 73–76. https://doi.org/10.1126/science.2321027

Dennhag, N., Liu, J. X., Nord, H., Hofsten, J. von, & Domellöf, F. P. (2020). Absence of desmin in myofibers of the zebrafish extraocular muscles. *Translational Vision Science and Technology*, *9*(10), 1–12. https://doi.org/10.1167/tvst.9.10.1

Dietrich, H., Glasauer, S., & Straka, H. (2017). Functional Organization of Vestibulo-Ocular Responses in Abducens Motoneurons. *The Journal of Neuroscience*, *37*(15), 4032–4045. https://doi.org/10.1523/JNEUROSCI.2626-16.2017

Dimitrova, D. M., Allman, B. L., Shall, M. S., & Goldberg, S. J. (2009). Polyneuronal Innervation of Single Muscle Fibers in Cat Eye Muscle: Inferior Oblique. *Journal of Neurophysiology*, *101*(6), 2815–2821. https://doi.org/10.1152/jn.90828.2008

Dunn, T. W., Mu, Y., Narayan, S., Randlett, O., Naumann, E. A., Yang, C.-T., Schier, A. F., Freeman, J., Engert, F., & Ahrens, M. B. (2016). Brain-wide mapping of neural activity controlling zebrafish exploratory locomotion. *ELife*, *5*(MARCH2016), 1–29. https://doi.org/10.7554/eLife.12741

Easter, S. S., & Nicola, G. N. (1996). The Development of Vision in the Zebrafish (Danio rerio). *Developmental Biology*, *180*(2), 646–663. https://doi.org/10.1006/dbio.1996.0335

Eckmiller, R. (1974). Hysteresis in the static characteristics of eye position coded neurons in the alert monkey. *Pflügers Archiv European Journal of Physiology*, *350*(3), 249–258. https://doi.org/10.1007/BF00587804

Eisen, J. S., Myers, P. Z., & Westerfield, M. (1986). Pathway selection by growth cones of identified motoneurones in live zebra fish embryos. *Nature*, *320*(6059), 269–271. https://doi.org/10.1038/320269a0

Elsalini, O. A., & Rohr, K. B. (2003). Phenylthiourea disrupts thyroid function in developing zebrafish.

Development Genes and Evolution, *212*(12), 593–598. https://doi.org/10.1007/s00427-002-0279-3

Emran, F., Rihel, J., Adolph, A. R., Wong, K. Y., Kraves, S., & Dowling, J. E. (2007). OFF ganglion cells cannot drive the optokinetic reflex in zebrafish. *Proceedings of the National Academy of Sciences of the United States of America*, *104*(48), 19126–19131. https://doi.org/10.1073/pnas.0709337104

Engeszer, R. E., Patterson, L. B., Rao, A. A., & Parichy, D. M. (2007). Zebrafish in the wild: A review of natural history and new notes from the field. *Zebrafish*, *4*(1), 21–40. https://doi.org/10.1089/zeb.2006.9997

Escudero, M., de la Cruz, R. R., & Delgado-García, J. M. (1992). A physiological study of vestibular and prepositus hypoglossi neurones projecting to the abducens nucleus in the alert cat. *The Journal of Physiology*, *458*, 539–560. http://www.ncbi.nlm.nih.gov/pubmed/1302278

Euler, T., Hausselt, S. E., Margolis, D. J., Breuninger, T., Castell, X., Detwiler, P. B., & Denk, W. (2009). Eyecup scope—optical recordings of light stimulus-evoked fluorescence signals in the retina. *Pflügers Archiv - European Journal of Physiology*, *457*(6), 1393–1414. https://doi.org/10.1007/s00424-008-0603-5

Evinger, C., Graf, W. M., & Baker, R. (1987). Extra- and intracellular HRP analysis or the organization of extraocular motoneurons and internuclear neurons in the guinea pig and rabbit. *Journal of Comparative Neurology*, *262*(3), 429–445. https://doi.org/10.1002/cne.902620307

Fadool, J., & Dowling, J. (2008). Zebrafish: A model system for the study of eye genetics. *Progress in Retinal and Eye Research*, *27*(1), 89–110. https://doi.org/10.1016/j.preteyeres.2007.08.002

Félix, R. (2020). *Sensory and motor representations in the inferior olive of larval zebrafish. PhD Thesis*. Universidade Nova de Lisboa.

Felix, R., Markov, D. A., Renninger, S. L., Tomás, R., Laborde, A., Carey, M. R., Orger, M. B., & Portugues, R. (2021). *Structural and functional organization of visual responses in the inferior olive of larval zebrafish*. https://doi.org/https://doi.org/10.1101/2021.11.29.470378

Fetcho, J. R., Cox, K. J. A., & O'Malley, D. M. (1998). Monitoring activity in neuronal populations with single-cell resolution in a behaving vertebrate. *Histochemical Journal*, *30*(3), 153–167. https://doi.org/10.1023/A:1003243302777

Fetcho, J. R., & Liu, K. S. (1998). Zebrafish as a Model System for Studying Neuronal Circuits and Behaviora. *Annals of the New York Academy of Sciences*, *860*(1 NEURONAL MECH), 333–345. https://doi.org/10.1111/j.1749-6632.1998.tb09060.x

Finger, S. (2009). Chapter 10 The birth of localization theory. In *Handbook of Clinical Neurology* (3rd ed., Vol. 95, Issue C, pp. 117–128). Elsevier B.V. https://doi.org/10.1016/S0072-9752(08)02110-6

Fisher, D., Olasagasti, I., Tank, D. W., Aksay, E. R. F., & Goldman, M. S. (2013). A modeling framework for deriving the structural and functional architecture of a short-term memory microcircuit. *Neuron*, *79*(5), 987–1000. https://doi.org/10.1016/j.neuron.2013.06.041

Freeman, J., Vladimirov, N., Kawashima, T., Mu, Y., Sofroniew, N. J., Bennett, D. V, Rosen, J., Yang, C.-T., Looger, L. L., & Ahrens, M. B. (2014). Mapping brain activity at scale with cluster computing. *Nature Methods*, *11*(9). https://doi.org/10.1038/nmeth.3041

Fritsches, K. A., & Marshall, N. J. (2002). Independent and conjugate eye movements during optokinesis in teleost fish. *Journal of Experimental Biology*, *205*(9), 1241–1252. https://doi.org/10.1242/jeb.205.9.1241

Fuchs, A. F., Scudder, C. A., & Kaneko, C. R. (1988). Discharge patterns and recruitment order of identified

motoneurons and internuclear neurons in the monkey abducens nucleus. *Journal of Neurophysiology*, *60*(6), 1874–1895. https://doi.org/10.1152/jn.1988.60.6.1874

Fukushima, K., Kaneko, C. R., & Fuchs, a F. (1992). The neuronal substrate of integration in the oculomotor system. *Progress in Neurobiology*, *39*(6), 609–639. https://doi.org/10.1016/0301-0082(92)90016-8

Garbutt, S., Harwood, M. R., & Harris, C. M. (2001). Comparison of the main sequence of reflexive saccades and the quick phases of optokinetic nystagmus. *The British Journal of Ophthalmology*, *85*(12), 1477–1483. https://doi.org/10.1136/bjo.85.12.1477

Gerlach, J. von. (1872). *Von dem Rückenmarke, in: Handbuch der Lehre von den Geweben des Menschen und der Thiere*. (S. Stricker & J. Arnold (eds.); 1st ed.). Engelmann, W.

Gestri, G., Link, B. A., & Neuhauss, S. C. F. (2012). The visual system of zebrafish and its use to model human ocular Diseases. *Developmental Neurobiology*, *72*(3), 302–327. https://doi.org/10.1002/dneu.20919

Gestrin, P., & Sterling, P. (1977). Anatomy and physiology of goldfish oculomotor system. II. Firing patterns of neurons in abducens nucleus and surrounding medulla and their relation to eye movements. *Journal of Neurophysiology*, *40*(3), 573–588. https://doi.org/10.1152/jn.1977.40.3.573

Ghasia, F. F., Meng, H., & Angelaki, D. E. (2008). Neural correlates of forward and inverse models for eye movements: Evidence from three-dimensional kinematics. *Journal of Neuroscience*, *28*(19), 5082–5087. https://doi.org/10.1523/JNEUROSCI.0513-08.2008

Giolli, R. A., Blanks, R. H. I., & Lui, F. (2006). The accessory optic system: basic organization with an update on connectivity, neurochemistry, and function. *Progress in Brain Research*, *151*, 407–440. https://doi.org/10.1016/S0079-6123(05)51013-6

Glickstein, M. (2006). Golgi and Cajal: The neuron doctrine and the 100th anniversary of the 1906 Nobel Prize. *Current Biology*, *16*(5), 147–151. https://doi.org/10.1016/j.cub.2006.02.053

Goldman, M. S. (2009). Memory without Feedback in a Neural Network. *Neuron*, *61*(4), 621–634. https://doi.org/10.1016/j.neuron.2008.12.012

Goldstein, H. P., & Robinson, D. A. (1986). Hysteresis and slow drift in abducens unit activity. *Journal of Neurophysiology*, *55*(5), 1044–1056. https://doi.org/10.1152/jn.1986.55.5.1044

Gonçalves, P. J. (2012). A neural circuit model of the oculomotor integrator: theory for optogenetic dissection. *PhD Thesis*. Universite Pierre et Marie Curie.

Gonçalves, P. J., Arrenberg, A. B., Hablitzel, B., Baier, H., & Machens, C. K. (2014). Optogenetic perturbations reveal the dynamics of an oculomotor integrator. *Frontiers in Neural Circuits*, *8*(February), 10. https://doi.org/10.3389/fncir.2014.00010

Grant, G. (2007). How the 1906 Nobel Prize in Physiology or Medicine was shared between Golgi and Cajal. *Brain Research Reviews*, *55*(2), 490–498. https://doi.org/10.1016/j.brainresrev.2006.11.004

Greaney, M. R., Privorotskiy, A. E., D'Elia, K. P., & Schoppik, D. (2016). Extraocular motoneuron pools develop along a dorsoventral axis in zebrafish, Danio rerio. *Journal of Comparative Neurology*, *78*, 65–78. https://doi.org/10.1002/cne.24042

Grienberger, C., & Konnerth, A. (2012). Imaging calcium in neurons. *Neuron*, *73*(5), 862–885. https://doi.org/10.1016/j.neuron.2012.02.011

Grunwald, D. J., & Eisen, J. S. (2002). Headwaters of the zebrafish — emergence of a new model vertebrate. *Nature Reviews Genetics*, *3*(9), 717–724. https://doi.org/10.1038/nrg892

Harpaz, R., Nguyen, M. N., Bahl, A., & Engert, F. (2021). Precise visuomotor transformations underlying collective behavior in larval zebrafish. *Nature Communications*, *12*(1), 6578. https://doi.org/10.1038/s41467-021-26748-0

Helmholtz, H. von. (2005). *Treatise on Physiological Optics, Volume III* (J. P. Southall (ed.)). Dover Publications.

Hernández, R. G., Calvo, P. M., Blumer, R., de la Cruz, R. R., & Pastor, A. M. (2019). Functional diversity of motoneurons in the oculomotor system. *Proceedings of the National Academy of Sciences*, *116*(9), 3837–3846. https://doi.org/10.1073/pnas.1818524116

Hirata, Y. (2021). Roles of Cerebellum-Brainstem Loops in Predictive Optokinetic Eye Velocity Control in Fish, Mice, and Humans. In H. Mizusawa & S. Kakei (Eds.), *Contemporary Clinical Neuroscience* (pp. 183–198). Springer International Publishing. https://doi.org/10.1007/978-3-030-75817-2_9

Horn, A. K. E., & Straka, H. (2021). Functional Organization of Extraocular Motoneurons and Eye Muscles. *Annual Review of Vision Science*, *7*, 793–825. https://doi.org/10.1146/annurev-vision-100119-125043

Howe, K., Clark, M. D., Torroja, C. F., Torrance, J., Berthelot, C., Muffato, M., Collins, J. E., Humphray, S., McLaren, K., Matthews, L., McLaren, S., Sealy, I., Caccamo, M., Churcher, C., Scott, C., Barrett, J. C., Koch, R., Rauch, G.-J., White, S., … Stemple, D. L. (2013). The zebrafish reference genome sequence and its relationship to the human genome. *Nature*, *496*(7446), 498–503. https://doi.org/10.1038/nature12111

Huang, K.-H., Rupprecht, P., Frank, T., Kawakami, K., Bouwmeester, T., & Friedrich, R. W. (2020). A virtual reality system to analyze neural activity and behavior in adult zebrafish. *Nature Methods*, *17*(3), 343–351. https://doi.org/10.1038/s41592-020-0759-2

Huang, L., Ledochowitsch, P., Knoblich, U., Lecoq, J., Murphy, G. J., Reid, R. C., de Vries, S. E. J., Koch, C., Zeng, H., Buice, M. A., Waters, J., & Li, L. (2021). Relationship between simultaneously recorded spiking activity and fluorescence signal in gcamp6 transgenic mice. *ELife*, *10*. https://doi.org/10.7554/eLife.51675

Huang, Y.-Y. (2008). The optokinetic response in zebrafish and its applications. *Frontiers in Bioscience*, *13*(13), 1899. https://doi.org/10.2741/2810

Igusa, Y., Sasaki, S., & Shimazu, H. (1980). Excitatory premotor burst neurons in the cat pontine reticular formation related to the quick phase of vestibular nystagmus. *Brain Research*, *182*(2), 451–456. https://doi.org/10.1016/0006-8993(80)91202-0

Irons, T. D., MacPhail, R. C., Hunter, D. L., & Padilla, S. (2010). Acute neuroactive drug exposures alter locomotor activity in larval zebrafish. *Neurotoxicology and Teratology*, *32*(1), 84–90. https://doi.org/10.1016/j.ntt.2009.04.066

Jacoby, J., Chiarandini, D. J., & Stefani, E. (1989). Electrical properties and innervation of fibers in the orbit layer of rat extraocular muscles. *Journal of Neurophysiology*, *61*(1), 116–125. https://doi.org/10.1152/jn.1989.61.1.116

Jao, L.-E., Appel, B., & Wente, S. R. (2012). A zebrafish model of lethal congenital contracture syndrome 1 reveals Gle1 function in spinal neural precursor survival and motor axon arborization. *Development*, *139*(7), 1316–1326. https://doi.org/10.1242/dev.074344

Jesuthasan, S. (2012). Fear, anxiety, and control in the zebrafish. *Developmental Neurobiology*, *72*(3), 395–403. https://doi.org/10.1002/dneu.20873

Johnston, L., Ball, R. E., Acuff, S., Gaudet, J., Sornborger, A., & Lauderdale, J. D. (2013). Electrophysiological Recording in the Brain of Intact Adult Zebrafish. *Journal of Visualized*

Experiments, *81*, 1–11. https://doi.org/10.3791/51065

Joshua, M, & Lisberger, S. G. (2015). A tale of two species: Neural integration in zebrafish and monkeys. *Neuroscience*, *296*, 80–91. https://doi.org/10.1016/j.neuroscience.2014.04.048

Joshua, Mati, Medina, J. F., & Lisberger, S. G. (2013). Diversity of Neural Responses in the Brainstem during Smooth Pursuit Eye Movements Constrains the Circuit Mechanisms of Neural Integration. *Journal of Neuroscience*, *33*(15), 6633–6647. https://doi.org/10.1523/JNEUROSCI.3732-12.2013

Judge, S. J., & Cumming, B. G. (1986). Neurons in the monkey midbrain with activity related to vergence eye movement and accommodation. *Journal of Neurophysiology*, *55*(5), 915–930. https://doi.org/10.1152/jn.1986.55.5.915

Jurisch-Yaksi, N., Yaksi, E., & Kizil, C. (2020). Radial glia in the zebrafish brain: Functional, structural, and physiological comparison with the mammalian glia. *Glia*, *68*(12), 2451–2470. https://doi.org/10.1002/glia.23849

Kalderon, D., Roberts, B. L., Richardson, W. D., & Smith, A. E. (1984). A short amino acid sequence able to specify nuclear location. *Cell*, *39*(3 Pt 2), 499–509. https://doi.org/10.1016/0092-8674(84)90457-4

Kalueff, A. V., Gebhardt, M., Stewart, A. M., Cachat, J. M., Brimmer, M., Chawla, J. S., Craddock, C., Kyzar, E. J., Roth, A., Landsman, S., Gaikwad, S., Robinson, K., Baatrup, E., Tierney, K., Shamchuk, A., Norton, W., Miller, N., Nicolson, T., Braubach, O., … Schneider, H. (2013). Towards a comprehensive catalog of zebrafish behavior 1.0 and beyond. *Zebrafish*, *10*(1), 70–86. https://doi.org/10.1089/zeb.2012.0861

Kalueff, A. V., Stewart, A. M., & Gerlai, R. (2014). Zebrafish as an emerging model for studying complex brain disorders. *Trends in Pharmacological Sciences*, *35*(2), 63–75. https://doi.org/10.1016/j.tips.2013.12.002

Kanda, T., Sullivan, K. F., & Wahl, G. M. (1998). Histone–GFP fusion protein enables sensitive analysis of chromosome dynamics in living mammalian cells. *Current Biology*, *8*(7), 377–385. https://doi.org/10.1016/S0960-9822(98)70156-3

Kanwisher, N. (2010). Functional specificity in the human brain: A window into the functional architecture of the mind. *Proceedings of the National Academy of Sciences of the United States of America*, *107*(25), 11163–11170. https://doi.org/10.1073/pnas.1005062107

Kasprick, D. S., Kish, P. E., Junttila, T. L., Ward, L. a, Bohnsack, B. L., & Kahana, A. (2011). Microanatomy of adult zebrafish extraocular muscles. *PloS One*, *6*(11), e27095. https://doi.org/10.1371/journal.pone.0027095

Khona, M., & Fiete, I. R. (2022). Attractor and integrator networks in the brain. *Nature Reviews Neuroscience*, *23*(12), 744–766. https://doi.org/10.1038/s41583-022-00642-0

Kim, C. K., Miri, A., Leung, L. C., Berndt, A., Mourrain, P., Tank, D. W., & Burdine, R. D. (2014). Prolonged, brain-wide expression of nuclear-localized GCaMP3 for functional circuit mapping. *Frontiers in Neural Circuits*, *8*(November), 1–12. https://doi.org/10.3389/fncir.2014.00138

Kimmel, C. B. (1982). Reticulospinal and Vestibulospinal Neurons in the Young Larva of a Teleost Fish, Brachydanio rerio. *Progress in Brain Research*, *57*(C), 1–23. https://doi.org/10.1016/S0079-6123(08)64122-9

King, W. M. (2011). Binocular coordination of eye movements - Hering's Law of equal innervation or uniocular control? *European Journal of Neuroscience*, *33*(11), 2139–2146. https://doi.org/10.1111/j.1460-9568.2011.07695.x

King, W. M., Fuchs, A. F., & Magnin, M. (1981). Vertical eye movement-related responses of neurons in midbrain near interstitial nucleus of Cajal. *Journal of Neurophysiology*, *46*(3), 549–562. https://doi.org/10.1152/jn.1981.46.3.549

King, W. Michael, & Zhou, W. (1995). Initiation of disjunctive smooth pursuit in monkeys: Evidence that Hering's law of equal innervation is not obeyed by the smooth pursuit system. *Vision Research*, *35*(23–24), 3389–3400. https://doi.org/10.1016/0042-6989(95)00134-Z

King, W. Michael, & Zhou, W. (2000). New ideas about binocular coordination of eye movements: is there a chameleon in the primate family tree? *The Anatomical Record*, *261*(4), 153–161. https://doi.org/10.1002/1097-0185(20000815)261:4<153::AID-AR4>3.0.CO;2-4

King, W. Michael, Zhou, W., Tomlinson, R. D., McConville, K. M. V., Page, W. K., Paige, G. D., & Maxwell, J. S. (1994). Eye position signals in the abducens and oculomotor nuclei of monkeys during ocular convergence. *Journal of Vestibular Research : Equilibrium & Orientation*, *4*(5), 401–408. https://doi.org/10.3233/VES-1994-4509

Kinkhabwala, A., Riley, M., Koyama, M., Monen, J., Satou, C., Kimura, Y., Higashijima, S. -i., & Fetcho, J. (2011). A structural and functional ground plan for neurons in the hindbrain of zebrafish. *Proceedings of the National Academy of Sciences*, *108*(3), 1164–1169. https://doi.org/10.1073/pnas.1012185108

Knogler, L. D., Kist, A. M., & Portugues, R. (2019). Motor context dominates output from purkinje cell functional regions during reflexive visuomotor behaviours. *ELife*, *8*, 1–36. https://doi.org/10.7554/elife.42138

Knogler, L. D., Markov, D. A., Dragomir, E. I., Štih, V., & Portugues, R. (2017). Sensorimotor Representations in Cerebellar Granule Cells in Larval Zebrafish Are Dense, Spatially Organized, and Non-temporally Patterned. *Current Biology*, *27*(9), 1288–1302. https://doi.org/10.1016/j.cub.2017.03.029

Knüfer, A., Diana, G., Walsh, G. S., Clarke, J. D., & Guthrie, S. (2020). Cadherins regulate nuclear topography and function of developing ocular motor circuitry. *ELife*, *9*, 1–25. https://doi.org/10.7554/eLife.56725

Kramer, A., Wu, Y., Baier, H., & Kubo, F. (2019). Neuronal Architecture of a Visual Center that Processes Optic Flow. *Neuron*, *103*(1), 118-132.e7. https://doi.org/10.1016/j.neuron.2019.04.018

Kubo, F., Hablitzel, B., Dal Maschio, M., Driever, W., Baier, H., & Arrenberg, A. B. (2014). Functional architecture of an optic flow-responsive area that drives horizontal eye movements in zebrafish. *Neuron*, *81*(6), 1344–1359. https://doi.org/10.1016/j.neuron.2014.02.043

Labandeira-Garcia, J. L., Guerra-Seijas, M. J., Segade, L. A. G., & Suarez-Nuñez, J. M. (1987). Identification of abducens motoneurons, accessory abducens motoneurons, and abducens internuclear neurons in the chick by retrograde transport of horseradish peroxidase. *Journal of Comparative Neurology*, *259*(1), 140–149. https://doi.org/10.1002/cne.902590110

Lambert, F. M., Beck, J. C., Baker, R., & Straka, H. (2008). Semicircular canal size determines the developmental onset of angular vestibuloocular reflexes in larval Xenopus. *Journal of Neuroscience*, *28*(32), 8086–8095. https://doi.org/10.1523/JNEUROSCI.1288-08.2008

Lee, M. M., Arrenberg, A. B., & Aksay, E. R. F. (2015). A Structural and Genotypic Scaffold Underlying Temporal Integration. *Journal of Neuroscience*, *35*(20), 7903–7920. https://doi.org/10.1523/JNEUROSCI.3045-14.2015

Leigh, R. J., & Zee, D. S. (2006). *The Neurology of Eye Movements* (4th ed.). Oxford University Press.

Lemasson, B., Tanner, C., Woodley, C., Threadgill, T., Qarqish, S., & Smith, D. (2018). Motion cues tune

social influence in shoaling fish. *Scientific Reports*, *8*(1), 1–10. https://doi.org/10.1038/s41598-018-27807-1

Levin, E. D., & Cerutti, D. T. (2009). Behavioral Neuroscience of Zebrafish. In *Methods of Behavior Analysis in Neuroscience* (2nd ed.). CRC Press/Taylor & Francis, Boca Raton (FL). http://europepmc.org/books/NBK5216

Leyden, C., Brysch, C., & Arrenberg, A. B. (2021). A distributed saccade-associated network encodes high velocity conjugate and monocular eye movements in the zebrafish hindbrain. *Scientific Reports*, *11*(1), 1–17. https://doi.org/10.1038/s41598-021-90315-2

Li, S., Constantinidis, C., & Qi, X. L. (2021). Drifts in Prefrontal and Parietal Neuronal Activity Influence Working Memory Judgments. *Cerebral Cortex*, *31*(8), 3650–3664. https://doi.org/10.1093/cercor/bhab038

Li, S., Zhou, X., Constantinidis, C., & Qi, X. L. (2020). Plasticity of Persistent Activity and Its Constraints. *Frontiers in Neural Circuits*, *14*(May), 1–14. https://doi.org/10.3389/fncir.2020.00015

Lin, T. F., Mohammadi, M., Fathalla, A. M., Pul, D., Lüthi, D., Romano, F., Straumann, D., Cullen, K. E., Chacron, M. J., & Huang, M. Y. Y. (2019). Negative optokinetic afternystagmus in larval zebrafish demonstrates set-point adaptation. *Scientific Reports*, *9*(1), 1–14. https://doi.org/10.1038/s41598-019-55457-4

Lister, J. A., Robertson, C. P., Lepage, T., Johnson, S. L., & Raible, D. W. (1999). nacre encodes a zebrafish microphthalmia-related protein that regulates neural-crest-derived pigment cell fate. *Development (Cambridge, England)*, *126*(17), 3757–3767. http://www.ncbi.nlm.nih.gov/pubmed/10433906

Liu, J.-X., & Domellöf, F. P. (2018). A Novel Type of Multiterminal Motor Endplate in Human Extraocular Muscles. *Investigative Opthalmology & Visual Science*, *59*(1), 539. https://doi.org/10.1167/iovs.17-22554

Liu, Y. H., Zhu, J., Constantinidis, C., & Zhou, X. (2021). Emergence of prefrontal neuron maturation properties by training recurrent neural networks in cognitive tasks. *IScience*, *24*(10), 103178. https://doi.org/10.1016/j.isci.2021.103178

Lopez-Barneo, J., Darlot, C., Berthoz, A., & Baker, R. (1982). Neuronal activity in prepositus nucleus correlated with eye movement in the alert cat. *Journal of Neurophysiology*, *47*(2), 329–352. https://doi.org/10.1152/jn.1982.47.2.329

López-Muñoz, F., Boya, J., & Alamo, C. (2006). Neuron theory, the cornerstone of neuroscience, on the centenary of the Nobel Prize award to Santiago Ramón y Cajal. *Brain Research Bulletin*, *70*(4–6), 391–405. https://doi.org/10.1016/j.brainresbull.2006.07.010

Ma, L.-H., Grove, C. L., & Baker, R. (2014). Development of oculomotor circuitry independent of hox3 genes. *Nature Communications*, *5*(May), 4221. https://doi.org/10.1038/ncomms5221

Ma, L.-H., Punnamoottil, B., Rinkwitz, S., & Baker, R. (2009). Mosaic hoxb4a neuronal pleiotropism in zebrafish caudal hindbrain. *PloS One*, *4*(6), e5944. https://doi.org/10.1371/journal.pone.0005944

Major, Guy;, Baker, R., Aksay, E., Mensh, B., Seung, H. S., & Tank, D. W. (2004a). Plasticity and tuning by visual feedback of the stability of a neural integrator. *Proceedings of the National Academy of Sciences of the United States of America*, *101*(20), 7739–7744. https://doi.org/10.1073/pnas.0401970101

Major, Guy;, Baker, R., Aksay, E., Seung, H. S., & Tank, D. W. (2004b). Plasticity and tuning of the time course of analog persistent firing in a neural integrator. *Proceedings of the National Academy of Sciences of the United States of America*, *101*(20), 7745–7750. https://doi.org/10.1073/pnas.0401992101

Major, G., Markowitz, D. A., Baker, R., & Tank, D. W. (2005). Goldfish oculomotor neural integrator neurons exhibit an unexpected relationship between threshold and temporal integration of vestibular inputs. 290.22; 2005 Neuroscience Meeting Planer. Washington, DC: Society for Neuroscience, 2005. Online. https://www.sfn.org/meetings/past-and-future-annual-meetings/abstract-archive/abstract-archive-details?absID=4995&absyear=2005

Masseck, O. A., & Hoffmann, K.-P. (2009). Comparative Neurobiology of the Optokinetic Reflex. *Annals of the New York Academy of Sciences*, *1164*(1), 430–439. https://doi.org/10.1111/j.1749-6632.2009.03854.x

Matsuda, K., & Kubo, F. (2021). Circuit Organization Underlying Optic Flow Processing in Zebrafish. *Frontiers in Neural Circuits*, *15*(July), 1–8. https://doi.org/10.3389/fncir.2021.709048

Mays, L. E. (1984). Neural control of vergence eye movements: convergence and divergence neurons in midbrain. *Journal of Neurophysiology*, *51*(5), 1091–1108. https://doi.org/10.1152/jn.1984.51.5.1091

Mays, L. E., Porter, J. D., Gamlin, P. D., & Tello, C. A. (1986). Neural control of vergence eye movements: neurons encoding vergence velocity. *Journal of Neurophysiology*, *56*(4), 1007–1021. http://www.ncbi.nlm.nih.gov/pubmed/3783225

McConville, K., Tomlinson, R. D., King, W. M., Paige, G., & Na, E.-Q. (1994). Eye Position Signals in the Vestibular Nuclei: Consequences for Models of Integrator Function. *Journal of Vestibular Research*, *4*(5), 391–400. https://doi.org/10.3233/VES-1994-4508

McCrea, R. A., & Baker, R. (1985). Anatomical connections of the nucleus prepositus of the cat. *The Journal of Comparative Neurology*, *237*(3), 377–407. https://doi.org/10.1002/cne.902370308

McCrea, R. A., Strassman, A., & Highstein, S. M. (1986). Morphology and physiology of abducens motoneurons and internuclear neurons intracellularly injected with horseradish peroxidase in alert squirrel monkeys. *The Journal of Comparative Neurology*, *243*(3), 291–308. https://doi.org/10.1002/cne.902430302

McCrea, Robert A., & Horn, A. K. E. (2006). Nucleus prepositus. In *Progress in Brain Research* (Vol. 151, pp. 205–230). https://doi.org/10.1016/S0079-6123(05)51007-0

McFarland, J. L., & Fuchs, a F. (1992). Discharge patterns in nucleus prepositus hypoglossi and adjacent medial vestibular nucleus during horizontal eye movement in behaving macaques. *Journal of Neurophysiology*, *68*(1), 319–332. https://doi.org/10.1152/jn.1992.68.1.319

Mearns, D. S., Donovan, J. C., Fernandes, A. M., Semmelhack, J. L., & Baier, H. (2020). Deconstructing Hunting Behavior Reveals a Tightly Coupled Stimulus-Response Loop. *Current Biology*, *30*(1), 54-69.e9. https://doi.org/10.1016/j.cub.2019.11.022

Mensh, B. D., Aksay, E., Lee, D. D., Seung, H. S., & Tank, D. W. (2004). Spontaneous eye movements in goldfish: oculomotor integrator performance, plasticity, and dependence on visual feedback. *Vision Research*, *44*(7), 711–726. https://doi.org/10.1016/j.visres.2003.10.015

Mettens, P., Godaux, E., Cheron, G., & Galiana, H. L. (1994). Effect of muscimol microinjections into the prepositus hypoglossi and the medial vestibular nuclei on cat eye movements. *Journal of Neurophysiology*, *72*(2), 785–802. https://doi.org/10.1152/jn.1994.72.2.785

Migault, G., van der Plas, T. L., Trentesaux, H., Panier, T., Candelier, R., Proville, R., Englitz, B., Debrégeas, G., & Bormuth, V. (2018). Whole-Brain Calcium Imaging during Physiological Vestibular Stimulation in Larval Zebrafish. *Current Biology*, *28*(23), 3723-3735.e6. https://doi.org/10.1016/j.cub.2018.10.017

Miki, S., Urase, K., Baker, R., & Hirata, Y. (2020). Velocity storage mechanism drives a cerebellar clock for

predictive eye velocity control. *Scientific Reports*, *10*(1), 1–13. https://doi.org/10.1038/s41598-020-63641-0

Miklósi, Á, & Andrew, R. . (1999). Right eye use associated with decision to bite in zebrafish. *Behavioural Brain Research*, *105*(2), 199–205. https://doi.org/10.1016/S0166-4328(99)00071-6

Miklósi, Ádám, & Andrew, R. J. (2006). The Zebrafish as a Model for Behavioral Studies. *Zebrafish*, *3*(2), 227–234. https://doi.org/10.1089/zeb.2006.3.227

Miklósi, Ádám, Andrew, R. J., & Gasparini, S. (2001). Role of right hemifield in visual control of approach to target in zebrafish. *Behavioural Brain Research*, *122*(1), 57–65. https://doi.org/10.1016/S0166-4328(01)00167-X

Miller, J. M., Bockisch, C. J., & Pavlovski, D. S. (2002). Missing lateral rectus force and absence of medial rectus co-contraction in ocular convergence. *Journal of Neurophysiology*, *87*(5), 2421–2433. https://doi.org/10.1152/jn.00566.2001

Miller, J. M., Davison, R. C., & Gamlin, P. D. (2011). Motor nucleus activity fails to predict extraocular muscle forces in ocular convergence. *Journal of Neurophysiology*, *105*, 2863–2873. https://doi.org/10.1152/jn.00935.2010

Miri, A., Bhasin, B. J., Aksay, E. R. F., Tank, D. W., & Goldman, M. S. (2022). Oculomotor plant and neural dynamics suggest gaze control requires integration on distributed timescales. *The Journal of Physiology*, *600*(16), 3837–3863. https://doi.org/10.1113/JP282496

Miri, A., Daie, K., Arrenberg, A. B., Baier, H., Aksay, E., & Tank, D. W. (2011a). Spatial gradients and multidimensional dynamics in a neural integrator circuit. *Nature Neuroscience*, *14*(9), 1150–1159. https://doi.org/10.1038/nn.2888

Miri, A., Daie, K., Burdine, R. D., Aksay, E., & Tank, D. W. (2011b). Regression-Based Identification of Behavior-Encoding Neurons During Large-Scale Optical Imaging of Neural Activity at Cellular Resolution. *Journal of Neurophysiology*, *105*(2), 964–980. https://doi.org/10.1152/jn.00702.2010

Mo, W., Chen, F., Nechiporuk, A., & Nicolson, T. (2010). Quantification of vestibular-induced eye movements in zebrafish larvae. *BMC Neuroscience*, *11*, 110. https://doi.org/10.1186/1471-2202-11-110

Mu, Y., Bennett, D. V., Rubinov, M., Narayan, S., Yang, C. T., Tanimoto, M., Mensh, B. D., Looger, L. L., & Ahrens, M. B. (2019). Glia Accumulate Evidence that Actions Are Futile and Suppress Unsuccessful Behavior. *Cell*, *178*(1), 27-43.e19. https://doi.org/10.1016/j.cell.2019.05.050

Mueller, K. P., & Neuhauss, S. C. F. (2010). Quantitative measurements of the optokinetic response in adult fish. *Journal of Neuroscience Methods*, *186*(1), 29–34. https://doi.org/10.1016/j.jneumeth.2009.10.020

Nakai, J., Ohkura, M., & Imoto, K. (2001). A high signal-to-noise Ca2+ probe composed of a single green fluorescent protein. *Nature Biotechnology*, *19*(2), 137–141. https://doi.org/10.1038/84397

Naumann, E. A., Fitzgerald, J. E., Dunn, T. W., Rihel, J., Sompolinsky, H., & Engert, F. (2016). From Whole-Brain Data to Functional Circuit Models: The Zebrafish Optomotor Response. *Cell*, *167*(4), 947-960.e20. https://doi.org/10.1016/j.cell.2016.10.019

Naumann, E. A., Kampff, A. R., Prober, D. A., Schier, A. F., & Engert, F. (2010). Monitoring neural activity with bioluminescence during natural behavior. *Nature Neuroscience*, *13*(4), 513–520. https://doi.org/10.1038/nn.2518

Neher, E., & Sakaba, T. (2008). Multiple Roles of Calcium Ions in the Regulation of Neurotransmitter Release. *Neuron*, *59*(6), 861–872. https://doi.org/10.1016/j.neuron.2008.08.019

Neuhauss, S. C. F. (2003). Behavioral genetic approaches to visual system development and function in

zebrafish. *Journal of Neurobiology*, *54*(1), 148–160. https://doi.org/10.1002/neu.10165

Neuhauss, S. C. F. (2010). Zebrafish vision: Structure and function of the zebrafish visual system. In *Fish Physiology* (Vol. 29, Issue 10). Elsevier. https://doi.org/10.1016/S1546-5098(10)02903-1

Neuhauss, S. C. F., Biehlmaier, O., Seeliger, M. W., Das, T., Kohler, K., Harris, W. A., & Baier, H. (1999). Genetic Disorders of Vision Revealed by a Behavioral Screen of 400 Essential Loci in Zebrafish. *The Journal of Neuroscience*, *19*(19), 8603–8615. https://doi.org/10.1523/JNEUROSCI.19-19-08603.1999

Nevin, L. M., Taylor, M. R., & Baier, H. (2008). Hardwiring of fine synaptic layers in the zebrafish visual pathway. *Neural Development*, *3*(1), 36. https://doi.org/10.1186/1749-8104-3-36

Nikolaou, N., Lowe, A. S., Walker, A. S., Abbas, F., Hunter, P. R., Thompson, I. D., & Meyer, M. P. (2013). Parametric Functional Maps of Visual Inputs to the Tectum. *Neuron*, *77*(5), 992. https://doi.org/10.1016/j.neuron.2013.02.020

Nüsslein-Volhard, C. (2012). The zebrafish issue of development. *Development (Cambridge)*, *139*(22), 4099–4103. https://doi.org/10.1242/dev.085217

Nygren, E., Ramirez, A., McMahan, B., Aksay, E., & Senn, W. (2019). Learning temporal integration from internal feedback. *BioRxiv*, 2019.12.29.890509. https://doi.org/https://doi.org/10.1101/2019.12.29.890509

Olt, J., Allen, C. E., & Marcotti, W. (2016). In vivo physiological recording from the lateral line of juvenile zebrafish. *The Journal of Physiology*, *594*(19), 5427–5438. https://doi.org/10.1113/JP271794

Omejc, N. (2019). Ontogeny of the oculomotor hindbrain in zebrafish. Graduate School of Neural & Behavioral Sciences, University of Tübingen; Master thesis.

Optican, L. M., Zee, D. S., & Miles, F. A. (1986). Floccular lesions abolish adaptive control of post-saccadic ocular drift in primates. *Experimental Brain Research*, *64*(3), 596–598. https://doi.org/10.1007/BF00340497

Orger, M. B. (2016). The Cellular Organization of Zebrafish Visuomotor Circuits. *Current Biology*, *26*(9), R377–R385. https://doi.org/10.1016/j.cub.2016.03.054

Pallucchi, I., Bertuzzi, M., Michel, J. C., Miller, A. C., & El Manira, A. (2022). Transformation of an early-established motor circuit during maturation in zebrafish. *Cell Reports*, *39*(2), 110654. https://doi.org/10.1016/j.celrep.2022.110654

Palmer, L. M., & Mensinger, A. F. (2004). Effect of the anesthetic tricaine (MS-222) on nerve activity in the anterior lateral line of the oyster toadfish, Opsanus tau. *Journal of Neurophysiology*, *92*(2), 1034–1041. https://doi.org/10.1152/jn.01151.2003

Parichy, D. M., Elizondo, M. R., Mills, M. G., Gordon, T. N., & Engeszer, R. E. (2009). Normal table of postembryonic zebrafish development: Staging by externally visible anatomy of the living fish. *Developmental Dynamics*, *238*(12), 2975–3015. https://doi.org/10.1002/dvdy.22113

Park, H. C., Kim, C. H., Bae, Y. K., Yeo, S. Y., Kim, S. H., Hong, S. K., Shin, J., Yoo, K. W., Hibi, M., Hirano, T., Miki, N., Chitnis, A. B., & Huh, T. L. (2000). Analysis of upstream elements in the HuC promoter leads to the establishment of transgenic Zebrafish with fluorescent neurons. *Developmental Biology*, *227*(2), 279–293. https://doi.org/10.1006/dbio.2000.9898

Pastor, A. M., Calvo, P. M., de la Cruz, R. R., Baker, R., & Straka, H. (2019). Discharge properties of morphologically identified vestibular neurons recorded during horizontal eye movements in the goldfish. *Journal of Neurophysiology*, *121*(5), 1865–1878. https://doi.org/10.1152/jn.00772.2018

Pastor, A M, De la Cruz, R. R., & Baker, R. (1994). Eye position and eye velocity integrators reside in

separate brainstem nuclei. *Proceedings of the National Academy of Sciences of the United States of America*, *91*(2), 807–811. http://www.ncbi.nlm.nih.gov/pubmed/8290604

Pastor, Angel M., Blumer, R., & de la Cruz, R. R. (2022). Extraocular Motoneurons and Neurotrophism. In M. J. O'Donovan & M. Falgairolle (Eds.), *Vertrebrate Motoneurons* (pp. 281–319). Springer. https://doi.org/10.1007/978-3-031-07167-6_12

Pastor, Angel M, & Gonzalez-Forero, D. (2003). Recruitment order of cat abducens motoneurons and internuclear neurons. *Journal of Neurophysiology*, *90*(4), 2240–2252. https://doi.org/10.1152/jn.00402.2003

Pastor, Angel M, Torres, B., Delgado-Garcia, J. M., & Baker, R. (1991). Discharge characteristics of medial rectus and abducens motoneurons in the goldfish. *Journal of Neurophysiology*, *66*(6), 2125–2140. https://doi.org/10.1152/jn.1991.66.6.2125

Peng, M., Poukens, V., da Silva Costa, R. M., Yoo, L., Tychsen, L., & Demer, J. L. (2010). Compartmentalized Innervation of Primate Lateral Rectus Muscle. *Investigative Opthalmology & Visual Science*, *51*(9), 4612. https://doi.org/10.1167/iovs.10-5330

Pietri, T., Romano, S. A., Pérez-Schuster, V., Boulanger-Weill, J., Candat, V., & Sumbre, G. (2017). The Emergence of the Spatial Structure of Tectal Spontaneous Activity Is Independent of Visual Inputs. *Cell Reports*, *19*(5), 939–948. https://doi.org/10.1016/j.celrep.2017.04.015

Pologruto, T. A., Yasuda, R., & Svoboda, K. (2004). Monitoring neural activity and [Ca2+] with genetically encoded Ca2+ indicators. *The Journal of Neuroscience : The Official Journal of the Society for Neuroscience*, *24*(43), 9572–9579. https://doi.org/10.1523/JNEUROSCI.2854-04.2004

Portugues, R., & Engert, F. (2009). The neural basis of visual behaviors in the larval zebrafish. *Current Opinion in Neurobiology*, *19*(6), 644–647. https://doi.org/10.1016/j.conb.2009.10.007

Portugues, R., Feierstein, C. E., Engert, F., & Orger, M. B. (2014). Whole-brain activity maps reveal stereotyped, distributed networks for visuomotor behavior. *Neuron*, *81*(6), 1328–1343. https://doi.org/10.1016/j.neuron.2014.01.019

Portugues, R., Haesemeyer, M., Blum, M. L., & Engert, F. (2015). Whole-field visual motion drives swimming in larval zebrafish via a stochastic process. *Journal of Experimental Biology*, *March*. https://doi.org/10.1242/jeb.118299

Qian, H., Zhu, Y., Ramsey, D. J., Chappell, R. L., Dowling, J. E., & Ripps, H. (2005). Directional Asymmetries in the Optokinetic Response of Larval Zebrafish (Danio rerio). *Zebrafish*, *2*(3), 189–196. https://doi.org/10.1089/zeb.2005.2.189

Quinet, J., Schultz, K., May, P. J., & Gamlin, P. D. (2020). Neural control of rapid binocular eye movements: Saccade-vergence burst neurons. *Proceedings of the National Academy of Sciences of the United States of America*, *117*(46), 29123–29132. https://doi.org/10.1073/pnas.2015318117

Ramirez, A. D., & Aksay, E. R. F. (2021). Ramp-to-threshold dynamics in a hindbrain population controls the timing of spontaneous saccades. *Nature Communications*, *12*(1), 4145. https://doi.org/10.1038/s41467-021-24336-w

Ramón y Cajal, S. (1888). Estructura de los centros nerviosos de las aves. *Rev. Trim. Histol. Norm. Pat*, *1*, 1–10.

Raphan, T., Matsuo, V., & Cohen, B. (1979). Velocity storage in the vestibulo-ocular reflex arc (VOR). *Experimental Brain Research*, *35*(2), 229–248. https://doi.org/10.1007/BF00236613

Rick, J. M., Horschke, I., & Neuhauss, S. C. F. (2000). Optokinetic behavior is reversed in achiasmatic

mutant zebrafish larvae. *Current Biology*, *10*(10), 595–598. https://doi.org/10.1016/S0960-9822(00)00495-4

Riley, M. R., & Constantinidis, C. (2016). Role of Prefrontal Persistent Activity in Working Memory. *Frontiers in Systems Neuroscience*, *9*(JAN2016), 1–14. https://doi.org/10.3389/fnsys.2015.00181

Rinkwitz, S., Mourrain, P., & Becker, T. S. (2011). Zebrafish: An integrative system for neurogenomics and neurosciences. *Progress in Neurobiology*, *93*(2), 231–243. https://doi.org/10.1016/j.pneurobio.2010.11.003

Rinner, O., Rick, J. M., & Neuhauss, S. C. F. (2005). Contrast sensitivity, spatial and temporal tuning of the larval zebrafish optokinetic response. *Investigative Ophthalmology and Visual Science*, *46*(1), 137–142. https://doi.org/10.1167/iovs.04-0682

Robinson, D. A. (1964). The mechanics of human saccadic eye movement. *The Journal of Physiology*, *174*(2), 245–264. https://doi.org/10.1113/jphysiol.1964.sp007485

Robinson, D. A. (1989). Integrating with neurons. *Annual Review of Neuroscience*, *12*, 33–45. https://doi.org/10.1146/annurev.ne.12.030189.000341

Robles, E., Laurell, E., & Baier, H. (2014). The Retinal Projectome Reveals Brain-Area-Specific Visual Representations Generated by Ganglion Cell Diversity. *Current Biology*, *24*(18), 2085–2096. https://doi.org/10.1016/j.cub.2014.07.080

Roeser, T., & Baier, H. (2003). Visuomotor Behaviors in Larval Zebrafish after GFP-Guided Laser Ablation of the Optic Tectum. *The Journal of Neuroscience*, *23*(9), 3726–3734. https://doi.org/10.1523/JNEUROSCI.23-09-03726.2003

Rombough, P. (2002). Gills are needed for ionoregulation before they are needed for O2 uptake in developing zebrafish, Danio rerio. *Journal of Experimental Biology*, *205*(12), 1787–1794. https://doi.org/10.1242/jeb.205.12.1787

Rombough, P. (2007). The functional ontogeny of the teleost gill: Which comes first, gas or ion exchange? *Comparative Biochemistry and Physiology Part A: Molecular & Integrative Physiology*, *148*(4), 732–742. https://doi.org/10.1016/j.cbpa.2007.03.007

Rombough, P., & Drader, H. (2009). Hemoglobin enhances oxygen uptake in larval zebrafish (Danio rerio) but only under conditions of extreme hypoxia. *Journal of Experimental Biology*, *212*(6), 778–784. https://doi.org/10.1242/jeb.026575

Rose, T., Goltstein, P. M., Portugues, R., & Griesbeck, O. (2014). Putting a finishing touch on GECIs. *Frontiers in Molecular Neuroscience*, *7*(November), 1–15. https://doi.org/10.3389/fnmol.2014.00088

Rubinstein, A. L. (2003). Zebrafish: from disease modeling to drug discovery. *Current Opinion in Drug Discovery & Development*, *6*(2), 218–223. http://www.ncbi.nlm.nih.gov/pubmed/12669457

Saito, Y., & Sugimura, T. (2020). Different activation mechanisms of excitatory networks in the rat oculomotor integrators for vertical and horizontal gaze holding. *ENeuro*, *7*(1). https://doi.org/10.1523/ENEURO.0364-19.2019

Saito, Y., & Sugimura, T. (2021). Distinct purinergic receptor-mediated currents of rat oculomotor integrator neurons characterized by different firing patterns. *Journal of Neurophysiology*, *126*(4), 1045–1054. https://doi.org/10.1152/jn.00209.2021

Schiller, P. H. (1970). The discharge characteristics of single units in the oculomotor and abducens nuclei of the unanesthetized monkey. *Experimental Brain Research*, *10*(4), 347–362. https://doi.org/10.1007/BF02324764

Schiller, P. H. (1996). On the specificity of neurons and visual areas. *Behavioural Brain Research*, *76*(1–2), 21–35. https://doi.org/10.1016/0166-4328(95)00186-7

Schilling, T. F., & Kimmel, C. B. (1997). Musculoskeletal patterning in the pharyngeal segments of the zebrafish embryo. *Development*, *124*(15), 2945–2960. https://doi.org/10.1242/dev.124.15.2945

Schmitt, E. A., & Dowling, J. E. (1994). Early-eye morphogenesis in the zebrafish,Brachydanio rerio. *The Journal of Comparative Neurology*, *344*(4), 532–542. https://doi.org/10.1002/cne.903440404

Schoonheim, P. J., Arrenberg, A. B., Del Bene, F., & Baier, H. (2010). Optogenetic Localization and Genetic Perturbation of Saccade-Generating Neurons in Zebrafish. *Journal of Neuroscience*, *30*(20), 7111–7120. https://doi.org/10.1523/JNEUROSCI.5193-09.2010

Schoppik, D., Bianco, I. H., Prober, D. A., Douglass, A. D., Robson, D. N., Li, J. M. B., Greenwood, J. S. F., Soucy, E., Engert, F., & Schier, A. F. (2017). Gaze-Stabilizing Central Vestibular Neurons Project Asymmetrically to Extraocular Motoneuron Pools. *The Journal of Neuroscience*, *37*(47), 11353–11365. https://doi.org/10.1523/JNEUROSCI.1711-17.2017

Schuller, J. (2017). FUNCTIONAL ORGANIZATION AND ONTOGENY OF THE OPTOKINETIC REFLEX IN XENOPUS LAEVIS. *PhD Thesis*. Ludwig-Maximilians-Universität München. https://doi.org/10.5282/edoc.25344

Scudder, C., Kaneko, C., & Fuchs, A. (2002). The brainstem burst generator for saccadic eye movements. *Experimental Brain Research*, *142*(4), 439–462. https://doi.org/10.1007/s00221-001-0912-9

Seung, H. S. (1996). How the brain keeps the eyes still. *Proceedings of the National Academy of Sciences*, *93*(23), 13339–13344. https://doi.org/10.1073/pnas.93.23.13339

Seung, H.Sebastian, Lee, D. D., Reis, B. Y., & Tank, D. W. (2000). Stability of the Memory of Eye Position in a Recurrent Network of Conductance-Based Model Neurons. *Neuron*, *26*(1), 259–271. https://doi.org/10.1016/S0896-6273(00)81155-1

Shadmehr, R. (2017). Distinct neural circuits for control of movement vs. holding still. *Journal of Neurophysiology*, *117*(4), 1431–1460. https://doi.org/10.1152/jn.00840.2016

Simpson, J. I. (1984). The accessory optic system. *Annual Review of Neuroscience*, *7*, 13–41. https://doi.org/10.1146/annurev.ne.07.030184.000305

Soeller, C., & Cannell, M. B. (1999). Two-photon microscopy: Imaging in scattering samples and three-dimensionally resolved flash photolysis. *Microscopy Research and Technique*, *47*(3), 182–195. https://doi.org/10.1002/(SICI)1097-0029(19991101)47:3<182::AID-JEMT4>3.0.CO;2-4

Soodak, R. E., & Simpson, J. I. (1988). The accessory optic system of rabbit. I. Basic visual response properties. *Journal of Neurophysiology*, *60*(6), 2037–2054. https://doi.org/10.1152/jn.1988.60.6.2037

Sovrano, V. (1999). Roots of brain specializations: preferential left-eye use during mirror-image inspection in six species of teleost fish. *Behavioural Brain Research*, *106*(1–2), 175–180. https://doi.org/10.1016/S0166-4328(99)00105-9

Sparks, D. L., Mays, L. E., & Porter, J. D. (1987). Eye movements induced by pontine stimulation: interaction with visually triggered saccades. *Journal of Neurophysiology*, *58*(2), 300–318. https://doi.org/10.1152/jn.1987.58.2.300

Spence, R., Gerlach, G., Lawrence, C., & Smith, C. (2008). The behaviour and ecology of the zebrafish, Danio rerio. *Biological Reviews*, *83*(1), 13–34. https://doi.org/10.1111/j.1469-185X.2007.00030.x

Spencer, R. F., & Porter, J. D. (2006). Biological organization of the extraocular muscles. *Progress in Brain Research*, *151*, 43–80. https://doi.org/10.1016/S0079-6123(05)51002-1

Steiger, H.-J., & Büttner-Ennever, J. (1978). Relationship between motoneurons and internuclear neurons in the abducens nucleus: a double retrograde tracer study in the cat. *Brain Research*, *148*(1), 181–188. https://doi.org/10.1016/0006-8993(78)90387-6

Sterling, P. (1977). Anatomy and physiology of goldfish oculomotor system. I. Structure of abducens nucleus. *Journal of Neurophysiology*, *40*(3), 557–572. https://doi.org/10.1152/jn.1977.40.3.557

Stewart, A., Desmond, D., Kyzar, E., Gaikwad, S., Roth, A., Riehl, R., Collins, C., Monnig, L., Green, J., & Kalueff, A. V. (2012a). Perspectives of zebrafish models of epilepsy: What, how and where next? *Brain Research Bulletin*, *87*(2–3), 135–143. https://doi.org/10.1016/j.brainresbull.2011.11.020

Stewart, A., Gaikwad, S., Kyzar, E., Green, J., Roth, A., & Kalueff, A. V. (2012b). Modeling anxiety using adult zebrafish: A conceptual review. *Neuropharmacology*, *62*(1), 135–143. https://doi.org/10.1016/j.neuropharm.2011.07.037

Straka, H., & Dieringer, N. (1991). Internuclear neurons in the ocular motor system of frogs. *The Journal of Comparative Neurology*, *312*(4), 537–548. https://doi.org/10.1002/cne.903120405

Straka, Hans, Beck, J. C., Pastor, A. M., & Baker, R. (2006). Morphology and Physiology of the Cerebellar Vestibulolateral Lobe Pathways Linked to Oculomotor Function in the Goldfish. *Journal of Neurophysiology*, *96*(4), 1963–1980. https://doi.org/10.1152/jn.00334.2006

Strassman, A., Highstein, S. M., & McCrea, R. A. (1986a). Anatomy and physiology of saccadic burst neurons in the alert squirrel monkey. I. Excitatory burst neurons. *The Journal of Comparative Neurology*, *249*(3), 337–357. https://doi.org/10.1002/cne.902490303

Strassman, A., Highstein, S. M., & McCrea, R. A. (1986b). Anatomy and physiology of saccadic burst neurons in the alert squirrel monkey. II. Inhibitory burst neurons. *The Journal of Comparative Neurology*, *249*(3), 358–380. https://doi.org/10.1002/cne.902490304

Straube, A., Kurzan, R., & Büttner, U. (1991). Differential effects of bicuculline and muscimol microinjections into the vestibular nuclei on simian eye movements. *Experimental Brain Research*, *86*(2), 517–530. https://doi.org/10.1007/BF00228958

Streisinger, G., Walker, C., Dower, N., Knauber, D., & Singer, F. (1981). Production of clones of homozygous diploid zebra fish (Brachydanio rerio). *Nature*, *291*(5813), 293–296. https://doi.org/10.1038/291293a0

Sun, S., Zuo, Z., Ma, M. M., Qian, C., Chen, L., Zhou, W., Drasbek, K. R., & Zuxiang, L. (2019). Neural circuits mediating visual stabilization during active motion in zebrafish. *BioRxiv*, 1–42. https://doi.org/http://dx.doi.org/10.1101/566760

Svoboda, K., & Yasuda, R. (2006). Principles of Two-Photon Excitation Microscopy and Its Applications to Neuroscience. *Neuron*, *50*(6), 823–839. https://doi.org/10.1016/j.neuron.2006.05.019

Sylvestre, P. a., Choi, J. T. L., & Cullen, K. E. (2003). Discharge Dynamics of Oculomotor Neural Integrator Neurons During Conjugate and Disjunctive Saccades and Fixation. *Journal of Neurophysiology*, *90*(2), 739–754. https://doi.org/10.1152/jn.00123.2003

Sylvestre, P. A., & Cullen, K. E. (2002). Dynamics of abducens nucleus neuron discharges during disjunctive saccades. *Journal of Neurophysiology*, *88*(6), 3452–3468. https://doi.org/10.1152/jn.00331.2002

Takeuchi, M., Matsuda, K., Yamaguchi, S., Asakawa, K., Miyasaka, N., Lal, P., Yoshihara, Y., Koga, A., Kawakami, K., Shimizu, T., & Hibi, M. (2015). Establishment of Gal4 transgenic zebrafish lines for analysis of development of cerebellar neural circuitry. *Developmental Biology*, *397*(1), 1–17. https://doi.org/10.1016/j.ydbio.2014.09.030

Thevenaz, P., Ruttimann, U. E., & Unser, M. (1998). A pyramid approach to subpixel registration based on intensity. *IEEE Transactions on Image Processing*, *7*(1), 27–41. https://doi.org/10.1109/83.650848

Tian, L., Hires, S. A., & Looger, L. L. (2012). Imaging Neuronal Activity with Genetically Encoded Calcium Indicators. *Cold Spring Harbor Protocols*, *2012*(6). https://doi.org/10.1101/pdb.top069609

Torres, B., Pastor, A. M., Cabrera, B., Salas, C., & Delgado-García, J. M. (1992). Afferents to the oculomotor nucleus in the goldfish (Carassius auratus) as revealed by retrograde labeling with horseradish peroxidase. *The Journal of Comparative Neurology*, *324*(3), 449–461. https://doi.org/10.1002/cne.903240311

Tropepe, V., & Sive, H. L. (2003). Can zebrafish be used as a model to study the neurodevelopmental causes of autism? *Genes, Brain and Behavior*, *2*(5), 268–281. https://doi.org/10.1034/j.1601-183X.2003.00038.x

Ulrich, F., Grove, C., Torres-Vázquez, J., & Baker, R. (2016). Development of functional hindbrain oculomotor circuitry independent of both vascularization and neuronal activity in larval zebrafish. *Current Neurobiology*, *7*(2), 62–73. http://www.ncbi.nlm.nih.gov/pubmed/30135618

Valente, A., Huang, K.-H., Portugues, R., & Engert, F. (2012). Ontogeny of classical and operant learning behaviors in zebrafish. *Learning & Memory*, *19*(4), 170–177. https://doi.org/10.1101/lm.025668.112

Van Gisbergen, J. A. M., Robinson, D. A., & Gielen, S. (1981). A quantitative analysis of generation of saccadic eye movements by burst neurons. *Journal of Neurophysiology*, *45*(3), 417–442. https://doi.org/10.1152/jn.1981.45.3.417

Venkatraman, P., Mills-Henry, I., Padmanabhan, K. R., Pascuzzi, P., Hassan, M., Zhang, J., Zhang, X., Ma, P., Pang, C. P., Dowling, J. E., Zhang, M., & Leung, Y. F. (2020). Rods Contribute to Visual Behavior in Larval Zebrafish. *Investigative Opthalmology & Visual Science*, *61*(12), 11. https://doi.org/10.1167/iovs.61.12.11

Vishwanathan, A., Daie, K., Ramirez, A. D., Lichtman, J. W., Aksay, E. R. F., & Seung, H. S. (2017). Electron Microscopic Reconstruction of Functionally Identified Cells in a Neural Integrator. *Current Biology*, *27*(14), 2137-2147.e3. https://doi.org/10.1016/j.cub.2017.06.028

Vishwanathan, A., Ramirez, A. D., Wu, J., Sood, A., Yang, R., Kemnitz, N., Ih, D., Turner, N., Lee, K., Tartavull, I., Silversmith, W. M., Jordan, C. S., David, C., Bland, D., Goldman, M. S., Aksay, E. R. F., Seung, H. S., & Eyewirers, T. (2022). Predicting modular functions and neural coding of behavior from a synaptic wiring diagram. *BioRxiv*, https://doi.org/https://doi.org/10.1101/2020.10.28.359620

Waespe, W., & Henn, V. (1978). Reciprocal changes in primary and secondary optokinetic after-nystagmus (OKAN) produced by repetitive optokinetic stimulation in the monkey. *Archiv Fur Psychiatrie Und Nervenkrankheiten*, *225*(1), 23–30. https://doi.org/10.1007/BF00367349

Walz, W. (2011). *Zebrafish Models in Neurobehavioral Research* (A. V. Kalueff & J. M. Cachat (eds.); Vol. 52). Humana Press. https://doi.org/10.1007/978-1-60761-922-2

Wang, K., Hinz, J., Haikala, V., Reiff, D. F., & Arrenberg, A. B. (2019). Selective processing of all rotational and translational optic flow directions in the zebrafish pretectum and tectum. *BMC Biology*, *17*(1), 1–18. https://doi.org/10.1186/s12915-019-0648-2

Wang, K., Hinz, J., Zhang, Y., Thiele, T. R., & Arrenberg, A. B. (2020). Parallel Channels for Motion Feature Extraction in the Pretectum and Tectum of Larval Zebrafish. *Cell Reports*, *30*(2), 442-453.e6. https://doi.org/10.1016/j.celrep.2019.12.031

Wei, Z., Lin, B. J., Chen, T. W., Daie, K., Svoboda, K., & Druckmann, S. (2020). A comparison of neuronal population dynamics measured with calcium imaging and electrophysiology. *PLoS Computational*

Biology, *16*(9), 1–29. https://doi.org/10.1371/journal.pcbi.1008198

White, R. M., Sessa, A., Burke, C., Bowman, T., LeBlanc, J., Ceol, C., Bourque, C., Dovey, M., Goessling, W., Burns, C. E., & Zon, L. I. (2008). Transparent Adult Zebrafish as a Tool for In Vivo Transplantation Analysis. *Cell Stem Cell*, *2*(2), 183–189. https://doi.org/10.1016/j.stem.2007.11.002

Wilson, S. W., & Houart, C. (2004). Early steps in the development of the forebrain. *Developmental Cell*, *6*(2), 167–181. https://doi.org/10.1016/S1534-5807(04)00027-9

Wolf, Sébastien, Dubreuil, A. M., Bertoni, T., Böhm, U. L., Bormuth, V., Candelier, R., Karpenko, S., Hildebrand, D. G. C. C., Bianco, I. H., Monasson, R., & Debrégeas, G. (2017). Sensorimotor computation underlying phototaxis in zebrafish. *Nature Communications*, *8*(1), 1–12. https://doi.org/10.1038/s41467-017-00310-3

Wolf, Sebastien, Le Goc, G., Cocco, S., Debrégeas, G., & Monasson, R. (2022). Emergence of time persistence in an interpretable data-driven neural network model. *BioRxiv*. https://doi.org/https://doi.org/10.1101/2022.02.02.478841

Wu, Y. (2019). Neural Basis of Visual Motion Perception : An Illusory Perspective. *PhD thesis*. Ludwig-Maximilians-Universität München. https://doi.org/10.5282/edoc.25243

Wu, Y., dal Maschio, M., Kubo, F., & Baier, H. (2020). An Optical Illusion Pinpoints an Essential Circuit Node for Global Motion Processing. *Neuron*, *108*(4), 722-734.e5. https://doi.org/10.1016/j.neuron.2020.08.027

Xie, J., Jusuf, P. R., Bui, B. V., & Goodbourn, P. T. (2019). Experience-dependent development of visual sensitivity in larval zebrafish. *Scientific Reports*, *9*(1), 1–11. https://doi.org/10.1038/s41598-019-54958-6

Xu, C., Volkery, S., & Siekmann, A. F. (2015). Intubation-based anesthesia for long-term time-lapse imaging of adult zebrafish. *Nature Protocols*, *10*(12), 2064–2073. https://doi.org/10.1038/nprot.2015.130

Yaksi, E., Jamali, A., Diaz Verdugo, C., & Jurisch-Yaksi, N. (2021). Past, present and future of zebrafish in epilepsy research. *The FEBS Journal*, *288*(24), 7243–7255. https://doi.org/10.1111/febs.15694

Yang, E., Zwart, M. F., Rubinov, M., James, B., Wei, Z., Narayan, S., Vladimirov, N., Mensh, B. D., Fitzgerald, J. E., & Ahrens, M. B. (2021). A brainstem integrator for self-localization and positional homeostasis. *BioRxiv*, 2021.11.26.468907. https://doi.org/https://doi.org/10.1101/2021.11.26.468907

Yu, L., Tucci, V., Kishi, S., & Zhdanova, I. V. (2006). Cognitive aging in zebrafish. *PLoS ONE*, *1*(1). https://doi.org/10.1371/journal.pone.0000014

Zhang, M., Liu, Y., Wang, S. zhi, Zhong, W., Liu, B. hua, & Tao, H. W. (2011). Functional elimination of excitatory feedforward inputs underlies developmental refinement of visual receptive fields in zebrafish. *Journal of Neuroscience*, *31*(14), 5460–5469. https://doi.org/10.1523/JNEUROSCI.6220-10.2011

Zhang, Y., Gamlin, P. D. R., & Mays, L. E. (1991). Antidromic identification of midbrain near response cells projecting to the oculomotor nucleus. *Experimental Brain Research*, *84*(3), 525–528. https://doi.org/10.1007/BF00230964

Zhang, Yue, Huang, R., Nörenberg, W., & Arrenberg, A. B. (2022). A robust receptive field code for optic flow detection and decomposition during self-motion. *Current Biology*, *32*(11), 2505-2516.e8. https://doi.org/10.1016/j.cub.2022.04.048

Zhao, X. C., Yee, R. W., Norcom, E., Burgess, H., Avanesov, A. S., Barrish, J. P., & Malicki, J. (2006). The Zebrafish Cornea: Structure and Development. *Investigative Opthalmology & Visual Science*, *47*(10),

4341. https://doi.org/10.1167/iovs.05-1611

Zhou, Wu, & King, W. M. (1998). Premotor commands encode monocular eye movements. *Nature*, *393*(6686), 692–695. https://doi.org/10.1038/31489

Zhou, WU, & King, W. M. (1996). Ocular selectivity of units in oculomotor pathways. *Annals of the New York Academy of Sciences*, *781*(1), 724–728. https://doi.org/10.1111/j.1749-6632.1996.tb15770.x

Zhou, X., Zhu, D., Katsuki, F., Qi, X. L., Lees, C. J., Bennett, A. J., Salinas, E., Stanford, T. R., & Constantinidis, C. (2014). Age-dependent changes in prefrontal intrinsic connectivity. *Proceedings of the National Academy of Sciences of the United States of America*, *111*(10), 3853–3858. https://doi.org/10.1073/pnas.1316594111

Zhou, X., Zhu, D., Qi, X. L., Lees, C. J., Bennett, A. J., Salinas, E., Stanford, T. R., & Constantinidis, C. (2013). Working memory performance and neural activity in prefrontal cortex of peripubertal monkeys. *Journal of Neurophysiology*, *110*(11), 2648–2660. https://doi.org/10.1152/jn.00370.2013

Zhou, X., Zhu, D., Qi, X. L., Li, S., King, S. G., Salinas, E., Stanford, T. R., & Constantinidis, C. (2016). Neural correlates of working memory development in adolescent primates. *Nature Communications*, *7*, 1–11. https://doi.org/10.1038/ncomms13423

Zimmermann, M. J. Y., Nevala, N. E., Yoshimatsu, T., Osorio, D., Nilsson, D.-E., Berens, P., & Baden, T. (2018). Zebrafish Differentially Process Color across Visual Space to Match Natural Scenes. *Current Biology*, *28*(13), 2018-2032.e5. https://doi.org/10.1016/j.cub.2018.04.075

Zola-Morgan, S. (1995). Localization of Brain Function: The Legacy of Franz Joseph Gall (1758-1828). *Annual Review of Neuroscience*, *18*(1), 359–383. https://doi.org/10.1146/annurev.ne.18.030195.002043

Acknowledgments

Most of all, I want to thank my supervisor Prof. Arrenberg for the opportunity to pursue my thesis in his lab and for his continuous support, valuable input, and patience over all those years. Starting from the early days in Freiburg, over the move to Tübingen until today I always had an open door when I encountered problems during my research.

I would like to thank Prof. Hafed and Prof. Euler for being on my advisory board and their advice and discussions during our meetings. I would also like to thank Prof. Ilg for being a member of my examination board.

I want to express my gratitude to Prof. Driever under whom I started my project. Until the lab in Tübingen was fully set up, he provided refuge for me, my colleague, and our fish so we could continue our work without delay.

I want to thank Kun Wang for being a very close friend and all the discussions about science and life during our time in Freiburg and Tübingen. From cooking authentic Chinese food, giving me his honest opinion about work and life, and at least trying to make a sportier person out of me, I am grateful to have met him.

I also want to thank Claire Leyden, Nina Omejc and Eleanor Schaber for helping me with the recordings and Nina for adapting the setup for older larvae.

I would like to thank all the lab members from Freiburg and Tübingen for creating such a nice atmosphere and all the laughs during those years, including Kun, Claire, Florian Dehmelt, Yue Zhang, Tim Hladnik, Giulia Soto, Nina, Christian Altbürger, Christian Sigloch, Theresa Schredelseker, Sebastian Reinig, Maximilian Wandl, Rebecca Meier, Julian Hinz and Sabrina Fuchs.

I also want to thank Rebecca and Maxi for all their additional support, helping to bring the fish from Freiburg and with Lidia García-Pradas, Sabine Götter, Sabrina and Timo Brüggemann for the excellent fish care.

I want to express my gratitude to the University of Freiburg, University of Tübingen, University Hospital Tübingen and the Graduate Training Centre of Neuroscience for their support during this study.

Last, but not least, I want to thank my family. Without their continuous support this work would not have been possible.

Statement of contribution

Prof. Aristides Arrenberg planned the study and secured the funding. AA and Christian Brysch designed the experiments. Data was recorded by CB (~70 %) and Claire Leyden (~30 %) with assistance from Nina Omejc and Eleanor Schaber. CB, CL, NO and ES did the pre-analysis (ROI-selection and registration) with minor re-analysis by CB. The code for the pre-analysis was written by Bastian Hablizel (ROI identification & extraction, reference brain registration) and modified by CB (multiple regressor identification/parallel processing). A precursor version of ZebEyeTrack was modified by CB to allow for monocular/ocular rivalry stimulation and to perform the closed-loop experiments. The final analysis was done by CB and the analysis code was written by CB. The design and assembly of Figure 1-3, Figure 1-7 and all figures in chapters 3 & 4 was done by CB with input from AA, except for Figure 4-1, which was done by NO. NO designed and adapted the setup for late-stage larvae with input from AA and CB. This statement of contribution applies to all the data presented in this thesis. Some data was previously published by me (Brysch, C., Leyden, C., and Arrenberg, A.B. (2019). Functional architecture underlying binocular coordination of eye position and velocity in the larval zebrafish hindbrain. BMC Biology 17.).

Appendix

Supplemental figures:

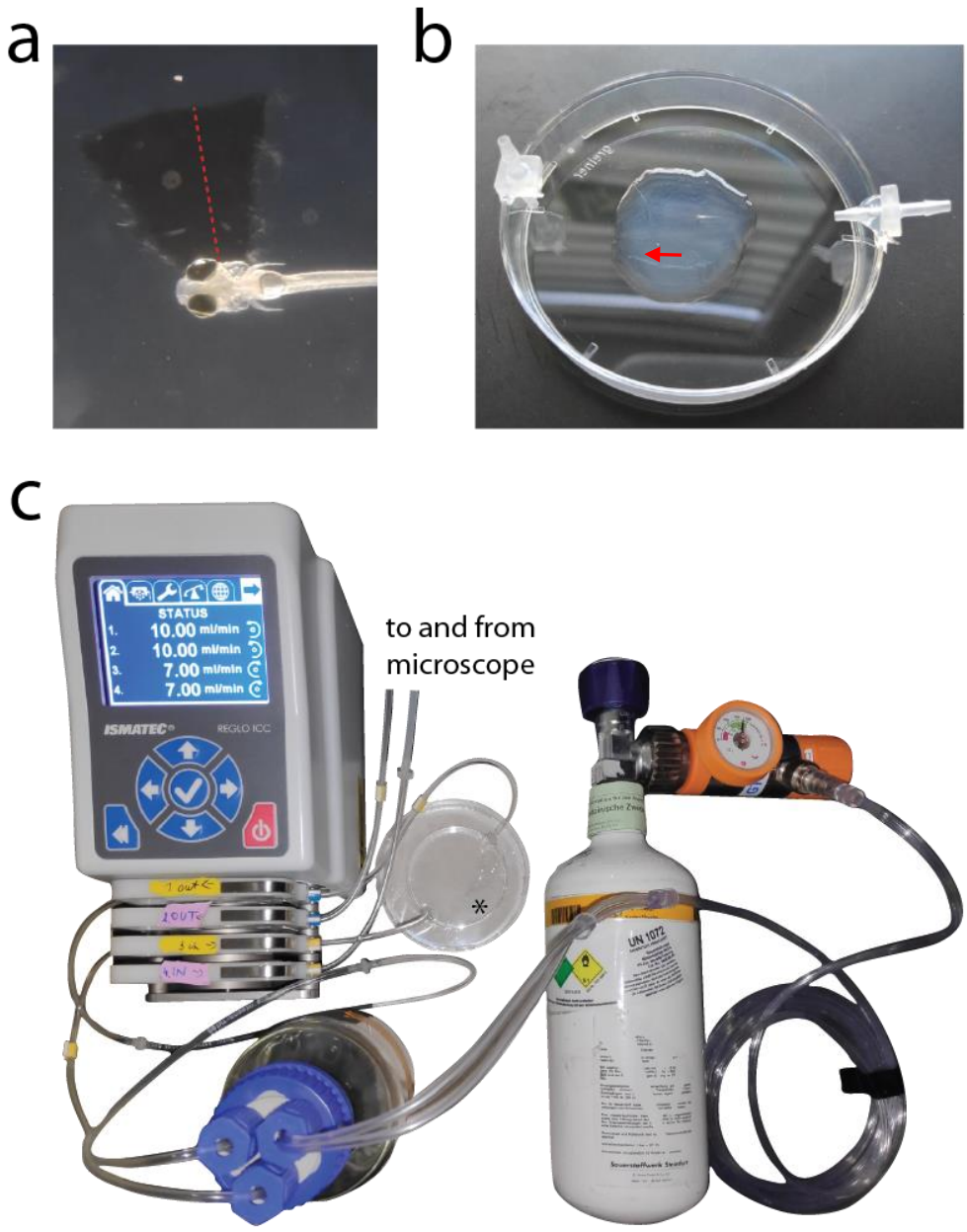

Supplemental Figure 1: Fish mounting and perfusion setup for late-stage larvae

a: 14 dpf late-stage larvae mounted in 3 % agarose with its right eye and gills cut free of agarose. The red dashed line indicates the additional area cut free for the late-stage larvae to ensure Ringer's solution flow over the gills for better oxygen uptake. **b:** 14 dpf larvae mounted in a petri dish lid with the Luer connectors glued to it. The red arrow indicates fish orientation (in direction of the head). Note the different level of the connectors with the input connector (left, at the side of the larvae's head) being lower to ensure mixture of the solution and the output connector being higher to ensure that the larvae stay fully submerged. **c:** Picture of the perfusion setup with the O_2 bottle (right) and peristaltic pump (left). Note the different input and output speeds, with the output speeds being higher to prevent flooding of the microscope. The asterisk indicates a 2nd location to keep a mounted fish oxygenated.

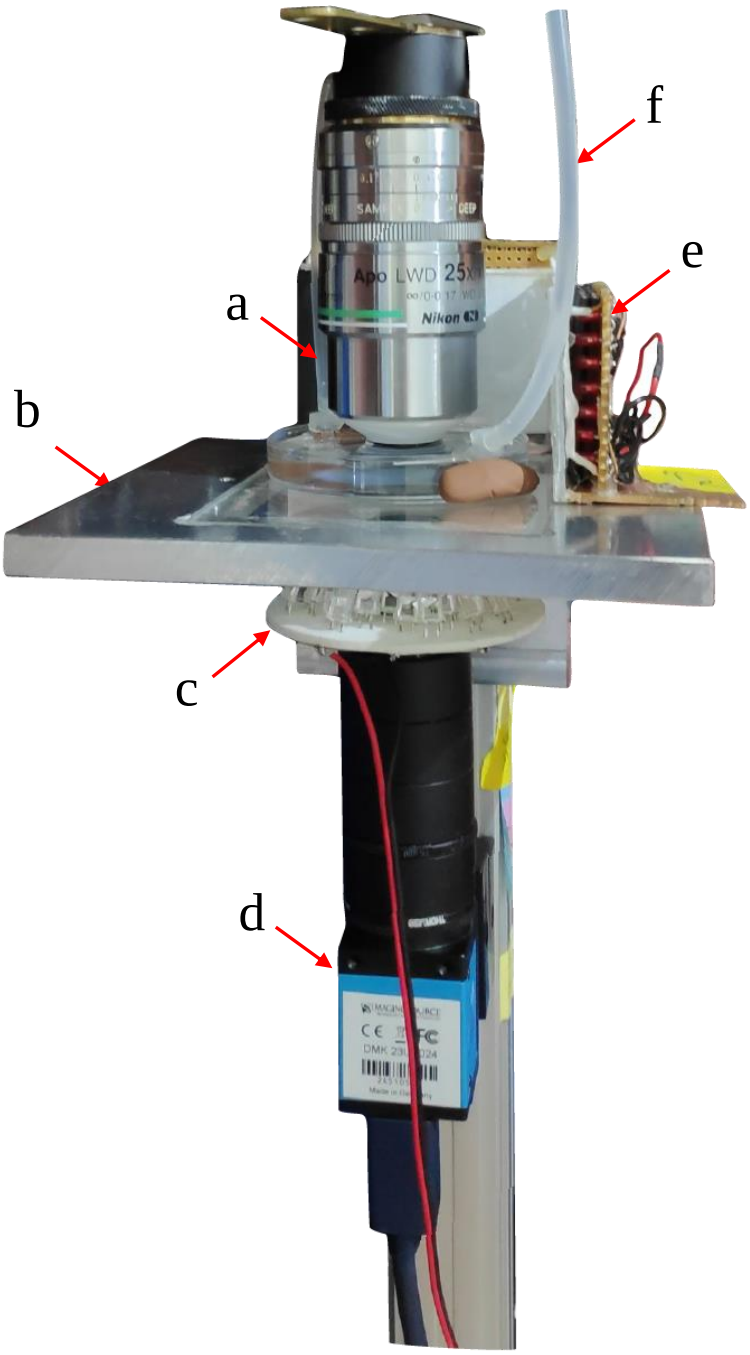

Supplemental Figure 2: Modified setup for late-stage larvae

a: Input tube for oxygenated Ringer's solution. **b:** Modified stage with a plexiglass cutout in the middle to record eye movements. **c:** Additional IR-LED ring to provide illumination of the eyes independent of objective position. **d:** CMOS camera to record eye movements. **e:** One half of the LED arena (2 panels, used for stimulation of the right eye). Note the diffusor in front of the LEDs and the black foil in front of the binocular zone (partially hidden by the objective, behind the input tube). **f:** Output tube for deoxygenated Ringer's solution.

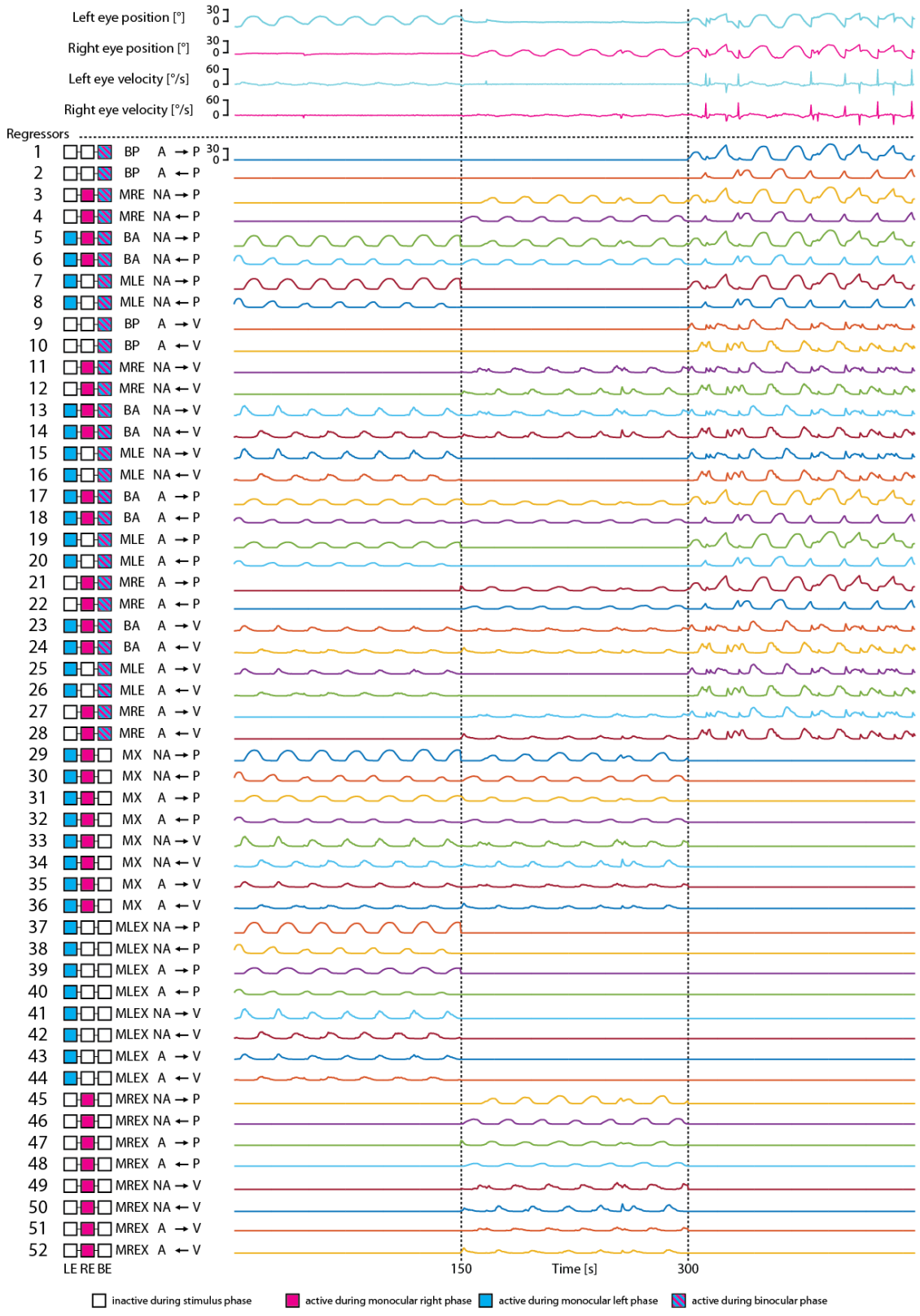

Supplemental Figure 3: Example regressors for one recording

All 52 regressors from the recording depicted in Figure 3-3a and Figure 3-4a. Scale bar from regressor 1 accounting for all regressors. Abbreviations similar as for Figure 3-4. Figure adapted under CC BY 4.0 from Brysch et al. (2019b).

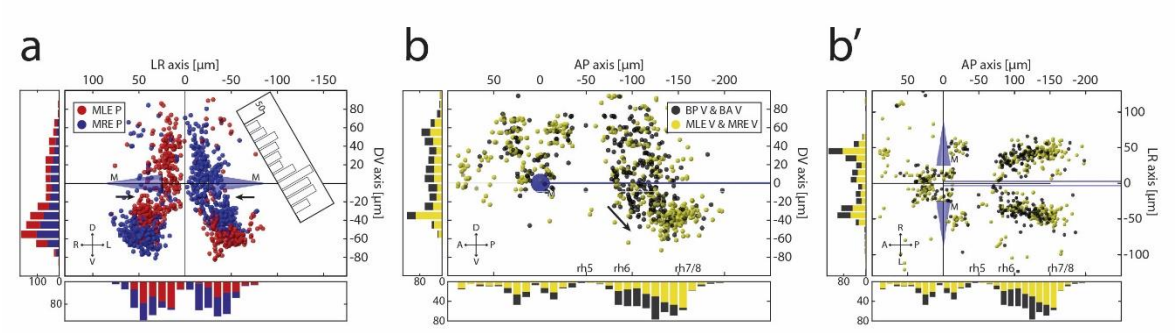

Supplemental Figure 4: Additional monocular and binocular cell maps

Additional cell maps highlighting the arrangement of monocular neurons in rh5/6 and alignment of mono- and binocular velocity neurons in young larvae. **a:** Transversal projection of monocular position encoding neurons in rh5 & 6. The two black arrows indicate the faint gap between the two INN clusters. The bar plot shows the number of neurons in D-V for the left hemisphere rotated by 30 ° with the reduced number of neurons visible in the middle. D: dorsal, L: left, M: Mauthner cells, MLE: monocular left eye, MRE: monocular right eye, P: position, R: right, V: ventral. **b & b':** Sagittal and dorsal view of mono- and binocular velocity encoding neurons. The black arrow in b shows the shift of velocity coding neurons from intermingled towards monocular. A: anterior, BA: binocular always, BP: binocular preferred, L: left, P: posterior, R: right, rh: rhombomere, V: velocity. Figure adapted under CC BY 4.0 from Brysch et al. (2019b).

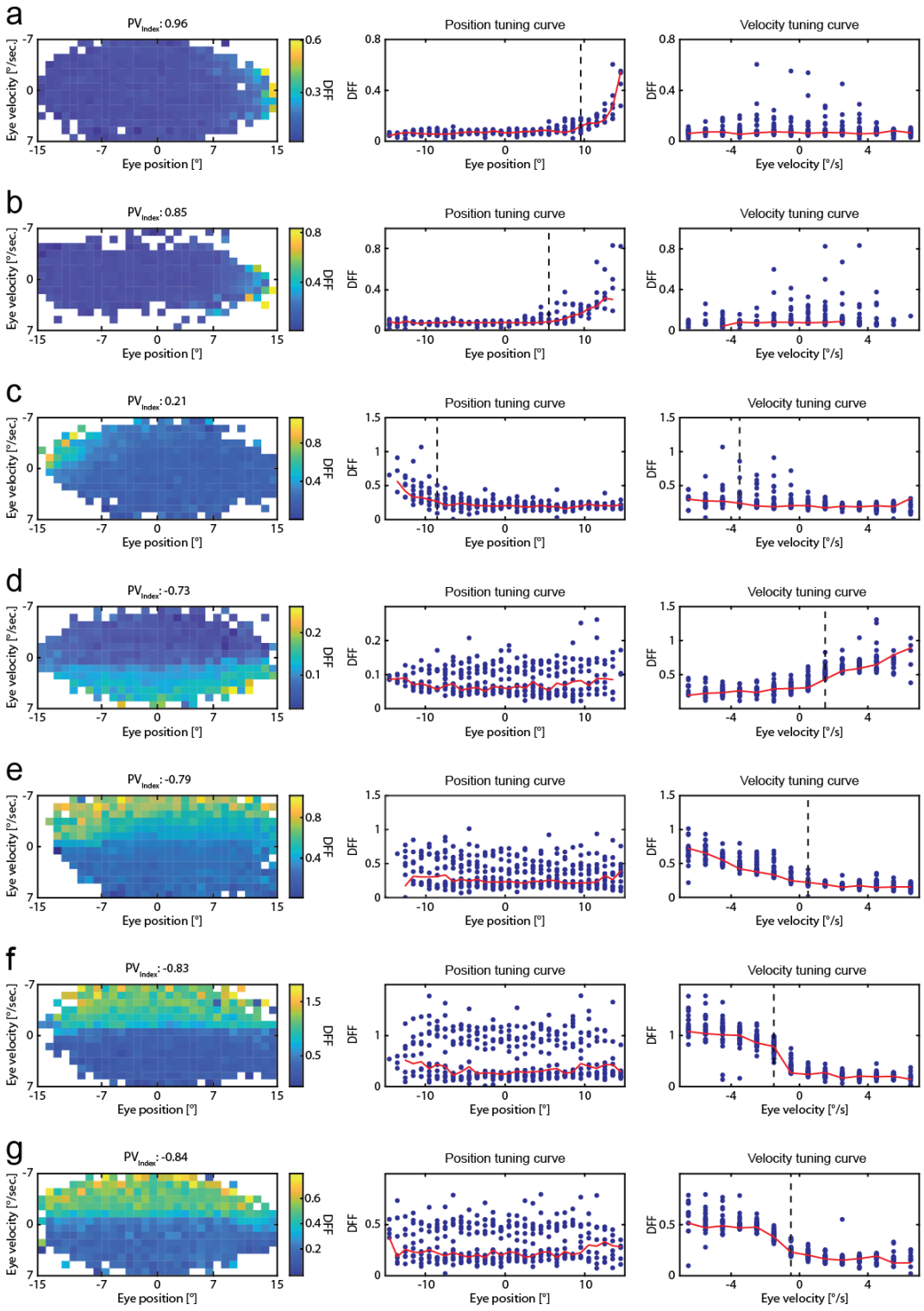

Supplemental Figure 5: Additional tuning curves from experiment 2

a-g: Left column: two-dimensional tuning curves with the DFF color-coded for eye position (x-axis) and slow-phase eye velocity (y-axis). Middle column: eye position tuning curve. Red line shows the averaged eye position tuning between ± 1 °/sec. Blue dots show the datapoints for the remaining velocities. The black dashed line shows the respective firing threshold, if identified. Right column: same as in middle column but for slow-phase eye-velocity with the red column showing the eye velocity between ± 1 °. Figure adapted under CC BY 4.0 from Brysch et al. (2019b).

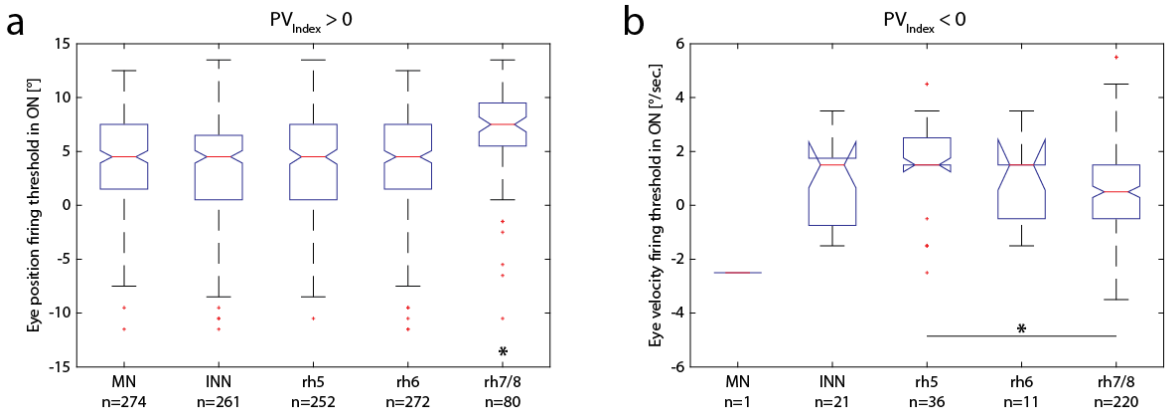

Supplemental Figure 6: Firing thresholds for different anatomical locations in young larvae

a: Eye position firing thresholds pooled in ON direction for eye position encoding neurons ($PV_{Index} > 0$) for different neuronal groups. INN: internuclear neurons, MN: motoneurons, rh: rhombomere. All other groups are significantly different from rh7/8 (Kruskal-Wallis test, $p < 0.05$). **b:** Eye velocity firing thresholds pooled in ON direction for eye velocity encoding neurons ($PV_{Index} < 0$) for different neuronal groups. Rh5 significantly differs to rh7/8 (Kruskal-Wallis test, $p < 0.05$). Please note the low number of velocity encoding neurons outside of rh7/8, which limits comparability.

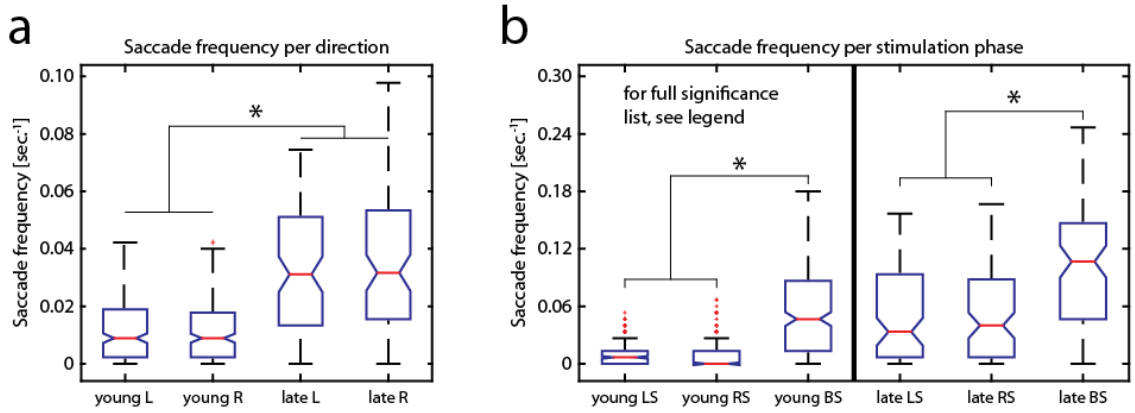

Supplemental Figure 7: Saccade frequency for each direction and stimulation phase

Late-stage larvae show increased saccadic frequency in both directions in comparison to young larvae and most saccades are triggered during the binocular stimulation phase for experiment 1 & 3. **a:** Saccadic frequency in each direction over the whole experiment. No differences in direction were observed, but frequency increased with development (Kruskal-Wallis test: $p < 0.05$). L: saccade to the left; R: saccade to the right. **b:** Saccadic frequency for each stimulation phase for young and late-stage larvae (Kruskal-Wallis test: $p < 0.05$: YLS-YBS, YLS-LLS, YLS-LRS, YLS-YBS, YRS-YBS, YRS-LLS, YRS-LRS, YRS-YBS, YBS-LBS, LLS-LBS, LRS-LBS). BS: both eyes stimulated, LS: left eye stimulated, RS: right eye stimulated.

a

Neuron numbers per brain

	Position		Velocity	
	young	late	young	late
MLE	90	116	23	21
MRE	102	68	20	13
BA	34	88	29	6
BP	41	40	5	7
MLEX	7	29	2	5
MREX	3	5	2	3
Σ	277	346	81	55

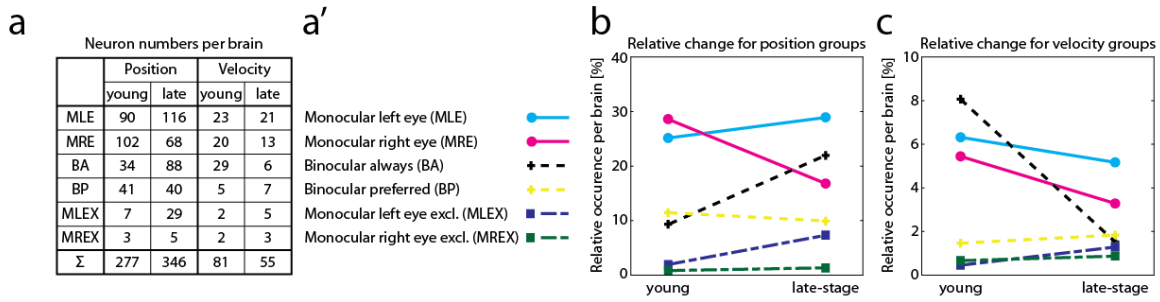

Supplemental Figure 8: Neuron number comparison caudal to the Mauthner cells

a: Number of identified neurons for each response group per brain caudal of the Mauthner cells (mean, upscaled for late-stage). **a':** Color-code for subfigures b & c. **b:** Change of each eye position encoding response group for young and late-stage larvae (relative to the total, average number of neurons identified for the respective developmental stage). **c:** same as in b, but for velocity encoding groups.

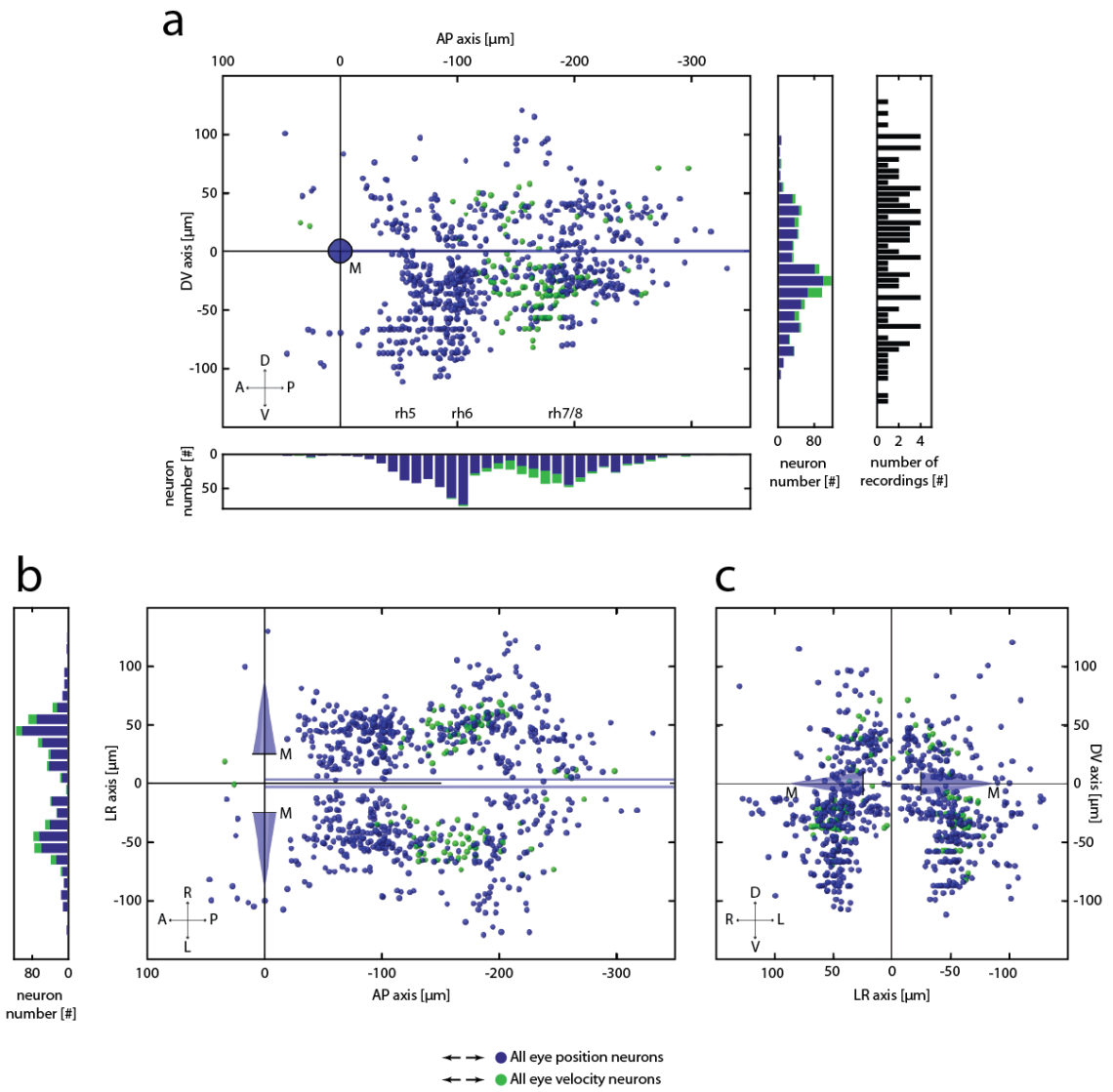

Supplemental Figure 9: Maps for all identified eye position and velocity neurons in late-stage larvae:

Spatial locations of all identified neurons in late-stage larvae color-coded for eye position and velocity. **a-c:** Sagittal, dorsal, and transversal views. Each dot represents one neuron identified in one recording. A: anterior, D: dorsal, L: left, M: Mauthner cells, P: posterior, R: right, rh: rhombomere, V: ventral.

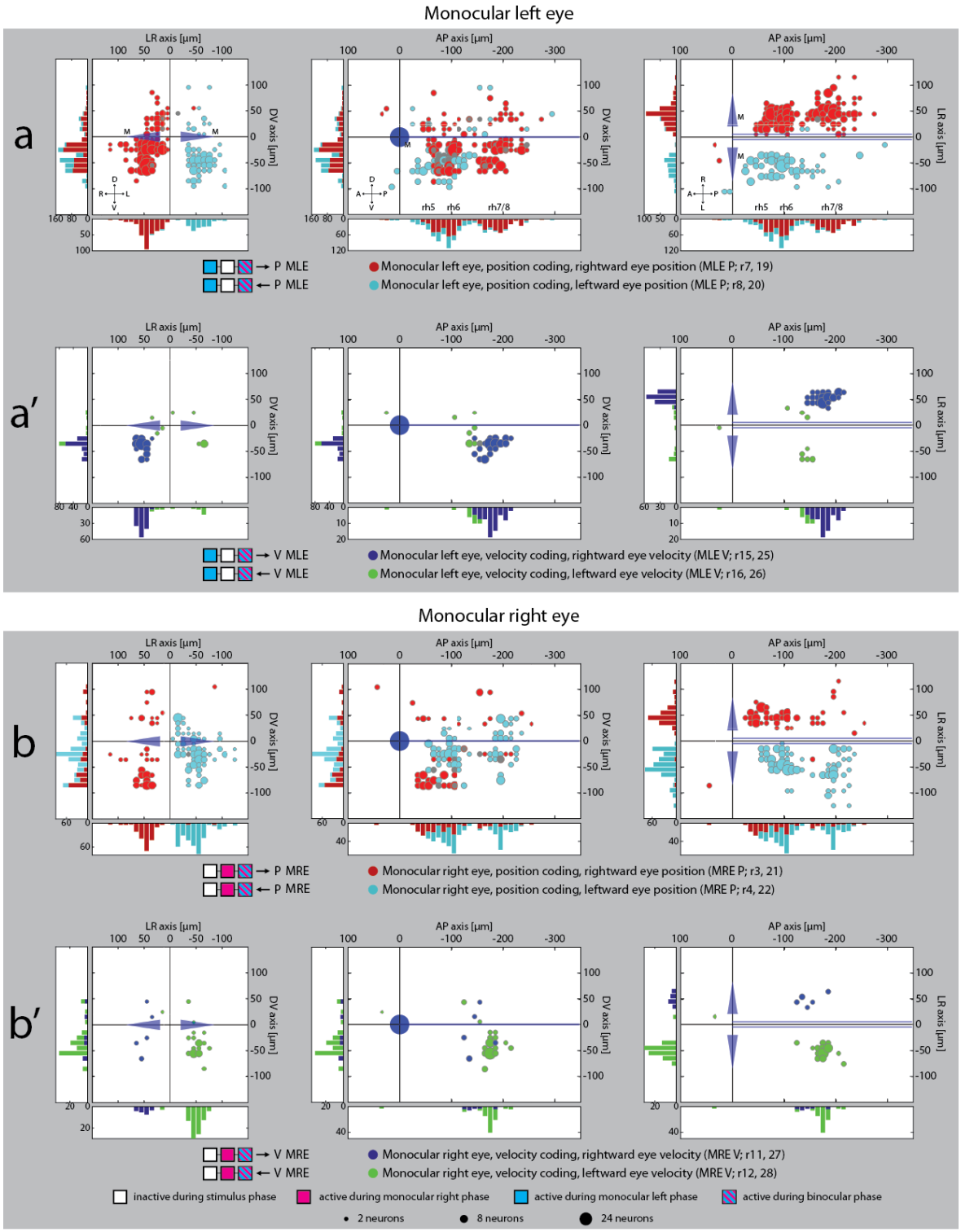

Supplemental Figure 10: Upscaled monocular cell maps for late-stage larvae

Spatial locations of upscaled monocular neurons. **a-b':** Transversal, sagittal and dorsal views for MLE eye position (a), MLE velocity (a'), MRE position (b) and MRE velocity (b') encoding neurons. Each dot represents one 10 x 10 x 10 µm voxel upscaled to 8 brains in 5µm increments. A: anterior, D: dorsal, L: left, M: Mauthner cells, P: posterior/position, R: right/regressor, rh: rhombomere, V: ventral/velocity.

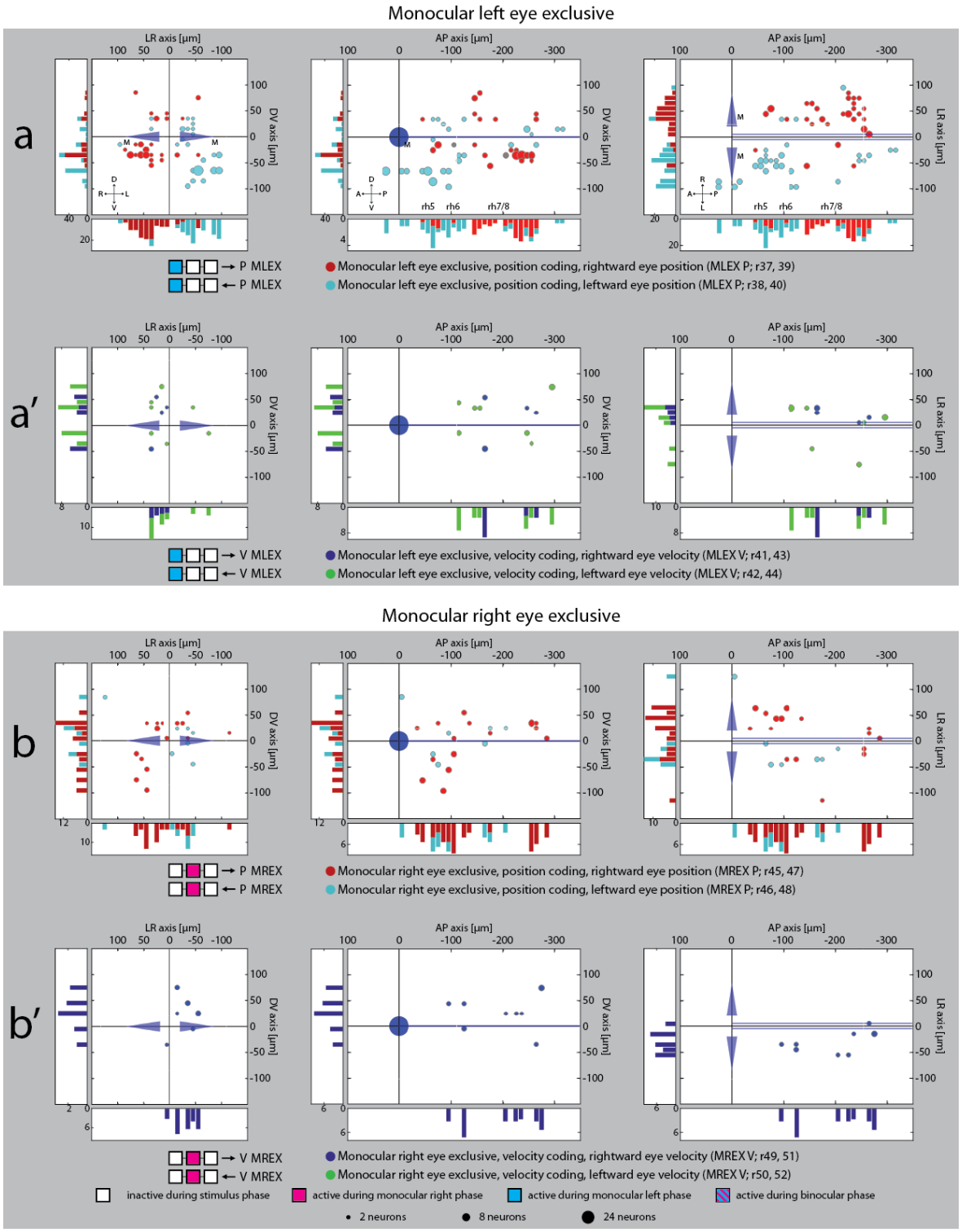

Supplemental Figure 11: Upscaled monocular exclusive cell maps for late-stage larvae

Spatial locations of upscaled monocular exclusive neurons. **a-b':** Transversal, sagittal and dorsal views for MLEX eye position (a), MLEX velocity (a'), MREX position (b) and MREX velocity (b') encoding neurons. Each dot represents one 10 x 10 x 10 µm voxel upscaled to 8 brains in 5µm increments. A: anterior, D: dorsal, L: left, M: Mauthner cells, P: posterior/position, R: right/regressor, rh: rhombomere, V: ventral/velocity.

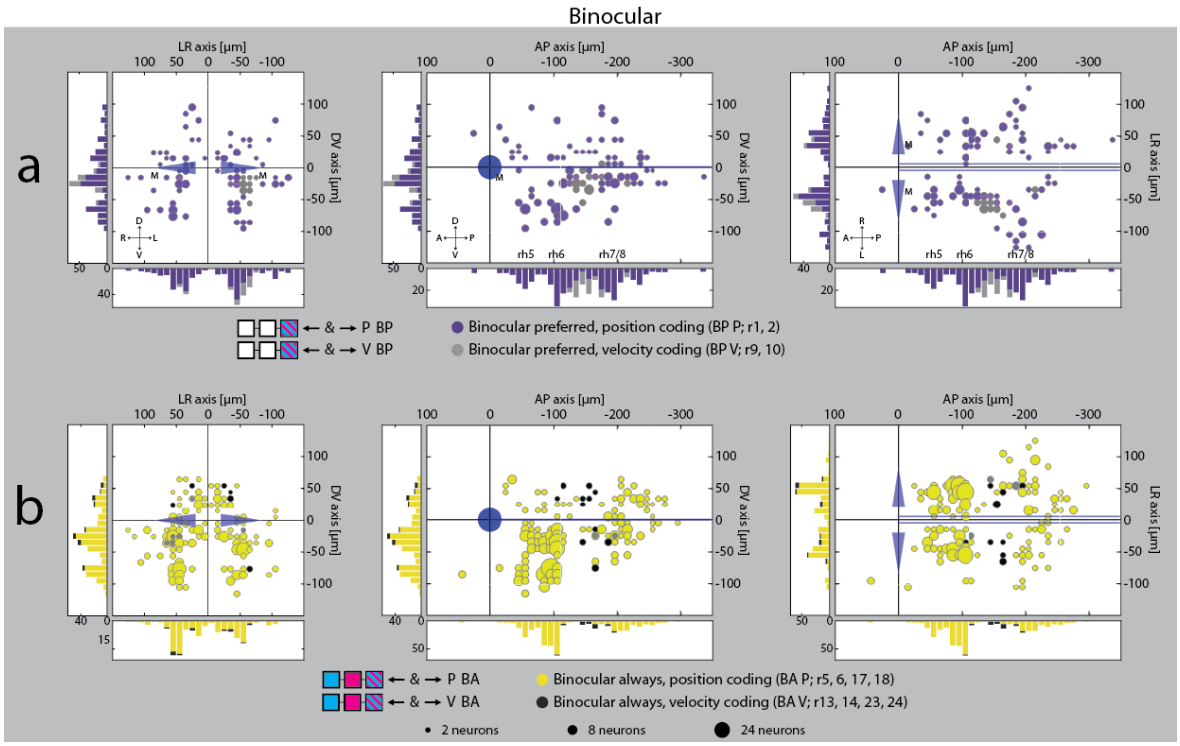

Supplemental Figure 12: Upscaled binocular cell maps for late-stage larvae

Spatial locations of upscaled binocular neurons. **a-b':** Transversal, sagittal and dorsal views for BP (a) and BA (b) encoding neurons. Each dot represents one 10 x 10 x 10 µm voxel upscaled to 8 brains in 5µm increments. A: anterior, D: dorsal, L: left, M: Mauthner cells, P: posterior/position, R: right/regressor, rh: rhombomere, V: ventral/velocity.

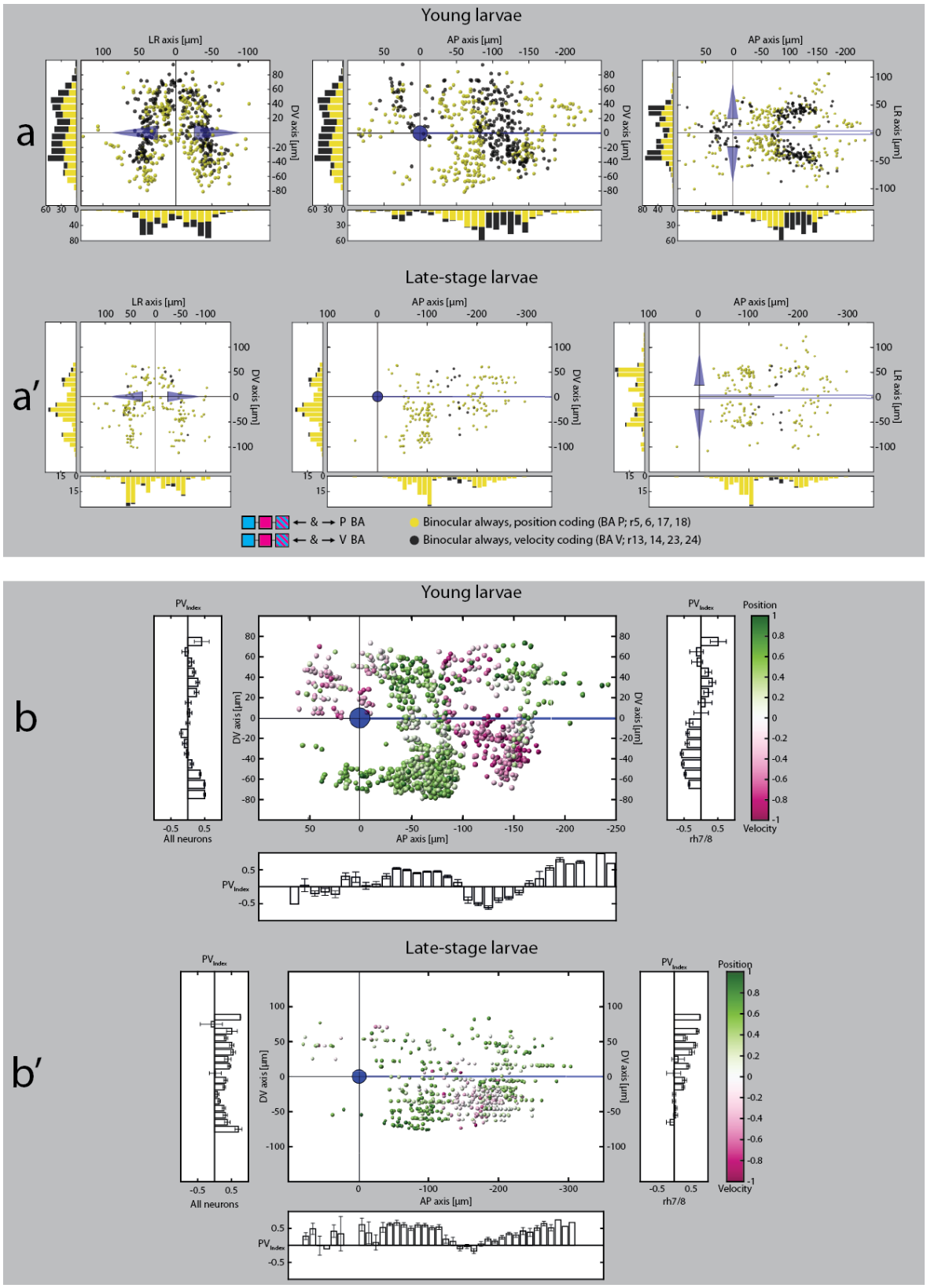

Supplemental Figure 13: Comparison of BA neurons and the PVIndex between young and late-stage larvae

a & **a'**: Transversal, sagittal and dorsal views of identified BA neurons in young and late-stage larvae. Data from Figure 3-9a' and Figure 4-6a'. Note the different size of the pictured hindbrain patch which was kept

similar to the other figures of the respective developmental stage. Each dot represents one neuron identified in one recording with its highest correlation to the regressor in the respective legend. M: Mauthner cells, P: position, R: regressor, V: velocity. **b** & **b'**: Color-coded PV_{Index} for neurons identified in experiment 2 and 4. Data from Figure 3-13a and Figure 4-10a. Note the different size of the pictured hindbrain patch which was kept similar to the other figures of the respective developmental stage. Error bars are SEM.

Supplemental Table 1: Number of identified neurons for each regressor for Exp 1

Regressor number	Tuning	Total # (per brain)	**Regressor number**	Tuning	Total # (per brain)
1	BP P → NA	173 (22)	**27**	MRE V → A	23 (3)
2	BP P ← NA	221 (28)	**28**	MRE V ← A	36 (5)
3	MRE P → NA	221(28)	**29**	MX P → NA	0 (0)
4	MRE P ← NA	273 (34)	**30**	MX P ← NA	0 (0)
5	BA P → NA	26 (3)	**31**	MX P → A	0 (0)
6	BA P ← NA	22 (3)	**32**	MX P ← A	0 (0)
7	MLE P → NA	282 (35)	**33**	MX V → NA	0 (0)
8	MLE P ← NA	107 (13)	**34**	MX V ← NA	0 (0)
9	BP V → NA	39 (5)	**35**	MX V → A	0 (0)
10	BP V ← NA	19 (2)	**36**	MX V ← A	0 (0)
11	MRE V → NA	45 (6)	**37**	MLEX P → NA	20 (3)
12	MRE V ← NA	96 (9)	**38**	MLEX P ← NA	7 (1)
13	BA V → NA	31 (4)	**39**	MLEX P → A	19 (2)
14	BA V ← NA	39 (5)	**40**	MLEX P ← A	22 (3)
15	MLE V → NA	114 (14)	**41**	MLEX V → NA	7 (1)
16	MLE V ← NA	51 (6)	**42**	MLEX V ← NA	9 (1)
17	BA P → A	113 (14)	**43**	MLEX V → A	2 (0)
18	BA P ← A	142 (18)	**44**	MLEX V ← A	3 (0)
19	MLE P → A	252 (32)	**45**	MREX P → NA	10 (1)
20	MLE P ← A	127 (16)	**46**	MREX P ← NA	15 (2)
21	MRE P → A	150 (19)	**47**	MREX P → A	3 (0)
22	MRE P ← A	250 (32)	**48**	MREX P ← A	12 (2)
23	BA V → A	99 (12)	**49**	MREX V → NA	22 (3)
24	BA V ← A	98 (12)	**50**	MREX V ← NA	4 (1)
25	MLE V → A	49 (6)	**51**	MREX V → A	12 (2)
26	MLE V ← A	27 (3)	**52**	MREX V ← A	10 (1)

A: averaged, BA: binocular always, BP: binocular preferred, MLE: monocular left eye, MLEX: monocular left eye exclusive, MRE: monocular right eye, MREX: monocular right eye exclusive, MX: monocular exclusive, NA: non-averaged P: position, V: velocity

Supplemental Table 2: Number of recordings of late-stage larvae per z-level

Z-level	# of recordings	**Z-level**	# of recordings	**Z-level**	# of recordings
130	1	**40**	6	**-50**	3
120	1	**30**	5	**-60**	3
110	1	**20**	6	**-70**	3
100	4	**10**	5	**-80**	3
90	4	**0**	5	**-90**	3
80	3	**-10**	4	**-100**	3
70	4	**-20**	4	**-110**	1
60	4	**-30**	3	**-120**	1
50	5	**-40**	4	**-130**	1

Gray shaded entries indicate dorsal-ventral area which was upscaled to 8 brains

Supplemental Table 3: Number of identified neurons for each regressor for Exp 3

Regressor number	Tuning	Total # (upscaled, per brain)	**Regressor number**	Tuning	Total # (upscaled, per brain)
1	BP P → NA	42 (20)	**27**	MRE V → A	2 (1)
2	BP P ← NA	43 (20)	**28**	MRE V ← A	4 (2)
3	MRE P → NA	30 (16)	**29**	MX P → NA	0 (0)
4	MRE P ← NA	50 (24)	**30**	MX P ← NA	0 (0)
5	BA P → NA	37 (18)	**31**	MX P → A	0 (0)
6	BA P ← NA	28 (14)	**32**	MX P ← A	0 (0)
7	MLE P → NA	117 (56)	**33**	MX V → NA	0 (0)
8	MLE P ← NA	45 (26)	**34**	MX V ← NA	0 (0)
9	BP V → NA	2 (1)	**35**	MX V → A	0 (0)
10	BP V ← NA	13 (6)	**36**	MX V ← A	0 (0)
11	MRE V → NA	3 (2)	**37**	MLEX P → NA	23 (11)
12	MRE V ← NA	17 (9)	**38**	MLEX P ← NA	21 (11)
13	BA V → NA	2 (1)	**39**	MLEX P → A	10 (4)
14	BA V ← NA	1 (0)	**40**	MLEX P ← A	9 (4)
15	MLE V → NA	25 (14)	**41**	MLEX V → NA	1 (0)
16	MLE V ← NA	4 (2)	**42**	MLEX V ← NA	8 (4)
17	BA P → A	65 (34)	**43**	MLEX V → A	3 (1)
18	BA P ← A	44 (22)	**44**	MLEX V ← A	0 (0)
19	MLE P → A	40 (23)	**45**	MREX P → NA	14 (6)
20	MLE P ← A	26 (13)	**46**	MREX P ← NA	7 (3)
21	MRE P → A	23 (10)	**47**	MREX P → A	3 (1)
22	MRE P ← A	40 (18)	**48**	MREX P ← A	1 (1)
23	BA V → A	5 (3)	**49**	MREX V → NA	8 (4)
24	BA V ← A	5 (2)	**50**	MREX V ← NA	0 (0)
25	MLE V → A	5 (3)	**51**	MREX V → A	0 (0)
26	MLE V ← A	5 (3)	**52**	MREX V ← A	0 (0)

A: averaged, BA: binocular always, BP: binocular preferred, MLE: monocular left eye, MLEX: monocular left eye exclusive, MRE: monocular right eye, MREX: monocular right eye exclusive, MX: monocular exclusive, NA: non-averaged P: position, V:velocity

List of figures

List of supplemental figures

List of tables

List of supplemental tables:

List of equations

Copyright

Figure 1-2: Figure adapted from: Amores, A., Catchen, J., Ferrara, A., Fontenot, Q., and Postlethwait, J.H. (2011). Genome evolution and meiotic maps by massively parallel DNA sequencing: Spotted gar, an outgroup for the teleost genome duplication. Genetics *188*, 799–808. Reproduced by permission of Oxford University Press. Copyright © 2011.

Figure 1-4: **a:** Figure adapted from: Grienberger, C., and Konnerth, A. (2012). Imaging Calcium in Neurons. Neuron *73*, 862–885. Republished with permission of Elsevier Science & Technology Journals; permission conveyed through Copyright Clearance Center, Inc.; Copyright © 2012 **b:** Adapted by permission from Springer Nature: Chen, T.W., Wardill, T.J., Sun, Y., Pulver, S.R., Renninger, S.L., Baohan, A., Schreiter, E.R., Kerr, R.A., Orger, M.B., Jayaraman, V., et al. (2013). Ultrasensitive fluorescent proteins for imaging neuronal activity. Nature *499*, 295–300. Copyright © 2013. **c-c''**: Reprinted from: Svoboda, K., and Yasuda, R. (2006). Principles of Two-Photon Excitation Microscopy and Its Applications to Neuroscience. Neuron *50*, 823–839, with permission from Elsevier. Copyright © 2006. **d-d'**: Reprinted from: Soeller, C., and Cannell, M.B. (1999). Two-photon microscopy: Imaging in scattering samples and three- dimensionally resolved flash photolysis. Microscopy Research and Technique *47*, 182–195, with permission from John Wiley and Sons. Copyright © 1999.

Figure 1-5b: Republished with permission of Society of Neuroscience, from Neuhauss, S.C.F., Biehlmaier, O., Seeliger, M.W., Das, T., Kohler, K., Harris, W.A., and Baier, H. (1999). Genetic disorders of vision revealed by a behavioral screen of 400 essential loci in zebrafish. Journal of Neuroscience *19*, 8603–8615; permission conveyed through Copyright Clearance Center, Inc.; Copyright © 1999.

Figure 1-6: Reprinted from: Masseck, O.A., and Hoffmann, K.P. (2009). Comparative neurobiology of the optokinetic reflex. In Annals of the New York Academy of Sciences, (Blackwell Publishing Inc.), pp. 430–439, with permission from John Wiley and Sons. Copyright © 2009.

Figure 1-8: **a & b:** Reprinted with permission from Springer Nature: Aksay, E., Gamkrelidze, G., Seung, H.S., Baker, R., and Tank, D.W. (2001). In vivo intracellular

recording and perturbation of persistent activity in a neural integrator. Nature Neuroscience *4*, 184–193. Copyright © 2001. **b:** Adapted from National Academy of Science: Seung, H.S. (1996). How the brain keeps the eyes still. Proceedings of the National Academy of Sciences of the United States of America *93*, 13339–13344. Copyright © (1996) National Academy of Sciences. Written permission for noncommercial and educational use not required.

Figure 1-9: **a:** Reprinted with permission from The American Physiological Society: Aksay, E., Baker, R., Seung, H.S., and Tank, D.W. (2000). Anatomy and discharge properties of pre-motor neurons in the goldfish medulla that have eye-position signals during fixations. Journal of Neurophysiology *84*, 1035–1049. Copyright © 2000. **b:** Preprinted from: Aksay, E., Major, G., Goldman, M.S., Baker, R., Seung, H.S., and Tank, D.W. (2003). History Dependence of Rate Covariation between Neurons during Persistent Activity in an Oculomotor Integrator. Cerebral Cortex *13*, 1173–1184., by permission of Oxford University Press. Copyright © 2003.

All other figures did not require written permission and are attributed at the appropriate sections if applicable.

List of abbreviations

2-P: 2-photon
ABN: abducens nucleus
AF: arborization field
AOS: accessory optic system
APT: area pretectalis
ARTR: anterior rhombencephalic turning region
BA: binocular always
BE: both eyes
BP: binocular preferred
CCW: counterclockwise
CIRF: calcium impulse-response function
cpEGFP: circularly permuted enhanced green fluorescent protein
CW: clockwise
DC: double cone
dpf: days post fertilization
DS: direction-selective
EBN: excitatory burst neuron
EM: electron microscopy
EOM: extraocular muscle
Ephys: electrophysiology
GECI: genetically encoded calcium indicator
IBN: inhibitory burst neuron
INC: interstitial nucleus of Cajal
INN: internuclear neuron
IO: inferior olive
IOb: inferior oblique
IR: inferior rectus
LE: left eye
LR: lateral rectus
LSC: long single cone
MIF: multiply innervated muscle fiber
MLE: monocular left eye
MLEX: monocular left eye exclusive
MLF: medial longitudinal fasciculus
MN: motoneuron
MR: medial rectus
MRE: monocular right eye
MREX: monocular right eye exclusive
MVN: medial vestibular nucleus
MX: monocular exclusive
nIII-nVI: cranial nerve III-VI
NPH: nucleus prepositus hypoglossi
OI: oculomotor integrator
OKAN: optokinetic after-nystagmus
OKR: optokinetic response
OMN: oculomotor nucleus
OMR: oculomotor response
OPN: omnipause neuron
RE: right eye
RGC: retinal ganglion cell
rh: rhombomere
ROI: region of interest
SIF: singly innervated muscle fiber
SL: standard length
SOb: superior oblique
SR: superior rectus
SSC: short single cone
VGCC: voltage-gated calcium channel
VOR: vestibulo-ocular reflex
VPNI: velocity to position neuronal integrator
VSM: velocity storage mechanism
YI: Yoking index
ZIRC: Zebrafish International Resource Center